



HAL
open science

Suspended sediment production and transfer in mesoscale catchments: a new approach combining flux monitoring, fingerprinting and distributed numerical modeling

Magdalena Uber

► **To cite this version:**

Magdalena Uber. Suspended sediment production and transfer in mesoscale catchments: a new approach combining flux monitoring, fingerprinting and distributed numerical modeling. Applied geology. Université Grenoble Alpes [2020-..], 2020. English. NNT: 2020GRALU011 . tel-02926078

HAL Id: tel-02926078

<https://theses.hal.science/tel-02926078>

Submitted on 31 Aug 2020

HAL is a multi-disciplinary open access archive for the deposit and dissemination of scientific research documents, whether they are published or not. The documents may come from teaching and research institutions in France or abroad, or from public or private research centers.

L'archive ouverte pluridisciplinaire **HAL**, est destinée au dépôt et à la diffusion de documents scientifiques de niveau recherche, publiés ou non, émanant des établissements d'enseignement et de recherche français ou étrangers, des laboratoires publics ou privés.

THÈSE

Pour obtenir le grade de

DOCTEUR DE L'UNIVERSITÉ GRENOBLE ALPES

Spécialité : **Océan, Atmosphère, Hydrologie**

Arrêté ministériel : 25 Mai 2016

Présentée par

Magdalena Uber

Thèse dirigée par **Cédric Legout**
et coencadrée par **Guillaume Nord**

préparée au sein d' **Institut des Géosciences de l'Environnement (IGE)**
dans l'École Doctorale **Terre Univers Environnement**

Suspended sediment production and transfer in mesoscale catchments: a new approach combining flux monitoring, fingerprinting and distributed numerical modeling

Thèse soutenue le **9 juin 2020**,
devant le jury composé de :

Frédéric Liébault

Directeur de Recherche, INRAE Grenoble, Président

Núria Martínez-Carreras

Researcher, Luxembourg Institute of Science and Technology, Rapporteur

Axel Bronstert

Professeur, University of Potsdam, Rapporteur

Agnès Ducharne

Directrice de Recherche, METIS, Sorbonne Université, Examinatrice

Anne Probst

Directrice de Recherche, ECOLAB, Examinatrice

Luis Cea

Senior lecturer, Universidade da Coruña, Examineur

Cédric Legout

Maître de conférences, Université Grenoble Alpes, Directeur de thèse



Acknowledgements

I would like to thank many people at IGE or elsewhere, without them this work would not have been possible or less pleasant:

First and foremost a big thank you to Cédric and Guillaume for the excellent supervision, for having initiated this PhD project, for your support, creativity, encouragement and understanding throughout the last three-and-a-half years. This thesis is a result of team work and it was always a pleasure to work with you!

I also want to thank those who contributed to this thesis in one way or another: Jérôme Poulenard, Christian Crouzet, François Demory, Nico Hachgenei, Brice Boudevillain, Olivier Evrard, Irène Lefèvre and especially Luis Cea. Thank you, Luis, for welcoming me in A Coruña, for your ongoing support in the modeling studies and for your fast help whenever I encountered a problem.

Further, I would like to thank Luis, Brice, Jérôme and Isabelle Braud for the very fruitful and always constructive discussions during the meetings of my *Comité de thèse*. I also thank the reviewers of this thesis, Núria Martínez-Carreras and Axel Bronstert for their detailed lecture of the manuscript, their very constructive comments and their interest and acknowledgement of this work as well as the other members of the Jury Frédéric Liébault, Anne Probst, Agnès Ducharne and Luis Cea for the very pleasant and fruitful discussion during the PhD defense. Thanks to all the researchers, students and technicians involved in the OHMCV and Draix-Bléone observatories for having generated such valuable data sets and for the inspiring meetings in Grenoble and Draix.

I also want to thank IGE's administrative service, especially Carméline, Odette and Valérie, Christine and Florence from the doctoral school for your constant help with administrative issues as well as to Mondher for the help with the calculations. Most of the calculations presented here were performed using the GRICAD infrastructure whose staff I want to thank for this service.

A big thank you also to my friends in the lab, the fellow PhD students and interns for all the time we spent together and for being there for each other: Catherine, Claudio, Maria Belen, Ana, Stefano, Mathilde and Alessandra; Pati and Gabriela, you were wonderful office mates, thank you for the nearly three years we spent in office 108. Thank you also to Nico, An and Romane for your company and the nice moments during those last stressful months of writing and to the many other PhD students and colleagues who made IGE a very pleasant working environment.

Thank you to my friends outside the lab for having made the time in Grenoble such a wonderful experience: to Johannes for the nice hikes in the mountains; to Nico and many others at *Les pouces verts* for sharing more than fruits and vegetables; to Meike, Jan, Arthur, Melli, Fabien, Agnieszka, Cecilia, Andrea, Pauline and Alban for sharing the parenting experience; to Océ, Laura, Nadia, Diego, Nino, Abdul, Arturo and Thomas for your conviviality and friendship.

To all my friends in Berlin, especially to Lea, Johan and Paula for always welcoming us in your flat and for making me feel as if I never left when I was back in my home town. You are the best!

I also owe a big thank you to the regular and occasional babysitters, without you I would still be writing the introduction! Especially to Bernd, who always came running from various parts of Europe to take care of a sick granddaughter when we needed help and to Gertrud, Helmut and Silja for your invaluable aid during the last months in home office and Corona confinement.

Last but not least a big thank you to Linus for all your support and companionship during all those years and to Flora for being the best kid ever. You are the best family I could imagine and I am looking forward to new adventures with you!

Résumé

L'étude des mécanismes d'érosion hydrique des sols et de transfert de matières en suspension (MES) des bassins versants vers les rivières revêt des enjeux environnementaux et socio-économiques prégnants face à une pression anthropique grandissante et au changement climatique. L'objectif de cette thèse est de comprendre comment la variabilité de la pluie contrôle l'activation de différentes zones sources de MES et la dynamique des flux hydro-sédimentaires dans deux bassins versants méditerranéens de méso-échelle, la Claduègne (42 km^2) et le Galabre (20 km^2) membres de l'infrastructure de recherche sur la zone critique OZCAR.

Dans la première partie, les contributions des zones d'érosion aux MES à l'exutoire de la Claduègne ont été quantifiées à haute résolution temporelle avec une approche low-cost de traçage. Deux ensembles de traceurs (spectres colorimétriques et de fluorescence X) et trois modèles de mélange ont été comparés pour évaluer la sensibilité des contributions de sources à ces choix méthodologiques. Les principales sources de MES identifiées sont les zones de badlands marno-calcaires. Une approche similaire conduite sur le bassin versant du Galabre a mis en avant la dominance des badlands sur molasses dans les flux de MES. La comparaison des traceurs et des modèles de mélange, a montré que les choix méthodologiques génèrent des différences importantes, qui amènent à recommander une approche d'ensemble multi-traceurs-multi-modèle pour obtenir des résultats plus robustes. L'application de cette approche à un grand nombre d'échantillons de MES a souligné l'importante variabilité inter et intra événements des contributions des différentes sources de MES, soulevant des questions sur les processus hydro-sédimentaires à l'origine de la variabilité des flux de MES.

Le concept de connectivité hydrosédimentaire a été testé en posant l'hypo-

thèse que cette variabilité résultait de distributions des temps de transfert des MES très variables contrôlées par i) les caractéristiques inhérentes aux bassins versants comme la localisation des différentes sources de MES et la façon dont elles sont liées à l'exutoire (i.e. connectivité structurelle) et ii) les caractéristiques spatio-temporelles des événements pluvieux qui activent et impactent les vitesses de transfert (i.e. connectivité fonctionnelle). Ainsi, dans la deuxième partie, un modèle numérique distribué basé sur la résolution des équations de Saint Venant couplé à un module d'érosion multi-sources de MES, a été utilisé pour évaluer les rôles respectifs des connectivités structurelle et fonctionnelle. L'analyse de sensibilité aux choix de discrétisation et de paramétrisation (i.e. seuil d'aire drainée pour distinguer la rivière des versants, valeurs de coefficients de frottement sur les versants et la rivière) a montré que la localisation des sources de MES dans le bassin versant était plus importante que les choix de modélisation à condition que les paramètres soient dans une gamme réaliste et limitée. Un schéma général de réponse temporelle du bassin versant par type de sources a été observé, cohérent avec les résultats de l'approche de traçage et la distribution des distances des sources à la rivière et à l'exutoire. Ce même schéma persiste pour différentes durées ou intensités des précipitations mais devient beaucoup plus variable lorsque des hyétogrammes bimodaux ou des précipitations variables dans l'espace sont appliquées. En outre, la localisation de la pluie par rapport aux sources détermine les contributions moyennes des sources et donc les différences entre les événements de pluie.

Les deux approches de traçage des MES et de modélisation numérique se sont avérées complémentaires et leur application combinée présente un fort potentiel pour comprendre comment les interactions entre connectivité structurelle et fonctionnelle contrôlent la dynamique des flux de MES aux exutoires de bassins versants de méso-échelle.

Abstract

The study of soil erosion by water and the transfer of suspended solids from watersheds to rivers is crucial given the environmental and socio-economic issues with regards to growing human influence and the expected intensification of these processes under climate change. The objective of this thesis is to understand how rainfall variability controls the activation of different sediment source zones and the dynamics of hydro-sedimentary flows in two mesoscale Mediterranean catchments, i.e. the Claduègne (42 km^2 , subcatchment of the Ardèche) and the Galabre (20 km^2 , subcatchment of the Durance) which are members of the OZCAR critical zone research infrastructure.

In the first part, the contributions of the erosion zones to sediment fluxes at the outlet of the Claduègne catchment were quantified at high temporal resolution with a low-cost sediment fingerprinting approach. Two sets of tracers (color and X-ray fluorescence tracers) and three mixing models were compared to assess the sensitivity of estimated source contributions to these methodological choices. Marly-calcareous badlands were identified as the main sediment source. A similar approach carried out on the Galabre catchment area showed that badlands on molasses were the main source. The comparison of tracer sets and mixing models, showed that the methodological choices generated important differences. Thus, we suggest a multi-tracer-multi-model ensemble approach to obtain more robust results. The application of this approach to a large number of sediment samples highlighted the important within and between event variability in the contributions of different sediment sources, raising questions about the hydro-sedimentary processes that cause this variability.

We hypothesized that this variability resulted from variable suspended sediment transit time distributions governed by the interplay of (i) catch-

ment characteristics such as the location of different sources and how they are linked to the outlet (referred to as structural sediment connectivity) and (ii) the spatio-temporal characteristics of rain events that activate and impact transfer velocities (i.e. functional connectivity).

Thus, in the second part, a distributed numerical model based on the resolution of the Saint Venant equations coupled to a multi-source erosion module was used to evaluate the respective roles of structural and functional connectivity. Sensitivity analysis of the discretization and parameterization choices (i.e. threshold of contributing drainage area to identify the river network, values of roughness coefficients on hillslopes and the river) showed that the location of the sediment sources in the watershed was more important than the modeling choices when the parameters were limited to realistic range. A general temporal pattern of source contributions was observed. This was consistent with the results of the fingerprinting approach and the distribution of distances from the sources to the river and the outlet. The same pattern persists for different rainfall durations or intensities but became much more variable when bimodal hyetographs or spatially variable precipitation was applied. In addition, the location of the rainfall with respect to the sources determined the average contributions of the sources and thus differences between rainfall events.

The two approaches, sediment fingerprinting and numerical modeling, were found to complement each other. Their combined application has a high potential for understanding how interactions between structural and functional connectivity control the dynamics of sediment fluxes in mesoscale catchments.

Contents

Acknowledgements	2
Résumé	4
Abstract	6
List of Figures	14
List of Tables	15
1 Introduction	16
1.1 Motivation	16
1.2 Scientific context	20
1.2.1 Soil erosion and sediment transport	20
1.2.2 Sediment connectivity	24
1.2.3 Sediment fingerprinting	29
1.2.4 Modeling soil erosion and sediment transport	33
1.3 Objectives	42
2 Study sites	45
2.1 Claduègne catchment	46
2.1.1 Introduction	46
2.1.2 Geology, soils and topography	46
2.1.3 Land cover	48
2.1.4 Erosion zones	49
2.1.5 Climate	50
2.1.6 Hydrology	51
2.1.7 Soil erosion and sediment export	55
2.1.8 Data availability	56
2.2 Galabre catchment	59

2.2.1	Introduction	59
2.2.2	Geology, soils and topography	60
2.2.3	Land cover and erosion zones	61
2.2.4	Climate	62
2.2.5	Hydrology	63
2.2.6	Soil erosion and sediment export	66
2.2.7	Data availability	67

3	High temporal resolution quantification of suspended sediment source contributions in two mesoscale Mediterranean catchments	70
3.1	Claduègne	70
3.1.1	Introduction	72
3.1.2	Methods	73
3.1.2.1	Sampling	73
3.1.2.2	Measurements of tracer properties	74
3.1.2.3	Tests of assumptions	76
3.1.2.4	Source quantification with mixing models	77
3.1.2.5	Error assessment	79
3.1.3	Results	82
3.1.3.1	Verification of fingerprinting assumptions	82
3.1.3.2	Comparison of the mixing models	83
3.1.3.3	Comparison of the tracer sets	85
3.1.3.4	Errors of the fingerprinting approaches	89
3.1.4	Discussion	92
3.1.4.1	Performance and errors of the various fingerprinting approaches	92
3.1.4.2	Interests of using multi-tracer-model ensemble predictions to detect main sources, within- and between event variability in a mesoscale catchment	94
3.1.5	Conclusions and perspectives	100
3.2	Galabre	102
3.2.1	Introduction	102
3.2.2	Materials and methods	102
3.2.3	Results and discussion of the previous studies	103
3.2.4	Conclusions and perspectives	106
3.3	Temporal variability of suspended sediment fluxes	107
3.3.1	Variability between flood events	107
3.3.2	Variability within flood events	108
3.3.3	Discussion and perspectives	111

4	Variability in source soil contributions to suspended sediments: the role of modeling choices and structural connectivity	115
4.1	Introduction	115
4.2	Methods	117
4.2.1	Characteristics of the modeled study sites	117
4.2.2	Model description	120
4.2.3	Model discretization and input data	122
4.2.4	Modeling scenarios	124
4.2.5	Comparison of scenarios	127
4.3	Results and discussion	128
4.3.1	Impact of modeling choices on modeled sediment dynamics	128
4.3.1.1	Varying the contributing drainage area threshold	128
4.3.1.2	Varying Manning's n	133
4.3.2	The role of structural connectivity on the dynamics of sus- pended sediment fluxes at the outlet	136
4.4	Conclusions and perspectives	141
5	Variability in source soil contributions to suspended sediments: the role of spatio-temporal rainfall variability	143
5.1	Introduction	143
5.2	Precipitation data quality control	147
5.3	Methods	153
5.3.1	Selected rain events	153
5.3.1.1	Claduègne	153
5.3.1.2	Galabre	155
5.3.2	Rainfall forcing used in the modeling scenarios	158
5.3.2.1	Temporal rain variability	158
5.3.2.2	Spatial rain variability	159
5.3.2.3	Location of the storm	161
5.4	Results and discussion	162
5.4.1	How does temporal variability of rainfall forcing impact sim- ulated hydro-sedimentary fluxes of different sediment sources?	162
5.4.2	Does spatial variability of rainfall forcing impact modeled hydro-sedimentary fluxes in mesoscale catchments?	169
5.4.2.1	Impact of simplifications of rainfall patterns	169
5.4.2.2	Impact of neglecting spatial rainfall variability	174
5.4.3	How does the location of rain cells with respect to the sources determine source contributions to sediment fluxes at the out- let?	177
5.5	Conclusions and perspectives	179

6	Conclusions and perspectives	182
6.1	Comparison of model results with source contributions estimated with sediment fingerprinting	182
6.2	Synthesis and future research directions	188
6.2.1	Where do suspended sediments passing the outlet of two mesoscale catchments originate and how do the contributions of different sources vary within and between flood events?	188
6.2.2	What are the reasons for the observed variability of source contributions between and within events?	190
6.2.3	Benefits of combining sediment fingerprinting and distributed numerical modeling	195
	Appendices	197
A	Calculation of specific sediment yield	198
B	Supplementary information for Chapter 3.1	200
B.1	Additional figures and tables	200
B.2	Comparison of the alternative tracer sets with conventional fingerprinting	203
C	Supplementary information for Chapter 4	206
C.1	Additional figures and tables	206
D	Supplementary information for Chapter 5	210
D.1	Precipitation data criticism (Chapter 5.2)	210
D.2	Additional figures	213
	Bibliography	218

List of Figures

1.1	Sediment yield in Europe (Vanmaercke et al., 2011)	18
1.2	Map of soil loss in Europe (Panagos et al., 2015b)	19
1.3	Types of soil erosion by water	21
1.4	Sediment transport in rivers	23
1.5	Factors controlling water and sediment connectivity (Keesstra et al., 2018).	25
1.6	Conceptual framework of connectivity by Fryirs (2013).	27
1.7	Scheme of sediment fingerprinting	30
1.8	Variability in $SSC - Q_t$ relation	36
1.9	Observed and simulated soil loss (Jetten et al., 1999)	37
1.10	Observed and simulated soil loss (Alewell et al., 2019)	38
1.11	Combining fingerprinting and erosion modeling (Palazón et al., 2016)	41
2.1	Location of the study sites	45
2.2	Geology and pedology of the Claduègne catchment	47
2.3	Land cover of the Claduègne catchment	48
2.4	Erosion zones in the Claduègne catchment	49
2.5	Claduègne river during low flow and during a flash flood	52
2.6	Initial soil moisture and event based runoff coefficients	53
2.7	Annual hydro-sedimentary dynamics (Claduègne)	54
2.8	Geology of the Galabre catchment	60
2.9	Land cover of the Galabre catchment	61
2.10	Monthly precipitation at Laval (Mathys, 2006)	63
2.11	Intra-annual hydro-sedimentary dynamics (Galabre)	64
2.12	Galabre river during low flow and during a flash flood	65
3.1	Sampling sites for sediment fingerprinting (Claduègne).	74
3.2	Comparison of different mixing models in sediment fingerprinting	84
3.3	Comparison of different tracer sets in sediment fingerprinting	86
3.4	Source contributions during a flood event in 2013	87
3.5	Calculated and measured X_{lf} of sediment samples	88

3.6	Comparison of spectral tracers with radionuclids	89
3.7	Mean source contributions in the Claduègne and Gazel	95
3.8	Mean source contributions in the Gazel catchment	97
3.9	Between event variability of sediment source contributions	98
3.10	Within event variability of source contributions	99
3.11	Sampling sites for sediment fingerprinting (Galabre)	103
3.12	Discrimination of sources with color and DRIFTS tracers	104
3.13	Comparison of results obtained with color and DRIFTS tracers	105
3.14	Between event variability of source contributions (Claduègne).	107
3.15	Between event variability of source contributions (Galabre).	108
3.16	Scheme of classification of events due to sediment flux variability	109
3.17	Within event variability of source contributions	110
3.18	Source contributions during different stages of the hydrograph	111
3.19	Distributed event Precipitation for two events	114
4.1	Distance of the sources to the outlet and the stream	118
4.2	Characteristic times of hydrographs and sedigraphs	127
4.3	Simulated hydrographs with different CDA thresholds	129
4.4	Sensitivity to characteristic times to changing model parameters	130
4.5	Simulated sedigraphs with different CDA thresholds	131
4.6	Modeled source contributions with varying CDA thresholds	132
4.7	Modeled hydrographs and sedigraphs with varying Manning's n	133
4.8	Modeled source contributions $n_{hillsl.} = 0.2$	134
4.9	Hydro-sedimentary fluxes: distance to the outlet (Galabre)	138
4.10	Hydro-sedimentary fluxes: distance to the stream (Galabre)	139
5.1	Comparison of radar and rain gauge data (Galabre)	150
5.2	Difference of rainfall in the north and south of the catchments	152
5.3	Rain events in the Claduègne catchment	154
5.4	Rain events in the Galabre catchment	156
5.5	Scheme of rainfall forcing: temporal variability	158
5.6	Scheme of rainfall forcing: spatial variability	160
5.7	Locations of artificial storms passing the catchments	164
5.8	Modeled source contributions with varying rain intensity and duration	165
5.9	Modeled hydro-sedimentary fluxes obtained with bimodal hyetographs	166
5.10	Hydro-sedimentary fluxes modeled with real and approximated hyetographs	168
5.11	Comparison of distributed radar data and elliptic approximation	171
5.12	Comparison of distributed radar data and approximated precipitation gradient	172

5.13	Comparison of distributed and uniform precipitation	175
5.14	Role of the location of the storm	178
6.1	General pattern of modeled source contribution	184
6.2	Modeled source contributions during different stages of the hydrograph	186
A.1	SSC - T relation in the two catchment	199
B.1	Effect of particle size on tracer values	202
B.2	Predicted vs. real source contributions to artificial mixtures	202
B.3	Source contributions predicted with radionuclids	205
C.1	Structural connectivity of potential sediment sources	207
C.2	Hydro-sedimentary fluxes: distance to the outlet (Claduègne)	209
C.3	Hydro-sedimentary fluxes: distance to the stream (Claduègne)	209
D.1	Cumulated radar precipitation data	211
D.2	Criticism of rain gauge data (Galabre)	212
D.3	Residuals of radar and rain gauge data (Claduègne)	213
D.4	Seasonality of agreement of radar and rain gauge data (Claduègne)	214
D.5	Seasonality of agreement of radar and rain gauge data (Galabre)	215
D.6	Surface weather maps	216

List of Tables

2.1	Specific yield of Mediterranean catchments	56
3.1	Sampling for sediment fingerprinting and tests of assumptions . . .	75
3.2	Estimates of error of the 3 mixing models and 2 tracer sets	90
4.1	Characteristics of the catchments and the erosion zones	119
4.2	Modeling scenarios	125
4.3	Scheme of responses of Q_l and Q_s to changes in Manning's n . . .	134
5.1	Scores of agreement of radar and rain gauge data	149
5.2	Modeling scenarios: temporal rain variability	159
5.3	Modeling scenarios: spatial rain variability and storm location . .	162
5.4	Characteristics of modeled hydrographs and sedigraphs: temporal variability	163
5.5	$\Delta_{t,crit}$ for independent events	167
5.6	Characteristics of modeled hydrographs and sedigraphs: spatial variability	170
6.1	Group classification in Fingerprinting and modeling	183
B.1	Selected tracer statistics	201
B.2	Selected radionuclid tracers	203
B.3	Error due to source heterogeneity (radionuclid tracers)	204
C.1	Characteristics of modeled hydrographs and sedigraphs	208

Chapter 1

Introduction

1.1 Motivation

Soil erosion and sediment transport are important processes that shape the critical zone, i.e. “the thin layer of the Earth’s terrestrial surface and near-surface environment that ranges from the top of the vegetation canopy to the bottom of the weathering zone” (Guo and Lin, 2016). These natural processes create diverse ecosystems such as braided river systems and river deltas that are a habitat to many species. However, as human activities in the Anthropocene are exerting profound influence on all compartments of the environment (Crutzen, 2006; Zalasiewicz et al., 2008), there is an increasing anthropogenic impact on these processes (Syvitski and Kettner, 2011; Poesen, 2018). Via land cover changes and climate change, erosion is accelerated in a way that it now exceeds rates of soil production by many in large parts of the world (Montgomery, 2007). On the other hand, sediments are retained in reservoirs behind dams and do not reach the ocean, leading to a disturbance of natural balances in floodplains and deltas (Syvitski and Kettner, 2011).

Excess erosion and sediment export from headwater catchments to river systems and the ocean can cause important on-site and off-site problems. The former concerns mainly soil loss and the associated loss of nutrients and fertile topsoil and thus a decrease of agricultural productivity (Pimentel et al., 1995; Amundson et al., 2015; Panagos et al., 2015b). Soil erosion by water is considered one of the main threats to soils in Europe (Panagos et al., 2015b). Off-site problems on the other hand, include disturbances in

the sediment balance of downstream water bodies which cause the loss of reservoir capacities due to siltation and thus necessitate regular and costly dredging activities or flushing (Camenen et al., 2013; Wisser et al., 2013; Kondolf et al., 2014). The estimated annual loss rate of reservoir capacity due to siltation is estimated to be in the order of 0.5% globally, but can be up to 5% for some reservoirs (Wisser et al., 2013; Kondolf et al., 2014). Furthermore, suspended sediments are a preferential transport vector for adsorbed nutrients and contaminants (Blake et al., 2003; Owens et al., 2005; Ciszewski and Grygar, 2016). Thus, they can contribute to eutrophication and pollution of downstream water bodies and to toxic impacts on fish and other aquatic organisms and to human health problems after consumption (Owens et al., 2005; Bilotta and Brazier, 2008; Sánchez-Chardi et al., 2009; Mueller et al., 2020). In Europe, these issues are increasingly recognized and addressed in the Water Framework Directive (Brils, 2008). Further off-site impacts of soil erosion include muddy floodings and extra costs for drinking water treatment due to increased turbidity (Boardman et al., 2019).

These issues are expected to become even more pressing in the future. The IPCC reported, that “it was likely that annual heavy precipitation events had disproportionately increased compared to mean changes between 1951 and 2003 over many mid-latitude regions, even where there had been a reduction in annual total precipitation” (Hartmann et al., 2013). This intensified hydrological regime is expected to lead to an increase in soil erosion (Nearing et al., 2005). This is attributed to both the increase of total precipitation and to higher precipitation intensity. Simulation studies reviewed by Nearing et al. (2004) suggest that per 1% change of annual precipitation, soil erosion will change by 1.7%. Furthermore, expected land cover changes such as the increase of cropland due to an increasing demand on agricultural production have a high potential to lead to more soil erosion (Yang et al., 2003; Nearing et al., 2005).

Mediterranean and mountainous regions are especially prone to soil erosion (Panagos et al., 2015b; Vanmaercke et al., 2011, 2012; Fig. 1.1 and 1.2). This is due to high rainfall erosivity and steep slopes. Further, in some regions a low vegetative cover exacerbates the erosion risk (Panagos et al., 2015b). The Mediterranean and mountainous regions are prone to high-intensity rain events that can lead to flash floods and associated high sediment exports. These events that are short in time contribute nonetheless

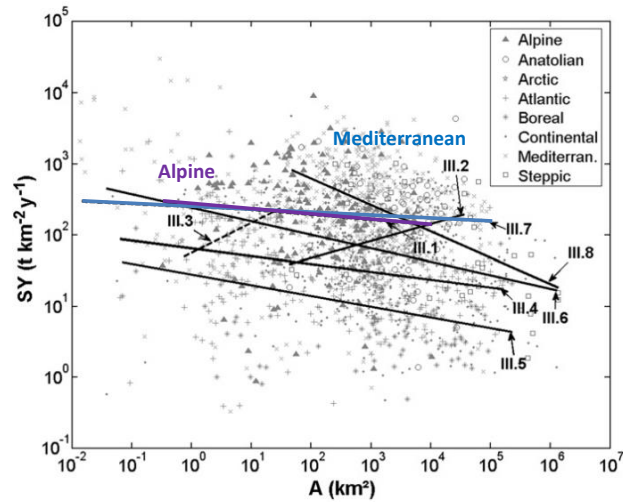


Figure 1.1: Sediment yield (SY) in different geographic regions in Europe plotted against catchment / plot area (A). The regression lines for the Mediterranean and the Alpine zones are highlighted. From [Vanmaercke et al. \(2011\)](#).

importantly to sediment loads in such areas. For example, for four alpine catchments in France, [Mano et al. \(2009\)](#) found that 38 – 84 % of sediment load was discharged in only 2 % of the time. [González-Hidalgo et al. \(2007\)](#) compiled more than 60 years of time series of daily soil erosion of 16 sites in western Mediterranean areas and found that the three most erosive events always contribute to more than 50 % of annual soil erosion. Soil erosion in the Mediterranean mountainous context is also highly variable in space. For example, the Durance river contributes only 4 % of the total discharge of the Rhône, but to 24 % of its suspended sediment flux while the Saône contributes to 25 % of discharge but only to 5 % of suspended sediment flux ([Poulier et al., 2019](#)). Such variability is often due to “hotspots” of soil erosion such as badlands that can be found in mountainous areas in the Mediterranean climate ([Gallart et al., 2002](#); [Mathys et al., 2005](#); [Francke et al., 2008b](#); [Nord et al., 2017](#)). These highly erodible zones with no or very sparse vegetative cover and clear signs of gully erosion are usually small in surface but contribute a high proportion of the sediment loads in downstream water bodies. Another important specificity of alpine and Mediterranean regions is that the relationship between sediment yield and area are not as significant as in other environments (Fig. 1.1, [Vanmaercke et al., 2011](#)). This smaller dependency to scale indicates a wide range of processes and factors. For this

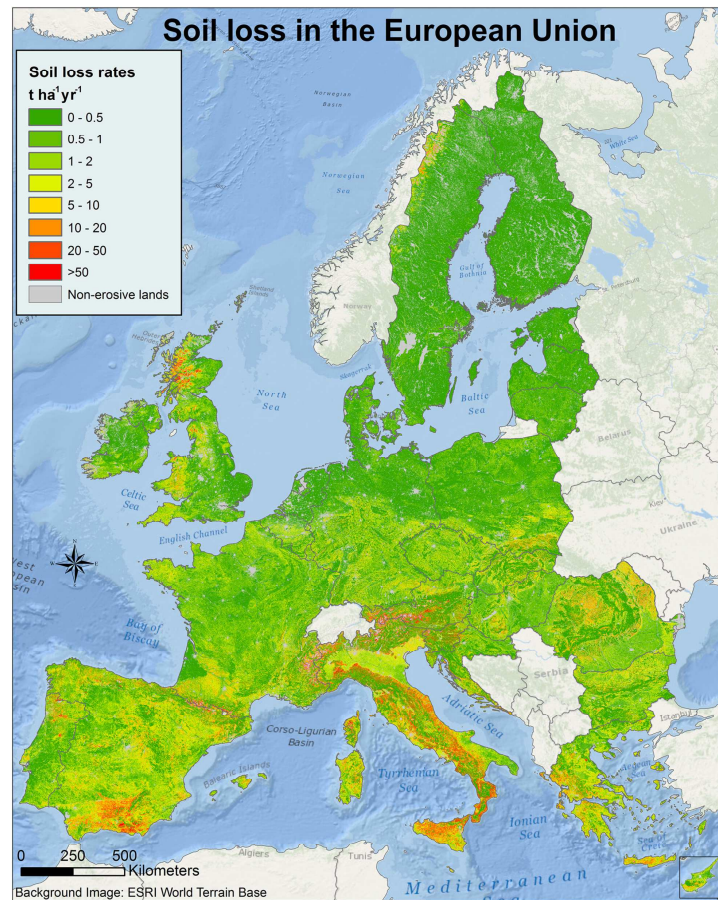


Figure 1.2: Map of modeled soil loss in Europe. From [Panagos et al. \(2015b\)](#)

reason simple empirical regression equations including the drainage area as an explanatory variable might not be suitable in these environments. In the Mediterranean region the precipitation regime was observed to become more extreme in recent years and this trend is predicted to continue in a changing climate ([Alpert et al., 2002](#); [Tramblay et al., 2012](#); [Blanchet et al., 2018](#)). Also mountainous regions are highly sensitive to climate change and a raising snowline, and intensified precipitation in zones with sparse vegetation cover are assumed to lead to increasing erosion ([Alewell et al., 2008](#)). Thus, questions arise on the evolution of soil erosion and sediment yields in these vulnerable areas.

The issues mentioned above show that sediment management is a crucial part of a sustainable river management, to protect soil and water resources and to attend a good ecological status of water bodies as is set as a goal of the European Water Framework Directive. Erosion control measures or steps to interrupt the pathways of sediments from source to sink can help to prevent on- and off-site impacts of erosion and sediment loads in water bodies, but to be effective they require knowledge on these processes. Thus, the study of soil erosion and sediment transport are important to deal with these issues. Important questions that have to be answered include the following ones:

- Where are the main erosion zones?
- What are the main pathways of sediments through the catchment?
- How long does it takes them to travel from the sources to the outlet of the catchment?
- What processes lead to erosion and sediment transport and where do they occur?
- What can be done to hinder these processes?
- How can soil erosion and sediment transport be measured / predicted?

To address these questions, scientists rely on observations and modeling. However, both methodologies are prone to many errors and most answers to the above mentioned questions remain very uncertain ([Jetten et al., 1999](#); [Merritt et al., 2003](#); [Wainwright et al., 2008](#); [de Vente et al., 2013](#); [Alewell et al., 2019](#)). Thus, innovative observation strategies are needed and novel model applications as well as methodologies to improve model structure and performance remain an active research topic.

1.2 Scientific context

1.2.1 Soil erosion and sediment transport

Erosion is the process of detachment of soil particles and physically or chemically weathered rock fragments from their original assemblage by natural agents such as water, wind and glaciers ([Grotzinger et al., 2007](#); [Osman, 2014](#)). The eroded particles or sediments are transported downstream by wind, water, glaciers and gravity and get deposited further away. The magnitude of erosion and the travel distances of sediments are highly scale-

dependent. As an example at short time scales, particles get redistributed within the same field, while at geological time scales eroded particles get transported to the oceans where they are deposited in layers and finally transformed by pressure, temperature and chemical reactions to sedimentary rocks (Grotzinger et al., 2007).

The main natural agents of soil erosion are water and wind (Osman, 2014) but there are also anthropogenic forms of erosion such as tillage erosion on agricultural surfaces and erosion due to constructions, land leveling and soil quarrying (Poesen, 2018). While wind erosion is mainly an issue in arid and semiarid regions with sparse vegetation and low rainfall, soil erosion by water is the most crucial reason of soil degradation in many regions in the temperate, Mediterranean and tropical climate zones (Osman, 2014; Amundson et al., 2015). Thus, here we focus on soil erosion by water.

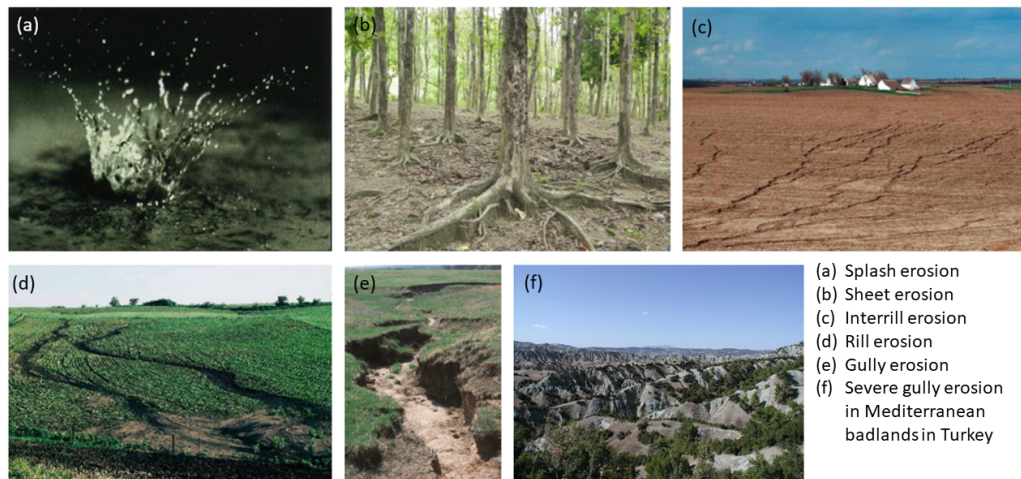


Figure 1.3: Different types of soil erosion by water. Pictures (a) - (e) are taken from Osman (2014), (f) is taken from <https://www.wur.nl/en/show/Temperate-Mediterranean-Badlands-A-pre-Holocene-or-Anthropocene-phenomenon.htm>.

There are different types of water erosion. **Splash erosion** can be called the first step of soil erosion by water. It refers to the detachment of soil particles due to the impact of rain drops on the soil surface (Fernández-Raga et al., 2017; Fig 1.3a). It acts by transporting particles a short distance away from the location of rainfall impact and by destroying aggregates that are easier to entrain by flowing water afterwards. **Sheet erosion** is the removal

of a thin, more or less uniform layer of soil surface by splash erosion and shallow surface flow that occurs on an entire hillslope (Osman, 2014). Thus, it removes the fertile topsoil that is rich in nutrients and organic matter. Figure 1.3b shows tree roots that were exposed after sheet erosion. Splash erosion and sheet erosion are diffuse forms of erosion that do not occur in concentrated channels (Oakes et al., 2012). However, most slopes are not uniform so water concentrates in small channels. Thus, the resulting erosion is called **interrill erosion** (Fig. 1.3c). It is often referred to as the diffuse form of erosion that is opposed to **rill erosion** occurring when overland flow on hillslopes entrains sediments that are transported by the kinetic energy of the flowing water (Fig. 1.3d). This form of erosion is concentrated in linear features. Once linear features become deeper, this type of erosion is called **gully erosion** (Fig. 1.3e). Gullies develop when a lot of water accumulates in a channel with high slopes. Thus, water velocity and kinetic energy are high which leads to high rates of entrainment and high transport capacities (Osman, 2014). Gully erosion usually involves vertical incision, lateral erosion and backward or retrograde erosion. Gullies can become permanent features which cannot be remediated by tilling practices. Gullying processes can be caused by inappropriate cultivation or irrigation, overgrazing or road building. In their most extreme form, gullies can form **badlands**, i.e. highly erodible areas with missing or sparse vegetation that are characterized by steep slopes, lack of soil cover and clear v-shaped gully morphology (Fig. 1.3f). They cannot be cultivated and are often a main source of sediment, thus they are responsible for many off-site effects such as reservoir siltation (Valentin et al., 2005). A further highly effective and highly concentrated form of erosion are **mass movements** of consolidated and unconsolidated movement of rock and soil such as landslides, landslips, debris flow or mud flow. They are caused by unstable geological conditions, intense rainfalls that saturate soil, or earthquakes. Another form of soil erosion by water is **riverbank** or **streambank erosion** due to the removal of bank material by water flowing in river and collapse of unstable river banks (Osman, 2014).

Eroded particles are transported downhill by overland flow until they get deposited or reach a water body. The time scale of the sediment transport to a water body, usually a stream or a river, and the rate of sediments that reach a river or a downstream river section depend on the connectivity of the watershed and the river network (Chapter 1.2.2).

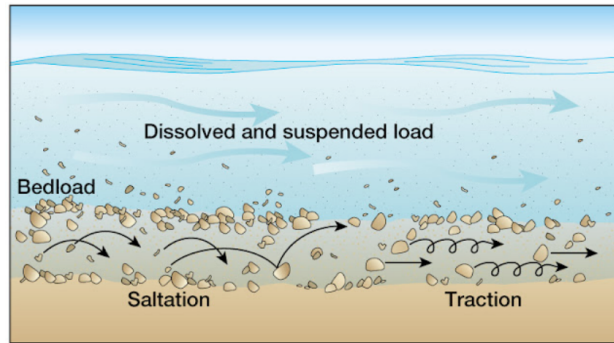


Figure 1.4: Sediment transport in rivers as bedload and suspended load. Source: <http://www.geologyin.com/2016/01/how-do-streams-transport-and-deposit.html>.

Turbulent flow in rivers, can carry sediments that are transported in two modes. While the coarse particles (usually boulder to sand size classes) are transported at the bottom of the riverbed via saltation, rolling or traction, the finer particles (fine sand to clay size) are transported within the water column when they are kept in suspension by turbulence (Grotzinger et al., 2007). In most environments suspended load constitutes the majority of total sediment flux, even in gravel bed rivers where bedload fluxes are significant (Misset, 2019). Moreover, the smaller particles are the most important ones for many of the off-site effects of soil erosion such as reservoir siltation and the detrimental transport of nutrient and contaminants. Thus, we concentrate on suspended sediment transport even if bedload transport as well as the interaction between the two transport modes deserve attention.

Whether or not a suspended sediment particle can be transported or is deposited in the river depends on the ratio between the upward and downward directed forces that act on the particle. This can be quantified with the Rouse number Z_R (Garcia, 2006)

$$Z_R = \frac{v_s}{\kappa u_*}$$

where v_s is the settling velocity that depends on particle size, shape and density, κ is the Von Kármán constant ($\kappa = 0.4$) and u_* is the shear velocity at the bottom of the riverbed.

How the suspended sediment load interacts with the river bed is an active

research topic (Misset, 2019). Early studies suggested that there is a part of suspended load that passes river sections without interaction with the bed. This fraction was called washload by Einstein et al. (1940) who observed that fine particles are not present in the river bed. Thus, they assumed that they originate from upstream sources and “get washed” through the system without deposition and resuspension from the river bed. Several authors have tried to define the washload fraction of suspended sediment. Besides the presence in the river bed, particle size was used to try to define this fraction. However, as Hill et al. (2017) point out, this is difficult as the critical particle size depend a lot on local flow condition and vary between $400\ \mu\text{m}$ and $3\ \mu\text{m}$. Thus, Hill et al. (2017) suggest that washload should be defined based on a small particle size relative to bed material size, a Rouse number smaller than 0.8, and a low rate of fine sediment supply relative to transport capacity.

The fraction of suspended sediment that does interact with the riverbed was called bed material load (Einstein et al., 1940; Hill et al., 2017). Several recent studies have shown that there is an interaction even of very fine particles with the riverbed, e.g. via infiltration and capture of fines into the gravel matrix (Misset, 2019). Thus, the river bed can be a sink or source of fine sediment, depending on the flow conditions and the mobility of gravels. This is the case in specific geomorphological configurations, i.e. in well developed alluvial rivers with wide active river beds, while it was often not observed in small to mesoscale watersheds (Misset et al., 2019b).

1.2.2 Sediment connectivity

The concept of sediment connectivity has been increasingly used in recent years to address the spatial and temporal variability in sediment fluxes (Wainwright et al., 2011; Bracken et al., 2015; Parsons et al., 2015). The efficiency of catchments to deliver sediments to the outlet is a longstanding research question. The fact that in most larger catchments only a fraction of the sediment eroded on the hillslopes will arrive at the outlet in the short term was called the sediment delivery problem by Walling (1983) but it dates back to the 1950s (Parsons et al., 2006). Consequently, much use has been made of the sediment delivery ratio, i.e. a dimensionless number that gives the ratio of gross eroded sediment and sediment yield at the outlet. However, this simple black box concept has several flaws and has to be replaced by a new concept that can help to understand sediment pathways from source

to sink at different spatial and temporal scales (Parsons et al., 2006; Fryirs, 2013). This is the aim of recent literature on sediment connectivity.

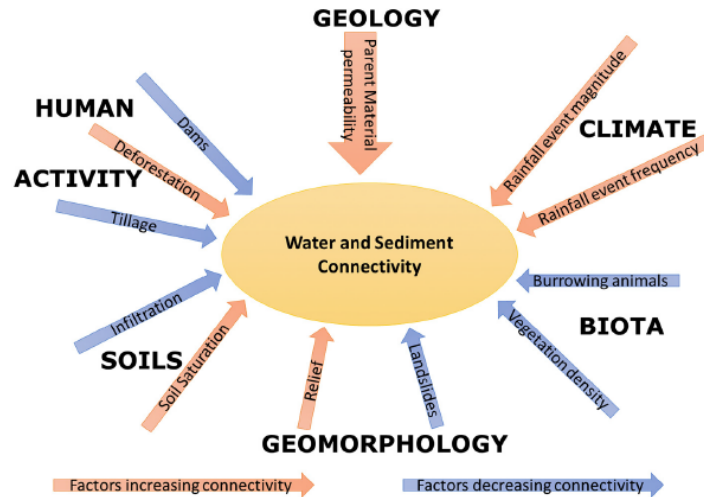


Figure 1.5: Schematic representation of factors that control water and sediment connectivity. Source: Keesstra et al. (2018).

Sediment connectivity is defined as the potential of a sediment particle to be transported from the source to the sink via transport vectors such as water, wind and gravity (Borselli et al., 2014; Bracken et al., 2015; Heckmann et al., 2018). Many factors such as climate, geology, pedology and human activities influence water and sediment connectivity (Keesstra et al., 2018, Fig. 1.5). However, the term remains ambiguous and different ideas of connectivity exist (Wainwright et al., 2011). Fryirs (2013) developed a conceptual framework of sediment (dis-)connectivity where the catchment is represented as a system of linkages and blockages. Linkages can be longitudinal, lateral or vertical. Longitudinal linkages include the upstream-downstream linkage in the river network or the tributary-trunk linkage. They influence the transport along the river network, the transport from bar to bar and the connectivity of tributaries. These linkages can be disrupted by barriers such as bedrock steps, valley constrictions, sediment slugs, dams or woody debris. Lateral linkages define the connectivity between the river network and the landscape. Thus, they include the slope-channel linkage and the floodplain-channel linkage. Buffers are features that interrupt lateral linkages. They are often large sediment sinks outside of the channel network, e.g. alluvial

fans, floodplains, piedmont zones or terraces. They prevent sediments from entering the river network and sediments often have long residence times of hundreds to thousands of years. Vertical linkages represent the surface-subsurface interaction and are controlled by the bed material and the characteristics of the soil or the regolith at the hillslopes surface. Blankets are features that disrupt vertical linkages. Examples given are sand sheets, bed armour and fine material in the interstices of gravel bars.

The concept explained above, depends mainly on the structure of the catchment, of the distribution of sources in the catchment and on how landscape units are linked to each other. This is what [Wainwright et al. \(2011\)](#) refer to as structural connectivity. What is defined as landscape units depends on the scale and on study objectives. Structural connectivity can be measured using indices of contiguity (e.g. [Borselli et al., 2008](#); [Cavalli et al., 2013](#); [Heckmann et al., 2018](#)). It usually does not consider interactions, directionality and feedbacks ([Wainwright et al., 2011](#)). However, connectivity also depends on the processes that link landscape units to one another and their hydro-meteorological forcing. This is referred to as functional ([Wainwright et al., 2011](#)) or process-based connectivity ([Bracken et al., 2013](#)). Functional connectivity accounts for the way in which interactions and feedbacks between the landscape and its processes affect hydrologic, geomorphic and ecologic processes. Its measurement or quantification is more difficult and need distributed measurements and modeling ([Wainwright et al., 2011](#)). Spatial and temporal dynamics have to be accounted for to describe system responses. As the functional connectivity of a system depends on the intensity of the processes that link landscape units, it depends on the magnitude of an event. For example, landscape units can be disrupted during frequent, low-magnitude events but can become connected during extreme, high-magnitude events ([Fryirs, 2013](#), Fig. 1.6). One of the main drivers of functional connectivity is the spatio-temporal variability of rainfall forcing. The intensity and duration of rain events determine the magnitude of the event and thus its hydro-sedimentary response, but also the spatial variability of rainfall can be an important factor. The results of several studies show that hydrological responses of catchments to highly variable rain events differ from the the ones during spatially homogeneous rain events ([Smith et al., 2004](#); [Seo et al., 2012](#); [Lobligeois et al., 2014](#); [Emmanuel et al., 2017](#); [Anggraheni et al., 2018](#)). Few studies addressed the impact of rainfall variability on sediment fluxes, but [Shen et al. \(2012\)](#) found out that sediment fluxes

were more sensitive to rainfall variability than liquid fluxes. [Adams et al. \(2012\)](#) observed that spatial variability led to increased erosion compared to homogeneous precipitation of the same intensity and also constitute that sensitivity of hydro-sedimentary fluxes to spatial rain variability depends on the size of the catchments.

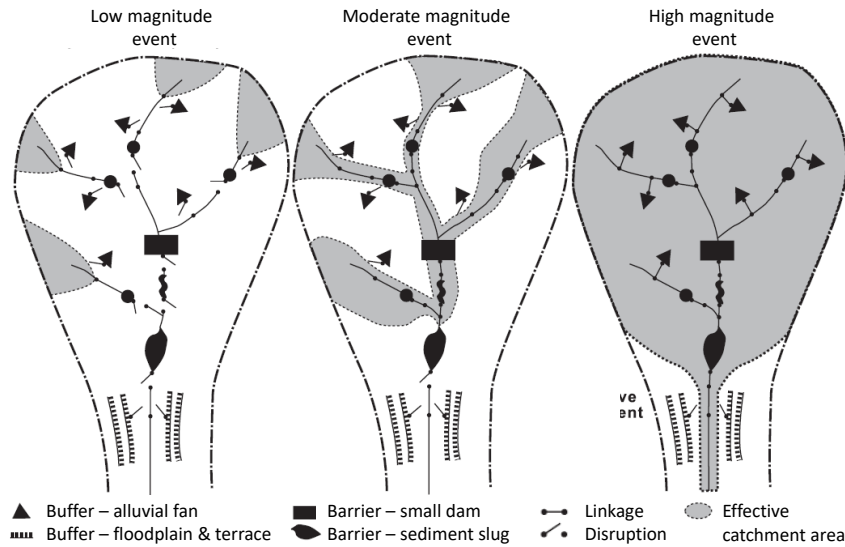


Figure 1.6: A conceptual framework of (dis)connectivity in a catchment as it is constituted by longitudinal and lateral linkages and the features that disrupt them: barriers and buffers. Whether or not a landscape feature disrupts a linkage depends on the magnitude of an event. Adapted from [Fryirs \(2013\)](#).

Connectivity indices aim to move from qualitative concepts such as the one proposed by [Fryirs \(2013\)](#) to (semi-)quantitative methods to describe connectivity ([Heckmann et al., 2018](#)). Today many indices of connectivity exist; for a review see [Heckmann et al. \(2018\)](#). Most indices are raster-based and can be calculated with GIS software, but there are also other approaches that are based on the calculation of effective catchment area or network based indices ([Heckmann et al., 2018](#)). The most widely used connectivity indicator is the one proposed by [Borselli et al. \(2008\)](#). It is a raster based indicator that uses a DEM and a land cover data set to calculate a dimensionless indicator of connectivity (IC) for every raster cell k . It consists of an upstream component (D_{up}) and a downstream component (D_{dn}) and is calculated as

$$IC_k = \log_{10}\left(\frac{D_{up,k}}{D_{dn,k}}\right) = \log_{10}\left(\frac{\overline{W}_k \overline{S}_k \sqrt{A}}{\sum_i \frac{d_i}{W_i S_i}}\right) \quad (1.1)$$

where A is the surface of the contributing area upslope of the cell k . \overline{W}_k is the average of a weighing factor in the contributing area and \overline{S}_k is the average of the slope in the contributing area. The downslope component is calculated for all cells along the downslope path from cell k to the sink and summed up. For cell i along the downslope path, d_i is distance from cell k to cell i along the flowline. W_i and S_i are the weighing factor and slope at cell i . The index is weighed with land cover, so the weighing factor W can be derived from land cover data and tables such as the one given in the original publication (Borselli et al., 2008). Cavalli et al. (2013) propose to weigh the IC not with land cover but with a roughness factor that is derived from a high-resolution DEM.

Several authors used concepts of connectivity to model water and sediment fluxes (e.g. Medeiros et al., 2010; Le Roux et al., 2013; Masselink et al., 2016; Cossart et al., 2018). For example, Medeiros et al. (2010) showed how spatially and temporally variable patterns of sediment connectivity help to explain non-linear catchment responses of sediment yield at the outlet. In this study, sediment connectivity was obtained from the pattern of deposition, using the deposition rate as an indicator of (dis-)connectivity. Masselink et al. (2016) combined modeling with indicators of vegetation and antecedent precipitation that were used to parameterize connectivity. Le Roux et al. (2013) found that farm dams and wetlands considerably influenced water and sediment connectivity represented in the Soil Water Assessment Tool (SWAT, Arnold et al., 1998) and consequently have a high impact on modeled sediment fluxes. López-Vicente et al. (2015) combined a distributed model with the IC by Borselli et al. (2008) to identify erosion hotspots that are well connected to the river network and concluded that the two tools are complementary because the combination yielded better results than each method separately. It further helped to interpret the obtained maps.

These studies showed that the concept of connectivity offers a high potential to interpret observations or modeling results and spatio-temporal variability of sediment fluxes. However, the examples given above also showed that the concept remains ambiguous and that many different definitions of

connectivity exists. Thus, the question how the concept of connectivity can be applied in measurement schemes and modeling studies is still an active research question (Keesstra et al., 2018). Determining the main sources of sediment in the catchment, quantifying their contribution to total sediment fluxes and assessing the spatio-temporal dynamics of these source contributions can help to understand which sediments arrive at the outlet and which are characteristic time scales of their arrival. Such information can be obtained with sediment fingerprinting. Furthermore, models of erosion and sediment transport can be used to test hypotheses of how sediment connectivity defines hydro-sedimentary fluxes at the outlet and thus contribute to a better understanding of these fluxes and the underlying processes in the catchment.

1.2.3 Sediment fingerprinting

Since the 1970s researchers used sediment fingerprinting to identify sources of fine sediment transported in rivers and to quantify the contribution of different sources to total loads (Davis and Fox, 2009; Smith et al., 2015). Knowledge of sediment provenance in catchments that are prone to erosion is therefore important for two reasons. Firstly, proposing best management practices requires applying the right erosion control measures to the right target areas in order to reduce soil loss within catchments or to ensure good ecological status of water bodies as demanded by the European Water Framework Directive (Brils, 2008; de Deckere et al., 2011; Perks et al., 2017). Secondly, improving our understanding of processes responsible for sediment transfer within the critical zone requires the capacity to analyze suspended sediment yields with other descriptors than only the hydrograph and suspended sediment concentrations at a single point.

The method usually involves three steps (Fig. 1.7). The first step consists in the identification and localization of erosion zones that are potential sediment sources and field sample collection. Different methods are used for the collection of source samples and fluvial sediment samples (Haddadchi et al., 2013). Sediment sources are often classified by land-use, geologic parent material, or by erosion process (e.g. streambank erosion, gully erosion or sheet and rill erosion, Davis and Fox, 2009). The second step is the laboratory analysis of the source and sediment samples. Several physico-chemical properties of sediment samples and their potential sources are used as tracers or

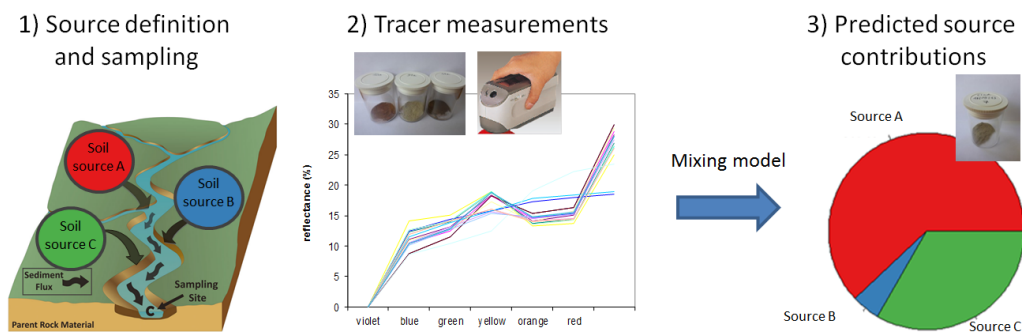


Figure 1.7: Scheme of a typical sediment fingerprinting methodology. The left figure is adapted from [Lacey et al. \(2019\)](#).

fingerprints, including radionuclides (e.g. [Motha et al., 2003](#); [Evrard et al., 2011, 2013](#); [Ben Slimane et al., 2013](#); [Palazón et al., 2016](#); [Huon et al., 2017](#); [Palazón and Navas, 2017](#); [Pulley et al., 2017b](#)), organic or inorganic geochemistry (e.g. [Collins et al., 1997, 2010](#); [Douglas et al., 2009](#); [Evrard et al., 2011, 2013](#); [Koiter et al., 2013a](#); [Cooper et al., 2014](#); [Haddadchi et al., 2014](#); [Lacey and Olley, 2015](#); [Du and Walling, 2017](#); [Huon et al., 2017](#)), magnetic properties (e.g. [Walling et al., 1979](#); [Dearing et al., 1981, 1986, 2001](#); [Maher, 1986](#); [Yu and Oldfield, 1993](#)), particle color (e.g. [Martínez-Carreras et al., 2010c,a](#); [Legout et al., 2013](#); [Brosinsky et al., 2014a,b](#)) or composite fingerprints that comprise several of these tracers. There are some important requirements to the tracers that are used. First of all, they have to be conservative, i.e. the measured properties must not change during the processes of erosion, transport and possible phases of deposition and resuspension. Secondly, they have to be able to discriminate between the different source classes. Several statistical tests are used to estimate the discriminative power of possible tracers. Based on such analyses, all measured tracers or a subset is selected. The third step involves the application of a mixing model to quantify the contribution of each source class to the sediment samples. Traditionally, mixing models are based on chemical mass balances for each tracer, but recently new models based on Bayesian statistics are becoming more widely used ([Douglas et al., 2009](#); [Koiter et al., 2013b](#); [Cooper et al., 2014](#); [Nosrati et al., 2014, 2018](#); [Barthod et al., 2015](#); [Garzon-Garcia et al., 2016](#); [Ferreira et al., 2017](#); [Boudreault et al., 2019](#)).

In recent years, awareness of the limitations, challenges and uncertainty

is increasing and much research has focused on these issues (Smith et al., 2015). Pulley et al. (2017a,b) addressed the uncertainty that is inherent in the source group classification. They criticized that “the classification of source groups is perhaps the least thoroughly explored stage of the sediment fingerprinting approach, but in many ways is the most important” (Pulley et al., 2017a). Uncertainties can be caused by the a-priori classification of sources where sources may be missed, by a high within-class variability that leads to a low signal-to-noise ratio in the tracers and by the fact that the fingerprint of a tracer is determined by a multitude of reasons such as land use, geology and human impacts (Pulley et al., 2017a). Alternatives can be source classification based on statistical methods such as cluster analysis or the consideration of individual samples instead of source classification but these methods are rarely used.

Another important challenge is the effect of particle size in sediment fingerprinting. Laceby et al. (2017) stated that the sorting effect of particles by size during erosion, sediment transport, and deposition is a key challenge of the requirements that tracers have to be conservative. This is often not the case because sediment samples are often finer than the source sample due to the particle size selectivity during erosion and transport processes and because tracers vary in the different particle size ranges (Legout et al., 2013; Pulley and Rowntree, 2016; Laceby et al., 2017). This problem is traditionally addressed by sieving source and sediment samples to the finest fraction (usually $< 10 \mu m$ or $< 63 \mu m$) or by applying particle size correction factors (Collins et al., 2010). However, both practices are increasingly challenged and new approaches such as edge-of-field sampling or tributary sampling (i.e. collecting already eroded particles with flumes on fields or sediments in different tributaries as source samples for tracing the origins of sediments collected downstream) were proposed by Laceby et al. (2017) to obtain source samples but both approaches are rarely applied so far. Another possible challenge to the assumption of conservative behavior of tracers are possible biogeochemical alterations of the tracer properties during transport or temporary storage of the sediments in the riverbed (Legout et al., 2013). This issue is rarely addressed in sediment fingerprinting studies so far.

A further source of uncertainty is inherent in the selection of tracers and mixing models. As outlined by Martínez-Carreras et al. (2010c); Evrard et al. (2013); Pulley et al. (2015); Zhang and Liu (2016); Nosrati et al. (2018), dif-

ferent results in the sediment source proportions can also be obtained when different tracer (sub-)sets or different composite fingerprints are used. Similar contradictory results can also be obtained when different mixing models are used (Haddadchi et al., 2013; Cooper et al., 2014; Laceby and Olley, 2015; Nosrati et al., 2018). These latter elements suggest a high sensitivity of the fingerprinting approaches to such methodological choices.

Besides addressing the challenges and limitations of the sediment fingerprinting approach, current research also focuses on developing and testing novel fingerprints. Compound specific stable isotopes can be highly discriminative between different land cover classes, because they use plant-specific biotracers such as fatty acids and alkanes as fingerprints (Reiffarth et al., 2016; Upadhayay et al., 2017). Environmental DNA has the potential to provide even more specific information of different plant species (Evrard et al., 2019). Moreover, recent studies evaluated the potential of different low-cost tracers for use in sediment fingerprinting. As the measurement of frequently used tracer sets such as radionuclides and element geochemistry can be expensive and time consuming, low-cost tracers offer the potential of significantly reducing analytic costs. In this way more samples can be analyzed and results can be obtained at higher temporal and spatial resolution, offering new research perspectives. Martínez-Carreras et al. (2010c,a), Legout et al. (2013) and Brosinsky et al. (2014a,b) obtained promising results with color tracers that are cheap and fast to measure. Pulley and Rowntree (2016) even used an office color scanner and concluded that color tracers performed comparably to mineral magnetic tracers. Another set of low-cost tracers can be obtained with X-ray fluorescence (XRF). In this way, elemental geochemistry can be measured in a cheaper way than with traditional measurement techniques such as mass-spectroscopy. The sediment fingerprinting studies by Motha et al. (2003), Douglas et al. (2009), Cooper et al. (2014), Laceby and Olley (2015) and Ferreira et al. (2017) successfully applied XRF tracers.

Recent studies that estimated source contributions of samples taken at high temporal resolutions with sediment fingerprinting found that sediment fluxes can be highly variable in time. Several studies showed that the contributions of potential sediment sources can differ considerably from one flood event to another and at different times of sampling within a single flood event (e.g. Evrard et al., 2011; Navratil et al., 2012c; Poulenard et al., 2012;

Legout et al., 2013; Brosinsky et al., 2014b; Gourdin et al., 2014; Cooper et al., 2015; Gellis and Gorman Sanisaca, 2018; Vercruyssen and Grabowski, 2019). At longer time scales (typically inter-annual), other authors applied the sediment fingerprinting methodology on samples obtained from long time records in sediment cores (Belmont et al., 2011; Navratil et al., 2012a; Miller et al., 2013; Chen et al., 2016). In these studies inter-annual variability was attributed to climate variability, human activities, different flood magnitudes, mass movements and bank collapse (Arnaud et al., 2012; Navratil et al., 2012a; Bajard et al., 2016) or to changes in sediment connectivity due to the construction of a drainage ditch (Miller et al., 2013). At the between event scale, possible reasons for variability of suspended sediment fluxes include seasonal variations of the climatic drivers of soil erosion and sediment transport, variability of the spatial distribution of rainfall, land cover changes and human interventions (Sun et al., 2016; Vercruyssen et al., 2017). At the within event scale, the distribution of sources in the catchment and thus different travel times of sediment sources to the outlet as well as rainfall dynamics are assumed to be the dominant reason for observed suspended sediment flux variability (Legout et al., 2013), but to our knowledge, no studies have systematically tested these hypotheses yet.

Here, there is a high potential for the combination of sediment fingerprinting studies with distributed physically-based modeling and the analyses of connectivity of the sources in the catchment to the river network. Sediment connectivity determines travel times of eroded particles, thus it governs arrival times of different classes of sediments at the outlet. Assessing patterns of the dynamics of source contributions together with connectivity of the sources can help to understand these fluxes. On the other hand, numerical models can be used to test hypotheses for the reasons of observed source variability and to test scenarios that cannot be done with observed data alone.

1.2.4 Modeling soil erosion and sediment transport

Modeling soil erosion and suspended sediment fluxes in rivers is important for catchment management, decision making, erosion control measures and for understanding soil erosion and suspended sediment transfer (Jetten et al., 1999; Merritt et al., 2003). It is a valuable tool that helps understanding and predicting the impact of agricultural practices and land use changes on sediment dynamics as well as reservoir sedimentation (Wainwright et al., 2008).

When field measurements are too costly and time consuming to conduct in large regions over long time spans, models can be used for long term erosion simulation in many conditions (Pandey et al., 2016). Information on soil erosion rates at regional and global scale can only be provided by models (de Vente et al., 2013). Such information is needed to deal with the increasing problems of soil erosion, its considerable uncertainty and the fact that it cannot be evaluated with observations has to be kept in mind nonetheless.

Soil erosion modeling has its origins in the 1920s when erosion problems in the mid-western dust bowl of the USA were increasingly recognized (Jetten and Favis-Mortlock, 2006). This resulted in the creation of a network of soil erosion experiment stations and the development of empirical models specific to this region (Jetten and Favis-Mortlock, 2006). In the 1970s this led to the development of the Universal Soil Loss Equation (USLE; Wischmeier and Smith, 1978) which is an empirical formula that aims to capture measurable parameters linked to soil erosion based on data of thousands of field plots and small watersheds (Alewell et al., 2019). The equation (or variations of it) is still widely used and it influences many of the most widely used soil erosion models such as the Soil and Water Assessment Tool (SWAT, Arnold et al., 1998), the Agricultural Non-Point Source Pollution Model (AGNPS, Cronshey and Theurer, 1998), and the Water and Tillage Erosion and Sediment Model (Watem/Sedem, Van Rompaey et al., 2001) (Jetten and Favis-Mortlock, 2006; Alewell et al., 2019).

In the 1980s and 90s awareness of the limitations of the USLE grew and efforts were made to develop alternatives. More physically-based models such as the Water Erosion Prediction Model (WEPP, Laflen et al., 1997), the European Soil Erosion Model (EUROSEM, Morgan et al., 1998) and the Pan-European Soil Erosion Risk Assessment (PESERA, Kirkby et al., 2008) were developed (Jetten and Favis-Mortlock, 2006; Pandey et al., 2016; Alewell et al., 2019). Physically-based models offer several advantages over purely empirical models. They are often spatially distributed and can thus be used to identify critical erosion zones (Pandey et al., 2016). Further, they can be used for process understanding, while empirical models are rather seen as a black-box. In theory, they can be used everywhere as the equations are assumed to be valid universally and independent of the study site. However, it has to be noted that to date, physically based models do not perform better than empirical models (Alewell et al., 2019; Jetten et al., 1999; see below).

Besides the differentiation based on model family (empirical models vs. physically-based models), models vary in their spatial scale. Some models are suited to the regional scale (e.g. PESERA) and USLE-based models are applied at large scale such as for continental Europe, China and Australia and even at global scale (Alewell et al., 2019). Most process-based models on the other hand are limited to the hillslope or the small catchment scale (Pandey et al., 2016). The development of process-based erosion models for large-scale applications remains a key area for future research (Alewell et al., 2019).

Concerning sediment transport, physically-based approaches as well as empirical, data driven ones are commonly used. The physically based equations usually estimate suspended and bedload based on the transport capacity of the flow. Hydraulic parameters (water velocity and depth, shear stress and stream power), properties of the sediment (particle size and density) as well as bed geometry are used in these equations (e.g. Engelund and Hansen, 1967; van Rijn, 1984; Pandey et al., 2016). Deposition can be calculated as a function of settling velocity and the profile of the sediment concentration in the water column (e.g. Cea et al., 2015). It has to be kept in mind that many models focus on suspended sediment transport and neglect bedload.

Empirical approaches usually try to relate sediment loads in rivers to measurable hydro-meteorological variables of rainfall and runoff (e.g. Francke et al., 2014; Buendia et al., 2016b; Tuset et al., 2016). One of the most frequently applied methods is the use of sediment rating curves, that relate suspended sediment concentrations (SSC) to discharge (Q_t) in the form

$$SSC = aQ_t^b$$

where a and b are parameters of the regression equation (Walling, 1977; Crawford, 1991; Asselman, 2000). The two parameters are calibrated based on instantaneous sediment samples. In this way, continuous estimates for sediment concentrations can be obtained from time series of discharge, but the method bears significant uncertainties. This is especially the case when low numbers of sediment samples are available or when there is a high scatter in the relation of SSC and Q_t (Mano et al., 2009; López Tarazón, 2011; Misset, 2019, Fig. 1.8). This scatter can be due to seasonality, hysteresis or

the exhaustion of sediment supply (Francke et al., 2014). Thus, when factors other than discharge alone control sediment fluxes, such a univariate model is no longer appropriate and more advanced approaches such as multivariate regression methods (Francke et al., 2008a,b; Mano et al., 2009; Zimmermann et al., 2012), neural networks (Nagy et al., 2002; Boukhrissa et al., 2013) and fuzzy logic (Kisi et al., 2006) have been applied (Francke et al., 2014).

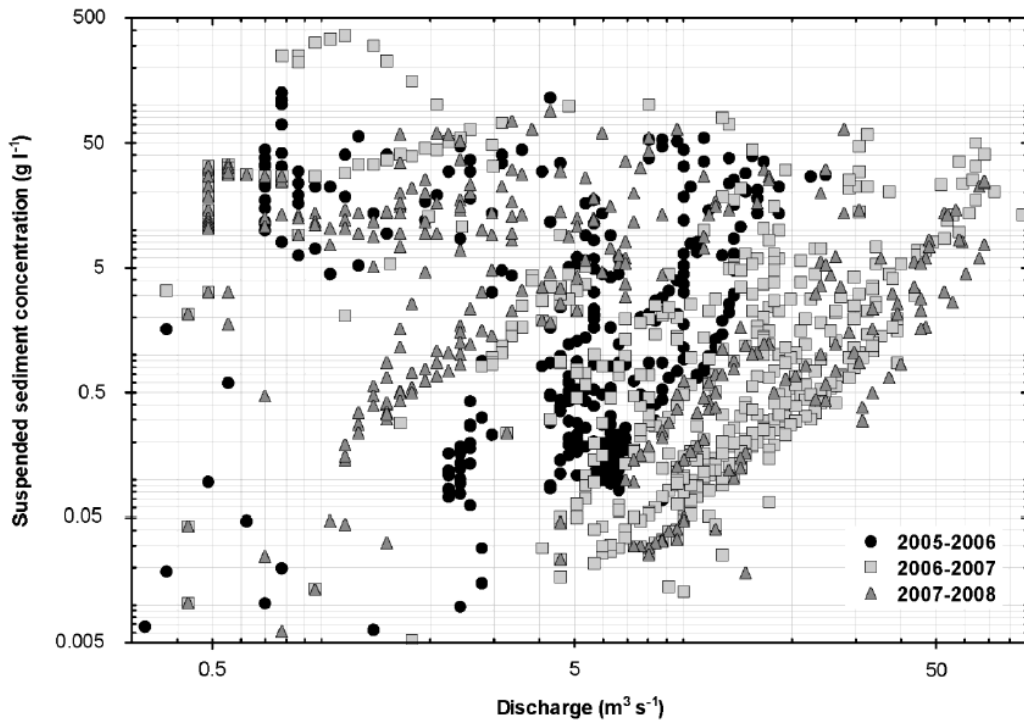


Figure 1.8: Very high variability in the relation of suspended sediment concentration and discharge in the Isábena catchment (445 km^2) in the southern central Pyrenees. The high scatter questions the applicability of sediment rating curves that establish a power law relation between the two variables. Source: López Tarazón (2011).

Currently, the available hydro-sedimentary models are not able to meet the needs of policy makers and other stakeholders (Jetten et al., 1999; Merritt et al., 2003; Wainwright et al., 2008; Alewell et al., 2019). In a model inter-comparison study, Jetten et al. (1999) showed that four commonly used models failed to reproduce observed yearly, monthly and daily soil loss (Fig. 1.9). Even though this study dates back 20 years now, it has not lost its relevance

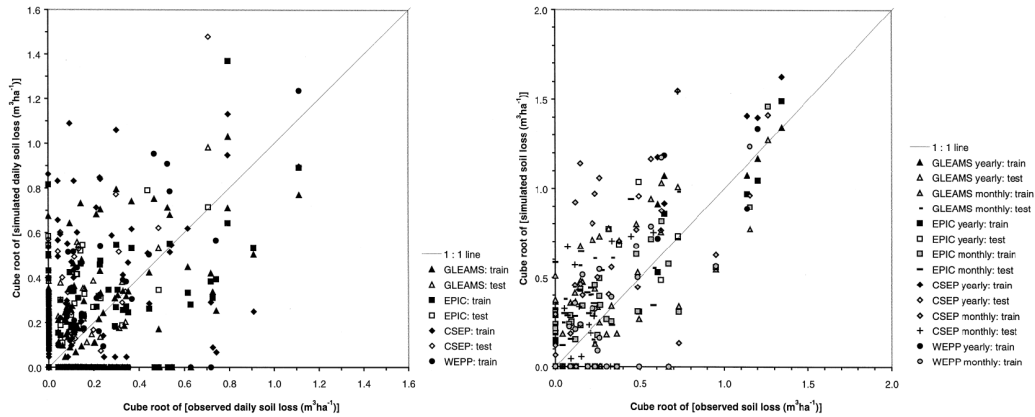


Figure 1.9: Comparison of observed and simulated daily (a) and monthly or yearly (b) soil loss. The models used are GLEAMS (Groundwater Loading Effects of Agricultural Management Systems modeling system, [Leonard et al. \(1987\)](#)), EPIC (Erosion Productivity Impact Calculator, [Williams \(1985\)](#)), CSEP (Climatic index for soil erosion potential, [Kirkby and Cox \(1995\)](#)) and WEPP (Water Erosion Prediction Project, [Lafren et al. \(1991\)](#)). From [Jetten et al. \(1999\)](#).

to the present. Recently, [Alewell et al. \(2019\)](#) compared the performance of Pesera model and USLE-based models by testing it against measured data from erosion plots in Europe compiled by [Cerdan et al. \(2010\)](#) (Fig 1.10). This study confirmed the results of [Jetten et al. \(1999\)](#) by concluding that neither type of modeling family performed well in reproducing observed data.

Despite these fairly negative conclusions on the performance of distributed, physically-based models, they have to be continued to be used and efforts have to be made to improve them. They are needed to understand the processes leading to soil erosion and sediment export from catchments, and to identify erosion hotspots and major sources of sediment ([Jetten et al., 1999](#); [Pandey et al., 2016](#)). However, past studies showed that simple, empirical or conceptual models often perform better than physically-based models. The latter rely heavily on calibration to perform equally well or to overcome conceptual flaws ([Jetten et al., 1999, 2003](#); [Jetten and Favis-Mortlock, 2006](#); [Wainwright et al., 2008](#); [de Vente et al., 2013](#)). As a striking example, [Jetten et al. \(2003\)](#) compare the studies by [Bathurst et al. \(1998\)](#) and by [Brochot and Meunier \(1995\)](#) in the Draix study area. While the former study uses the physically-based and distributed SHE model ([Abbott et al., 1986a,b](#)),

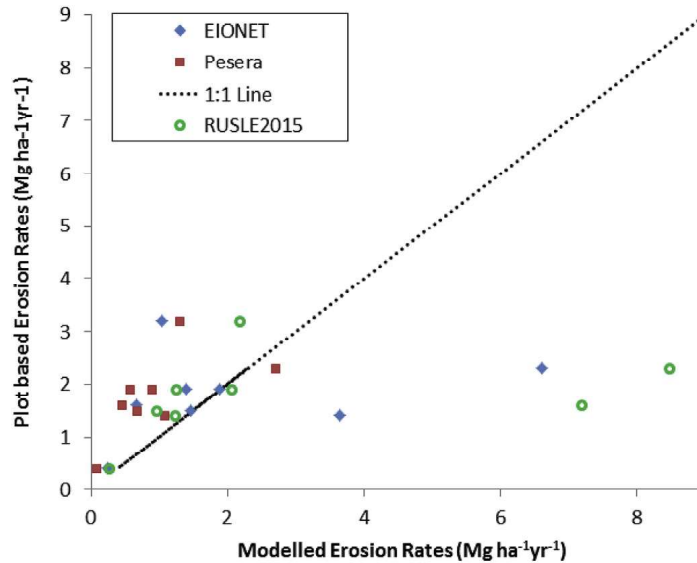


Figure 1.10: Comparison of erosion rates observed on plots (Cerdan et al., 2010) and simulated with USLE based models (EIONET, Panagos et al. (2014) and RUSLE2015, Panagos et al. (2015b)) and with the Pesera model Kirkby et al. (2008). From Alewell et al. (2019).

the latter one uses a simple regression model based on precipitation intensity and amount. Using the same data, Brochot and Meunier (1995) obtained better results with the lumped empirical model than the ones obtained with the physically-based model.

Many authors addressed the reasons for the poor model performance of physically based models and propose strategies for improvement. Two main sources of error can be identified; those associated to data quality and availability and those associated to model structure. Firstly, available data can be scarce and subject to measurement errors (Brazier et al., 2000; Alewell et al., 2019). Furthermore, many input parameters of erosion models such as soil characteristics are highly scale-dependent and the transfer of measured parameters at the plot scale to effective parameters that are applied to larger scale leads to high uncertainties (Brazier et al., 2000; Jetten et al., 2003).

Secondly, many models suffer from overparameterization which leads to unrealistic data requirements that are not met by the data that is usually

available to catchment managers or in research catchments ([Merritt et al., 2003](#); [de Vente and Poesen, 2005](#)). Further, a high number of parameters that is not warranted by the available data, leads to equifinality problems ([Beven, 1996](#)). During model calibration, good fits of the data can be obtained with many parameter sets that may be dispersed in the parameter space which hinders conclusions to be drawn from parameter values and model results and leads to errors in predictions ([Beven, 1996](#)). Another source of error is the misconception and misrepresentation of erosion and sediment transport processes. For example most models include rill and interrill erosion, but only a few have an implementation of gully, streambank or landslide erosion. Therefore, if the model is calibrated with total suspended sediment yield at the outlet, it has to overcompensate the missing processes with the ones implemented in the model ([de Vente and Poesen, 2005](#)).

The poor results in comparing measured and modeled fluxes at the outlet led the research community to several conclusions. [Alewell et al. \(2019\)](#) proposed to abandon the idea of exactly reproducing absolute fluxes at the outlet:

[Nearing \(2004\)](#) concluded that model validation is not just a matter of comparing measured to modelled data, one must also ask the question: 'How variable is nature?' We would like to add, that in bidding farewell to the idea of accurately predicting absolute values with models but rather concentrating on the prediction of relative differences, trends over times and systems reactions to processes and management practices, we can use models as tools to learn about the modelled systems and their reactions. In this conceptual approach, modelling in general and large-scale modelling specifically will per se not aim at an accurate prediction of point measurements. ([Alewell et al., 2019](#), p. 215)

They further stressed the potential of soil erosion models for hypothesis testing, process understanding and scenario development. Nonetheless, models have to be evaluated to ensure that the drawn conclusions are valid - even if they are of a more conceptual kind rather than based on absolute numbers.

Other authors stressed the need for alternative ways for model evaluation besides the classical split-sample test that makes use of data at the outlet

alone (Oreskes et al., 1994; Beven, 1996, 2002; Jetten et al., 2003; Palazón et al., 2016). Here, internal catchment information can be extremely valuable. The possibility to include such data is a major advantage of distributed models. Shifting the focus from the outlet alone to a more generalized view of the catchment can help to identify zones where the model is erroneous and can help to calibrate models. Advances in low-cost measurements and remote sensing can provide data at high spatial resolution. Measurement networks including internal points and nested catchments, increasingly provide such information (Braud et al., 2014; Nord et al., 2017; Francke et al., 2018). Several hydrological modeling studies used internal catchment information to calibrate or evaluate models (Anderton et al., 2002; Whitaker et al., 2003; Bathurst et al., 2004; Gallart et al., 2007). Gallart et al. (2007) show how distributed water table records and the extent of saturated zones help to reduce the uncertainty of discharge and baseflow prediction in a small catchment in the eastern Spanish Pyrenees. Whitaker et al. (2003) use internal catchment information that was not used for model calibration to evaluate model performance. They compared measured and modeled snow water equivalent at four climate stations and measured and modeled discharge in a subwatershed of their 25.8 km^2 study catchment.

In erosion modeling internal catchment information can be derived from maps of erosion and deposition. These can be realized via field mapping, from aerial photographs or calculated as the difference of two digital elevation models obtained at different dates. However, such information is rarely used for model calibration or validation (Jetten et al., 2003). Takken et al. (1999) mapped erosion features and measured rill and gully erosion as well as sediment deposition in a 290 *ha* agricultural catchment in Belgium at the event scale and compared it with erosion and deposition areas modeled in the physically-based and distributed LISEM model (Hessel et al., 2003b). The authors showed that the model performed reasonably well in reproducing overall sediment delivery ratio and deposition patterns, but poorly predicted erosion patterns on fields with different crop types. Jetten et al. (2003) applied a similar approach in a catchment in China. They found that the simulated and mapped patterns of erosion resembled each other in general. However, they ascribed this finding to rainfall spatial variability and observed that there were many discrepancies when the two maps were compared in detail. They quantified the differences between observed and simulated erosion at the scale of the grid cell (10 *m*) and at larger aggregations and showed

that the error decreased considerably with increasing resolution. This led them to the fairly negative conclusion that erosion models are not able to reproduce detailed spatial patterns.

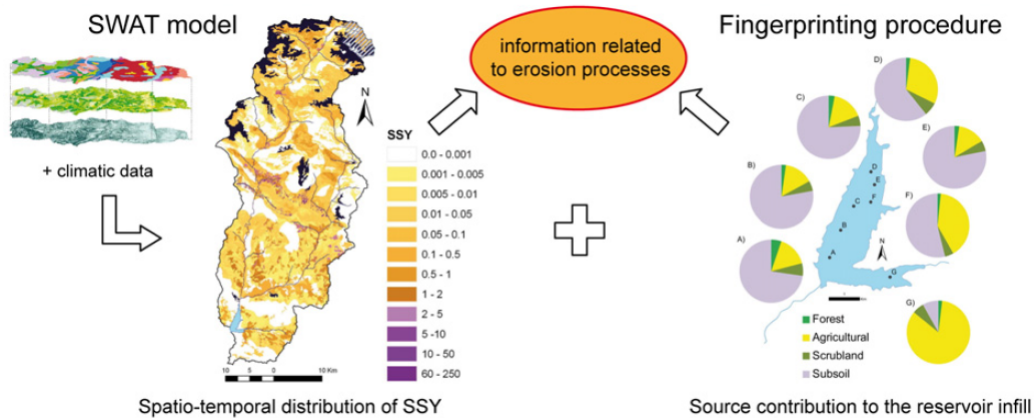


Figure 1.11: Combination of sediment fingerprinting with erosion modeling to obtain internal catchment information for model evaluation and understanding sediment dynamics. The modeled erosion hotspots that are displayed with purple color on the left figure correspond to the location of the badlands in the catchment. Source: Palazón et al. (2016).

Another approach to obtain internal catchment data for model calibration or evaluation is to apply sediment fingerprinting. A few studies combined erosion and sediment transport modeling with fingerprinting. Theuring et al. (2013) compared measured annual sediment export of a 15.000 km^2 catchment in Mongolia to values modeled with the semi-distributed sediment budget model SedNet. They also determined the contribution of surface erosion, riverbank and gully erosion with a sediment fingerprinting approach and found that modeled total suspended sediment output was in the same order of magnitude as measured one. However, the model underestimated riverbank erosion and overestimated surface erosion which showed that the model predicts the right output but for the wrong reasons. A similar finding was made by Wilkinson et al. (2013). In this study the model also underestimated the importance of gully erosion and the authors stressed the need to validate model results with additional information such as the one obtained from sediment fingerprinting. Palazón et al. (2014) conducted sediment fingerprinting and numerical modeling to identify the prevailing sources of sediment deposited in a reservoir at the outlet of the mountainous Benasque catchment

in the central Spanish Pyrenees and found that the main sources identified by the model and the fingerprinting approach did not agree. [Palazón et al. \(2016\)](#) also compared SWAT model output with sediment fingerprinting in the catchment of the Barasona reservoir in the Pyrenees. In their study, results from both procedures agreed that badlands are the main source of sediment (Fig. 1.11). [Mukundan et al. \(2010b,a\)](#) also found coherent results on main sediment sources identified with SWAT and sediment fingerprinting. These results are promising for the use of the models to determine main sediment source areas for management purposes and to help with process understanding. However, all of these studies are conducted at the long term scale concerning values averaged at the annual scale or longer. To understand hydro-sedimentary dynamics at shorter time scales we need comparisons of modeling and fingerprinting studies at the within and between event scale. To our knowledge, no such studies exist at the event scale yet.

1.3 Objectives

The aim of this thesis is to identify the origins of suspended sediments and to understand the dynamics of hydro-sedimentary fluxes in two mesoscale Mediterranean catchments that are prone to erosion by water and high sediment exports. Despite the long history of research on erosion and sediment transport, there are still major knowledge gaps that need to be addressed to better understand spatio-temporal patterns of soil erosion and pathways in the catchment ([Poesen, 2018](#)). Mediterranean mountainous areas are especially important because these regions are vulnerable and especially prone to erosion [Panagos et al. \(2015b\)](#); [Vanmaercke et al. \(2011, 2012\)](#). Mesoscale catchments (10 - 100 km) are of interest to catchment managers because it is the scale where erosion control and sediment retention measures are effective and feasible. For research it is important because it is the scale where the heterogeneity of geology, geomorphology, land cover and topography interact to define structural connectivity and where the spatio-temporal variability of hydro-meteorologic forcing can create variability of functional connectivity. Thus, this thesis work is focused on the mesoscale. Concerning the time scale we consider single rainfall-runoff events because solid fluxes in Mediterranean environments can occur during short time periods. Indeed, yearly solid yields can be transported in single extreme events [Navratil et al. \(2012c\)](#); [González-](#)

[Hidalgo et al. \(2007\)](#).

In the first part of the thesis we use sediment fingerprinting to address the following questions:

- Where do suspended sediments passing the outlet of two mesoscale catchments originate?
- How do the contributions of different sources vary within and between flood events?
- How certain can we be of the answers to the questions above?

The dynamics of suspended sediment fluxes at the outlet provide indirect information about the hydro-sedimentary processes within the catchments. Thus, these observations raise further questions:

- Where and when does erosion occur and how long does it take the eroded particles to reach the outlet?
- What are the reasons for differences in source contributions between and within events?

We hypothesize that the observed sediment flux variability is a result of the interplay of structural connectivity (governed by the location of the sources in the catchment with respect to the river network and the outlet) and spatio-temporal variability of the hydro-meteorological forcing. We address these questions in the second part of the thesis with the help of a physically-based, distributed numerical model.

In [Chapter 2](#) a description of the two mesoscale catchments that are the study sites of this thesis is given. The first one is the 42 km^2 catchment of the Claduègne which is a headwater catchment of the Ardèche. The second one is the 20 km^2 catchment of the Galabre, a headwater catchment of the Durance in the Southern French Prealps. In both catchments, suspended sediment samples are taken at the outlets at a high temporal resolution during floods. [Chapter 3](#) describes the quantification of the contribution of different erodible zones in the catchment to each of the sediment samples collected at the outlet using sediment fingerprinting. [Chapter 4](#) addresses the role of structural connectivity on the hydro-sedimentary fluxes at the outlets of the catchments. As the representation of connectivity of the sources to the

outlet in a distributed model depends not only on the actual configuration of the catchment but also on decisions taken during model discretization and parameterization, we first aim to assess the sensitivity of the model to such choices. We further examine how the structural connectivity of the sources impacts the simulated hydro-sedimentary dynamics at the outlet. Then, in Chapter 5 we include functional connectivity by examining how temporally and spatially variable rainfall patterns influence the modeled hydro-sedimentary fluxes. Finally, in Chapter 6 the results obtained from sediment fingerprinting and numerical modeling are compared and conclusions and open questions for further work are presented.

Chapter 2

Study sites

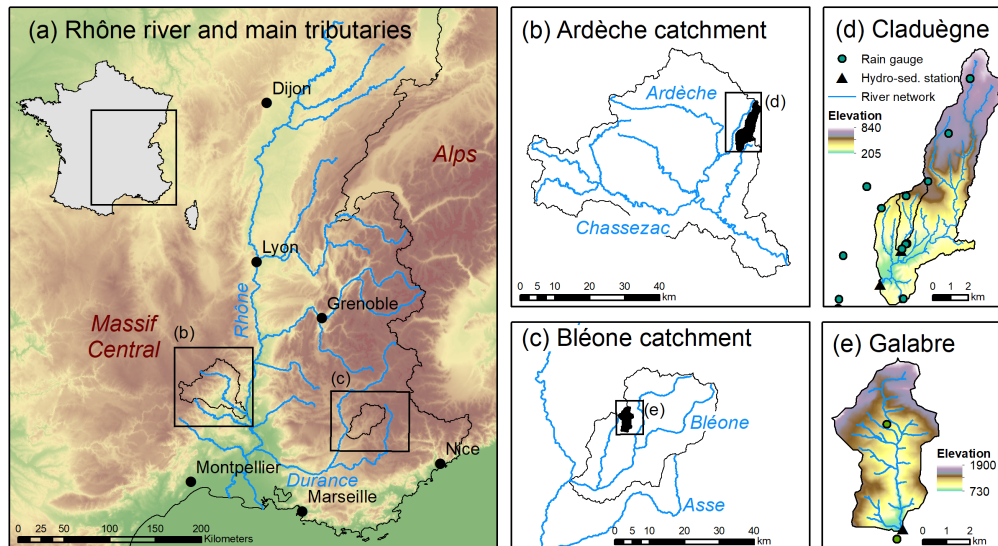


Figure 2.1: Location of the study sites in southeastern France (a). The catchments considered here are the 42.3 km^2 catchment of the Claduègne which is a headwater catchment of the Ardèche (b) and the 19.6 km^2 catchment of the Galabre, a headwater catchment of the Bléone which is a tributary of the Durance river. (d) Elevation of the Claduègne catchment and location of the rain gauges and the hydro-sedimentary stations at the outlets of the Claduègne and the nested Gazel catchment. (e) Elevation of the Galabre catchment.

2.1 Claduègne catchment

2.1.1 Introduction

The 42.3 km^2 Claduègne catchment is a research catchments within the Cévennes-Vivarais Mediterranean Hydrometeorological Observatory (OHM-CV, Boudevillain et al., 2011, <http://ohmcv.osug.fr>) which is part of the French network of critical zone observatories (OZCAR, Gaillardet et al., 2018, <https://www.ozcar-ri.org>). The devices and means of observation of the OHM-CV have been very useful to the HyMeX program and the FloodScale project. The 10 year HyMeX program (Hydrological Cycle in the Mediterranean Experiment, Drobinski et al., 2014; Ducrocq et al., 2014, <https://www.hymex.org/>, 2010 - 2020) is a monitoring program that aims at a better understanding of the hydrological cycle in the Mediterranean under climate change with a focus on extreme events. Within this program, the FloodScale project (Braud et al., 2014, 2016, <https://floodscale.irstea.fr/>, 2012 - 2015) was dedicated to the understanding and simulation of the hydrological processes leading to flash floods in the catchments of the Ardèche and the Gard. The project set up a multi-scale observation scheme with instrumentation covering (i) the hillslope scale (ii) the small-to-medium catchment scale (1 - 100 km^2) and (iii) the larger scale (100 - 1000 km^2 , Braud et al., 2014). Thus, to the benefit of this thesis a very rich data set of three nested subcatchments of the Ardèche, i.e. the Auzon (116 km^2), Claduègne (42.3 km^2) and Gazel (3.4 km^2) catchments is available (Nord et al., 2017). The observations in this study site aim at investigating the meteorological and hydro-sedimentary processes during heavy rain events and flash floods.

2.1.2 Geology, soils and topography

Both the Claduègne and the nested Gazel catchment can be clearly divided into two distinct geologies (Fig. 2.2). The northern part is constituted by the Coiron basaltic plateau that is bounded by a steep cliff of basaltic columns in the south, whereas the southern part of both catchments is a landscape of piedmont hills underlain by sedimentary limestone lithology (Nord et al., 2017). The basaltic plateau covers 51 % of the Claduègne catchment, whereas its fraction of the Gazel catchment is only 23 %. Thus, the northern part is dominated by silty and stony soils on pebble deposit of basaltic component, while the soils in the southern part are predominantly rendzinas or other

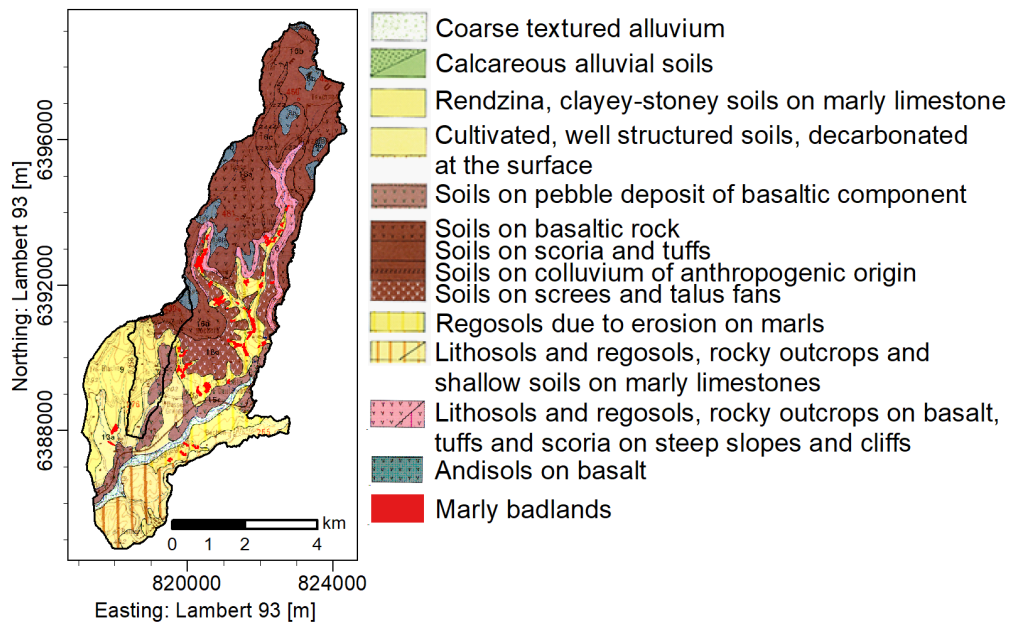


Figure 2.2: Map of the pedology of the Claduègne catchment and the Gazel subcatchment. Source: 1:100 000 soil map from INRA, Nord et al. (2017).

clay-stony soils, cultivated soils of loam and clay-loam and in the south of the Claduègne catchment lithosols and regosols (Nord et al., 2017, Fig. 2.2). Soil depths are generally less than two meters and shallow soils of less than 40 cm are common. In the central part of the Claduègne catchment, the river is deeply carved into the plateau, exposing the sedimentary rocks that lie below the basaltic plateau. Here, there are gorges with steep slopes and badlands with the typical aspects of gully erosion and low vegetation cover. Besides the steep slopes and cliffs at the edge of the basaltic plateau, the terrain is hilly with mean slopes of approximately 24%. The slopes are somewhat higher on the sedimentary geology than on the basaltic plateau (mean slope of 26% and 23% respectively). The elevation ranges from about 230 m at the outlet to about 820 m above sea level at the highest point of the catchment.

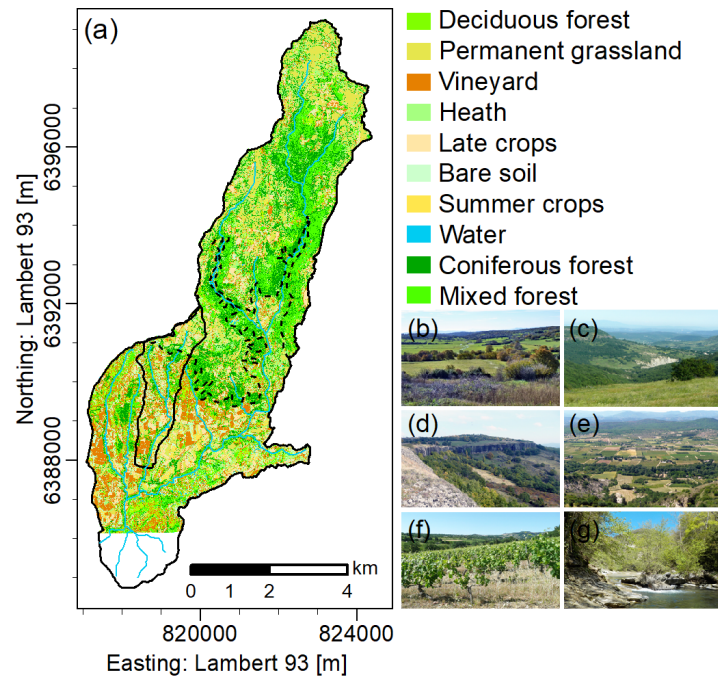


Figure 2.3: (a) Map of the land cover in the Claduègne and Gazel catchment (Andrieu, 2015). For the extreme south of the catchment the data is not available. The dashed line gives the border between the basaltic plateau and the sedimentary geology. Typical landscapes of the catchment: (b) grassland and open woodland on the Coiron plateau, (c) deep valleys of the river carved into the plateau, (d) basaltic cliffs at the southern end of the Coiron plateau, (e) marly limestone formation with regosols in the foreground, mosaic of agricultural landscape on the sedimentary geology in the background, (f) hillslope with vineyards and (g) river bed of the Claduègne, incised into marly-sedimentary bedrock. Pictures (b) - (f) are taken from Nord et al. (2017), Picture (g) taken by M. Hirigoyen.

2.1.3 Land cover

The catchment is characterized by extensive agriculture and natural vegetation. On the Coiron plateau permanent grassland and pastures dominate the land cover, complemented by open woodlands and shrublands. In well drained depression crops are grown. Oaks, chestnut trees and associated shrub flora are found on the slopes and screes (Nord et al., 2017).

In the southern part of the catchment natural vegetation consisting of downy oak woods, garrigues, Mediterranean open woodlands and dry grass-

lands is found mainly on the steeper slopes. On the more gentle slopes, this vegetation has been cleared to make place for cultivated fields (mainly cereals), grasslands and vineyards (Nord et al., 2017). According to the land cover map by Andrieu (2015), forests and shrublands cover 61 % of the catchment, followed by vineyards (16 %), grasslands and cultivated fields (11 % each, Fig. 2.3).

2.1.4 Erosion zones

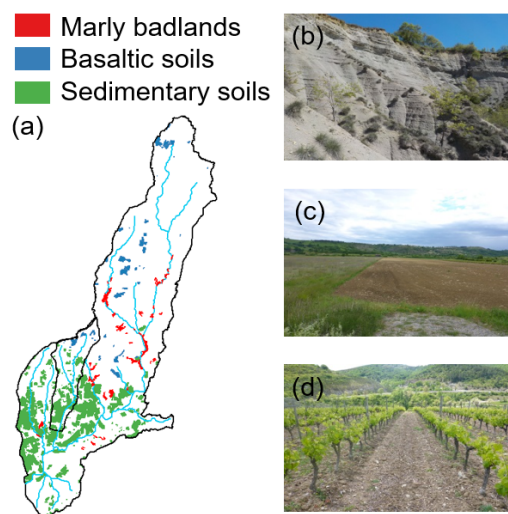


Figure 2.4: (a) Location of the erosion zones in the Claduègne catchment and pictures giving an example of each of the three zones: marly badlands (b), a cultivated field on basaltic geology that is bare after harvest (c) and a vineyard on sedimentary geology (d). Picture (b) was taken by M. Hirigoyen.

Based on the information on geology and land cover several erosion zones that are considered as potential sources of sediments passing the outlet can be identified (Fig. 2.4). Firstly, the marly badlands are assumed to be a main source of sediment. Several studies have shown the high erodibility of Mediterranean badlands and high sediment export of catchments with badlands (Gallard et al., 2005; Mathys, 2006; Francke et al., 2008b; Duvert et al., 2012). In the Claduègne catchment, the badlands cover an area of $0.3 km^2$ representing less than 1 % of the catchments surface (delineation on orthophotos of IGN, 2018a and verified during field trips). Many of the badlands are directly adjacent to the hydrographic network, thus, they are

very well connected (Fig. 2.4). In the Gazel catchment there are no badlands.

Besides the badlands, there are other potential erosion zones which are considered as diffuse erosion zones. The cultivated fields and vineyards are temporarily bare (Fig. 2.4b and 2.4c) so they are also assumed to provide sediment to the river. While the vineyards are located only on the sedimentary geology, cultivated fields are present in both geologic zones. Thus, in this study we differentiate between diffuse sources on basaltic geology and on sedimentary geology (Fig. 2.4). They were delineated based on a combination of land cover data obtained from Sentinel-2 satellite data (Inglada et al., 2017) and land register data of the agricultural parcels declared for direct subsidies of the Common Agricultural Policy of the European Union (DRAAF, 2017). On the basaltic plateau they cover a surface of about 0.5 km^2 corresponding to 1.2% of the surface of the Claduègne catchment (For the Gazel catchment: 0.06 km^2 , 2%). On the sedimentary geology, temporarily bare fields and vineyards cover about 4.2 km^2 representing 9.9% (Gazel: 0.6 km^2 , 18.5%). The basaltic sources are assumed to be less connected to the outlet due to their higher distance to the outlet and to the river network. The permanently covered land uses, i.e. forest, shrublands and grassland are not considered as potential erosion zones.

2.1.5 Climate

The study site is subject to both oceanic and Mediterranean climatic influences. Furthermore, the topography plays an important role in the rainfall generating processes. Average annual precipitation in the Auzon catchment is in the range of $850 - 900 \text{ mm}$ (Nord et al., 2017). There is an uneven seasonal distribution with highest monthly precipitation occurring in autumn and a second - but smaller - maximum in spring (Molinié et al., 2012, Fig. 2.7a). Boudevillain et al. (2016) distinguish three main types of rain events occurring in the Cévennes Vivarais region, i.e. widespread rainfall, localized convection and Cévennes rain events. Widespread rainfall events are usually associated with westerly frontal systems that lead to moderate total precipitation amounts ($40 - 50 \text{ mm}$) and rain intensities of usually less than 10 mm h^{-1} . Localized convective events occur typically at the end of summer or in autumn, last for a few hours and can reach high total rainfall amounts of up to 200 mm and high hourly rain rates of $50 - 100 \text{ mm h}^{-1}$ (Boudevillain et al., 2016). Cévennes rain events are a particularity of the region and can

reach high hourly rain rates and very high amounts of precipitation such as 30 mm h^{-1} and 600 mm of cumulative precipitation from November 1st to 6th, 2011 (Boudevillain et al., 2016) or $600 - 700 \text{ mm}$ and a maximum hourly rain rate of 120 mm h^{-1} during the catastrophic event of September 8th to 9th in the Gard river (Delrieu et al., 2005). These events occur usually in the end of summer or in autumn when the warm Mediterranean Sea feeds the air with moisture and an advective flow transports the warm and moist air masses northwards. The Rhône valley with the mountains of the Massif Central to the west and the Prealps to the east acts as a funnel and the warm air masses rise when reaching the slopes of the Cévennes (Boudevillain et al., 2011; Melese, 2019). These topographic and geographic factors make the region very vulnerable to precipitation extremes and the associated hydrologic risks. The elongated form of the rain bands and the small cell size of the localized convection events can lead to high spatio-temporal variability of rainfall even at the scale of catchments of less than 100 km^2 (Wijbrans et al., 2015). Furthermore, there is a spatial gradient of precipitation in the region with the highest hourly intensities recorded in the plains and the highest daily rain intensities recorded in the mountains (Molinié et al., 2012).

2.1.6 Hydrology

The extreme precipitation events occurring in the Cévennes-Vivarais make the region prone to flash floods with high economic damage and numbers of fatalities (Ruin et al., 2008; Braud et al., 2014). Based on Gaume et al. (2009), Braud et al. (2014) define flash floods as rapid flood events where the rise of the hydrograph takes no more than a few hours for catchments $< 100 \text{ km}^2$ and less than 24 h for larger catchments ($> 1000 \text{ km}^2$). Further, peak discharge has to exceed $0.5 \text{ m}^3 \text{ s}^{-1} \text{ km}^{-2}$. In the Claduègne catchment, such events occur mainly in autumn and to a lesser extent in spring or summer. Fig. 2.5 shows the Claduègne river close to the hydro-sedimentary station during low flow and during a flash flood.

The Claduègne catchment is characterized by a rapid hydrological response to rain events. Hachgenei (2018) quantified the lag time for several impulsive rain events, the time of rise and the time of concentration for the Claduègne catchment and 12 subcatchments ranging in size from 0.17 to 12.24 km^2 . The lag time (T_{lag}) was calculated as the time between the peak of precipitation and peak discharge (for impulsive events the peak of



Figure 2.5: (a) Claduègne river during low flow (Sep 13th, 2015) and (b) during a flash flood on October 4th, 2014. (b) is taken from [Nord et al. \(2015\)](#).

precipitation is assumed to be representative for the barycenter). The time of concentration (T_c) is defined as the time that it takes the water to travel from the hydraulically furthest point in the catchment to the outlet, calculated as the time difference between the end of effective precipitation and the end of event flow or rapid runoff ([Salimi et al., 2017](#); [Hachgenei, 2018](#)). The time of rise (T_r) is the time between the beginning of effective precipitation and the increase of discharge. T_c of the Claduègne catchment is in the order of $4.7 h$, the one of the Gazel catchment is about $2.7 h$ and the ones of the other subcatchments correlate well with their catchment length. T_{lag} of impulsive events was found to be a good indicator of the time of concentration ([Hachgenei, 2018](#)). The median T_r of the hydrographs of the Claduègne catchment during impulsive events is $2.7 h$, but it varies strongly between events. Further, the T_r normalized with catchment length varies strongly between catchments. In general, the southern part of the catchment on sedimentary geology reacts faster than the basaltic plateau. This is probably due to the steeper slopes, but might also be due to differences in soils and land cover ([Hachgenei, 2018](#)).

In the Gazel and Claduègne catchments it was further observed that the hydrological response depends strongly on initial soil moisture conditions ([Huza et al., 2014](#); [Uber et al., 2018](#)). There is a threshold of about 34% volumetric soil moisture below which the hydrologic response is very low, even for events with high cumulative precipitation (up to $78 mm$, Fig. 2.6). Above this threshold the hydrological response can be very high with event

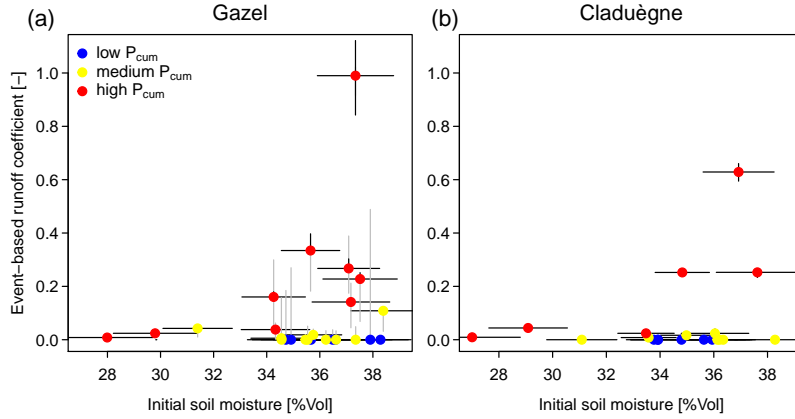


Figure 2.6: Relation between initial soil moisture and event based runoff coefficients in the Gazel (a) and Claduègne (b) catchments. The lines give estimates of the errors due to soil moisture heterogeneity (horizontal), the hydrograph separation method (vertical, grey; only estimated in the Gazel) and the stage-discharge relation (vertical, black). The color of the points indicates whether cumulative event precipitation is low ($P_{cum} < 1.5 \text{ mm}$), medium ($1.5 \text{ mm} < P_{cum} < 13 \text{ mm}$) or high ($P_{cum} > 13 \text{ mm}$). Adapted from Uber et al. (2018).

based runoff coefficients (i.e. the ratio of event runoff volume to total event rainfall volume) of up to 0.99 even if there is a high scatter (Uber et al., 2018).

This observation is important for the annual discharge dynamics. Soils are usually dry in summer and soil moisture increases in the beginning of autumn when more rain falls and potential evapotranspiration is lower than in summer (Braud et al., 2014). This is reflected in the low discharge during the summer months June, July and August (Fig. 2.7b). Most rainfall (about 40 % of annual precipitation occurs from September to November) as well as high monthly discharge occurs in autumn (mean discharge of $1.1 \text{ m}^3 \text{ s}^{-1}$ compared to mean discharge throughout the year of $0.7 \text{ m}^3 \text{ s}^{-1}$). However, there is a second peak in precipitation in late spring (Fig. 2.7a) that is hardly reflected in the annual dynamic in discharge (Fig. 2.7b). This is assumed to be due to differences in soil moisture.

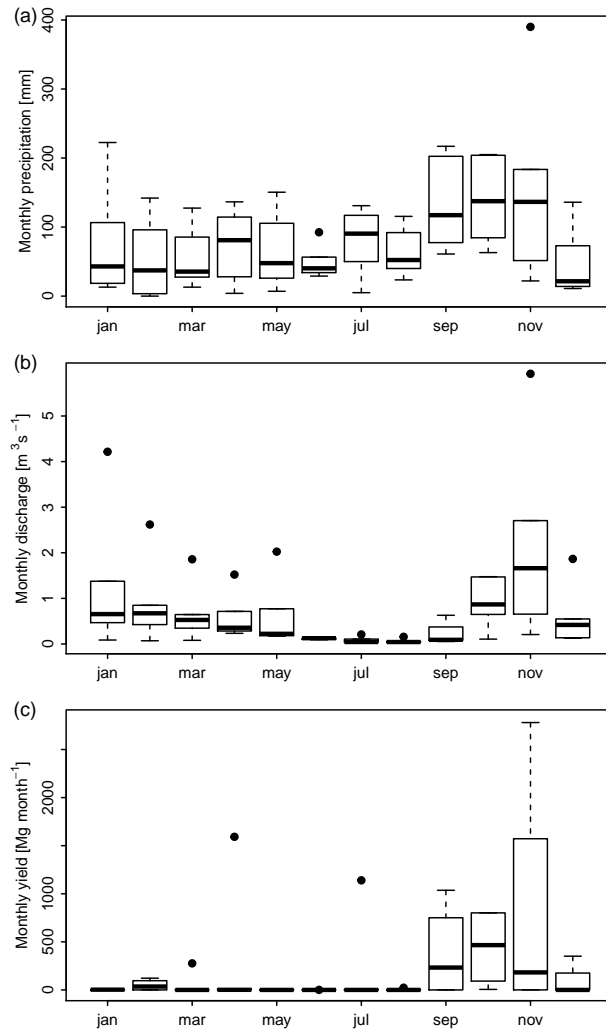


Figure 2.7: Annual dynamics of precipitation (a), discharge (b) and sediment yield (c) in the Claduègne catchment. The values are derived from the period 2011 - 2016. For better visualization, two outliers in Fig (c) are not shown. They correspond to May and October 2013 where two individual flood events (May 18th and October 23rd) each yielded $> 10000 Mg$ of sediment yield.

2.1.7 Soil erosion and sediment export

In the south of the Gazel catchment, close to its outlet, two soil erosion plots on vineyards were installed and monitored from December 2009 to October 2013 (OHM-CV, 2009; Nord et al., 2017). The two replicates are 60 m long and 2.2 m wide which corresponds to the distance between two rows of vine plants (Grangeon, 2006; Cea et al., 2015; Nord et al., 2017). The average slope along the length of the plots is about 15% and the vegetation between the vine plants is sparse. Water depth was measured every minute in a Parshall flume located at the lower end of the slope and an experimentally built stage-discharge rating curve allows the continuous calculation of discharge (Grangeon, 2006). A sequential sampler collected water and eroded particles and a mean erosion rate in the order of $5 \text{ t ha}^{-1} \text{ year}^{-1}$ was estimated (Cea et al., 2015). This estimate is similar to the mean erosion rate in Mediterranean vineyards reported by Cerdan et al. (2010) based on a literature review of erosion rates obtained from erosion plots in Europe under natural rainfall conditions ($8.6 \pm 27.4 \text{ t ha}^{-1} \text{ y}^{-1}$; mean \pm standard deviation).

The suspended sediment concentration at the outlet of the Claduègne catchment is very low between floods (in the order of $0.01 - 0.02 \text{ g l}^{-1}$). During floods it remains usually below 8 g l^{-1} which corresponds to the 95th percentile of the suspended sediment concentration of 238 instantaneous samples collected between 2011 and 2016. Nonetheless, it can temporarily reach high values with a maximum of 26.8 g l^{-1} . In the Gazel catchment the concentration is usually below 2.7 g l^{-1} (95th percentile) with a maximum of 13.8 g l^{-1} . These values are high enough to cause adverse effects for ecosystems (Bilotta and Brazier, 2008), but they are low compared to suspended sediment concentrations exceeding 350 g l^{-1} as reported e.g. by Esteves et al. (2019) or even as high as 800 g l^{-1} (Mathys et al., 2003) in the catchments of the Draix-Bléone Observatory. At the catchment scale, specific suspended sediment yield, i.e. the yearly mass of suspended sediment passing the outlet normalized by the size of the catchment, was quantified from the data set of discharge, turbidity and suspended sediment concentrations (Appendix A). In the Claduègne catchment, specific yield is estimated to be in the order of $380 \text{ t km}^{-2} \text{ y}^{-1}$. This value was calculated as the mean of five years, but it is subject to the error of the suspended sediment concentration - turbidity rating curve as well as to the error due to high temporal variability between the years (ranging from 13 - $1073 \text{ t km}^{-2} \text{ y}^{-1}$). It is in the range of values reported

Table 2.1: Literature values for specific yield of Mediterranean mountainous catchments at the smaller mesoscale (1 - 100 km^2). In all studies specific yield was obtained from the measurement of suspended sediment concentration and discharge at the outlet. References : (1) Jahn et al. (1989), (2) Buendia et al. (2016a), (3) Mathys et al. (2003), (4) Francke et al. (2014), (5) Lenzi et al. (2003), (6) Duvert et al. (2012), (7) Esteves et al. (2019), (8) this study.

Site	Location	Area [km^2]	Erosion sources	Specific yield [$t km^{-2} y^{-1}$]	Ref.
Portugal	S Portugal	6	NA	3	1
Canalda	Spain, Pre-Pyrennees	65	bare soils, rocky outcrops	4	2
Brusquet	SE France	1.1	Badlands: 13 %	80	3
Lascuarre	NE Spain	45	Badlands: < 1%	82	4
Cordon catchment	NE Italy	5	hillslopes (5.2%), channel bed, stream banks	171	5
Cal Rodo	E Spain, Pyrennees	4.2	Badlands: 2.8 %	250	6
Ceguera	NE Spain	28	Badlands: 0.93 %	361	4
Claduègne	SE France	42	Badlands (< 1%), agriculture	380	8
Ca l'Isard	E Spain, Pyrennees	1.3	Badlands: 4.5 %	440	6
Galabre	SE France	20	Badlands: 9 %	666	7
Carrasquero	NE Spain	25	Badlands: 1.95 %	627	4
Villacarli	NE Spain	42	Badlands: 5.57 %	3651	4

in the literature for Mediterranean catchments at the smaller mesoscale (i.e. < 100 km^2 ; Table 2.1).

However, there is a high seasonal variability of sediment fluxes. Thus, yearly sediment yield is not distributed evenly over the year (Fig. 2.7c). There usually is a maximum in autumn, but high monthly values can also be obtained when intense storms occur in spring. This was the case for example in May 2013 when a single flood event generated nearly 12000 t of suspended sediment yield during three days (May 18th - May 21st). In summer, sediment export is usually low due to low discharge.

2.1.8 Data availability

A comprehensive overview of the available data in the Claduègne and Gazel catchments is published in Nord et al. (2017) and data can be accessed at the publishers website. Thus, only a short summary of the data used here is given. Some of the data can also be visualized and downloaded at <https://bdoh.irstea.fr/OHM-CV/>

Precipitation Rainfall data were obtained from the HPiconet rain gauge network at a resolution of 1 *min*. The network consists of 19 tipping bucket rain gauges with a sampling surface of 1000 cm^2 and a resolution of 0.2 *mm*, out of which 12 are located in the Claduègne catchment or its close vicinity. Furthermore, two rain gauges operated by the French weather service Météo France are located in the catchment and data is available at 6 *min* resolution. Besides the rain gauge data, the region is also covered by two operational S-band radars located in Bollène (37 *km* southwest of the catchment centroid) and Nîmes (89 *km* south). They provide quantitative precipitation estimates at a resolution of 5 *min* and 1 km^2 (Météo France, 2018; Tabary, 2007).

Discharge Water level is continuously measured at the outlets of the two catchments with a pressure probe at 2 *min* resolution (Gazel) and a radar level sensor at 10 *min* resolution (Claduègne). The water level is converted to discharge with a stage–discharge relationship established using the BaRatin framework (Le Coz et al., 2014) that also gives the uncertainty of the rating curve that is quantified as the 90 % confidence interval of discharge. The rating curve is based on numerous discharge measurements performed from 2012 to 2014.

Suspended sediments At the hydrometric stations of the Gazel and Claduègne, turbidity is continuously measured with suspended solid probes that are optimized for high turbidity ranges (Visolid IQ 700). Thus, data between floods was set to zero because the low concentrations could not be accurately measured. At the outlets of the Gazel and Claduègne catchments, samples of about 1 *l* of water and suspended sediment are automatically taken every 10 and 40 *min*, respectively, with an automatic sequential water sampler (Teledyne ISCO 3700). Sampling is automatically triggered once critical thresholds of water level and turbidity are exceeded. Suspended sediment concentrations (*SSC*) of all of these samples were measured and a turbidity - *SSC* rating curve was established to calculate time series of *SSC* (Appendix A). Further, these samples were used to quantify source contributions with sediment fingerprinting (Chapter 3.1).

Spatial characterization data A bare earth digital elevation model (DEM) at 1 *m* resolution was derived from an aerial lidar data set obtained in 2012 (Braud et al., 2014; Nord et al., 2017; Fig. 2.1d). It covers all but the very

southern part of the Claduègne catchment. A DEM at 5 *m* is available for the entire catchment, derived from the fusion of the lidar DEM and smoothing of a DEM with a resolution of 25 *m*. A map of the geology at a scale of 1:500000 dating from 1996 was released by the French Geological Survey Bureau de Recherches Géologiques et Minières (BRGM) and a soil map at a scale of 1:100000 (Fig. 2.2) was released by the French National Institute for Agricultural Research (INRA) in 1977. Furthermore, during a field campaign Braud and Vandervaere (2015) conducted tests of infiltration at 17 locations in the catchment to document surface hydraulic properties. Soil samples were taken at the same sites and were analyzed for soil texture. For land cover several data sources are available. Firstly, a 0.5 *m* resolution land use map of the Claduègne catchment based on QuickBird satellite images is available (Andrieu, 2015; Fig. 2.3). There also is a land cover map for all of France at a resolution of 10 *m* provided by Centre d'Etudes Spatiales de la Biosphère (CESBIO). The map is based on Sentinel-2 satellite data (Inglada et al., 2017).

2.2 Galabre catchment

2.2.1 Introduction

The 19.6 km² Galabre catchment belongs to the Draix-Bléone Observatory (<https://oredraixbleone.inrae.fr/en/>) which is also part of the research infrastructure OZCAR (Gaillardet et al., 2018, <https://www.ozcar-ri.org>). The observatory was set up in 1983 to observe hydrological and erosive processes in a Mediterranean mountainous terrain called "Terres Noires" (Fig. 2.8a). This formation of Jurassic black marls is very susceptible to erosion. Thus, high sediment exports from headwater catchments are observed and extensive badlands can be found (Fig. 2.8b). Seven catchments ranging in size from 1300 m² to 22 km² are monitored as part of the Draix-Bléone Observatory.

Most of the research at the Draix-Bléone Observatory is dedicated to the study of erosion processes (Oostwoud Wijdenes and Ergenzinger, 1998; Antoine et al., 1995; Descroix and Olivry, 2002; Descroix and Gautier, 2002; Descroix and Mathys, 2003; Mathys et al., 2005; Mathys, 2006; Yamakoshi et al., 2009; Lofi et al., 2012) as well as suspended sediment and bedload transport (Navratil et al., 2010; Le Bouteiller et al., 2011; Navratil et al., 2011; Badoux et al., 2012; Grangeon et al., 2012; Liébault et al., 2012; Navratil et al., 2012b,c; Legout et al., 2013; Esteves et al., 2019), hydrology and hydrochemistry (Craz, 2005; Esteves et al., 2005; Cras et al., 2007; Montety et al., 2007; Thommeret et al., 2010; Garel et al., 2012; Neuville et al., 2012; Travelletti et al., 2012; Mallet, 2018). Further, the effect of vegetation on sediment retention is investigated (Lukey et al., 1995, 2000; Vallauri et al., 2002; Rey, 2004, 2009; Liébault et al., 2005; Burylo et al., 2012, 2014; Erktan and Rey, 2013; Erktan et al., 2013; Phillips et al., 2013; Rey and Burylo, 2014; Carrière, 2019).

The research conducted at the Draix-Bléone Observatory is not only important for science but also for practitioners. Sediment exports from the headwater catchments lead to siltation of downstream reservoirs such as the Malijai reservoir in the Durance river and the Barré Lagoon and consequently to economic and ecological problems (Accornero et al., 2008; Navratil et al., 2012c). On the other hand, the Durance is a major source of sediment for the Rhône delta. It contributes on average only 4% of the discharge of the

Rhône river but 24% of sediment fluxes (Poulier et al., 2019).

2.2.2 Geology, soils and topography

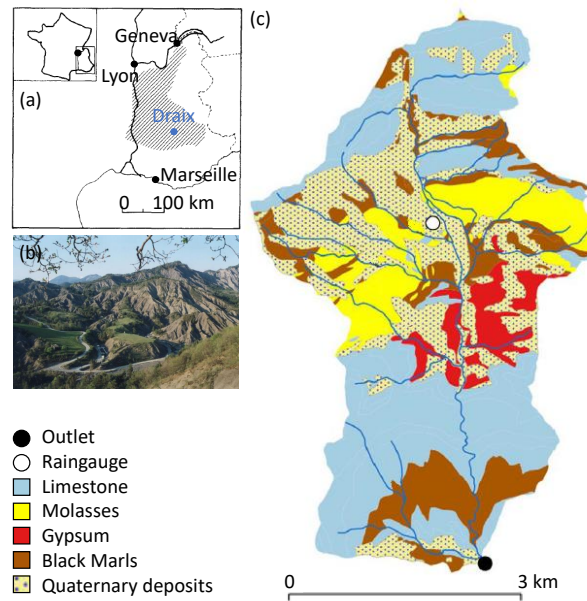


Figure 2.8: (a) Extent of the "Terres Noires" formation in southeastern France and location of the Draix-Bléone Observatory; adapted from Antoine et al. (1995). (b) Extended badlands on Jurassic black marls containing instrumented gullies that belong to the Draix-Bléone Observatory; Photo by D. Richard https://oredraixbleone.inrae.fr/en/photos/draix_panoram_dr/ (c) Map of the geology of the Galabre catchment; adapted from Esteves et al. (2019).

The Draix-Bléone Observaotry is located in the dark, predominantly marly "Terres Noires". This geologic formation was deposited in the Jurassic age in an extensive basin that covers large parts of southern France (Fig. 2.8a). The facies range from marls to clayey limestones (Antoine et al., 1995). The Terres Noires are known for their high susceptibility to weathering and erosion and badlands are frequent (Antoine et al., 1995; Descroix and Mathys, 2003).

While the other catchments of the Draix-Bléone Observatory are dominated by a rather homogeneous black marl geology, in the Galabre catchment

various sedimentary rocks can be found (Fig. 2.8b). Limestones cover about 34 %, marls and marly limestones 30 %, gypsum 9 %, molasses 9 % and Quaternary deposits 18 % (Esteves et al., 2019). The Quaternary deposits comprise unconsolidated material that is a mixture of the other facies (Legout et al., 2013). The soils are stony and shallow with a maximum depth of 60 cm (Legout et al., 2013).

The elevation of the Galabre catchment ranges from about 730 m at the outlet to about 1880 m above sea level at the ridges. The slopes are steep (mean \pm standard deviation of 54 ± 40 %) and the river is deeply incised into the bedrock in V-shaped valleys. In the northern part of the catchment there are several vertical cliffs.

2.2.3 Land cover and erosion zones

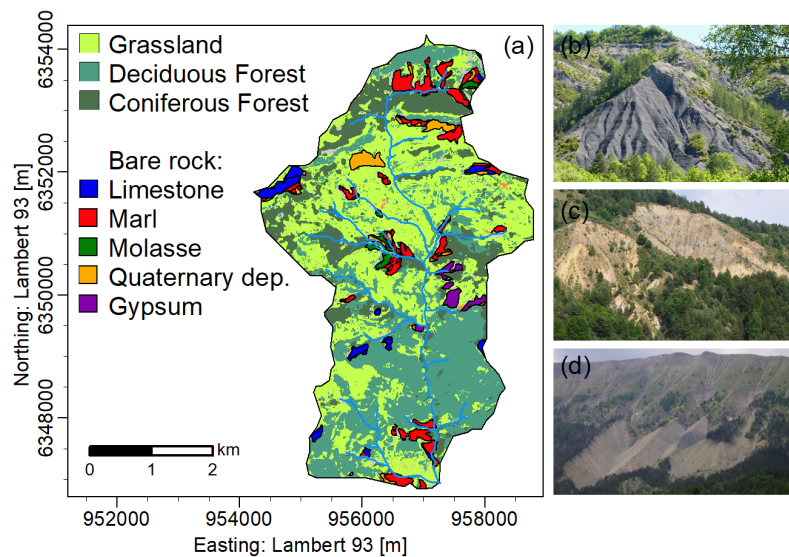


Figure 2.9: (a) Land cover map of the Galabre catchment. Adapted from CESBIO Land cover data (Inglada et al., 2017). The unvegetated badlands were delineated by Legout et al. (2013) and classified according to their geology. The pictures show badlands on black marl (b), molasse (c) and limestone (d).

The majority of the Galabre catchment is permanently covered by vegetation (Fig. 2.9a). Deciduous (34 %) and coniferous forests (17 %) cover more than half of the catchment. Further, grasslands and prairies cover about

40 %. Grasslands are mainly found where the slopes are more gentle while forests are found on the steeper slopes. Agricultural zones and sealed surfaces are hardly present in the catchment ($< 1\%$). Thus, the human impact on the catchment is very low. About 9 % of the catchment are covered by highly eroded surfaces. They show a clear badland topography with extensive gully development, steep slopes and lack of vegetation (Fig. 2.9b-d). They were delineated based on orthophotos and their location as well as their geology were validated during field observations by Legout et al. (2013). They are scattered throughout the catchment and are found on all types of geologies (Fig. 2.9a). They are usually close to the river network (distance to the stream $< 2000\text{ m}$) but the distribution of the distance to the streams varies for the different erosion zones. The ones on black marls are closest to the river. The badlands are considered to be the only source of suspended sediment in the river as the other land cover types are permanently protected by vegetation. We assume that the forests and grasslands are negligible as a source of erosion compared to the highly erodible badlands.

2.2.4 Climate

The climate of the study site is dominated by Mediterranean and mountainous influences. Mean annual temperature at an altitude of 400 m above sea level is 12°C but there is a high variability with monthly values varying by about 18°C between the coldest and the warmest month (Esteves et al., 2019). Mean annual precipitation at the Laval rain gauge about 13 km south-east of the catchment at an altitude of 851 m is 940 mm (data from 1984 - 2003, Mathys, 2006) and about 995 mm at Ainac in the Galabre catchment at an altitude of 1146 m (Esteves et al., 2019). The Mediterranean influence determines notably the high inner-annual variability of precipitation (Fig. 2.10 and 2.11a). There are two precipitation maxima, in spring (April to June) and in autumn (October to December, Fig. 2.11a). Summer is usually dry but there can be thunderstorms with high rain intensities. Indeed, the annual distribution of high intensity precipitation is monomodal with a maximum in July and August (Fig. 2.10, Mathys, 2006). This indicates that different types of precipitation are observed in the study site with high intensity storms occurring mainly in summer and less intense rain events occurring mainly in April / May as well as in October to December. Navratil et al. (2012c) distinguish two main types of rainfall regimes in the Southern French Alps. Firstly, widespread rain events are usually associated with low

pressure areas. Secondly local convective storms and rainfall generated at storm fronts cause air mass instabilities and convective precipitation. The latter storms are usually brief (few hours) and impact limited areas (a few km^2). Thus, single events can contribute strongly to monthly and annual precipitation. In the Galabre catchment maximum recorded daily precipitation is 94.2 mm . Twelve days in seven years exceeded 50 mm (Esteves et al., 2019). This is consistent with data from the other rain gauges of the Draix-Bléone Observatory which are located within 20 km distance of the Galabre and where longer time series are available. Maximum recorded daily values in the period 1984 - 2003 are about 100 mm and the estimated daily precipitation with a return time of 10 years is $80 - 90\text{ mm}$ (Mathys, 2006). Rainfall can also be highly variable in space. For example for an event in June 2015, 13 mm were recorded at Ainac in the central part of the catchment while 79 mm were recorded 5 km further south at La-Robine-sur-Galabre close to the outlet. Similar observations were made in Draix where a storm in June 1996 generated 36 mm at Pépinière and only 7 mm at Laval less than 4 km away (Mathys, 2006).

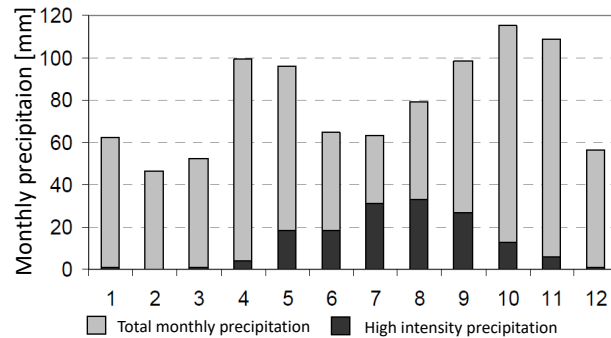


Figure 2.10: Mean monthly precipitation at the Laval rain gauge close to the Galabre catchment. The light gray bars show total precipitation, the dark gray bars only the fraction of precipitation that exceeds rain intensities of 15 mm h^{-1} (instantaneous rain intensity calculated every minute). Adapted from Mathys (2006).

2.2.5 Hydrology

Flow at the outlet of the Galabre catchment is perennial even though values as low as $0.02\text{ m}^3\text{ s}^{-1}$ are recorded in summer when high potential evaporation and low precipitation lead to a pronounced water deficit (Esteves et al.,

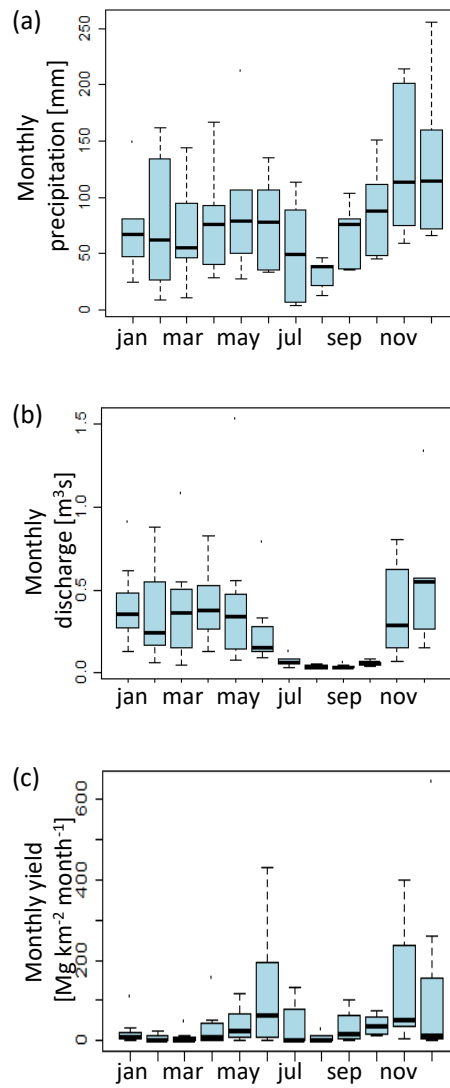


Figure 2.11: Intra-annual dynamics of rainfall, discharge and sediment yield in the Galabre catchment. The values represent mean monthly values in the period 2007 - 2014. Source: [Esteves et al. \(2019\)](#).

2019). Mean annual discharge at the outlet is $0.281 \text{ m}^3 \text{ s}^{-1}$; together with annual precipitation of 995 mm per year this leads to a mean runoff coefficient of 42.6% (Esteves et al., 2019). The flow regime of the Galabre is typical for Mediterranean mountainous streams with low flow in summer and floods occurring in spring, autumn and winter (Fig. 2.11). At the event scale, Micoud (2018) estimated event based runoff coefficients for nine floods to range between 2.6 and 49.1% . No data on soil moisture is available, thus these differences cannot be directly attributed to initial soil moisture conditions and no correlation was found between event based runoff coefficients and 15 day antecedent precipitation (Micoud, 2018).

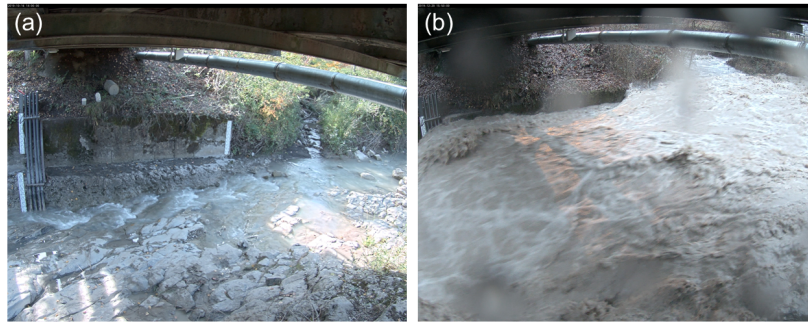


Figure 2.12: (a) Galabre river at the hydro-sedimentary station during low flow (Oct 16th, 2019) and (b) during a flash flood on December 20th, 2019.

The catchment is prone to flash floods with a fast hydrological response. Figure 2.12 shows the hydro-sedimentary station during low flow and during a flash flood. During the period October 2007 to December 2014, nine events with peak discharge exceeding $9.8 \text{ m}^3 \text{ s}^{-1}$ occurred. This corresponds to a specific discharge of $0.5 \text{ m}^3 \text{ s}^{-1} \text{ km}^{-2}$ that can be used as a threshold for an event to be considered as a flash flood (Braud et al., 2014). The maximum recorded instantaneous discharge was $34.0 \text{ m}^3 \text{ s}^{-1}$, corresponding to $1.7 \text{ m}^3 \text{ s}^{-1} \text{ km}^{-2}$ (Esteves et al., 2019). In the same study period 24 events exceeded $5 \text{ m}^3 \text{ s}^{-1}$. Floods that occur in spring are typically caused by local thunderstorms, while the ones in autumn are usually caused by widespread rain events (Esteves et al., 2019).

2.2.6 Soil erosion and sediment export

In the black marl badlands at Draix direct measurements of erosion were conducted in 2002 on four experimental plots of about 1 m^2 (Mathys, 2006). A metallic frame was fixed above the ground and contactless laser measurements of the distance to the surface were conducted at a high resolution throughout the year. In this way, mean net erosion rate of 8 mm a^{-1} was measured but this value is very variable. In the rills it was highest with 12 mm a^{-1} . Furthermore, single events contributed strongly to annual values. In July 2002, two storm events alone led to erosion rates that could locally exceed 7 mm in one month. In the Barronies, equally located in the Terres Noires, Lecompte et al. (1998) even reported values as high as 3.5 cm a^{-1} which are among the highest values reported globally (Burylo et al., 2014). Descroix and Mathys (2003) investigated erosion processes in the black marls of the Terres Noires and found that freeze-thaw and wet-dry cycles as well as the splash effect of rain are the main factors that cause rock disaggregation and generate a layer of highly erodible non-cohesive flakes of marls. Thus, erosion is higher on north facing slopes than on south facing slopes due to the higher number of freeze-thaw cycles. Further, the vegetation cover and the dip-slope angle influence local erosion rates (Descroix and Mathys, 2003).

At the outlets of small experimental catchments at Draix, solid fluxes are monitored since the 1980s and average suspended sediment yields range from $80\text{ t km}^{-2}\text{y}^{-1}$ at the Brusquet catchment (1.08 km^2 , 13 % bare surface) to $13600\text{ t km}^{-2}\text{y}^{-1}$ at the Roubine gully (drained surface of 1330 m^2 , 79 % bare surface). In the Galabre catchment average specific suspended sediment yield from 2007 – 2014 was estimated to be $666\text{ t km}^{-2}\text{y}^{-1}$ (Esteves et al., 2019, methodology described in Appendix A). This value is in the upper end of values obtained in other Mediterranean catchments (Table 2.1) and slightly above the median of values reported in badland catchments in the review by Nadal-Romero et al. (2011). It is also consistent with the results obtained by Vanmaercke et al. (2011) in Mediterranean and mountainous regions (Fig. 1.1). These results show that estimates of soil erosion and sediment yield depend strongly on the scale of the measurement.

Suspended sediment concentrations at the outlet were highly irregular and showed no clear seasonal tendency (Esteves et al., 2019). The maximum recorded value was 361 g l^{-1} in November 2012 (Esteves et al., 2019). Sus-

pended sediment discharge is also highly variable. Most of the events that lead to high values occur in late autumn or winter and early in summer (Fig. 2.11). The highest value of 1319 kg s^{-1} was reached in June 2010. The vast majority of solid discharge occurs in a small fraction of time during flood events. Navratil et al. (2011) found out, that 90 % of total suspended sediment yield passed the outlet in just 2 % of the time. This is coherent with the finding of Esteves et al. (2019) that the 30 events with highest suspended sediment yields accounted for 81 % of total suspended sediment yield in the 7-year study period. Single events could lead to more than 8000 t of sediment export in a few days.

When the intra-annual distributions of rainfall, discharge and sediment yield in the catchment are regarded, different periods of the year with distinct hydro-sedimentary processes can be differentiated (Fig. 2.11). In the beginning of the year, monthly sediment yield is very low despite high discharge. This indicates that transport capacity of the river is high but the availability of eroded material is limited. May and June represent a first peak in monthly yields. This can be associated to intense rain events that lead to extensive erosion (Esteves et al., 2019). During these events high suspended sediment concentrations are measured despite relatively low peak discharges. After that first period of high sediment exports, discharge decreases strongly in July and August, so there is a limited transport capacity especially of the intermittent network to transport eroded sediments. A second period of high sediment yield occurs in November and December when monthly values of precipitation and discharge increase strongly. Esteves et al. (2019) also assume that eroded particles that were not transported during the dry summer months get remobilized in autumn.

2.2.7 Data availability

Most of the hydro-meteo-sedimentary data set used here is presented in detail by Esteves et al. (2019). The data can be visualized and downloaded at <https://bdoh.irstea.fr/DRAIX/>. Thus, only a short summary of the data is given here.

Precipitation Since June 2008 rainfall is measured with an automatic tipping bucket rain gauge with a resolution of 0.254 mm per tip. The rain gauge is located at the hamlet of Ainac at the center of the catchment at an altitude of 1135 m . A second rain gauge was installed in August 2014 in La-Robine-sur-Galabre close to the outlet of the catchment. This tipping bucket rain gauge has a resolution of 0.1 mm per tip and a small weather station further measures air temperature and humidity as well as wind direction and speed at the same site. Operational rain gauges managed by Météo France are located in Thoard, Beaujeu and Digne-les-Bains at distances of 9.6 , 11.9 and 16.2 km respectively from the centroid of the catchment. Daily data is available from Thoard and Beaujeu and 6 min data is available at Digne. Further research rain gauges are located in the vicinity of the village of Draix at the outlet and the upper part of each of the other catchments monitored in the Draix-Bléone Observatory. They are located about 15 km to the east of the Galabre catchment.

Further, radar data is provided by Météo France (Météo France, 2018; Tabary, 2007). The three closest S band radars are located at Collobrières (111 km south of the catchment), Bollène (117 km to the west) and Nîmes (145 km to the west). However, due to the mountainous terrain and the high distance of the radar towers to the catchment, this data has to be treated carefully and we have to assume considerable errors in the quantitative precipitation estimates (Chapter 5.2). There are four X band radars located at distances of $32 - 83\text{ km}$ to the catchment centroid, but for the study period, this data has not yet been integrated into the available data yet.

Discharge and suspended sediment fluxes Liquid and solid fluxes are monitored since 2007 with the same instruments and sampling design as in the Claduègne catchment (Chapter 2.1.8). The stage-discharge rating curve was developed based on 35 discharge measurements with salt dilution and an electromagnetic current meter ranging from 0.017 to $0.948\text{ m}^3\text{ s}^{-1}$. This curve was extrapolated based on hydraulic modeling in HEC-RAS (Esteves et al., 2019). Turbidity was measured with a nephelometric turbidimeter and was transformed to suspended sediment concentrations and solid discharge as described in Appendix A. Suspended sediment samples were taken by automatic water samplers once thresholds of water level and turbidity were exceeded.

Spatial characterization data A digital elevation model at 1 *m* resolution is available ([IGN, 2018b](#)). A map of the geology is available at a scale of 1:50000 from the French Geological Survey BRGM and was used for the classification of the eroded zones. For land cover, the map at 10 *m* resolution provided by CESBIO ([Inglada et al., 2017](#); Fig. 2.9) was used. This land cover data was verified during field visits. While forests and grasslands were usually classified correctly, most of the bare surfaces were wrongly classified as urban land, mining land or dunes. Thus, the map shown in Fig. 2.9 was adapted to include the class “bare surfaces” with the patches of erosion zones delineated by [Legout et al. \(2013\)](#).

Chapter 3

High temporal resolution quantification of suspended sediment source contributions in two mesoscale Mediterranean catchments

3.1 Claduègne

The following chapter is based on the article “Comparing alternative tracing measurements and mixing models to fingerprint suspended sediment sources in a meso-scale Mediterranean catchment” by Magdalena Uber, Cédric Legout, Guillaume Nord, Christian Crouzet, François Demory and Jérôme Poulenard that was published in the *Journal of Soils and Sediments* in February 2019 ([Uber et al., 2019](#)). The article was slightly modified to avoid redundancies with previous chapters. In addition to the results presented in the article, a comparison of the alternative tracer sets with conventional fingerprinting with radionuclids is presented.

Abstract

Purpose Knowledge of suspended sediment provenance in mesoscale catchments is important for applying erosion control measures and best management practices as well as for understanding the processes controlling sediment transport in the critical zone. As suspended sediment fluxes are highly variable in time, particularly given the variability of soil and rainfall properties in mesoscale catchments, knowledge of sediment provenance at high temporal resolution is crucial.

Materials and methods Suspended sediment fluxes were analyzed at the outlet of a 42 km^2 Mediterranean catchment belonging to the French critical zone observatory network (OZCAR). Spatial origins of the suspended sediments were analyzed at high temporal resolution using low-cost analytical approaches (color tracers, X-ray fluorescence and magnetic susceptibility). As the measurements of magnetic susceptibility provide only one variable, they were used for cross-validation of the results obtained with the two alternative tracing methods. The comparison of the tracer sets and three mixing models (non-negative least squares, Bayesian mixing model SIMMR and partial least squares regression) allowed us to estimate different sources of errors inherent in sediment fingerprinting studies and to assess the challenges and opportunities of using these fingerprinting methods.

Results and discussion All tracer sets and mixing models could identify marly badlands as the main source of suspended sediments. However, the percentage of source contributions varied between 11 flood events in the catchment. The mean contribution of the badlands varied between 74 and 84 %, the one of topsoils on sedimentary geology ranged from 12 - 29 % and the one of basaltic topsoils from 1 - 8 %. While for some events the contribution remained constant, others showed a high within-event variability of the sediment provenance. Considerable differences in the predicted contributions were observed when different tracer sets (mean RMSE: 19.9 %) or mixing models (mean RMSE: 10.1 %) were used. Our result show that the choice of the tracer set was more important than the choice of the mixing model.

Conclusions These results highlighted the importance of using multi-tracer-multi-model approaches for sediment fingerprinting in order to obtain reliable

estimates of source contributions. As a given fingerprinting approach might be more sensitive to one type of error, i.e. source variability, particle size selectivity, multi-tracer ensemble predictions allow to detect and quantify these potential biases. High sampling resolution realized with low-cost methods is important to reveal within- and between event dynamics of sediment fluxes and to obtain reliable information of main contributing sources.

3.1.1 Introduction

Identifying the origins of suspended sediments and quantifying the contributions of different sources to sediment fluxes at the outlet of a catchment is important for efficient implementation of erosion control measures and mitigation strategies and to better understand the hydro-sedimentary processes (Chapter 1.2.3). In this chapter, we develop a sediment fingerprinting methodology that can be routinely applied on suspended sediment samples taken at a high resolution (within event scale) in the Claduègne catchment. In order to analyze a high number of samples it is necessary to use low-cost tracers. Here we use two tracer sets, i.e. X-ray fluorescence and spectrophotometry to quantify source contributions and a third one, i.e. magnetic tracers, to validate our results. By comparing different tracer sets, we estimate the error that is due to the choice of tracer set (Martínez-Carreras et al., 2010c; Evrard et al., 2013; Pulley et al., 2015). Furthermore, several authors have noted that different results are obtained with different mixing models (Haddadchi et al., 2013; Cooper et al., 2014; Laceby and Olley, 2015; Nosrati et al., 2018). However, these authors have compared Bayesian and frequentist mixing models that are all based on the same chemical mass balance approach. Here, we further include a third mixing model, based on partial least squares regression (PLSR), that is trained with artificial mixtures of known source contributions. In this way we assess the uncertainty due to the choice of mixing model with very contrasting model structures. We further quantify the errors due to source heterogeneity, particle size, biogeochemical alterations during immersion in the river and model structure.

Thus, the overall objective of this study is to quantify the contributions of the potential sediment sources identified in Chapter 2.1 to a high number of suspended sediment samples collected at the outlet of the Claduègne catchment and to assess the associated errors. As the area is prone to intense and highly variable rainfall that can lead to flash floods (Braud et al., 2014;

Nord et al., 2017), the hydro-sedimentary processes can change significantly between and within events. This motivated the use of low cost fingerprinting methods in combination with high resolution sampling to identify the variability of suspended sediment fluxes. The specific questions addressed in this study were: (i) whether low cost tracers could discriminate between major source of suspended sediments, (ii) to which extent the predicted proportions of source materials differ from mixing models and tracer sets, including associated errors and (iii) what were the variations of the source contributions between and within flood events that occurred during the 2011 - 2017 period in this Mediterranean mesoscale watershed?

3.1.2 Methods

3.1.2.1 Sampling

Source samples were collected at 56 locations in the Claduègne catchment (of which 21 are located in the nested Gazel catchment, Fig. 3.1). The sampling locations were chosen for accessibility and to represent the main variability of land use and soil types within each of the three groups assumed to contribute to the suspended sediment samples in the rivers, i.e. sedimentary badlands, bare soils on basaltic geology and bare soils on sedimentary geology. At each site 1 to 6 subsamples were taken within a radius of ca. 5 m. They were not combined in order to assess small-scale heterogeneity. In total, 178 subsamples were taken as surface scrapes of the top 3 - 5 cm with non-metallic shovels. 132 of them are taken in areas of the three potential sediment sources (Table 3.1). At the outlets of the Gazel and Claduègne catchments, suspended sediment samples are automatically taken every 10 and 40 minutes respectively once a threshold of turbidity and water level is exceeded. For this study 145 and 179 samples collected during 13 events between 2011 and 2017 in the Claduègne and Gazel catchments respectively are considered. For 27 suspended sediment samples taken during five events in the Claduègne catchment, grain size distributions were measured with a laser diffraction sizer (Malvern Mastersizer 2000) after ten min of sonication and stirring at maximum level in order to destroy aggregates (Grangeon et al., 2012). Source samples and suspended sediment samples were dried for 24 h at 105 °C, gently crushed and sieved to the particle size fraction < 63 μm.

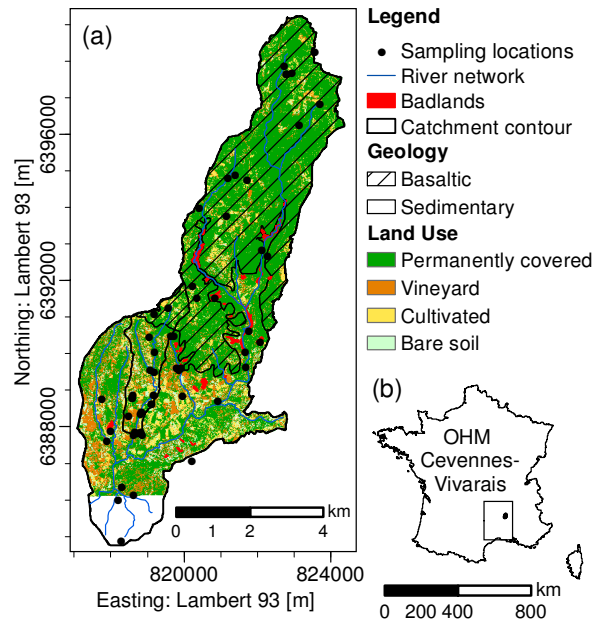


Figure 3.1: Study site: (a) Location of the 56 sampling sites of the source soil samples in the Claduègne catchment (42.3 km^2) and the nested Gazel catchment (3.4 km^2). The red polygons show the outline of the badlands that were digitized from satellite and aerial images. The geology can be roughly subdivided into the basaltic Coiron plateau in the north and Mesozoic sedimentary rocks (mainly marly-limestones) in the south. The land use data is based on quickbird satellite images (Andrieu, 2015). The class permanently covered comprises forests, permanent grasslands and heaths. (b) Location of the Cevennes-Vivarais Mediterranean Hydrometeorological Observatory (OHM) in France. The small dot represents the location of the Claduègne catchment.

3.1.2.2 Measurements of tracer properties

Spectrocolorimetry Color measurements were conducted using a portable diffuse reflectance spectrophotometer (Konica Minolta 2600d) that returns the reflectance spectra in the visible range between 360 and 740 nm in increments of 10 nm following Legout et al. (2013). For every sample the measurement was repeated three times after turning or shaking the tube in order to account for heterogeneity within the sample. The influence of sample quantity on the color tracers was assessed by repeating the measurement after increasing the sample quantity in the box and it was found that even sample quantities as low as 0.1 g barely influence the measurement. From the raw spectral data 15 color coefficients were calculated using the equations

Table 3.1: Numbers of samples measured and tests conducted for each analytic technique. Tracers in brackets are the ones that were discarded after the respective test.

	Spectro- colorimetry	XRF	Mineral magnetism
Number of samples:			
Source 1: Badlands	33	10	21
Source 2: Sedimentary soils	52	15	19
Source 3: Basaltic soils	27	11	10
Suspended sediments Claduègne	145	35	80
Suspended sediments Gazel	179	20	37
Artificial mixtures Claduègne	81	4	0
Artificial mixtures Gazel	81	0	0
Tests conducted:			
Kruskal Wallis test	✓(-)	✓(Co)	-
Linear Discriminant Analysis	✓	✓	-
Linear additivity	✓(-)	✓(P ₂ O ₅ , Cu, Y, Zr)	-
Range test	✓(-)	✓(P ₂ O ₅ , K ₂ O)	-
Convex hull range test	✓(-)	✓(Co, Zr)	-
Influence of particle size	✓	-	-
Influence of biogeochem. alterations	✓	-	-

given in [CIE, 2009](#). These include the xyz chromaticity coordinates, three parameters each of the L*a*b* color space and the Hunter Lab color space and 2 parameters each from the CIE 1976 UCS color diagram, the L*C*h* color space and the L*u*v* color space. Thus, in total 15 color coefficients were considered as color tracers.

X-Ray Fluorescence (XRF) The measurements were conducted with a portable Bruker Titan XRF analyzer. Using an internal calibration, the device automatically calculates the concentrations of Al₂O₃, SiO₂, P₂O₅, K₂O, CaO, TiO₂, V, MnO, Fe₂O₃, Co, Ni, Cu, Zn, Rb, Sr, Zr. To account for sample heterogeneity, the measurement was repeated three times for each sample turning the sample support 90° after each measurement. For practical reasons (availability of the measuring device and the higher sample quantity of about 1 g needed for XRF) only a subset of samples could be measured with XRF (Table 3.1).

Magnetic susceptibility Mineral magnetic properties were measured on a subset of 93 source samples and 126 suspended sediment samples at the

CEREGE laboratory (Aix Marseille University). For all samples specific low-field magnetic susceptibility X_{lf} was obtained from measurements with an AGICO MFK1-FA Kappabridge susceptibilimeter under a frequency of 976 Hz. The measured susceptibility was normalized using sample weight. X_{lf} values describe the ratio of the induced magnetization of a sample to the intensity of the magnetizing field. It is an indicator for the amount of ferromagnetic minerals (e.g. magnetite or hematite) present in a sample (Maher, 1986; Nizou et al., 2016). Mineral magnetic susceptibility was only used in this study to carry out a qualitative cross validation of the results obtained with the other two tracer sets.

3.1.2.3 Tests of assumptions

The ability of the different tracers to discriminate between the three source groups was tested with a Kruskal-Wallis test and by conducting linear discriminant analysis (LDA) using all tracers derived from each measuring technique (spectrocolorimetry or XRF).

In order to test the linear additivity of the tracers, 81 artificial mixtures with known proportions of the three source groups were prepared. First, for all the three sources, a composite sample was made from roughly equal contributions of many individual source samples from the respective group. This was well mixed and the artificial mixtures were prepared by mixing these three poles in known proportions as proposed in Legout et al. (2013). Spectrocolorimetric measurements were conducted on all the mixtures prepared as well as on the composite samples that represent the poles of 100% of any of the source classes. XRF measurements were only conducted on the three poles and four mixtures. The linear additivity of the tracer properties (15 color parameters for spectrocolorimetry tracers and 16 element concentrations for the XRF tracers) was quantified using the RMSE normalized with the mean of the measured tracer value.

A range test was conducted for every tracer property to check whether the suspended sediment samples were comprised within the range of the values measured for the source samples in order to detect problems concerning incomplete source sampling, conservative behavior of the tracers or linear additivity (Walden et al., 1997; Collins et al., 2017). A small tolerance of less than 5% of the mean of each tracer was applied and tracers for which the

range test was not passed were excluded from the mixing models. As outlined by Phillips et al. (2014), this univariate range test is a necessary but not a sufficient condition for mixing models to work. In order to ensure that the sediment samples can be represented as a combination of the sources, they also have to fall within the multi-dimensional convex hull spanned by the tracer values of the sources. Thus, a convex hull range test was additionally conducted by combining the tracer properties one-by-one, determining the 2d convex hull spanned by the sources and by checking whether the sediment samples lie within the hull.

In order to assess the influence of particle size on the color tracers, we sieved some source samples from the Claduègne catchment ($n = 14$, 4 badlands, 5 basaltic soils, 5 sedimentary soils) to the size fractions $> 500 \mu m$, $200 - 500 \mu m$, $100 - 200 \mu m$, $63 - 100 \mu m$, $40 - 63 \mu m$, $20 - 40 \mu m$ and $< 20 \mu m$. The spectrophotometry tracers were determined and compared for all these samples.

To evaluate the potential effect of biogeochemical alterations during transport and temporary storage, an in-situ biogeochemical experiment was conducted as described by Legout et al. (2013). Four composite samples of the $< 63 \mu m$ fraction of four to eleven individual samples from the same geology and land use (badland, cultivated fields on basalt, vineyard on sedimentary geology) were produced. Each one was divided into subsamples which were put into small bags of two layers of porous mesh with a mesh size of $20 \mu m$. Each subsample contained about $1 g$ of material. All bags were immersed in the river in April 2017 and after immersion times of 1, 3, 7 and 22 days two replicates of each composite sample were collected. No significant rainfall-runoff events occurred during the experiment. All subsamples were dried at $105^\circ C$ for $24 h$, gently crushed and weighed to check for weight loss. Spectrophotometric measurements were conducted and the influence of immersion time in the river on the color tracers was assessed by comparing the tracer values for the different immersion times.

3.1.2.4 Source quantification with mixing models

Non-negative least squares model (NNLS) For every sediment sample a system of linear equations based on a chemical mass balance can be set up as : $A \times c = s$ where $A_{(n \times m)}$ is the source matrix, m is the number

of sources and n is the number of tracers; $a_{i,j}$ being the matrix element giving the value of tracer j for source i . c is the unknown contribution vector that gives the contribution of each one of the m sources to the respective suspended sediment sample. s is the sediment sample vector that gives the measured values of the n tracers for the respective sediment sample. As this system of linear equations is usually overdetermined and there is no unique solution for c , it is approximated with the least squares method. In order to prevent the prediction of negative contributions, the model is constrained to non-negativity. The non-negative least squares (NNLS) algorithm implemented in the R function `nnls{nnls}` (Mullen and van Stokkum, 2015) following Lawson and Hanson (1974) was used. Besides the constraint for non-negativity, the model can also be constrained in a way that the sum of the predicted contributions adds up to 100%. In this study this constrained was not applied so that the test whether the contributions sum up to approximately 100% was used to detect problems in the fingerprinting approach.

Bayesian mixing model (SIMMR) The Bayesian mixing model implemented in the R package `simmr` (Stable Isotopes Mixing Models in R; Parnell, 2016) was used. It calculates a high number (default: $n = 10000$) of plausible solutions of source contributions to each sediment sample using Bayes theorem:

$$P(A|B) = \frac{P(B|A)P(A)}{P(B)} \quad (3.1)$$

where the posterior $P(A|B)$ is the contribution of a source to the sediment sample. The prior $P(A)$ is an initial guess of the contribution, which is randomly drawn from the Dirichlet distribution. Thus, the source contributions are independent from each other but sum up to 100%. B is the support knowledge that is provided to A and that is given by the measurements of the tracer properties for the sediment sample and the sources. The model is fitted with a Monte Carlo Markov Chain algorithm that produces plausible solutions for each source's contribution to each sediment sample (Parnell et al., 2010, 2013; Cooper et al., 2014). From these n realizations, the best estimate (mean or median) and an estimate for the uncertainty (standard deviation) can be derived.

Partial least squares regression mixing model (PLSR) PLSR is a multiple linear regression method that is commonly used in chemometrics for predicting a depended variable (response) from a set of predictor variables. Unlike other linear regression models, PLSR can deal with highly correlated, noisy and numerous predictor variables that are consequently not independent from each other and potentially redundant (Wold et al., 2001). Unlike the other two mixing models, the model is trained with artificial mixtures of known proportions of the possible sediment sources that were prepared as described in Chapter 3.1.2.3. As in Poulenard et al. (2012) and Legout et al. (2013), individual models were set up for each of three sources. In this way, the source contributions were not forced to sum up to 100 % for each sediment sample and the test whether or not that sum is close to 100 % allows to detect problems in the fingerprinting approach. The models were fitted in R with the function `pls` (Mevik et al., 2016) using six components. When applying the model to the color tracer set, the data set was split into a training and a testing data set (two thirds and one third of the data respectively) in order to check for overfitting and whether the model was able to predict the proportion of mixtures that were not used to set up the model. As the XRF measurements were only conducted on four artificial mixtures and the three poles, this validation step was not undertaken.

3.1.2.5 Error assessment

Source heterogeneity Source soil heterogeneity is treated differently in the three mixing models. Whereas it is smoothed out in the NNLS and PLSR mixing models, it is explicitly taken into account in the Bayesian SIMMR mixing model. The latter uses the mean and the standard deviation (sd) of each tracer property for each source as model input. Thus, for SIMMR the variability of model output is calculated and the mean of the sd obtained for all the sediment samples is given as an estimate of uncertainty due to source heterogeneity in every source category. In the NNLS mixing model, the source matrix A is initially parameterized with the mean of all samples in the respective source group for each tracer property. The potential error due to within-source group heterogeneity was assessed with a Monte-Carlo resampling algorithm (e.g. Franks and Rowan, 2000; Krause et al., 2003) using the sd of the predicted source contribution averaged over all suspended sediment samples as a measure of uncertainty due to source heterogeneity. In the PLSR mixing model source heterogeneity is also eliminated by creating

a composite sample of the source soils in the respective source category and using this composite for the creation of the artificial mixtures. Here, the potential error due to source heterogeneity is assessed by running the model on the source samples that belong unequivocally to one of the three source groups. Due to source heterogeneity, the signature of the individual samples will differ from the composite sample of the group. Hence, the predicted contributions will vary from 100 % or 0 % and the deviation of the predicted contribution from the real contribution (either 100 % or 0 %) was used to quantify this kind of error for each source:

$$\Delta_{sh} = \frac{1}{n} \sum_{i=1}^n |C_{real,i} - C_{pred,i}| \quad (3.2)$$

where n is the number of source samples in the respective source category, $C_{real,i}$ is the real source contribution and $C_{pred,i}$ is the predicted contribution of source category to the source sample i . In order to obtain a measure that is comparable between the three mixing models, this specific procedure is also applied with the NNLS and the SIMMR mixing models.

Tracer non-conservativeness: particle size None of the three mixing models takes this source of error into account. It was assessed for the three mixing models run with color tracers for the Claduègne catchment on the 14 source samples sieved to different particle size classes. The true contribution of the source categories was again either 100 % or 0 %. The deviation of the prediction of the fraction $< 63 \mu m$ from 100 % or 0 % was assumed to be due to source heterogeneity whereas particle size was assumed to be responsible of the deviation of the other size fractions from the fraction $< 63 \mu m$. In order to quantify this source of error in a way that allows for comparing between the mixing models, the difference between the $< 63 \mu m$ and the $< 20 \mu m$ fractions was calculated for every source category:

$$\Delta_{ps} = \frac{1}{n} \sum_{i=1}^n |C_{<63,i} - C_{<20,i}| \quad (3.3)$$

where n is the number of sources samples sieved to $< 20 \mu m$ in the respective source category, $C_{<63}$ is the predicted contribution of the source category to the fraction $< 63 \mu m$ and $C_{<20}$ the contribution to the fraction $< 20 \mu m$. The $< 20 \mu m$ fraction was chosen for this analysis, as this fraction

was found to be the dominant size class of the suspended sediment samples. The ratio of the fraction $< 20 \mu m$ to the fraction $< 63 \mu m$ ranged from 0.69 to 0.91 with a median of 0.78 for the 27 suspended sediment samples from the Claduègne where grain size distributions were measured.

Tracer non-conservativeness: biogeochemical alterations In order to quantify this source of error, the three mixing models run with the color tracers were applied to all the samples that were immersed in the river for different durations. The difference in predicted contributions before and after immersion in the river Δ_{bgc} was calculated for each source and each mixing model:

$$\Delta_{bgc} = \frac{1}{n} \sum_{i=1}^n |C_{0d,i} - C_{1d,i}| \quad (3.4)$$

where n is the number of samples for each source category, C_{0d} is the predicted contribution of the respective source to the composite sample before immersion in the river and C_{1d} is the predicted contribution after immersion in the river for 1 d . The immersion time of 1 d was chosen because it was found that the greatest change in tracer properties occurred already after 1 d whereas they remained stable afterwards. This is also the most likely maximum time of immersion in the river given the size of the catchment and the hydrological concentration time of a few hours.

Testing the mixing models with the artificial mixtures Besides their necessity for training the PLSR mixing model, the artificial mixtures were also used to test the predictive power of the three mixing models. The NNLS and the SIMMR mixing model were set up independently of the mixtures, so the models were tested on all mixtures (81 mixtures for color tracers, four mixtures and three poles for XRF tracers). For the PLSR mixing model the third of the mixtures that was not used for model training was used for testing it. The root mean squared error of the prediction RMSEP was calculated for each mixing model and each source from the known and the predicted proportions of the source classes.

3.1.3 Results

3.1.3.1 Verification of fingerprinting assumptions

Both tracer sets were able to discriminate between the three source groups. The main discriminating tracers were L^* , a^* and b^* for the spectrophotometry and Al_2O_3 , SiO_2 , CaO , Fe_2O_3 for XRF (Table B.1). When linear discriminant analysis was conducted with either all color tracers or all XRF tracers, all sources were correctly classified in the cross-validation.

With some exceptions, the linear additivity of the tracers was confirmed with the artificial mixtures. The normalized RMSE of the color tracers ranged between 0.2% and 6.3% and the one of the XRF tracers ranged between 1.1% and 16.8%. In the XRF tracer set the concentrations of P_2O_5 , Cu, Y and Zr had values for nRMSE > 10%. Because of this result, these four tracers were removed from the tracer set before the application of the mixing models.

When the univariate range test was conducted for the color tracers using only the source samples sieved to $< 63 \mu m$ the two color parameters L and L^* failed this range test. Thus, the univariate range test was repeated including the sources that were sieved to $< 20 \mu m$ which resulted in all color tracers passing the range test. Because of the results of the univariate range test, the samples $< 20 \mu m$ were included in the pairwise convex hull range test. When a small tolerance of $< 5\%$ of the range of each tracer was included in the test, all pairwise combinations passed the test. When the 16 XRF tracers were considered, the concentrations of P_2O_5 and K_2O did not pass the univariate range test with a tolerance of $< 5\%$ of the range. K_2O was removed from the tracer set in addition to P_2O_5 that was already excluded after the test for linear additivity. With the remaining 14 XRF tracers the pairwise convex hull range test was conducted. The combinations that did not pass the test were the following: Zr combined with 6 other concentrations and Co combined with SiO_2 . Thus, Zr and Co were discarded (Table 3.1).

Concerning the potential effect of particle size, the values of the L^* parameter decreased with increasing particle size in a relatively constant manner for the different samples (Fig. B.1). This effect could explain the fact that L^* failed the range test when considering source soil particles $< 63 \mu m$ while

it passed when source particles $< 20 \mu m$ were considered. This would suggest that the suspended sediment particles were enriched in particles $< 20 \mu m$ in comparison with the source soils, which was also consistent with the particle size measurements done on some suspended sediments (Chapter 3.1.2.1). For the a^* parameter the particle size effect was not systematic, notably for the badlands where the values were relatively independent of particle size. For only three tracers, h^* , u' and x , there was hardly any effect of particle size on the tracer values. While particle size affects some tracer values (e.g. L^* , L , b , v^*), others are less dependent on particle size which means that this effect might be smoothed as well as exacerbated in the final predictions performed on suspended sediment samples. Thus, the error that is introduced by this effect has to be assessed in the whole fingerprinting approach. This was quantified in Chapter 3.1.2.5 and taken into account in the interpretation of the results.

The in-situ biogeochemical experiment allowed analyzing the influence of immersion in the river on the color tracers. This effect was less important than the one of particle size. The changes were most important during the first day while all tracer values remained constant for longer immersion times. Even if the maximum immersion duration did not last more than 22 days, this is reassuring that the longest storage durations in the river did not affect the color parameters. The changes on the first day might also be due to the loss of fine particles through the bags with mesh size of $20 \mu m$. However, weight loss of the bags remained very small with values ranging from 0.5 to 3%. Weight loss did not increase with immersion time, so it occurred already during the first day. The impact of immersion on the tracers varied for the samples and the parameters. The basaltic samples changed most while the impact was least for the badlands. The most sensitive parameters were b , u^* and v^* but none of the parameters changed more than 10% for any sample and the median changes were $< 4\%$ for all parameters.

3.1.3.2 Comparison of the mixing models

As a first step the three mixing models were run with the two tracer sets on the artificial mixtures in order to calculate the contributions of the three sources basaltic bare soils, sedimentary bare soils and marly badlands. The models performed relatively well and could reproduce the known source contributions with RMSE below 7% source contribution with the exception of

the SIMMR model run with XRF tracers (Fig. B.2). This model failed to correctly reproduce the source contributions of mixtures with a high contribution of the sedimentary source, which were falsely predicted as a mixture of badlands and sedimentary sources.

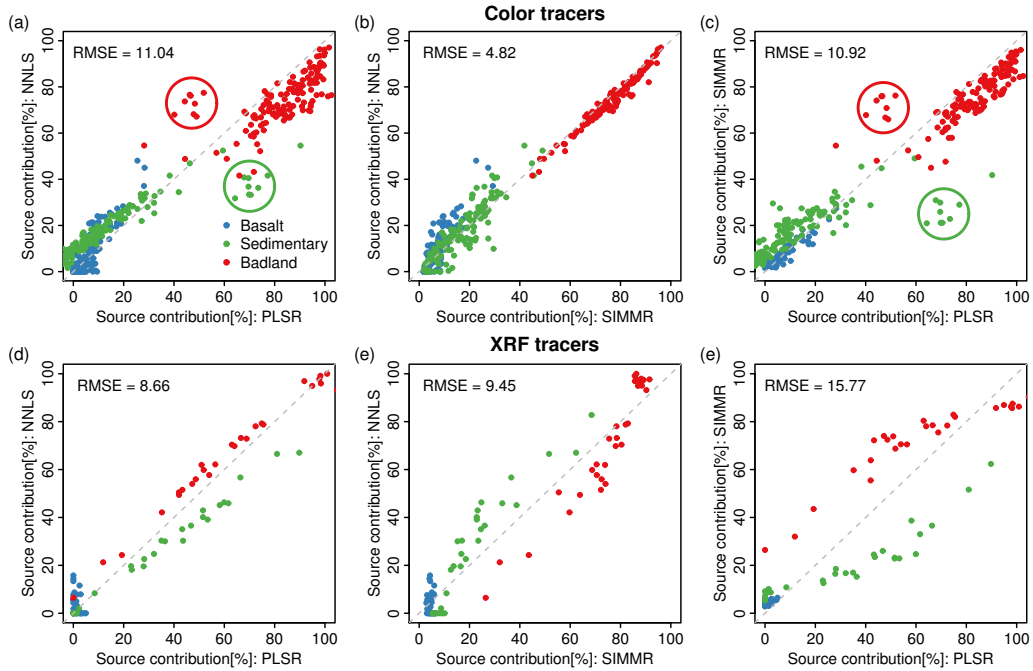


Figure 3.2: Comparison of the source contributions (in percent) to suspended sediment samples ($n = 145$ for spectrocolorimetry, $n = 35$ for XRF) from the Claduègne catchment predicted with color tracers (a – c) or XRF tracers (d – e) and different mixing models (NNLS: non-negative least squares, SIMMR: Bayesian stable isotope mixing model in R, PLSR: partial least squares regression). The encircled samples represent suspended sediment samples taken during the event of August 19th, 2014.

When the models were applied to the 145 suspended sediment samples this error increased (Fig. 3.2). Using color tracers, the SIMMR and the NNLS mixing model gave very similar results (Fig. 3.2b, RMSE of 4.8%). They agree on the mean source contributions and the correlations were high for all three sources. Also the results obtained with PLSR agreed well with the other two models with the exception of the flood event that occurred on August 19th, 2014 (Fig. 3.2a and 3.2c, RMSE of 8.2% and 9.5% when these samples were not included). Using XRF tracers, all three mixing models

agreed that the contribution of the basaltic sources to the suspended sediment samples in the Claduègne catchment was very low ($< 10\%$). The NNLS and SIMMR mixing model further agreed that the badlands were the dominant source and the two models correlated very well for the sedimentary and badland sources (Fig. 3.2e). The PLSR mixing model predicted approximately the same mean contribution of the sedimentary and the badland sources. Thus, there was a systematic difference between the results obtained with the PLSR mixing model and the other two models in so far that the two latter models predicted a considerably higher contribution of the badlands and a lower contribution of the sedimentary sources. There was, however, a high correlation between the results obtained with PLSR and with the other two models for the badland and sedimentary sources (Fig. 3.2d and 3.2f) so the within and between event dynamics of the source contribution were similar for all three mixing models.

3.1.3.3 Comparison of the tracer sets

In order to assess the effect of the choice of tracer sets on predicted source contributions, the results obtained with the two tracer sets were first compared for the artificial mixtures and then for the suspended sediment samples of the Claduègne (Fig. 3.3).

As the models performed well on the artificial mixtures, the tracer sets agreed on the predicted source contributions of the artificial mixtures when the NNLS and the PLSR mixing model were used (Fig 3.3a and 3.3c). With the SIMMR mixing model there were considerable differences between the two tracer sets (Fig. 3.3b) due to the bad performance of the SIMMR model driven with XRF tracers.

The differences in the predicted source contributions were much more pronounced when the suspended sediment samples were considered instead of the artificial mixtures. The correlations of the predicted contributions of the badlands were poor for all models and the mean RMSE was high (Fig. 3.3d to f). For the sedimentary sources the correlations were also poor and there was also a high mean RMSE of 22%. Using the PLSR model, the predictions obtained with the XRF tracers were systematically higher than the ones obtained with the with the color tracers. The mean RMSE for the basaltic samples was 9%, but considering the low predicted contributions of

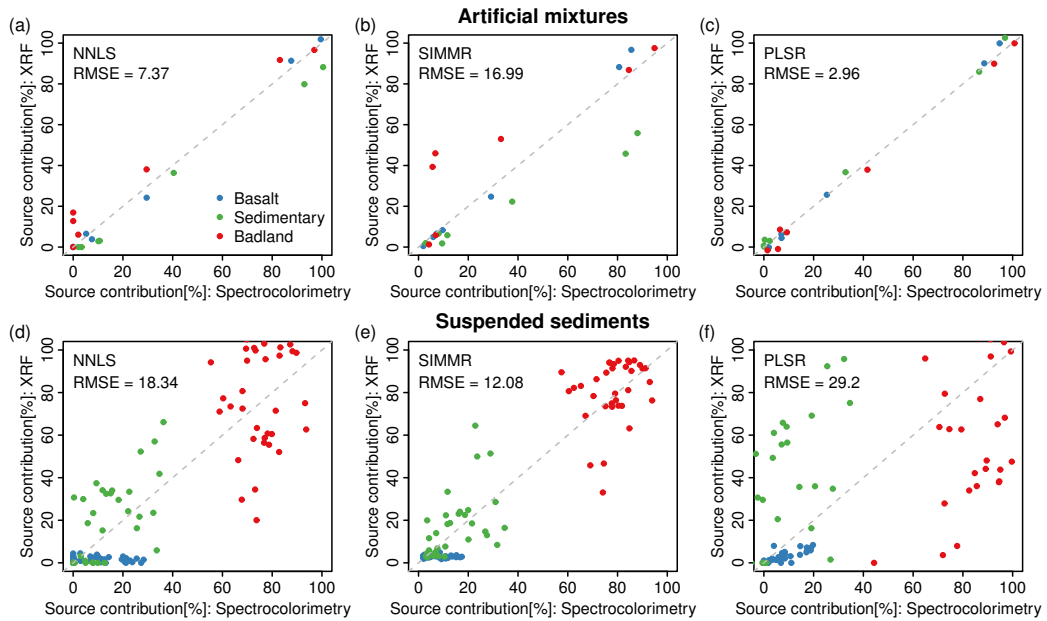


Figure 3.3: Correlations of predicted source contributions of the artificial mixtures (a to c) and the suspended sediment samples of the Claduègne catchment (d to f) using the same mixing model but different sets of tracers (color tracers or XRF tracers). The grey dashed line is the identity line.

the basaltic sources this value was large. There was some correlation between the two tracer sets when the PLSR model was used, but also a systematic difference in so far that the contributions predicted with the XRF tracers were always lower than the ones obtained with the color tracers. The poor correlations of the results obtained with the two tracer sets led to the within and between event dynamics being represented differently depending on which tracer set was used (Fig. 3.4).

Despite the poor accordance of the color tracers and the XRF tracers for single suspended sediment samples and the different prediction of within and between event dynamics, the two tracer sets agreed that the badlands were the main source of suspended sediment and that the contributions of the basaltic and sedimentary sources were rather small for that specific rainfall runoff event.

Owing to the large differences of the results obtained with the two tracer

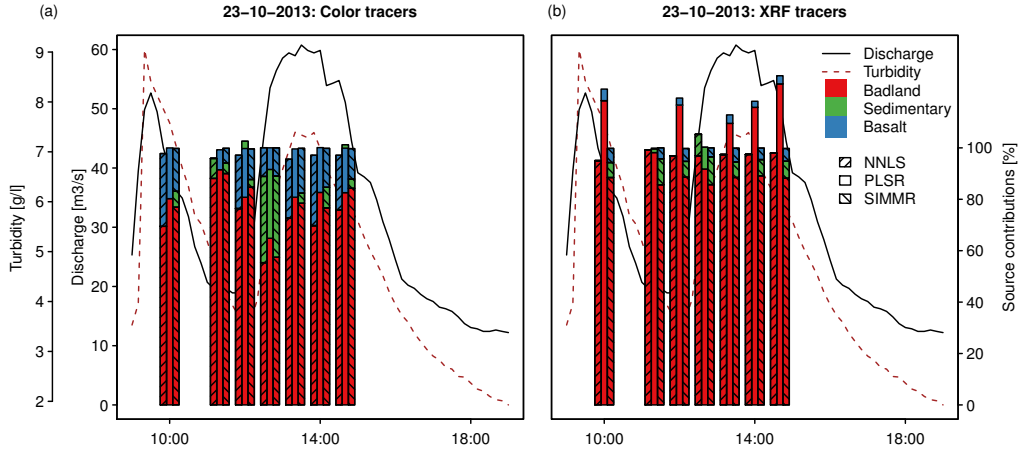


Figure 3.4: Time series of discharge and raw turbidity [$gl^{-1} SiO_2$] for a flood in 2013. The colored bars represent the source contributions of the suspended sediment samples predicted with the three mixing models using either the color tracers (a) or the XRF tracers (b).

sets, particularly for the basaltic contributions (from 5 to 10% on average for color tracers, from 0 to 2% for XRF), the measurements of magnetic susceptibility were used in order to assess in which tracer set to trust more. If the sediments really originated almost exclusively from the badlands, the values for X_{lf} measured for these suspended sediment samples should be close to the values measured in the badlands (mean \pm sd: $5.39 \pm 4.03 \cdot 10^{-8} m^3 kg^{-1}$, Table B.1). The measured values of the sediment samples of this event ranged from 19 to $88 \cdot 10^{-8} m^3 kg^{-1}$, with a mean and standard deviation of 57 and $19 \cdot 10^{-8} m^3 kg^{-1}$, respectively. Thus, they were considerably higher than the values of the badland source, slightly smaller than the values of the sedimentary sources ($75.92 \pm 79.40 \cdot 10^{-8} m^3 kg^{-1}$) and orders of magnitude smaller than the basaltic sources ($1323 \pm 551 \cdot 10^{-8} m^3 kg^{-1}$).

In order to assess more quantitatively the relation between predicted source contributions obtained with the two tracer sets and the X_{lf} values, X_{lf} was calculated as $X_{lf,calc} = \sum_{i=1}^s (X_{lf,source\ mean_i} \cdot c_i)$, where s is the number of sources ($s = 3$), $X_{lf,source\ mean_i}$ is the mean of the measured X_{lf} values of source i (Table B.1), and c_i is the contribution of source i predicted with the respective model. This was done with the three mixing models for the 35 sediment samples for which X_{lf} , XRF tracers and color tracers were

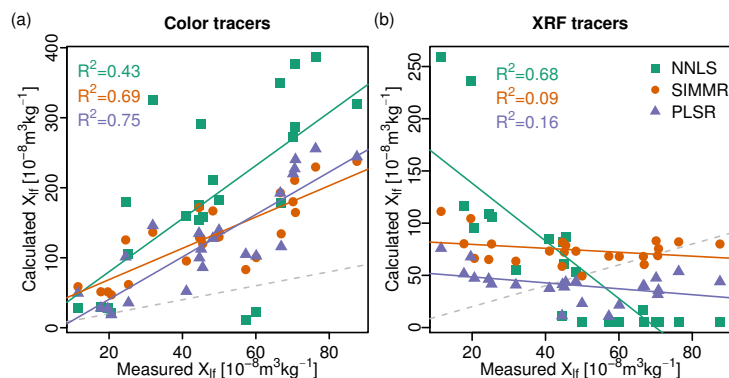


Figure 3.5: Calculated magnetic susceptibility (X_{lf}) of suspended sediment samples ($n = 23$) against measured ones. The calculated values were obtained using the predicted source contributions when using the color tracer set (a) or the XRF tracer set (b) and the different mixing models. The grey dashed line is the identity line.

available. The calculated values were compared to the measured values (Fig. 3.5). When the XRF tracers were used, the measured and the calculated X_{lf} values were either not correlated at all (SIMMR and PLSR mixing models) or even negatively correlated (NNLS model) which is not plausible at all (Fig. 3.5b). The correlations were better when the color tracers were used (Fig. 3.5a), especially with the PLSR model, indicating that the relation between the measured X_{lf} values of the sediment samples and the source contributions predicted with the mixing models were more plausible. However, the systematic overestimation of calculated X_{lf} values in Fig. 3.5a might be due to non-conservativeness (e.g. oxidation of magnetite present in the basaltic source leading to lower measured magnetic susceptibility) or non-additivity of the tracer or to a wrong estimation of the mean value for each source. The latter is certainly possible given the high within source variability. This is especially pronounced for the basaltic source where the natural variability of this parameter is the same order of magnitude as the one resulting from the variations of concentration. A further factor is the large difference (two orders of magnitude) between the measured values for basalts and the other sources.

Given the ambiguous results obtained with the alternative tracer sets, the source contributions with the spectral tracers, i.e. Color and XRF tracers were also compared to those predicted with conventional fingerprinting using radionuclid tracers (see Appendix B.2 for a description of the methodology

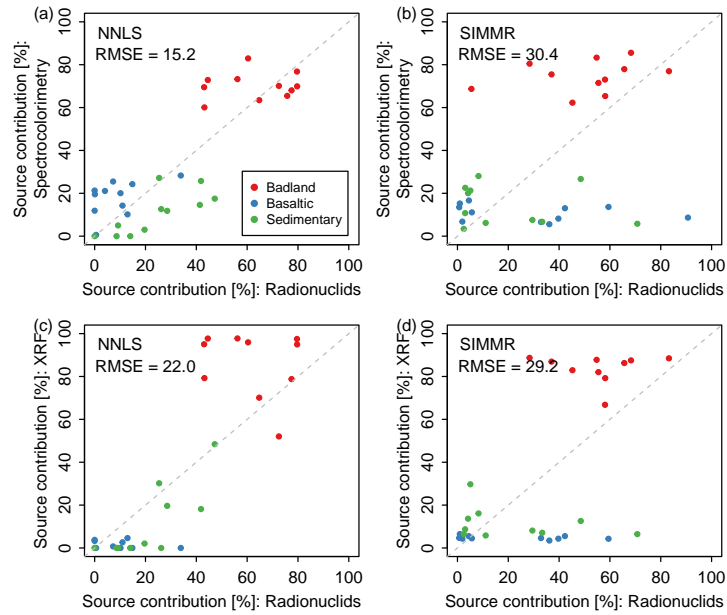


Figure 3.6: Comparison of predicted source contributions of suspended sediment samples obtained with spectral tracers (Color or XRF tracers) and with radionuclids (see Appendix B.2)

and further results). Figure 3.6 shows that there is a high scatter from the line of identity for both tracer sets as well as for the two mixing models NNLS and SIMMR. The agreement was best for the NNLS model run with color tracers and radionuclids (Fig. 3.6a) but the RMSE of 15.2% source contribution remained high but in the order of what should be considered as typical acceptable errors in fingerprinting studies. When the SIMMR mixing model was run with radionuclid tracers, high contributions of basaltic sources were predicted for single sediment samples. It has to be noted, that the number of source samples that were used to construct the models was much lower for the radionuclid tracer set ($n = 9$) than with the color ($n = 112$) and XRF tracers ($n = 36$).

3.1.3.4 Errors of the fingerprinting approaches

Errors due to source heterogeneity, tracer conservativeness and model structure were quantified as described in Chapter 3.1.2.5 and summed up in Table 3.2. For all three groups the errors varied strongly between tracer sets, mixing

models and sources.

Table 3.2: Estimates of error (in % source contribution) of the three mixing models applied with the color and XRF tracers. a) Calculated as described in Chapter 3.1.2.5, b) See Chapter 3.1.2.5, Eq. 3.2, c) See Chapter 3.1.2.5, Eq. 3.3, d) See Chapter 3.1.2.5, Eq. 3.4, e) Because the PLSR model driven with XRF tracers was calibrated only on 7 artificial mixtures, the data set was not split into training and testing data; the RMSE of leave-one-out cross-validation is given instead of the RMSE of the prediction.

		NNLS			SIMMR			PLSR		
		Badland	Sediment	Basalt	Badland	Sediment	Basalt	Badland	Sediment	Basalt
Color tracers										
Source heterogeneity	Mean SD ^{a)}	4.5	6.3	5.3	2.2	3.0	2.1	NA	NA	NA
	Δ_{sh} ^{b)}	3.3	13.2	6.3	3.3	18.4	13.7	4.2	13.2	17.5
Particle size	Δ_{ps} ^{c)}	17.6	19.5	9.0	15.9	14.0	12.1	11.8	13.1	35.4
Biogeochem. alterations	Δ_{bgc} ^{d)}	3.3	2.7	2.5	0.2	3.4	2.9	1.3	4.9	10.4
Verif. artif. mixtures	RMSEP	8.1	7.8	3.9	5.7	6.0	4.7	3.7	4.7	1.8
XRF tracers										
Source heterogeneity	Mean SD	18.4	16.9	3.9	8.8	9.0	1.6	NA	NA	NA
	Δ_{sh}	6.8	18.7	5.3	4.4	40.3	6.7	11.7	21.2	20.3
Verif. artif. mixtures	RMSEP	7.6	4.8	5.5	25.7	29.3	5.1	1.0 ^{e)}	1.3 ^{e)}	0.3 ^{e)}

Source heterogeneity Comparing the error due to source heterogeneity between the two tracer sets showed that the one of the XRF tracers was higher than the one of the color tracers with the exception of the basaltic sources. When the sources were compared, it can be seen that source heterogeneity was generally most pronounced in the sedimentary bare soils and smallest in the badland samples. The source heterogeneity of the basaltic sources varied between the mixing models. They could be unambiguously differentiated from the other sources but they were also a highly variable source (Table B.1). The PLSR mixing model seemed to be more sensitive to this within-source variability than the other two models as Δ_{sh} was high for both catchments and both tracer sets (Table 3.2).

Tracer conservativeness The impact of immersion in the water on the predicted source contributions was small ($\Delta_{bgc} < 5\%$) with the exception of the contribution of basalt predicted with the PLSR model (Table 3.2). Here, the difference in the predicted source contribution between the sample immersed for 1 d and the original one was $> 10\%$. A particular susceptibility of the basaltic samples to changes in the source prediction on immersion in the river was not confirmed by the other models, however.

The effect of particle size selectivity on the predicted source contributions was much more important than the one of biogeochemical alterations upon immersion in the river as Δ_{ps} was much higher than Δ_{bgc} for all sources and all mixing models (Table 3.2). The mixing models did not agree whether one source was particularly susceptible to the effect of particle size, but almost all values for Δ_{ps} were $> 10\%$ and could be up to $> 35\%$ for the basaltic sources predicted with the PLSR mixing model. This was also coherent with the need to including fine source material ($< 20 \mu m$) in the range test. Thus, knowing that the sediments are enriched in fine material, source contributions predicted for the sediment samples can be systematically over- or underestimated.

Model structure The error of the mixing models was quantified with the RMSE of the prediction of the artificial mixtures. When the color tracers were used all models perform well on predicting the contributions of the three sources with RMSEP $< 10\%$ for all sources and models (Table 3.2). The PLSR Model that was trained on two thirds of the artificial mixtures performed especially well on the remaining third of the data (RMSEP $< 5\%$ for all sources). Using the XRF tracers, the SIMMR model failed to correctly predict the source contributions of the mixtures, notably the one of the sedimentary sources.

Errors of the NNLS and PLSR model were also evaluated by summing up the predicted source contributions and checking whether the sum was close to 100%. Using the color tracers and the NNLS model, the sum of the predicted contributions of none of the suspended sediment samples and none of the artificial mixtures exceeded 110% or was below 90%. The PLSR model performed slightly worse with 9 out of 145 suspended sediment samples summing up to 110 – 120% but still the majority of the samples summed up to values very close to 100%. Using the XRF tracers, both models performed equally well in the Claduègne catchment and on the artificial mixtures.

3.1.4 Discussion

3.1.4.1 Performance and errors of the various fingerprinting approaches

Significant differences in predicting source contributions were put forward in this study due to the choice of tracers (Fig. 3.3) and models (Fig. 3.2). Such findings were already reported in a few studies. Concerning the choice of a tracer set, [Martínez-Carreras et al. \(2010c,b\)](#) and [Evrard et al. \(2013\)](#) found that alternative tracers (Color tracers and diffuse reflectance infrared Fourier transform spectroscopy) and conventional tracers did not agree on the main sediment source in all cases. [Pulley et al. \(2015\)](#) compared fingerprinting results obtained with magnetic tracers, geochemical tracers, radionuclides and combinations of these groups and found very important variations in mean contributions of three sources.

Concerning the choice of mixing model, the result that the NNLS and the SIMMR model generally resembled each other while the PLSR differed from the other two models is not surprising as it has a fundamentally different model set up. The NNLS and the SIMMR mixing model are both based on a mass balance approach, seeking to solve the same overdetermined system of linear equations while the PLSR model is based on artificial mixtures. While some studies already performed some comparisons between mixing models, these latter were only done for approaches similar to NNLS and SIMMR. [Cooper et al. \(2014\)](#) and [Nosrati et al. \(2014\)](#) obtained considerable differences in mean source contributions and in the widths of confidence intervals using different mixing models. [Haddadchi et al. \(2013\)](#) compared several variants of the NNLS mixing model and observed high differences in the source contributions predicted in two catchments. Thus, the comparison done in this study, adding a third mixing model with a different approach (i.e. artificial mixtures combined to PLSR), suggests that the differences in the prediction of source contributions due to the choice of a mixing model might be more important than the differences reported in the recent literature.

Among the various sources of errors considered in this study, the ones due to source heterogeneity and particle size were the most important ones. The high source heterogeneity of the sedimentary sources was an expected

result as they are very heterogeneous both in terms of land use and soil type. Moreover, some soils are poorly developed and might resemble the badlands. Soils close to the basaltic plateau or the soils on pebble deposit of basaltic component might contain basaltic elements. The lower source heterogeneity in the badland samples was not surprising either, as the badlands could be clearly distinguished from the other sources and resemble each other. Δ_{sh} , i.e. the measure of error due to source heterogeneity introduced here, is an effective measure to quantify this effect regardless of the mixing model and was found to be significant.

The observation that particle size effects were more important than the ones of biogeochemical alterations is consistent with the results obtained by [Legout et al. \(2013\)](#) who also quantified both effects. Both effects were found to be in the same order as the results obtained by these authors. The error due to biogeochemical alteration during immersion in the river was considered negligible when compared to the other sources of error. The sufficiently conservative behavior of color tracers and tracers from the infrared spectrum upon immersion in another Mediterranean river was also demonstrated by [Legout et al. \(2013\)](#) and [Poulenard et al. \(2012\)](#). This is promising and justifies the application of the sediment fingerprinting approach in our study site. In larger catchments, however, where longer storage durations in the river bed have to be assumed, this source of error can be important ([Vale, 2016](#)). The Error of the model structure that was quantified as the RMSE of the prediction varied strongly between the models and the sources.

It should be stressed that the different errors estimated in this study were not completely independent from each other, e.g. the failure of the SIMMR model driven with the XRF tracers to reproduce the sedimentary sources was reflected in Δ_{sh} and in the RMSEP that were both high for this model. Thus, the different sources of error could not be summed up to obtain a cumulative error. For the majority of the models and sources the maximum estimated error was below 20 %. For some models and concerning cumulative errors, however, this value could be exceeded. Many sediment fingerprinting studies only give the mean sd or other measures for dispersion in the obtained solutions as estimations of the error. The results obtained here indicated that this value was often rather small when compared to other sources of error, so the overall error of the fingerprinting approach is likely to be underestimated. Moreover, it did not include other sources of error than model structure and

source heterogeneity. Here, the most notable was the one due to particle size selectivity during erosion and sediment transport that creates systematic errors (over- or underestimation of source contributions).

These results also emphasized the importance to validate mixing models with artificial mixtures, to further address particle size issues and to carefully assess different sources of error. Another simple control procedure proposed by Poulénard et al. (2012) and successfully applied by Legout et al. (2013) and in this study is to not constrain the mixing model to sum up to 100%. This allows detecting problems associated to missing sources or uncertainty introduced during erosion processes and sediment transport. In our study this test was reassuring as it suggested that all relevant sources were sampled and that the errors discussed above did not lead to the prediction of completely unrealistic source contributions.

As the sensitivity of the mixing models and tracer sets to the different types of error was very heterogeneous, using only one tracer set and one mixing model could give faulty results that are biased by a certain source of error. Thus, this study highlights that there is a strong interest to compare different tracer sets and models and to use multi-tracer/multi-model ensemble predictions to obtain more robust results.

3.1.4.2 Interests of using multi-tracer-model ensemble predictions to detect main sources, within- and between event variability in a mesoscale catchment

Main sources In the Claduègne catchment all mixing models and tracer sets agreed that the badlands were the main source of suspended sediment sampled at the outlet (Fig. 3.7a). The contributions of this source averaged over eleven events from 2011 to 2017 ranged between 74 and 84% depending on the mixing model and the tracer set used. They also agreed that the mean contributions of the basaltic sources were small (1 - 8%) and the ones of the sedimentary sources ranged between 12 and 29%.

In order to assess to which extent the fingerprinting approach designed at the mesoscale of the 42 km² Claduègne catchment would be able to work correctly in a smaller sub-catchment, we applied the 6 model/tracers combinations to the suspended sediment collected at the outlet of the Gazel (3 km²). As the Gazel sub-catchment comprised no sedimentary badland ar-

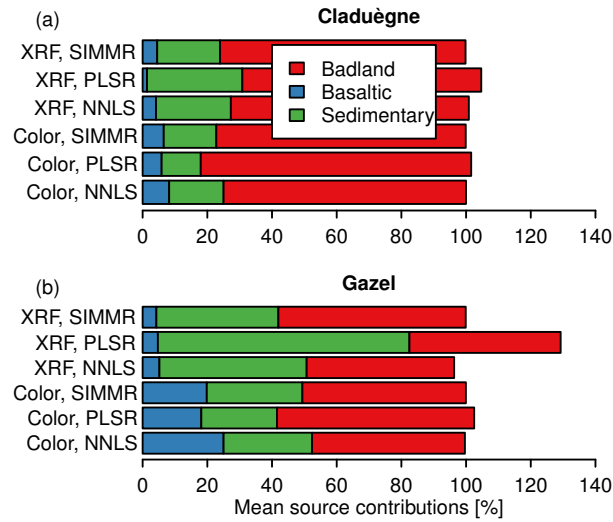


Figure 3.7: Mean source contributions of the suspended sediment samples of the Claduègne (a) and Gazel (b) catchments.

eas (Fig. 3.1), it was expected that the sediment samples were constituted of a mixture of the basaltic and the sedimentary samples. As can be seen in Fig. 3.7b this was not the case at first sight. Even though the predicted mean source contributions of the sedimentary badland source were smaller than in the Claduègne catchment, the badlands remained the main predicted source for five of the six ensemble predictions. This perturbing finding was a good example of fingerprinting approaches giving results that apparently contradict to physical reasoning without necessarily hinting at problems in the model set up. Indeed, the sum of contributions was close to 100% for these five ensemble predictions. Only one of them, the XRF-PLSR, predicted mainly sedimentary sources with sum of mean predicted source contributions exceeding 100% considerably. Out of the 20 tested suspended sediment samples the sum exceeded 110% for ten samples and was higher than 140% for eight samples with a maximum of 189%. The fact that one prediction differs significantly from the others emphasized the need of multi-model and multi-trace approaches as it can help to detect problems in the overall fingerprinting approach.

In order to understand the perturbing finding of sedimentary badlands being predicted in the suspended sediments of the Gazel despite their ab-

sence in the catchment, the catchment had to be regarded in detail. In some reaches, the riverbed is deeply incised into the marly-calcareous rocks. The thin erodible strata of marls could represent a highly connected source of fine material. Even though this source is very small in area, it might be an important sediment source. Thus, for the Gazel catchment, new mixing models were set up with the three sources (basaltic bare topsoils, sedimentary bare topsoils and eroded riverbanks in marly-calcareous rocks). The methodology used was identical to the one of the Claduègne and the estimates of the error were in the same order as the ones reported for the Claduègne catchment. Also the comparison of mixing models and tracer sets gave similar results.

The results of the mean source contributions predicted by these new models are shown in Fig. 3.8. A first striking result is that the new predicted proportions were not so different from those predicted initially in Fig. 3.7b, considering that badland contributions were replaced in similar proportions by marly calcareous eroded riverbanks. This result is consistent with the fact that the mean colorimetric signatures for eroded riverbanks (e.g. $L^*=61.44$, $a^*=2.88$, $b^*=14.91$) were almost identical as those for sedimentary badlands shown in Table B.1. This was also the case, albeit to a lesser extent for XRF tracers (e.g. $\text{CaO}=23.08$, $\text{Fe}_2\text{O}_3=1.51$). A second aspect is that there were some discrepancies in the prediction of source proportions ($< 20\%$) between the tracer sets. With the color tracers, the eroded riverbanks were predicted to be the main source of suspended sediments ranging from 48 - 65 %. With the XRF tracers the mean contribution of this source was predicted to be lower and similar to the mean contribution of the sedimentary sources (49 - 51 %). The mean contribution of the basaltic sources also varied between the two tracer sets. With the color tracers it ranged between 21 and 30 %, i.e. higher than the contribution of the sedimentary samples, while it was much lower with the XRF tracers (6 - 9 %). These absolute differences of less than 20 % on average have to be considered in the interpretation of the fingerprinting results, suggesting again the need to perform ensemble predictions obtained from various tracer sets and mixing models approaches.

Of course, the source class eroded riverbank on marly-calcareous rock is also present in the Claduègne catchment. As the fingerprinting properties of this class were very similar to the ones of the sedimentary badlands, the two classes could not be discriminated and the contribution of riverbanks were included in the badland source but were assumed to be of minor importance

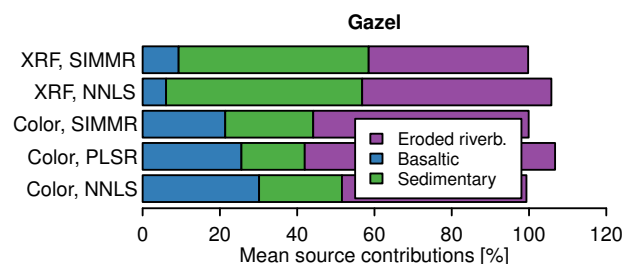


Figure 3.8: Mean source contributions of the suspended sediment samples of the Gazel catchment.

given their small extend compared to the badland areas. The finding that the badlands were the main contributing source for the Claduègne catchment despite their small area was consistent with the results of [Brosinsky et al. \(2014b\)](#) and [Palazón et al. \(2016\)](#). These latter found that the badlands, which cover less than 1 % of the surface of the Barasona reservoir catchment in the Spanish Pyrenees, were the main contributing source of suspended sediments in the reservoir. Given the high erodibility and good connectivity of this source this result was not surprising. The low contribution of the basaltic sources to the suspended sediments of the Claduègne catchment despite the large surface of this source, suggested either a low erodibility of these soils or a lower connectivity of the erosion zones to the river network.

Within and between event variability Figure 3.9 shows the mean predicted source contributions for eleven floods in the Claduègne catchment obtained with the different mixing models. The contributions of all three sources varied between events but there was no apparent seasonal variability. The between event variability seemed to be much higher when the XRF tracers were used than with the color tracers. This might, however, be an effect of sample size as much less samples were analyzed with XRF, so within event variability could not be evened out as much as with the color tracers. Indeed, looking only at events for which the sample size was more than five led to results that were more consistent between color and XRF tracers.

The event occurring on August 19th, 2014 stood out for the high predicted contribution of the sedimentary sources especially when the PLSR model or the XRF tracers were used. This might have been an indicator of distinct rainfall characteristics. It was indeed the only summer storm considered here

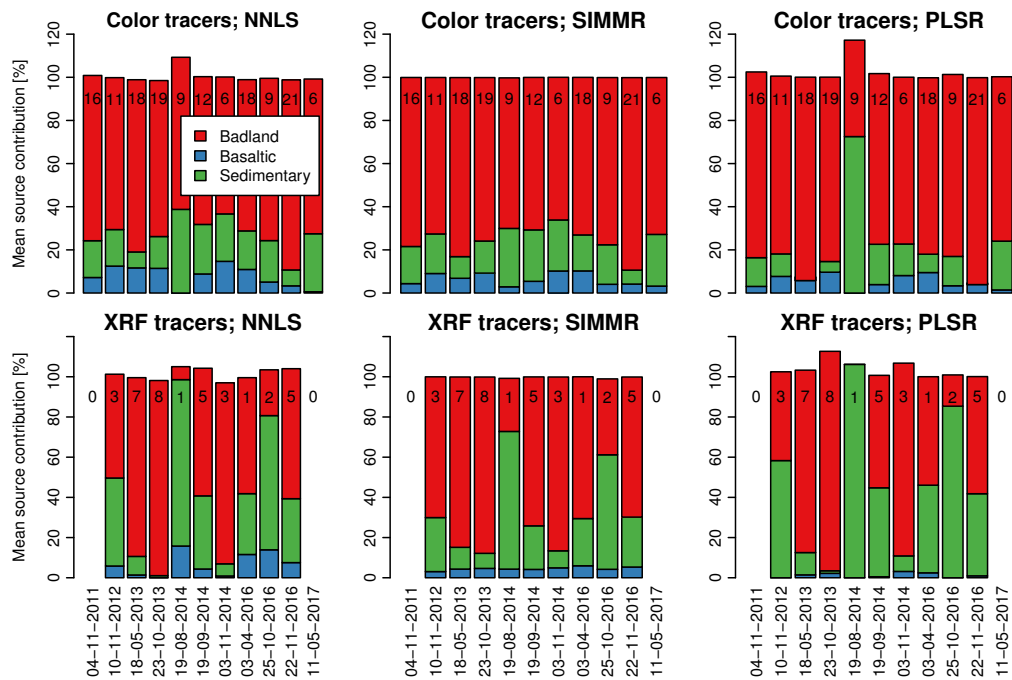


Figure 3.9: Between event variability. Mean source contributions for eleven events in the Claduègne catchment predicted with the color tracers (top row), the XRF tracers (bottom row) and the three mixing models. The numbers in the upper part of the bar give the number of samples analyzed per event.

while the other events were occurring in autumn or spring. However, this event was also the one that performed worst in the test whether the sum of contributions was close to 100 % and it was already identified as an outlier in the accordance of the mixing models (Fig. 3.2). This might point to problems with the PLSR mixing model driven with color tracers during this event.

The within event variability was very different between events. While for some events the source contributions were very similar for all samples (11-05-2017 in Fig. 3.10b or 23-10-2013 in Fig. 3.4), they varied a lot between samples for other events. Out of the eleven events in the Claduègne catchment considered here, five had a very low within event variability, while the remaining six had a higher within event variability such as in Fig. 3.10a.

Differences in within event variability of source contributions were also

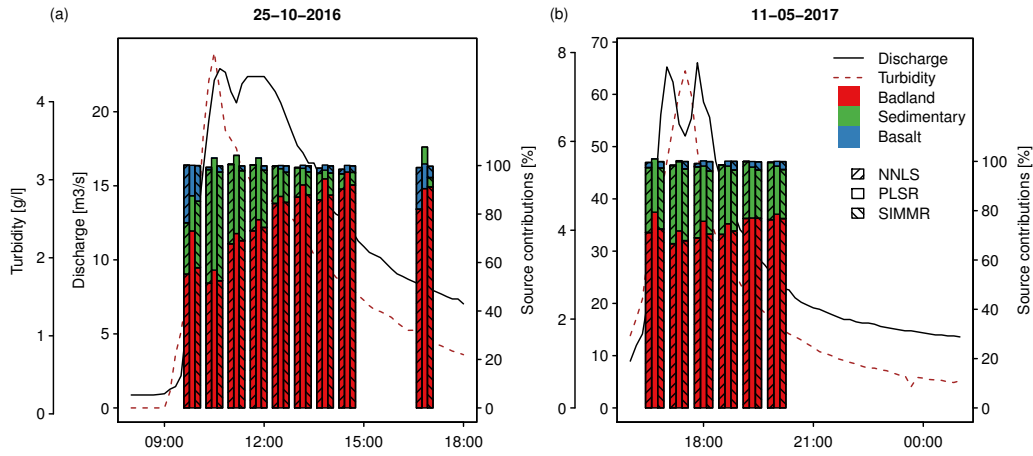


Figure 3.10: Within event dynamic of the source contributions predicted with the color tracers during two floods in the Claduègne catchment.

observed in other studies that conducted sediment fingerprinting at a high resolution. [Brosinsky et al. \(2014b\)](#) found a very high within-event variability for one out of four events in a catchment in the Spanish Pyrenees (445 km^2). [Legout et al. \(2013\)](#) classified 23 rain events in a mesoscale Mediterranean mountainous catchment (22 km^2) according to source contribution variability and found that more than half of the events could be considered as highly variable. Possible factors that influence the time of concentration of the eroded sediments to arrive at the outlet and thus the within event variability are the spatial distribution of the sources within the catchment and characteristics of the rain event. The latter include the intensity and duration of the rain event as well as rainfall variability (highly located vs. homogeneous rain), the displacement of the rain cells or fronts over the catchment. Variability in source contribution within an event may therefore act as a tracer for rainfall-runoff processes in the catchment. In this way, sediment fingerprinting at a high resolution could help to understand hydro-sedimentary processes in the critical zone.

Within- and between event variability also emphasized the importance to consider sediment samples taken at a high resolution or integrate samples when mean source contributions from a catchment are to be determined. When few instantaneous samples are considered the results might be very

sensitive to the time of sampling and “true” sources contributions might be considerably over- or underestimated.

3.1.5 Conclusions and perspectives

The alternative sediment fingerprinting techniques tested in this study, i.e. based on spectrophotometry and XRF measurements, could discriminate between three sources of suspended sediment (sedimentary badlands, bare topsoils on basaltic geology and bare topsoils on sedimentary geology). We investigated the different sources of error in sediment fingerprinting studies and examined the differences in predicted source contributions when different tracer sets or different mixing models were applied. We showed that the main source in the Mediterranean headwater catchment of the Claduègne (42 km^2) was sedimentary badlands. Despite their low proportion of the catchments surface ($< 1 \%$), whatever the mixing model and the tracer set used, mainly badlands contributed on average more than 70% to the suspended sediments sampled at the outlet.

In this study site which has a contrasted geology both low cost fingerprinting methods, i.e. spectrophotometry and XRF, were valid tools to conduct sediment fingerprinting at a high temporal resolution. Nonetheless, considerable uncertainties remained. These were mainly due to particle size selectivity, source heterogeneity, choice of fingerprinting properties. During erosion and sediment transport, the sediments were enriched in smaller particle size fractions which were shown to have a different fingerprinting signature than coarser particles. This challenges the assumption of conservative behavior of the tracers and led to errors that ranged between 9 and 35% depending on the source and the mixing model. Source heterogeneity was another major source of error which might lead to a wrong characterization of the source’s fingerprints and thus to false source predictions. It was quantified here as the error of predicted source contributions of the soil samples, ranging from < 5 to 18% .

Our results show that the choice of the tracer set was more important than the choice of the mixing model as different results were obtained using color or XRF tracers. This is a drawback of the two low-cost methods tested in this study as the two tracer sets don’t give unambiguous results. Notably, the mean source contribution of the basaltic soils was predicted

differently with the two methods and the correlation between predictions obtained with the two tracer sets was poor. The use of two additional methods (i.e. magnetic susceptibility and radionuclids) did not unambiguously answer the question which is the most suitable tracer set either. The comparison with these tracer sets was biased by the lower number of samples that could be analyzed, so we are more confident in the results presented in the main part of the paper (i.e. the ones obtained with color and XRF tracers) due to the higher number of samples used to build the models. A major result of this study was that there is a strong need to use multiple tracer sets to justify the results of suspended sediment fingerprinting studies and to obtain reliable estimates of source contributions with multi-tracer ensemble predictions. Another reason for the need of multi-tracer/multi-model ensemble predictions is that the sensitivity of the three mixing models and the two tracer sets to several sources of error varied a lot. Thus, the results obtained when only one tracer set and one mixing model are used might be biased considerably by one kind of error. On the other hand, this can be detected and mitigated by running various mixing models with different tracer sets.

Another main finding of the study in the mesoscale catchment was the considerable within- and between event variability. This highlighted the importance of high resolution sampling and fingerprinting of suspended sediments to obtain reliable estimates of the main sources contributions. It is also important for process understanding as high resolution data on sediment sources has a high potential for a more distributed picture of rainfall-runoff-erosion-sediment transport processes in the catchment because the sediments act as tracers of the governing surface runoff and erosion processes.

Within- and between event variability was also observed in other study sites by other authors (see Chapter 1.2.3). However, the reasons for these suspended sediment flux dynamics have not been systematically investigated yet. We hypothesize that the spatial distribution of the erosion sources within the catchment (i.e. their structural connectivity, see Chapter 1.2.2) as well as the spatio-temporal rainfall variability are the most important drivers of the variability of sediment fluxes. To test this hypothesis, the results of this chapter are combined with an analysis of how structural connectivity (Chapter 4) and rainfall variability (Chapter 5) determine hydro-sedimentary fluxes simulated in a numerical modeling framework.

3.2 Galabre

A sediment fingerprinting framework for the Galabre catchment has been developed by [Poulenard et al. \(2012\)](#) and [Legout et al. \(2013\)](#) and the data set was updated by [Hachgenei \(2017\)](#) and [Ronzani \(2019\)](#) during their Master internships. Thus, here only a brief description of the sediment fingerprinting studies in this catchment is given.

3.2.1 Introduction

As a mountainous catchment in the southern French Alps with highly erodible badlands, the Galabre catchment is prone to flash floods with high sediment exports (Chapter 2.2). The hydro-sedimentary response to rain events is very fast and water and sediment fluxes are highly variable in time. Thus, the objectives of the studies by [Poulenard et al. \(2012\)](#) and [Legout et al. \(2013\)](#) were to assess whether low cost spectroscopic tracers are able to discriminate between potential sediment sources, to assess whether the signatures are preserved during erosion and sediment transport and to quantify source contributions and their uncertainties for a high number of suspended sediment samples taken during flood events.

3.2.2 Materials and methods

48 source samples were taken exclusively in the badlands of different lithology. Badlands on five different lithologies (black marl, limestone, molasse, gypsum and Quaternary deposits) were identified as the main erodible areas and thus the main sources of sediment in the Galabre catchment (Chapter 2.2, Fig. 3.11). Suspended sediment samples are taken automatically at the outlet once thresholds of turbidity and discharge are exceeded. Since 2007 more than 600 samples were taken during 77 events.

Two spectral measurements were applied to develop sediment fingerprinting protocols. [Poulenard et al. \(2012\)](#) used Diffuse Reflectance Infrared Fourier Transform Spectrometry (DRIFTS) and the reflectance on wavenumbers in the range of 3800 - 2400 cm^{-1} and 2300 - 650 cm^{-1} were directly used as tracers. [Legout et al. \(2013\)](#) measured reflectance in the visible spectrum

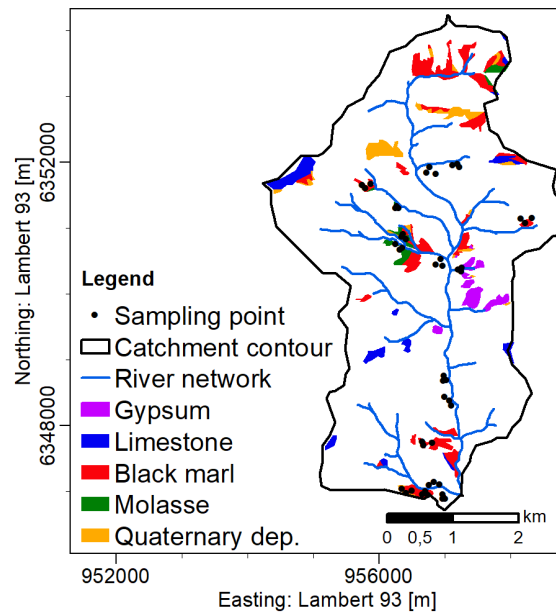


Figure 3.11: Location of the sampling sites in the Galabre catchment.

and used 15 color parameters as tracers as was done in the Claduègne catchment (see Chapter 3.1.2.2). Both studies use partial least squares regression (PLSR) mixing models to quantify the contribution of the sources (Poulenard et al., 2012; Legout et al., 2013, Chapter 3.1.2.4). Several errors were also assessed. Both studies tested the predictive power of the PLSR mixing model and the conservativeness of the tracers during immersion in the river bed was tested with in-situ biogeochemical experiments as was done in the Claduègne catchment (Chapter 3.1.2.5). Legout et al. (2013) further tested how particle size affected color tracers in the Galabre catchment.

3.2.3 Results and discussion of the previous studies

A first important result by Poulenard et al. (2012) was that gypsum was absent in the suspended sediment samples. This was expected as gypsum is highly soluble and is thus present in the solute load and not in the suspended sediment load. Thus, it was excluded as a source of suspended sediment.

It was shown that both the color tracers (Fig. 3.12a) as well as the DRIFTS tracers (Fig. 3.12b) could well discriminate the sources limestone, molasse, black marls and gypsum. The Quaternary deposits, however, are a very heterogeneous source as they comprise a mixture of the material of the other sources. Thus, they were not considered as a primary source and were not included in the mixing model.

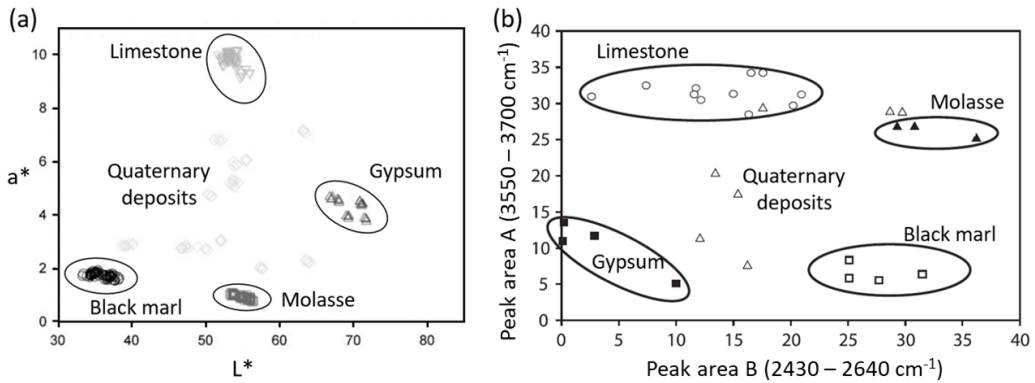


Figure 3.12: Discrimination of the sources of suspended sediment with two color tracers (a) and DRIFTS tracers (b). Figure (a) is adapted from Legout et al. (2013), (b) from Poulenard et al. (2012). a^* and L^* are two color parameters that quantify the hue (a^* , here the “redness”) and the shade (L^*), peak areas A and B are two parameters derived from the DRIFTS spectrum.

Concerning the assessment of error, it was shown that the PLSR mixing models performed well with both tracer sets. Poulenard et al. (2012) gave a RMSE of the prediction between 1.9 and 3.5 % source contribution. Legout et al. (2013) found a median absolute error of the PLSR model of 1.1 %. When spatial heterogeneity of the source samples was considered, this value increased to 3.9 %. When particle size fractions other than the fraction $< 63 \mu\text{m}$ were used the median error increased to 11.5 % and to 3.1 % when samples immersed in the river were used. The model also performed well in so far that the average of the sum of the predictions is 106 %, thus it deviates only marginally from 100 % (Legout et al., 2013). When comparing the results obtained in the Galabre catchment to the ones from the Claduègne catchment, it can be concluded that the error due to source heterogeneity is smaller in the Galabre catchment as the sources are more distinct from each other. It was coherent that the error due to particle size was more

important than the one due to biogeochemical alterations during immersion in the river.

For some instantaneous sediment samples, source contributions were estimated with both low-cost tracer sets as well as with a more conventional sediment fingerprinting approach (Navratil et al., 2012c). A comparison of the estimated contribution of black marls obtained with the three tracer sets showed that in general the results are consistent (Fig. 3.13). Nonetheless, the results differed depending on the tracer set and the uncertainty of the methods remained important. This underlines the finding that the choice of tracers is an important source of error (Chapter 3.1, Martínez-Carreras et al., 2010c; Evrard et al., 2013; Pulley et al., 2015; Zhang and Liu, 2016).

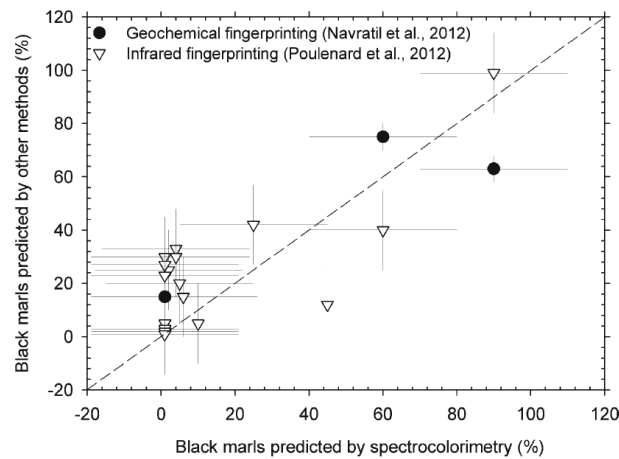


Figure 3.13: Comparison of the results obtained with color tracers to the ones obtained with DRIFTS tracers and geochemical tracers. The gray bars correspond to the estimated uncertainty, the dashed line is the line of identity. Source: Legout et al. (2013).

As was observed in the Claduègne catchment and elsewhere (e.g. Brosinsky et al., 2014b) there is a high variability between and within flood events. For half of the 23 runoff events analyzed by Legout et al. (2013) a considerable within flood variability was observed. This is regarded further in Chapter 3.3.

3.2.4 Conclusions and perspectives

The studies by [Poulenard et al. \(2012\)](#) and [Legout et al. \(2013\)](#) showed that low-cost spectral fingerprinting methodologies were successfully applied in the Galabre catchment. Especially the spectrophotometric fingerprinting could be applied routinely to quantify the source contributions of the primary sources to a high number of suspended sediment samples (to date more than 600). Thus, a very rich data set has been created.

Even though the results of the studies are promising and the estimated source contributions obtained with different tracer sets agreed in general, there is still some disparity between the methods. This finding further stresses the need of multi-tracer approaches in sediment fingerprinting and gives reason for the use of a multi-tracer mean as the best estimate of predicted source contributions (see Chapter [3.1.4](#)). Due to their low costs and low effort, spectral tracers can be used to complement traditional fingerprinting approaches.

A high variability of mean source contributions was observed between and within events. The reasons for this variability could not be identified with sediment fingerprinting alone and justified further analyses.

3.3 Temporal variability of suspended sediment fluxes

The sediment fingerprinting studies described above have created two rich data sets of suspended sediment source contributions determined for many samples taken during 11 flood events at the outlet of the Claduègne catchment and 77 flood events at the outlet of the Galabre catchment. In the Claduègne catchment the sampled events represent 46.1 % of sediment yield from 2012 to 2016, in the Galabre catchment they represent 54.8 % of sediment yield from 2008 to 2014.

3.3.1 Variability between flood events

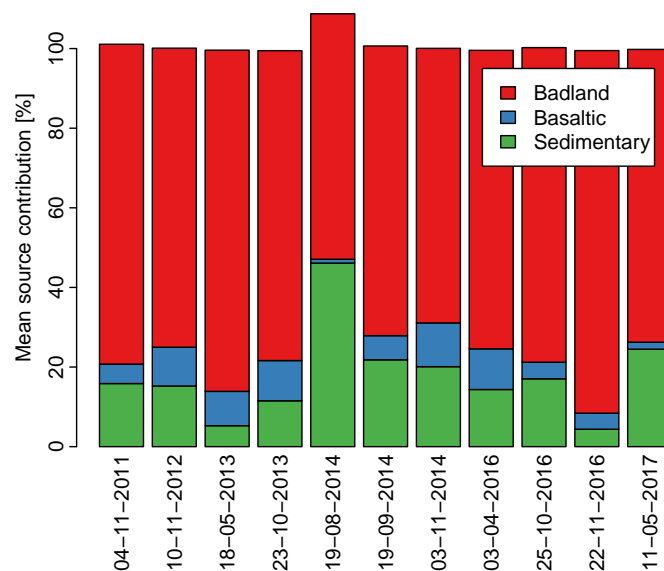


Figure 3.14: Mean source contributions to suspended sediment samples taken during 11 flood events in the Claduègne catchments. The bars show the multi-model mean of results obtained with the color tracers.

In the Claduègne catchment the contribution of the basaltic sources was constantly low for all events (1 - 11 %, Fig. 3.14). The contributions of the badlands and the sedimentary sources, however, varied from one event

to another (badlands: 62 - 91 %, sedimentary: 4 - 46 %). The event of August 19th, 2014 stood out for the high contribution of the sedimentary source.

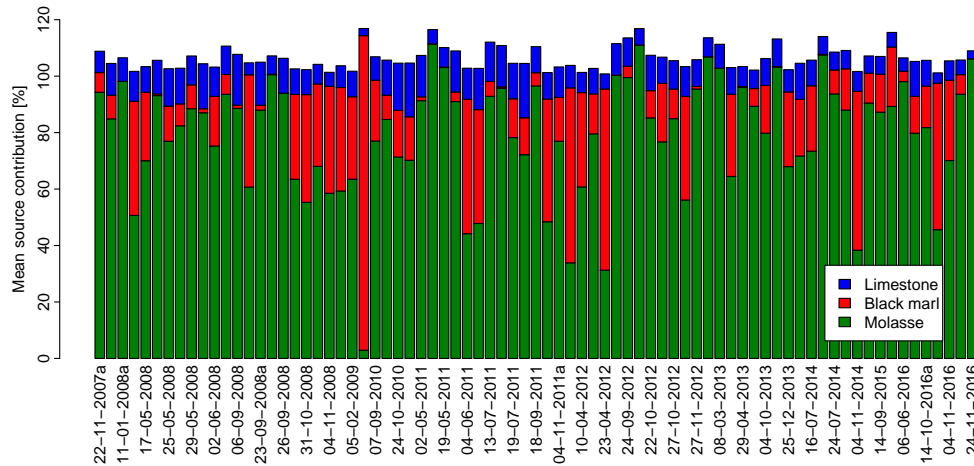


Figure 3.15: Mean source contributions to suspended sediment samples taken during 77 flood events in the Galabre catchment. Adapted from Hachgenei (2017).

In the Galabre catchment the contribution of the badlands on limestone was low and more or less constant between events (3 - 19 %). The contribution of the badlands on black marls and on molasses varied strongly from one event to another (Fig. 3.15). The event on June 23rd, 2010 stood out for its unusually high contribution of black marls (> 100 %) and low contribution of molasses (3 %). For the other events the contribution of black marls ranged from 0 to 64 % and the one of molasses ranged from 31 to > 100 % predicted with the PLSR mixing model and color tracers.

3.3.2 Variability within flood events

In both catchments the variability within flood events differed between flood events. While there were some events where source contributions varied strongly from one sample to another, there were other floods where the source contributions remained almost constant throughout the event. Slightly adapting the classification proposed by Legout et al. (2013) we classified the events in three groups:

- The first group comprises events with a low variability between the samples taken during the event. The criterion was set to a maximum of 25 % in range of one source. In other words, the difference between the minimum and the maximum of predicted source contribution for the most variable source cannot exceed 25 %
- Events of the second group also have a low variability, but one or two samples (usually in the beginning of the event) vary strongly from the rest of the samples.
- The third group comprises those events that are highly variable from one sample to another, i.e more than two samples exceed the critical range of 25 %.

Fig. 3.16 shows a scheme of the variability of source contributions in the three groups and 3.17 shows examples of flood events in the two catchments belonging to each of the three classes. The results of all events can be found in an interactive figure that complements Chapter 4 and can be found at https://modeloutputiber.shinyapps.io/interactive_fig_app/. In the Galabre catchment 15 events were classified as belonging to the first group, 18 events belonged to the second group and 13 events to the third group. In the Claduègne catchment six events belonged to the first group and five events to the third group. The second group was not present in the Claduègne catchment.

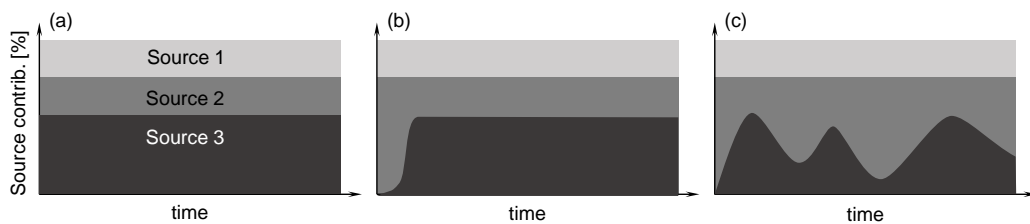


Figure 3.16: Scheme of the classification of events due to their sediment flux variability: (a) low variability of source contributions, (b) low variability with the exception of the very beginning of the event, (c) high variability of source contributions.

When all available sediment samples were classified according to the stage of the hydrograph at the time of sampling (rising limb, peak flow or falling

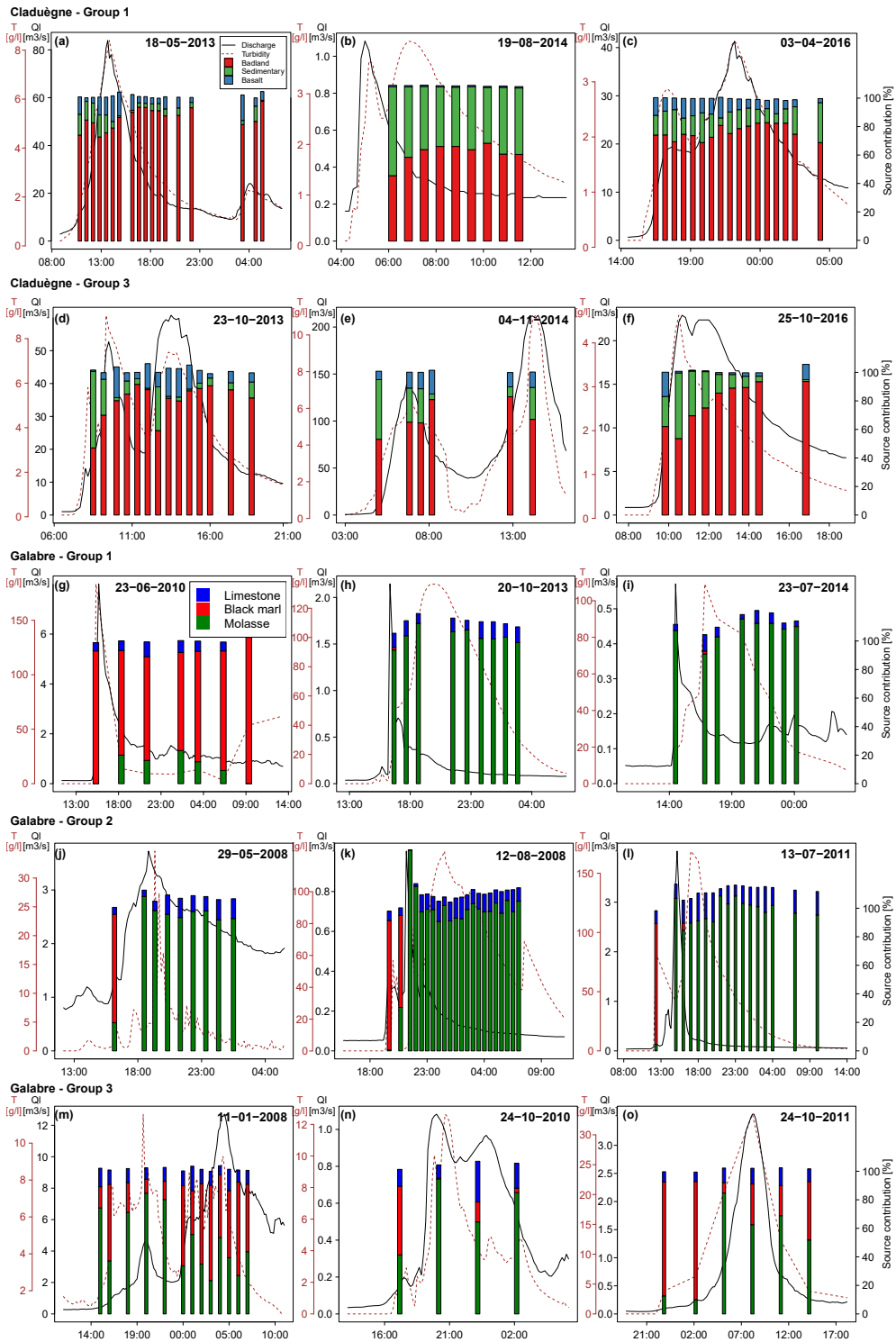


Figure 3.17: Examples of flood events that were classified according to within event variability of source contributions. The first two rows show events of groups 1 (a-c) and group 3 (d-f) in the Claduègne catchment. The third to fifth row show events of group 1 (g-i), group 2 (j-l) and group 3 (m-o) in the Galabre catchment. The black line gives liquid discharge (Q_l), the brown, dashed line shows turbidity (T) and the bars give the percentage source contributions to total solid discharge.

limb) and source contributions of the samples were regarded, a general pattern could be observed. In the Galabre catchment the contribution of the badlands on molasse was lowest during the rising limb of the hydrograph and increased during the peak and the falling limb of the hydrograph (Fig. 3.18a). The inverse was the case for the black marls where the contribution was highest during the rising limb and lowest during the falling limb of the hydrograph. But there was a large spread of the data, indicating that many events diverged from this general pattern. Nonetheless, this general pattern could be related to a higher connectivity and a faster transition time of the black marls due to their location close to the outlet and the stream (Fig 4.1c, d). This assumption was examined in Chapter 4. In the Claduègne catchment the differences between the different stages of the hydrograph were much less pronounced (Fig. 3.18b). Given the uncertainty of the sediment fingerprinting approach they were not significant.

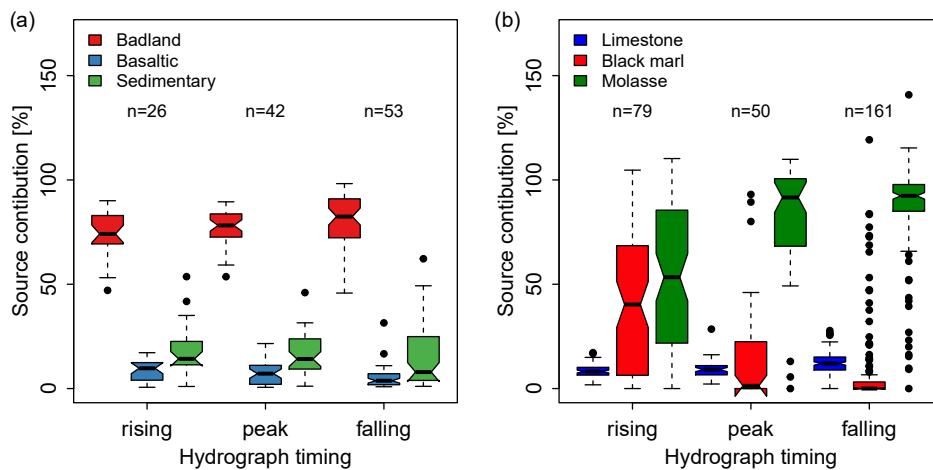


Figure 3.18: Source contributions to instantaneous sediment samples classified by the stage of the hydrograph (a) in the Claduègne and (b) in the Galabre catchment. The number of samples in each class (n) is given above the boxplots.

3.3.3 Discussion and perspectives

Other authors have observed within and between event variability of suspended sediment sources contributions estimated with sediment fingerprinting. [Brosinsky et al. \(2014b\)](#) analyzed source contributions of badlands, forests and grasslands and other sources during four flood events in the

Isábena catchment (445 km^2) in northern Spain. Similarly to our study, they obtained the result that mean source contribution differed from one flood to another. Further, for three events the source contributions stayed relatively constant throughout the flood while for the fourth event the variability within the flood was high (contribution of the source class “others” ranged from about 15 % to nearly 50 %). [Cooper et al. \(2015\)](#) estimated source contributions of arable topsoils, road verges and subsurface sources (including channel banks and field drains) to sediment samples taken during five floods in a 20 km^2 catchment in England. They observed a high within event variability for all events. [Gellis and Gorman Sanisaca \(2018\)](#) reported very high variability between flood events in the Smith creek catchment, Virginia, USA (246 km^2). Estimated contributions from channel banks varied from 43 to 100 %. In a 44 km^2 subcatchment this variability was even more extreme with contributions ranging from 0 to 100 %. [Martínez-Carreras et al. \(2010c\)](#) also assessed between event variability of source contributions in three catchments in Luxembourg ($0.7 - 4.4 \text{ km}^2$). While source contributions in the two smaller catchments remained more constant throughout the study period, in the third catchment the contribution of the main source grassland topsoils varied between about 20 % and nearly 100 % when color tracers were used.

[Cooper et al. \(2015\)](#) observed a regular pattern of within event sediment fluxes, where sediment transport was dominated by subsurface sources during low flow conditions and dominated by surface sources during the main part of the event. This pattern could be explained by distinct erosion processes during different stages of the event. In our study sites as well as in the other studies cited above, on the other hand, the reasons for the observed variability of sediment fluxes remained vague.

The most obvious explanation for between event variability of source contributions is distinct rainfall characteristics of the events that differ from the others. [Hachgenei \(2017\)](#) found out, that the contribution of the molasses in the Galabre catchment was somewhat higher in summer than in winter, while the opposite was the case for black marls. However, these differences were not statistically significant, so seasonality was not a sufficient explanation for the observed variability between flood events and events have to be regarded one by one.

In other studies, observed between event variability could not be related easily to precipitation and discharge dynamics either. [Gellis and Gor-](#)

man Sanisaca (2018) found no correlation between the contribution of channel banks to event sediment yield with possible explanatory variables such as peak discharge. Brosinsky et al. (2014b) note that even though discharge and precipitation characteristics were similar for two of the events, sediment fluxes were very different.

Studies that analyzed source contributions at the within event scale also struggled to explain the observed variability or lack thereof. Compared to other samples, Brosinsky et al. (2014b) found low contributions of the badland sources at the end of the falling limb of one of their events, but the reasons for this variation remained unknown. The authors assumed that exhaustion of available sediment might be the reason for the low contribution of this source at the end of the long event. In the Galabre catchment a general pattern of marls contributing mainly during the rising limb of the hydrograph and molasses contributing during the peak and falling limb was observed. This indicated that the location of the sources in the catchment played an important role on within event sediment flux variability. Legout et al. (2013) further assumed that spatio-temporal variability of the rain event influence sediment dynamics at the event scale. The location of the rain field in the catchment determines where erosion occurs and which sources are activated. Further, movement of rain cells with respect to the catchment causes a temporal dynamic of erosion and subsequent sediment transport.

Indeed, the two events that differed strongly from the other ones (i.e. the event of August 19th, 2014 in the Claduègne catchment and the one of June 23rd, 2009 in the Galabre catchment) showed distinct precipitation characteristics. The event of August 2014 in the Claduègne catchment, that was characterized by a high contribution of the sedimentary sources, was caused by a localized rain cell that passes the catchment from the west to the east in the southern part of the catchment (Fig. 3.19a). Similarly, the rain event in June 2009 in the Galabre catchment was highly localized in the very south of the catchment (Fig. 3.19b). Sediment flux was dominated by black marls. In both cases the location of the rain event corresponded to the location of the main sediment source during the respective event. The role of the localization of the rain cell with respect to the sources on sediment fluxes is further examined in Chapter 5.

Thus, we hypothesized that the interplay of structural connectivity and

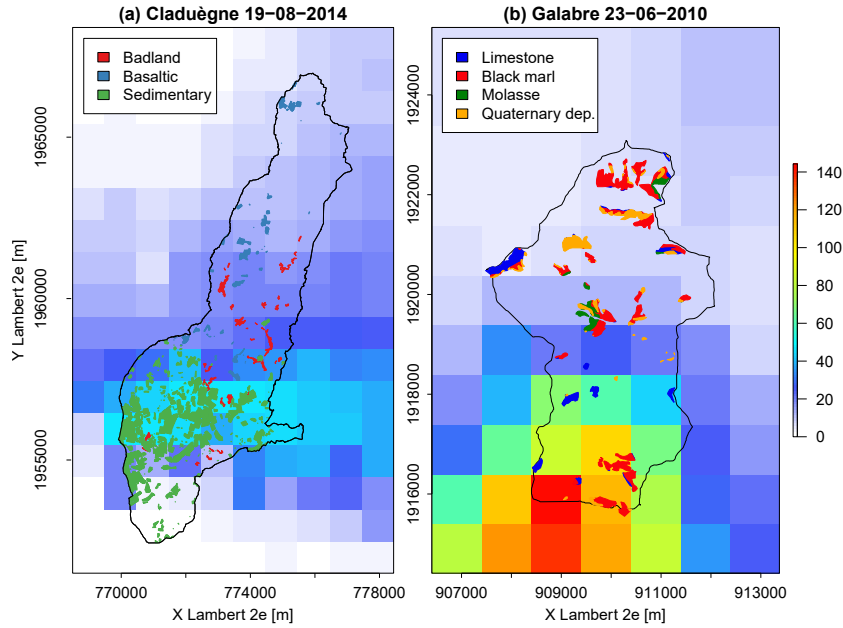


Figure 3.19: Distributed precipitation accumulated over the flood event (P_{cum} [mm]) in the Claduègne on August 19th, 2014 (a) and the one in the Galabre catchment on June 23rd, 2010 (b). The colored patches show the locations of the sediment sources.

spatio-temporal rainfall variability determined the between and within event variability of suspended sediment fluxes. Structural connectivity is determined by the location of the sources in the catchment and their potential to get transported to the outlet. The location and movements of rain fields on the other hand differ from event to event and are assumed to play an important role on sediment dynamics. In the following chapters this hypothesis was tested with a distributed numerical model by applying different scenarios that assessed the role of structural connectivity (Chapter 4) and the one of rainfall forcing (Chapter 5). While other studies showed the benefits of combining sediment fingerprinting with modeling to estimate mean sediment sources over longer time scales (Theuring et al., 2013; Wilkinson et al., 2013; Palazón et al., 2016), to our knowledge no studies made use of numerical models to understand sediment flux dynamics observed with sediment fingerprinting.

Chapter 4

Variability in source soil contributions to suspended sediments: the role of modeling choices and structural connectivity

4.1 Introduction

The following chapter is based on the draft of an article that is currently in the process of exchanging between coauthors, Magdalena Uber, Guillaume Nord, Cédric Legout and Luis Cea and will be submitted in the coming months. The introduction and the presentation of the study site were modified to avoid redundancies. The paper is complemented by a set of interactive figures that can be found at https://modeloutputiber.shinyapps.io/interactive_fig_app/.

Given the observed variability of suspended sediment fluxes within and between events and the lack of studies that analyze the reasons for this dynamic, there is a knowledge gap in our understanding of the hydro-sedimentary

processes that act during flood events and how they differ between events (Chapter 3.3). We hypothesize that the variability of sediment fluxes in mesoscale catchments is governed by two factors and their interplay: structural connectivity and functional connectivity. The latter is mainly governed by spatio-temporal dynamics of the rain event. Structural connectivity is governed by the distribution of the sources in the catchment and how landscape units are linked to each other (Wainwright et al., 2011; Fryirs, 2013). In order to isolate the two factors and to test this hypothesis, distributed, physically based models of soil erosion and sediment transport run at the event scale are powerful tools. They can help to understand the effect of the location of sources in the catchment, their linkage to the outlet, their travel times and characteristics of the rain events.

However, modeling soil erosion and sediment transport remains a challenge as there is no optimal model to represent all erosion and hydrological processes in the catchment and there is no standard protocol for the choice and set-up of the model (Merritt et al., 2003; Wainwright et al., 2008). Indeed, the outputs of hydro-sedimentary models are very sensitive to choices made by the modeler in the way processes are implemented, as well as during model discretization, parameterization, forcing and initialization. Especially the spatial structure and the discretization of the model, as well as its parameterization can crucially influence how structural connectivity of the catchment is represented in the model. In mesoscale catchments, the connectivity of sources to the outlet depends a lot on the distance to the stream. In many cases, however, the definition of the stream is not unambiguous (Tarboton et al., 1991; Turcotte et al., 2001). In most cases, the river network is based on topographic analysis in GIS software, where a stream is made up of all the cells of the digital elevation model (DEM) that exceed a threshold of contributing drainage area (CDA, Tarboton et al., 1991; Colombo et al., 2007). The CDA of a DEM cell is the cumulative size of all cells that are located upstream of the given cell and that drain into that cell. Thus, the definition of the stream and in consequence the connectivity of active erosion sources to the outlet is highly dependent on the choice of the CDA threshold (Colombo et al., 2007). Concerning parameterization, travel times of the sources to the outlet and thus structural connectivity also depend on how surface water and sediment fluxes are calculated and parameterized. Many distributed models use the depth-integrated shallow water equations (Saint Venant equations) or different approximations of them, such as the kinematic

or the diffusive wave approximations, for routing surface water to the outlet of the catchment (Pandey et al., 2016). These equations are highly sensitive to the roughness parameter (Baffaut et al., 1997; Tiemeyer et al., 2007; Fraga et al., 2013; Cea et al., 2015).

This chapter contributes to improve our understanding of the hydro-sedimentary processes leading to sediment flux variability. We focus on the role of structural connectivity using a distributed physical based model, applied to the catchments of the Claduègne and the Galabre. Since model outputs are highly sensitive to the choices made during model discretization and parameterization, the first objective is to assess the impact of these choices on the representation of structural connectivity. A second objective is to assess how structural connectivity in turn impacts modeled suspended sediment flux dynamics for both catchments.

4.2 Methods

4.2.1 Characteristics of the modeled study sites

The study is conducted in the two catchments of the Claduègne and the Galabre. A general description of the study sites can be found in Chapter 2. The two catchments differ in size and the slopes in the Galabre catchment are steeper than in the Claduègne catchment, both on the hillslopes and in the river network (Table 4.1). Furthermore, the erodibility differs between the two catchments and between sources. Catchment specific suspended sediment yield was estimated to be about $380 \text{ t km}^{-2} \text{ y}^{-1}$ in the Claduègne catchment and about $666 \text{ t km}^{-2} \text{ y}^{-1}$ in the Galabre catchment (Calculated as described in Appendix A). These values were calculated with the entire surface of the catchments. As we assume, however, that erosion occurs only on the erosion zones defined in Chapter 2.1.4 and 2.2.3 specific yield could be calculated per source. To this end, catchment specific yield was split into the contributions of the different sources using the estimates obtained from sediment fingerprinting. The source specific yields differed strongly between sources (Table 4.1).

To quantify sediment connectivity of the erosion zones, four indicators were calculated, i.e. the distance to the outlet, distance to the stream and

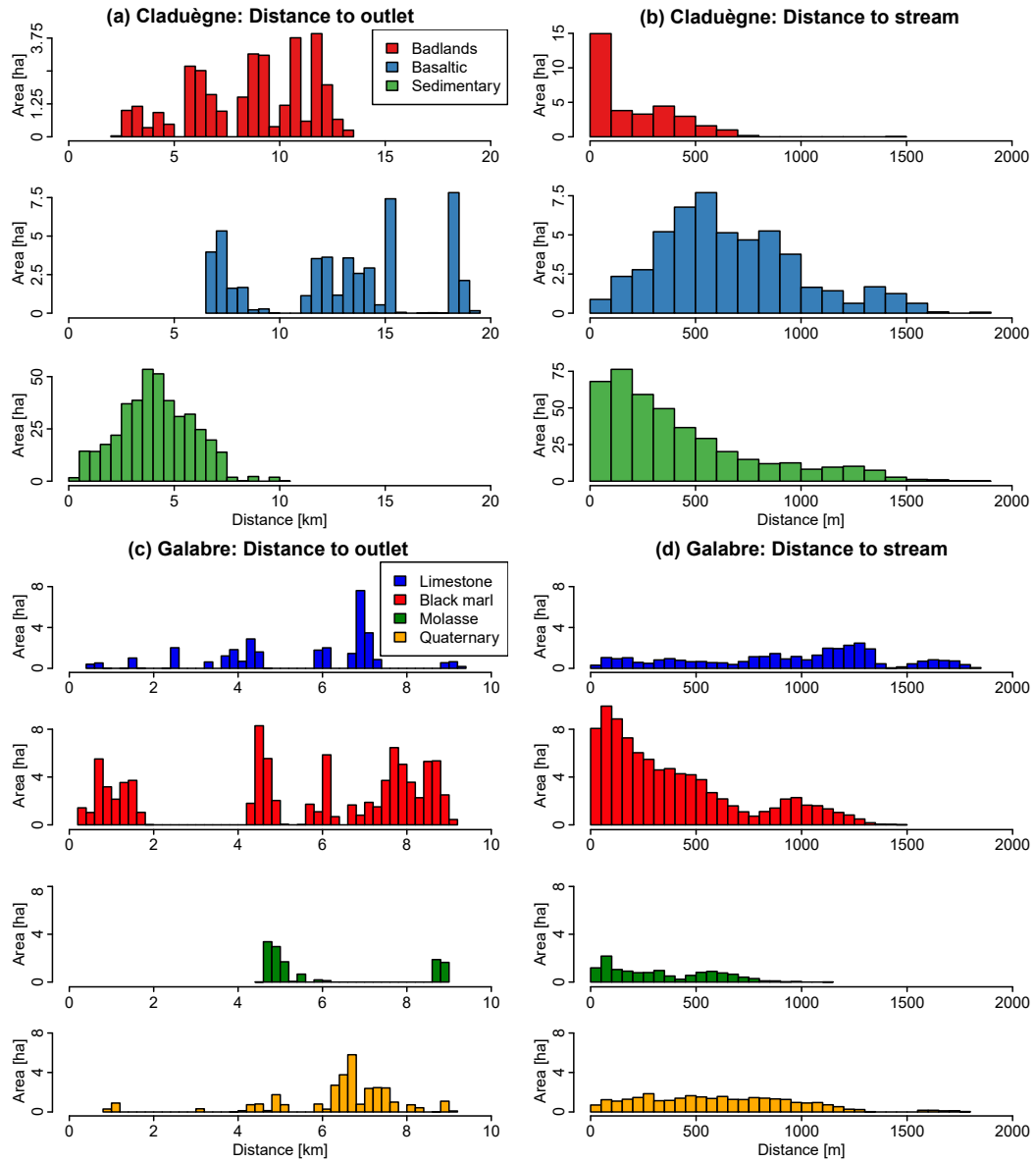


Figure 4.1: Distribution of the distance of the sources to the outlet (a for the Claduègne, c for the Galabre) and the stream (b for the Claduègne, d for the Galabre). The stream was defined with a threshold of contributing drainage area of 50 *ha*. The values represent distances along the flowlines that water and sediments travel following the gradient of the relief. They were calculated with TauDEM (Tarboton et al., 2015).

Table 4.1: Characteristics of the two catchments and the erosion zones. K_G is Gravelius' compactness indicator defined as the ratio between the catchment perimeter (P) and the one of a circle with equal surface. The values given for the slopes on the hillslopes, the distance to the outlet, the distance to the streams and the two connectivity indicators (IC) represent the mean \pm standard deviation. The mean slopes in the river network are given for the entire network including intermittent streams (defined with a threshold of CDA of 15 ha) and for the main, perennial network (CDA of 500 ha). a) The values correspond to the slope in the river network on the basaltic plateau and on sedimentary geology and are not limited to the erosion zones. b) Rainfall erodibility α corresponds to the mass of sediment detached on 1 m² by 1 mm of rain (Cea et al., 2015).

	Claduègne				Galabre				
	Entire catchment	Badland	Basaltic	Sedimentary	Entire catchment	Limestone	Marl	Molasse	Quaternary deposits
Catchment morphology									
Area [km ²]	42.24	0.32	0.52	4.19	19.55	0.34	0.93	0.13	0.33
K_G [-]	1.87	-	-	-	1.47	-	-	-	-
Slope, hillslopes	24 \pm 30	82 \pm 68	11 \pm 21	12 \pm 13	54 \pm 40	101 \pm 127	67 \pm 38	56 \pm 30	54 \pm 33
Slope, river network									
Intermittent streams	6.78	-	9.22 ^{a)}	6.06 ^{a)}	19.17	-	-	-	-
Main stream	2.72	-	4.93 ^{a)}	2.50 ^{a)}	5.71	-	-	-	-
Connectivity									
Distance to outlet [km]	9.18 \pm 5.10	8.59 \pm 2.82	12.91 \pm 3.92	4.15 \pm 1.73	4.75 \pm 2.17	5.49 \pm 1.99	5.28 \pm 2.91	6.03 \pm 1.72	6.25 \pm 1.65
Distance to stream [km]	0.44 \pm 0.35	0.21 \pm 0.19	0.67 \pm 0.34	0.42 \pm 0.36	0.53 \pm 0.37	0.89 \pm 0.47	0.39 \pm 0.35	0.34 \pm 0.24	0.57 \pm 0.35
IC (Borselli et al., 2008)	-9.18 \pm 0.61	-8.35 \pm 0.43	-9.30 \pm 0.37	-8.75 \pm 0.66	-8.84 \pm 0.75	-7.94 \pm 0.39	-7.95 \pm 0.60	-8.19 \pm 0.36	-8.03 \pm -0.42
IC (Cavalli et al., 2013)	-5.85 \pm 0.53	-5.50 \pm 0.34	-6.34 \pm 0.50	-5.73 \pm 0.50	-4.56 \pm 0.50	-4.52 \pm 0.33	-4.57 \pm 0.55	-4.81 \pm 0.35	-4.56 \pm 0.40
Erodibility									
Suspended sediment yield [t y ⁻¹]	15947	12394	1084	2469	12856	953	1956	7474	2473
Specific yield [t km ⁻² y ⁻¹]	380	38623	2087	589	666	2780	2113	57075	7418
Rain erodibility α^b [g mm ⁻¹ m ⁻²]	3.1	37.5	2.0	0.6	7.4	2.8	2.1	57.1	7.4

the two indices of connectivity (IC) proposed by Borselli et al. (2008) and Cavalli et al. (2013). Maps of the distance to the outlet along the flowlines (i.e. the distance that water and sediments travel following the gradient of the relief) and the distance to the stream were created (Fig. C.1). For the latter, the stream network with a CDA threshold of 50 ha was chosen. The distance to the outlet and the distance to the stream of a given position in the catchment serve as proxies of longitudinal and lateral connectivity in the sense of Fryirs (2013). Both maps were created using TauDEM (Tarboton, 2010) and a digital elevation model at a resolution of 1m (Claduègne: bare earth Lidar DEM, Nord et al., 2017; Galabre: RGE ALTI product of IGN, 2018b).

However, neither of these indicators takes into account surface roughness and slope. Thus, two of the most widely used indicators of connectivity, i.e. the IC proposed by Borselli et al. (2008) and the adjusted version of IC proposed by Cavalli et al. (2013), were calculated (see Chapter 1.2.2). Both indicators were calculated for each pixel of a DEM and take into account the CDA of that pixel and the distance to the stream along the flow lines. They also both include a weighting factor for the mean slope in the CDA and along

the downstream path as well as a second weighting factor W . Borselli et al. (2008) weight the index with land cover, thus the factor W was derived from the values proposed by Panagos et al. (2015a) for the land cover data that was obtained from Inglada et al. (2017). Cavalli et al. (2013) on the other hand propose a roughness index as the weighting factor W that represents a local measure of topographic surface roughness that is calculated for a 5×5 cell moving window. Both indicators were calculated using the program Sed-InConnect (Crema and Cavalli, 2017).

All these indicators (distance to the outlet, distance to the stream, IC proposed by Borselli et al., 2008, IC proposed by Cavalli et al., 2013) were calculated for each pixel within the catchments and values on the erosion zones were extracted. Mean values and standard deviations are given in Table 4.1 and the distributions of the distance to the outlet and to the stream are shown in Fig. 4.1. These characteristics of the catchments indicated that not only erodibility but also structural connectivity differs strongly between the two catchments and between sources.

4.2.2 Model description

The 2D hydrodynamic model Iber was originally developed for the simulation of free surface flows in rivers, estuaries and engineering applications (Bladé et al., 2014). It is a fully distributed physically-based model. In addition to the hydrodynamic model, there are optional modules for turbulence (Cea et al., 2007), bedload transport, suspended sediment transport, water quality (Cea et al., 2016), hydrology (Cea and Bladé, 2015) as well as soil erosion. The latter was developed and applied at the plot scale by Cea et al. (2015). This study presents the first application of the erosion model at the catchment scale.

The hydrodynamic module Water depths and water flow velocity fields are derived from the resolution of the full St. Venant equations applied both on the hillslopes and in the river network. Including rainfall and infiltration terms as well as Manning's formula for bed friction they can be written as (Cea et al., 2015):

$$\frac{\partial h}{\partial t} + \frac{\partial q_x}{\partial x} + \frac{\partial q_y}{\partial y} = R - i \quad (4.1)$$

$$\frac{\partial q_x}{\partial t} + \frac{\partial}{\partial x} \left(\frac{q_x^2}{h} \right) + \frac{\partial}{\partial y} \left(\frac{q_x q_y}{h} \right) = -gh \frac{\partial z_s}{\partial x} - g \frac{n^2}{h^{7/3}} |\mathbf{q}| q_x \quad (4.2)$$

$$\frac{\partial q_y}{\partial t} + \frac{\partial}{\partial x} \left(\frac{q_x q_y}{h} \right) + \frac{\partial}{\partial y} \left(\frac{q_y^2}{h} \right) = -gh \frac{\partial z_s}{\partial y} - g \frac{n^2}{h^{7/3}} |\mathbf{q}| q_y \quad (4.3)$$

where h is water depth, t is time, q_x and q_y are the components of unit discharge in the two horizontal directions, R is rainfall intensity, I is the infiltration rate, g is gravity acceleration, z_s is the elevation of the free surface and n is Manning's roughness parameter.

The soil erosion module The full description of the soil erosion model can be found in Cea et al. (2015). A summary is given here. The complete soil erosion model uses a two-layer soil structure that consists of a layer of previously eroded material over a layer of non-eroded cohesive soil. Given the results of Cea et al. (2015) that the two-layer structure of the model increased its complexity without significantly improving its predictive capacity in real applications, we only used a single-layer structure with vertically uniform erodibility. We assumed that the single-layer structure is adequate for the badlands where there usually is a thick regolith layer, and erosion from the underneath cohesive layer is negligible compared to the one of the regolith layer. In the complete model, two particle detachment processes are considered, i.e. rainfall-driven detachment and flow-driven entrainment. In this study, we only considered rainfall-driven detachment. This choice was made in order to minimize the number of parameters and because one of the objectives of the thesis was to relate the effect of rainfall variability to sediment flux variations.

We further assumed that all eroded particles are transported in suspension to the outlet and that deposition is negligible. This assumption corresponds to the wash load hypothesis first proposed by Einstein et al. (1940) (Chapter 1.2.1). This hypothesis led to a further simplification of the erosion model compared to the original one proposed by Cea et al. (2015), i.e. the omission of the deposition term. Thus, the suspended sediment concentration at every time step and in every model element was calculated with Eq.

4.4, which is a simplified version of equation 2 given in Cea et al. (2015) for the case of a single-layer structure with only rainfall-driven detachment and without deposition:

$$\frac{\partial hC}{\partial t} + \frac{\partial q_x C}{\partial x} + \frac{\partial q_y C}{\partial y} = D_{rdd} \quad (4.4)$$

where C [$kg\ m^{-3}$] is the depth-averaged sediment concentration in the water column. D_{rdd} [$kg\ m^{-2}s^{-1}$] is the rainfall-driven detachment rate that is calculated assuming a linear relationship between the detachment rate and the rain intensity; $D_{rdd} = \alpha R$, where α [$g\ mm^{-1}m^{-2}$] is the rainfall erodibility coefficient that represents the flux of sediment mass detached per unit area by a 1 mm of rain. The above mentioned assumptions can be considered as strong simplifications of hydro-sedimentary functioning. Nevertheless, they provided a modeling framework that could be kept the same for all simulations conducted here and allowed us to test other working hypothesis about the impact of model discretization, catchment characteristics and variable meteorological forcing.

Solution schemes The model equations are solved using the finite volume method, as it is very well suited to irregular geometries and is adequate for the modeling of wet-dry transitions and changes of the hydraulic regime (Bladé et al., 2014). As a numerical discretization scheme for solving the St. Venant equations, the decoupled hydrological discretization scheme (Cea and Bladé, 2015) is used in this study because of the low computation time and the good results and numerical stability of the scheme found by Cea and Bladé (2015). The temporal discretization is based on the Courant–Friedrichs–Lewy (CFL) condition, so the model determines the calculation time step in a way that the CFL number does not exceed a user-defined threshold. A detailed description of the numerical solution algorithm is given in Cea and Vázquez-Cendón (2012) and Cea and Bladé (2015).

4.2.3 Model discretization and input data

The geometry of the catchment was divided into three main modeling units, i.e. the hillslopes, the badlands and the river network. The badlands were delineated based on orthophotos and verified during field trips (Legout et al., 2013). The diffuse sources in the Claduègne catchment were delineated based

on land cover data (Inglada et al., 2017) and land register data (DRAAF, 2017; see Chapter 2.1.4). The river bed was delineated by (i) identifying the river network using TauDEM (Tarboton, 2010) and (ii) creating a polygon by “buffering” the line feature of the river. In order to take into account that the width of the river varies from upstream to downstream, we introduced a distinction between the perennial river network defined using a CDA of 500 *ha* and the intermittent river network obtained using a CDA of 15 *ha*. While the highest value of 500 *ha* is often used for cartography and large scale modeling studies (e. g. Colombo et al., 2007; Vogt et al., 2007; Bhowmik et al., 2015), the smallest value of 15 *ha* was found to create a river network that includes the intermittent streams observed in the catchment. This is coherent with the results of Schlunegger and Schneider (2005) who observed that at CDA threshold of 10 - 20 *ha* channel processes predominate while below that threshold hillslope processes prevail. For the perennial river a buffer of 10 *m* to both sides of the river was applied. For the intermittent streams, composed of small tributaries and in good agreement with field observations of the whole extension of the hydrographic network during floods, a buffer of 5 *m* was applied.

These principal modeling units (badlands, hillslopes and river network) were discretized as a finite volume mesh. The mesh elements are the fundamental numerical modeling units in which the erosion and transport equations are solved. In our study, we used an unstructured triangular mesh with variable mesh size in the different landscape elements. The smallest mesh size was required in the river network, where water and sediment fluxes are concentrated, so it was set to 5 *m*. On the hillslopes a coarser mesh size of 100 *m* was chosen in order to reduce the number of elements and thus computation time. In the badlands, where the fluxes are concentrated in the steep gullies, an intermediate mesh size of 20 *m* was used. At the border between two landscape units the meshsize increases gradually. With this discretization the model of the Claduègne consists of approx. 173.000 mesh elements, the one of the Galabre catchment of approx. 75.000 elements.

The potential erosion sources were classified according to their geology, consistently with the sediment fingerprinting studies (Chapter 3). In addition, they were classified based on their distance to the outlet and their distance to the stream network and separate sedigraphs were calculated for each source class. Equation 4.4 is solved in each element of the mesh for each

source class separately.

As input data the model is forced with a time series of spatially distributed or homogeneous precipitation data. As the focus of this chapter is on choices made during model set-up and how structural connectivity is represented, a synthetic triangular hyetograph was applied spatially homogeneous over the entire catchment. It has a duration of 12 h and a maximum rain intensity of $5 \text{ mm } h^{-1}$ representing effective precipitation (i.e. infiltration already deduced from rainfall). The model further needs parameters on infiltration, initial water depth, Manning's roughness coefficient n and rainfall erodibility α . All of these parameters and initial conditions can be applied spatially uniform or fully distributed. As we consider the precipitation input to be effective precipitation, infiltration was set to zero. The model does not represent subsurface water fluxes and baseflow, so we equally set initial water depth to zero (also in the river network). Thus, simulated fluxes at the outlet correspond to the fraction of the hydrograph resulting from surface runoff during the event.

4.2.4 Modeling scenarios

In order to test the effects of model discretization and parameterization on the representation of structural connectivity and on the computed suspended sediment fluxes, the modeling scenarios shown in Table 4.2 were tested.

Sc.1: Basic scenario In a first step, a basic scenario was set up. The threshold to define the river network based on CDA was set to 15 ha and the sources were classified according to their geology as in the sediment fingerprinting studies. In the river network, Manning's n was set to 0.05 and on the hillslopes it was set to 0.8. The value in the river network corresponds to what can be expected from values reported in the literature for streams comparable to the Claduègne and the Galabre (Te Chow, 1959; Barnes, 1967; Limerinos, 1970). For the values on the hillslopes there are fewer recommendations from the literature as the use of the St. Venant equations for the calculation of fluxes on hillslopes is much less common. Existing studies indicate that the values have to be considerably higher (Engman, 1986; Hessel et al., 2003a; Hallema, 2011; Fraga et al., 2013; Hallema et al., 2013). As these values are uncertain, the impact of this parameterization was assessed

Table 4.2: Model scenarios (Sc.) defined according to the value of the contributing drainage area threshold to define the river network (Th_{CDA}), the approach to classify the sources, the values for Manning’s roughness parameter (n) in the river network and on the hillslopes and the aim of the respective scenario.

Sc.	Aim	Th_{CDA} [ha]	Source classification	n_{river}	$n_{hillsl.}$
1	Basic scenario	15	Geology	0.050	0.8
2a	Impact of the river network threshold	35	Geology	0.050	0.8
2b		50	Geology	0.050	0.8
2c		150	Geology	0.050	0.8
2c		500	Geology	0.050	0.8
3a	Impact of the parameter-ization of Manning’s n	15	Geology	0.050	0.2
3b		15	Geology	0.050	0.4
3c		15	Geology	0.050	0.6
3d		15	Geology	0.025	0.8
3e		15	Geology	0.075	0.8
3f		15	Geology	0.100	0.8
4a	Dynamics between more and less connected sources	15	Distance to outlet	0.050	0.8
4b		15	Distance to stream	0.050	0.8
4c		15	Distance to outlet	0.100	0.2
4d		15	Distance to stream	0.100	0.2

in further scenarios.

The erodibility coefficient α was estimated from the available time series of suspended sediment concentrations (SSC), discharge and rainfall. Using the discharge and SSC , suspended sediment flux was calculated (Appendix A) and integrated over time for each recorded event to obtain event suspended sediment yield SSY_{ev} [g]. The value of α was estimated separately for each event and each source as:

$$\alpha_{s,ev} = \frac{SSY_{s,ev}}{R_{ev} \cdot A_s} \quad (4.5)$$

where A_s is the erodible surface of the respective source and R_{ev} [mm] was estimated as the water depth corresponding to the total event runoff volume divided by the watershed area. $SSY_{s,ev}$ is the contribution of source s to SSY_{ev} and was calculated based on the mean source contributions obtained from sediment fingerprinting. A mean value of α_s [$g\ mm^{-1}m^{-2}$] was calculated by averaging over all the available events (Table 4.1).

The basic scenario was used as the main reference to compare the other scenarios to and for the comparison between the two catchments.

Sc. 2: Impact of the CDA threshold We tested the impact of varying the CDA threshold on the modeled hydro-sedimentary response while keeping all other parameters unchanged compared to the basic scenario. As different values for Manning's n were applied in the river network area and on the hillslopes, the travel times of the sediments from source to sink vary depending on the length of the river network in the model. Five values were used: 15, 35, 50, 150 and 500 *ha*.

Sc. 3: Impact of the parameterization of Manning's n The model was run with different values for Manning's n in the river network and on the hillslopes. In the river network, values were varied spanning a range from 0.025 to 0.100. This corresponds to the full range of plausible values (Te Chow, 1959; Barnes, 1967; Limerinos, 1970). The value of 0.8 for n on hillslopes used in the basic scenario is already at the upper end of values reported in the literature (Te Chow, 1959; Engman, 1986; Hessel et al., 2003a; Hallema, 2011; Hallema et al., 2013). Thus, values in the range of 0.2 to 0.8 were tested.

Sc. 4: Source classification based on connectivity In order to test how the spatial distribution of the sources in the two distinct catchments contribute to the modeled sedigraphs at the outlet, the sources were classified into subclasses based on their distance to the outlet (Sc. 4a,c) and distance to the stream (Sc. 4b,d). These two measures serve as a proxy for the structural connectivity of the sources. The underlying hypothesis is that depending on their connectivity, several patches of the same source have different travel times to the outlet and can therefore lead to several peaks in the sedigraph of the source. In both scenarios, the sources were finally classified in two to three groups to simplify the interpretation. For example, in Sc. 4b, the badland sources in both catchments were classified as being directly adjacent to the river network or not. The diffuse sources in the Claduègne catchment i.e. soils on basaltic and sedimentary geology were classified using a threshold of distance to the river of 150 *m*.

4.2.5 Comparison of scenarios

To assess the impact of the changes done in each scenario with respect to the basic scenario, several characteristics of the modeled hydrograph and sedigraphs of all sources were calculated. The lag time of liquid discharge T_{lag,Q_l} is calculated as the time between the barycenter of the hyetograph and the barycenter of the hydrograph. The time of concentration of liquid discharge T_{c,Q_l} is defined as the time between the end of effective precipitation and the end of event flow since no infiltration is represented in this study. A third characteristic time, T_{spr,Q_l} , was defined to assess the spread of the hydrograph and thus a characteristic duration of the flood event (Fig. 4.2). All of these measures were also calculated for solid discharge (T_{lag,Q_s} , T_{c,Q_s} , T_{spr,Q_s}) and for each source separately. Further, maximum liquid discharge $Q_{l,max}$ and solid discharge $Q_{s,max}$ were determined for each scenario. Our simulations were truncated 12 h after the end of precipitation and in some cases fluxes did not recede to zero, so a threshold of $0.1 Q_{max}$ was used to calculate T_{lag} , T_c and T_{spr} for solid and liquid discharges.

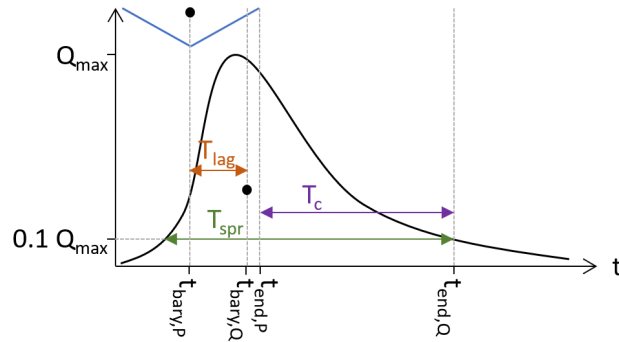


Figure 4.2: Scheme of the calculation of characteristic times T_{lag} , T_c and T_{spr} that were calculated using the simulated liquid and solid discharges. The points represent the barycenter of the hyetograph (blue curve) and of the fraction of discharge above the threshold of $0.1 \cdot Q_{max}$ (black curve).

4.3 Results and discussion

4.3.1 Impact of modeling choices on modeled sediment dynamics

4.3.1.1 Varying the contributing drainage area threshold

Results showed that the model is very sensitive to the choice of the CDA threshold to define the river network. Figure 4.3 shows the modeled hydrographs that were obtained when the CDA threshold was varied from 15 to 500 *ha*. For both catchments, higher values led to a less steep rising limb of the hydrograph, lower and later peak flow, slower recession and a flatter hydrograph. Thus, the lag time T_{lag} and time of concentration T_c of liquid discharge increased with increasing CDA threshold (Fig. 4.4a,b, Table C.1). In both catchments, the hydrographs obtained with thresholds of 15, 35 and 50 *ha* were relatively similar, but the results obtained with 150 and 500 *ha* differed considerably. In the Claduègne catchment peak flow was reduced by approximately a factor 2 when the threshold was increased from 15 to 500 *ha*, while in the Galabre catchment it decreased by about 20% (Table C.1). In the Claduègne catchment the hydrograph obtained with the threshold of 500 *ha* was much flatter than the one in the Galabre catchment and recession was very slow, so that even 12 *h* after the end of precipitation, discharge at the outlet persisted. This was not the case in the Galabre catchment.

The different hydrological response could not be attributed to the difference in size of the catchments alone, because a subcatchment of the Claduègne that has the same size as the Galabre catchment and a similar mean slope than the entire Claduègne catchment (Mean \pm sd: 25 \pm 32 %) also had a less steep rising limb of the hydrograph (Fig 4.3b). The T_{lag} of 3.2 *h* (basic scenario) was smaller than the one of the Claduègne catchment at the outlet (4 *h*) but also considerably larger than the one of the Galabre catchment (2.3 *h*). Thus, we assume that the fast rise and recession of the hydrograph in the Galabre catchment were mainly due to the steeper slopes in this catchment (Table 4.1) given that the lengths of the river networks are similar.

The modeled response of the sedigraph was also very sensitive to the CDA threshold. T_{lag} and T_c of solid discharge increased generally with increasing

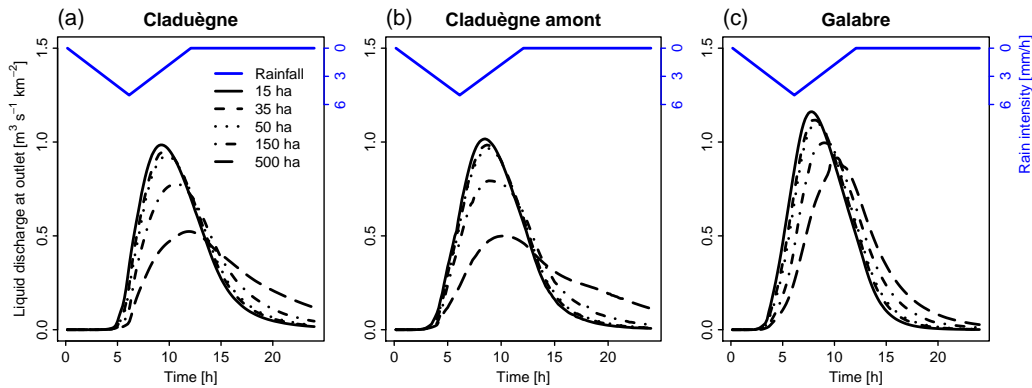


Figure 4.3: Simulated specific discharge obtained with different scenarios of model discretization at the outlet of the Claduègne (a) and the interior point Claduègne amont (b) where the size of the subcatchment is the same as the one of the Galabre catchment (c). The threshold for defining the river network is varied from 15 ha to 500 ha.

CDA threshold (Fig. 4.4a, b, Table C.1). In the Claduègne catchment, the sedigraphs obtained with CDA thresholds of 15, 35 and 50 ha were similar to each other, but when larger values were used, they varied substantially (Fig. 4.5). The sedigraphs of the basaltic and sedimentary sources were considerably delayed when higher thresholds were used. In the Galabre catchment the sedigraphs of all sources were highly sensitive to significant changes of the CDA threshold with changes in T_{lag,Q_s} and T_{c,Q_s} of more than 100% for the CDA threshold of 500 ha (Table C.1). When the threshold of 500 ha was used, the shape of the sedigraph of some sources differed. Indeed, for the badlands in the Claduègne catchment and the black marls and the molasses in the Galabre catchment, the single peak sedigraphs turned into multi peak sedigraphs (Fig. 4.5).

The differences in the modeled sedigraphs when different values for the CDA threshold were used are also obvious when the simulated contributions of the sources to total suspended sediment load are regarded (Fig. 4.6 and interactive figure). Increasing the CDA threshold from 15 to 500 ha notably prolonged the first flush of black marl dominated sediment in the Galabre catchment (marked as “1” in Fig. 4.6c and d). During the rising limb of the hydrograph and peak flow (marked “2”), the source contributions were variable while they remain relatively constant during the recession period (“3”) when the CDA threshold of 500 ha was used. This was not the case when

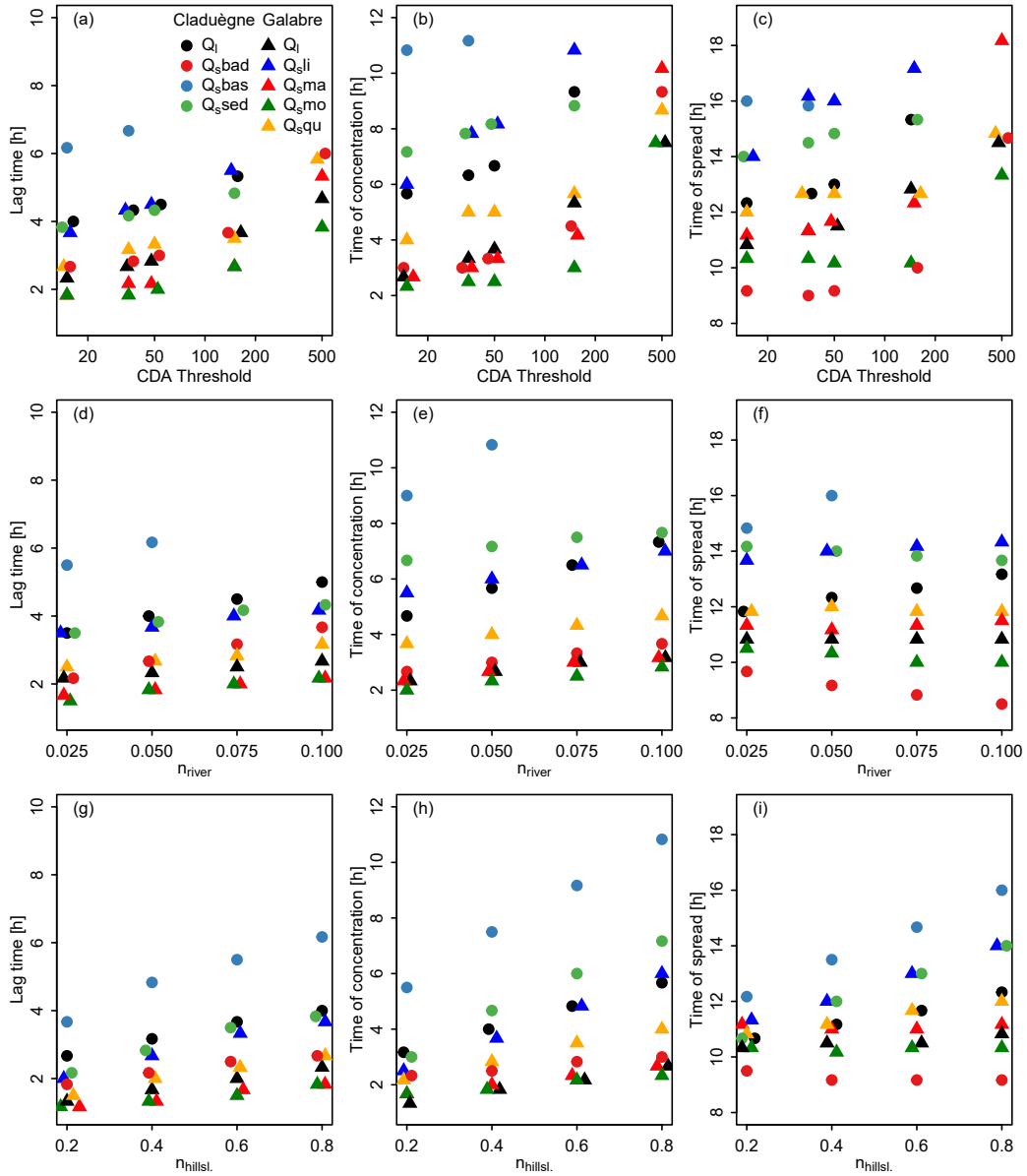


Figure 4.4: Sensitivity of lag times, times of concentration and time of spread to changing the CDA threshold (top row), Manning's n in the river network (middle row) and on the hillslopes (bottom row). For each catchment the characteristic times are given for liquid discharge (Q_l) and for solid discharge (Q_s) of the different source classes. Some symbols were slightly shifted on the x-axis if they were hard to see or overlapped by other symbols.

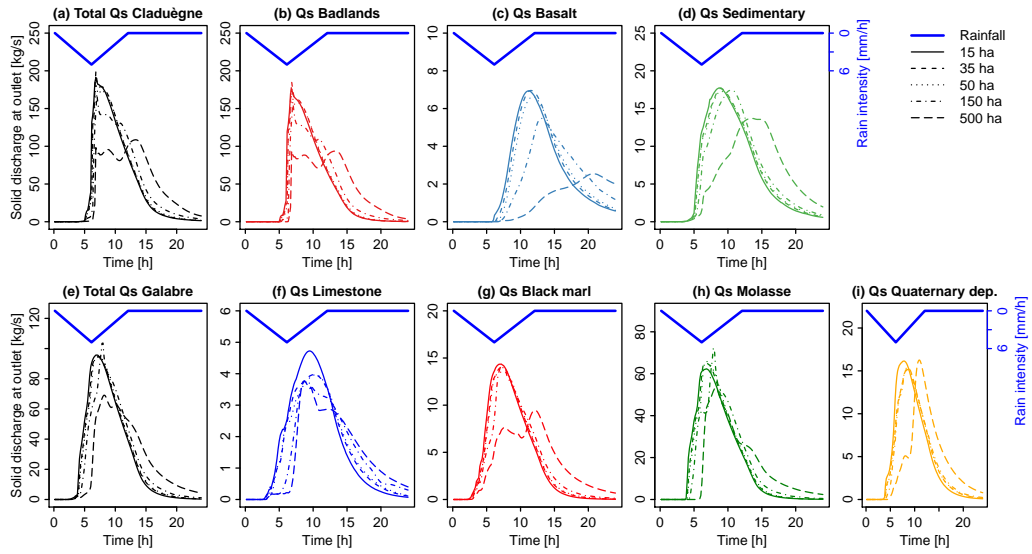


Figure 4.5: Simulated sedigraphs for total solid discharge (Q_s) and for each source in the two catchments when different values are used for the threshold of contributing drainage area (CDA) to define the river network.

the threshold was set to 15 ha . In this case, the contribution of molasses decreased steadily throughout the event while the one of limestone and Quaternary deposits increased (“2”, “3”, and “4” in Fig. 4.6c). In the Claduègne catchment notably the arrival of the basaltic sources at the outlet was much delayed when the CDA threshold of 500 ha was used compared to when the one of 15 ha was used. The shape of the sedigraph with multiple peaks that was modeled with a threshold of 500 ha resulted in a slower and less steady recession of the badland sources (Fig. 4.6b).

Overall, our results showed that the thresholds of 15 , 35 and 50 ha produced very similar results, i.e. the catchments are not highly sensitive to the CDA threshold in this range. The parameters given in Table C.1 (T_{lag,Q_l} , T_{c,Q_l} , T_{spr,Q_l} ; T_{lag,Q_s} , T_{c,Q_s} and T_{spr,Q_s} for all sources, $Q_{l,max}$ and $Q_{s,max}$) changed by a maximum of 37% compared to the basic scenario. Other authors showed that the CDA thresholds can vary spatially (i.e different values are found in different subcatchments) and temporally (CDA thresholds vary between seasons or between events) (Montgomery and Foufoula-Georgiou, 1993; Bischetti et al., 1998; Colombo et al., 2007). In the studied catchments, variability in this range seemed not to be of prime importance. However, the

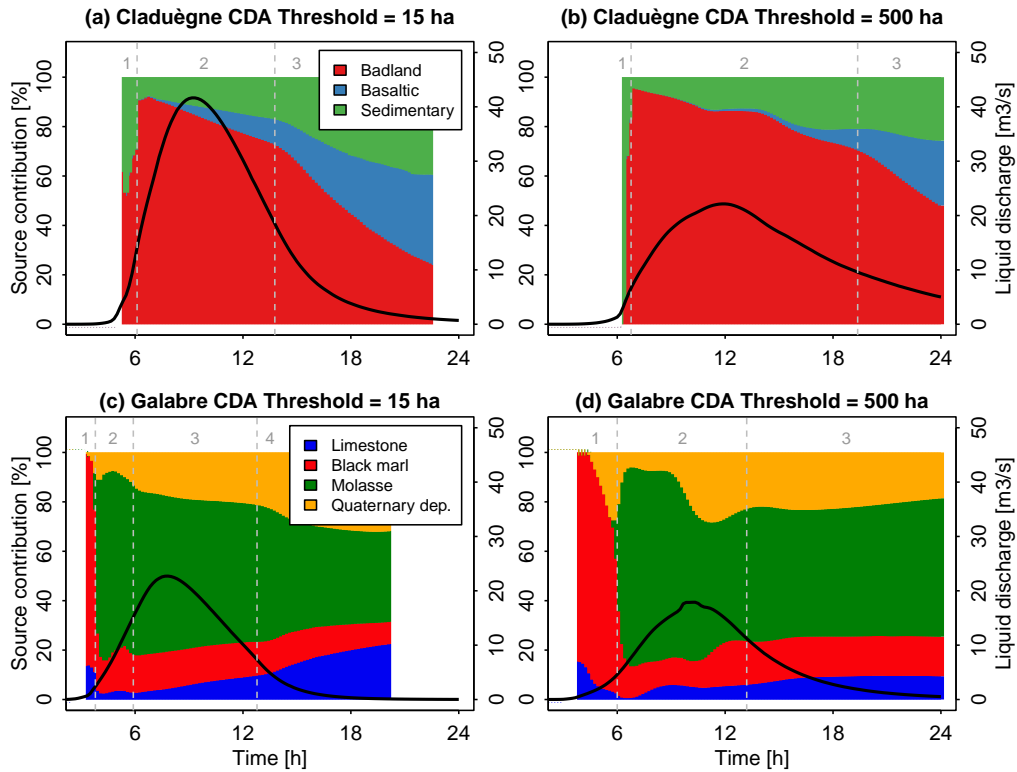


Figure 4.6: Modeled source contributions of the sediment sources in the Claduègne and Galabre catchments when the threshold of contributing drainage area (CDA) is set to 15 *ha* (left) or to 500 *ha* (right). The color shows the contribution of the different sources to total suspended sediment load in percent. The hydrograph is additionally shown to represent the timing of the event. The results obtained with all five CDA thresholds (15, 35, 50, 150 and 500 *ha*) for both catchments can be visualized at in the [interactive figure](#).

larger thresholds of 150 and 500 *ha* changed the modeled sediment dynamics considerably (changes of up to 280 % with respect to the basic scenario and several parameters changed > 150 %, Table C.1). This result showed that it is important to use a CDA threshold that is in the right order of magnitude compared to field observations or detailed maps (i.e. topographic map at scale 1:25000). Pradhanang and Briggs (2014) also tested the effect of CDA threshold on annual sediment yield and streamflow modeled with the AnnAGNPS model. In their study, they observed a high sensitivity of the model output to variations of the CDA threshold from 0.5 to 20 % of catchment area (5 - 25 *km*²). Differently to our study, they did not observe a

convergence of results in the “right” order of magnitude of the CDA threshold but results differed strongly between the six considered catchments.

4.3.1.2 Varying Manning’s n

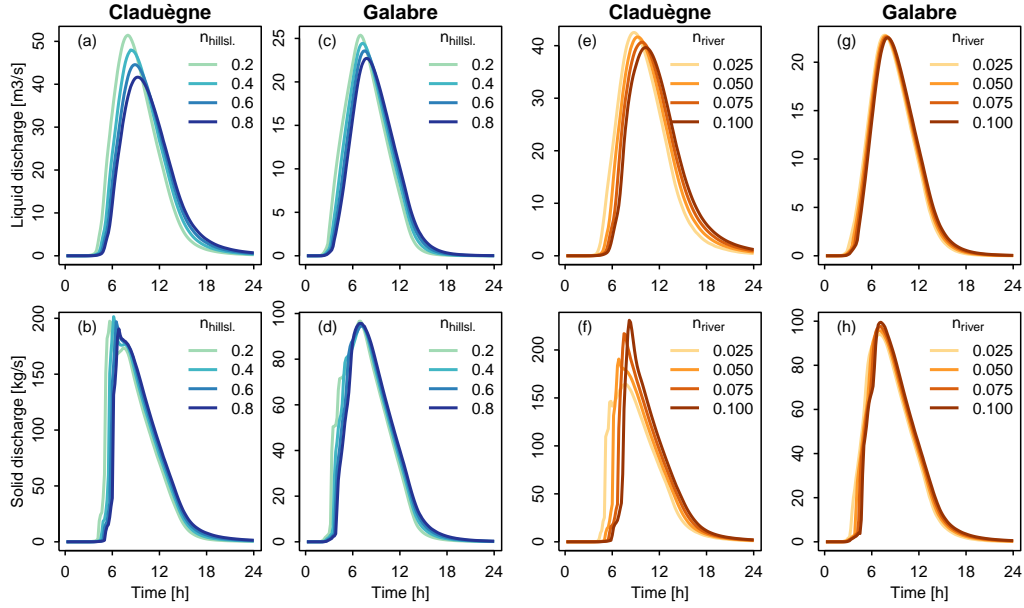


Figure 4.7: Sensitivity of modeled hydrographs (top row) and sedigraphs (bottom row) to changing Manning’s roughness parameter on the hillslopes (a-d) and in the river network (e-h). For subfigures a-d n_{river} was fixed to 0.05; for subfigures e-h $n_{hillst.}$ was fixed to 0.8.

Changing Manning’s n influenced the timing, the peak and the spread of both liquid and solid discharge (Fig. 4.7, Table 4.3). In general, increasing n led to a later time of rise of the hydrograph, a later time of peak and to slower recession with longer T_{lag} , T_c (Fig. 4.4, Table C.1). Considering the spreading of liquid discharges it seems that it is less sensitive to changes of Manning’s n in the Galabre than in the Claduègne catchment (Fig. 4.4, Table C.1). Increasing n also led to less maximum liquid discharge; interestingly, this was not the case for solid discharge. Peak solid discharge even increased with increasing n_{river} in the Claduègne catchment and to a lesser degree also in the Galabre catchment (Table C.1).

Table 4.3: Scheme of responses of liquid and solid discharges to changing the value for Manning’s n in the river network and on the hillslopes. ↗ means increase, ↘ decrease and → constant; two arrows correspond to strong increase or decrease.

	Claduègne				Galabre				
n_{river}	↗	$Q_{l,max}$	↘	$Q_{s,max}$	↗↗	$Q_{l,max}$	→	$Q_{s,max}$	→
$n_{hillsl.}$	↗	$Q_{l,max}$	↘↘	$Q_{s,max}$	→	$Q_{l,max}$	↘	$Q_{s,max}$	→

The larger catchment of the Claduègne was more sensitive than the smaller Galabre catchment (Table C.1, Fig. 4.7). Interestingly, in the Claduègne catchment liquid discharge was more sensitive to changes in $n_{hillsl.}$ than to n_{river} while solid discharge was more sensitive to n_{river} . In the Galabre this was not the case, both liquid and solid discharge were more sensitive to $n_{hillsl.}$.

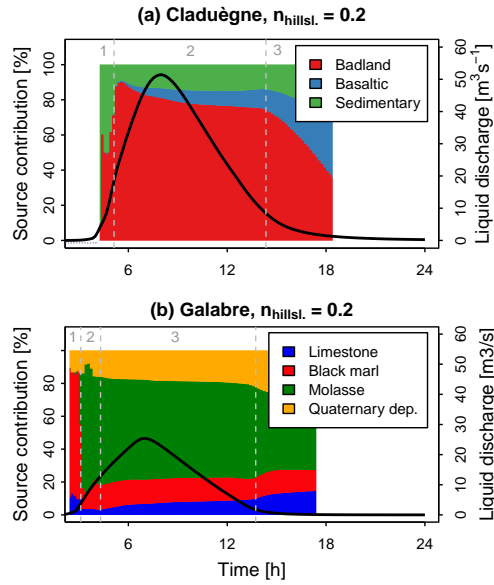


Figure 4.8: Modeled contributions of the sediment sources in the two catchments when Manning’s n on the hillslopes is set to 0.2.

Changing Manning’s n also influenced the temporal dynamics of source contributions. A low $n_{hillsl.}$ of 0.2 led to a multi-peaked sedigraph in the Claduègne catchment (Fig. 4.7b). This difference in the shape of the sedi-

graph also led to a difference in the modeled temporal dynamics of the percentage of source contributions (Fig. 4.8a). When $n_{hillsl.}$ was set to 0.2, the decrease of the contribution of the badland sources to total suspended sediment load in the Claduègne catchment was slower during the main part of the event (marked “2” in Fig. 4.8a) and the break point between phase 2 and 3 in the decrease of the badland source was more pronounced than in the basic scenario where $n_{hillsl.}$ was set to 0.8 (Fig 4.6a). In fact, for several hours during phase 2, the contributions of the three sources were nearly constant. This was not the case for the scenarios 3b and 3c where $n_{hillsl.}$ was set to 0.4 and 0.6. These scenarios hardly differed from the basic scenario (see [interactive figure](#)). In the Galabre catchment the scenarios 3b and 3c also hardly differed from the basic scenario. When $n_{hillsl.}$ was set to 0.2 the contributions during the main part of the event (“3” in Fig. 4.8b) remained more stable than in the basic scenario.

Changing n_{river} hardly changed the dynamics of the modeled source contributions in both catchments (results not shown, but can be seen in the [interactive figure](#)). Increasing n_{river} from 0.025 to 0.1 generally increased T_{lag} and T_c (Fig. 4.4) and led to a slight prolongation of the first flush of sediments from the sedimentary source (see [interactive figure](#)). In the Galabre this was also the case for the first flush of sediments originating from black marl, as it was the case for the changes in the CDA threshold shown in Fig. 4.6d.

Our results showed that even though modeled liquid discharge was sensitive to $n_{hillsl.}$, the sedigraphs of the main sources and thus of total suspended solid discharge were much less sensitive to this parameter (Fig. 4.7, Fig. 4.4). This was due to the fact that in both catchments the main sediment sources are located close to the river (Table 4.1), so only a small fraction of the trajectory of particles is located on the hillslopes. This was also represented in the modeled dynamics of the source contribution which barely changed unless the most extreme value of 0.2 was applied. This was again encouraging as this result suggested that it is sufficient to have a rough idea of the value of Manning’s n to study the dynamics of sediment fluxes. In the Claduègne catchment the modeled sedigraph was affected by variations of n_{river} which was less true for the Galabre catchment. This might be related to the difference of slopes of the river network in both catchments. Indeed, the mean slope in the river network is 2-3 times higher in the Galabre catch-

ment than in the Claduègne (Table 4.1). We assume that the model is more sensitive to changes in Manning’s n when slopes are low. However, also in the Claduègne catchment changes in n_{river} did not change the modeled dynamics of the source contributions, which was again encouraging for the use of our model to understand hydro-sedimentary dynamics.

4.3.2 The role of structural connectivity on the dynamics of suspended sediment fluxes at the outlet

The sedigraphs of the different sediment sources were strongly related to their location in the catchments and their structural connectivity. The lag times of the sources in the Claduègne catchment could generally be ranked as $T_{lag,Q_s}^{bad} < T_{lag,Q_s}^{sed} < T_{lag,Q_s}^{bas}$ (Fig. 4.4, Table C.1). This is consistent with the mean distance to the stream that is smallest for badlands and largest for the basaltic sources as well as with both connectivity indicators that are largest for the badlands and smallest for the basaltic sources (Table 4.1). Only the mean distance to the outlet is smaller for the sedimentary sources than for the badlands. In the Galabre catchment T_{lag,Q_s} and T_{c,Q_s} of the marls and molasses were always smaller than the ones of limestones and Quaternary deposits (Fig. 4.4, Table C.1). This is consistent with the distance to the streams but not with the other connectivity indicators (Table 4.1).

From figures 4.6 and 4.8, a general pattern of the contribution of the different sources to total solid discharge could be derived. In the Claduègne catchment at the onset of the event (“1”), the sediments originated from the sedimentary source and the badlands. During the phases 2 and 3 of the event the main source (i.e. the badlands that contribute most to annual sediment yield, Table 4.1) clearly dominated total solid discharge. The contribution of this source decreased gradually while the percentage of contribution of the other two sources increased. This is coherent with the structural connectivity of the sources. The sedimentary sources are closest to the outlet, while the badlands are closest to the stream and have the highest values of both connectivity indicators (Table 4.1). The basaltic sources are furthest from both the outlet and the stream and have the lowest IC values, which agrees to their late arrival at the outlet. In the Galabre catchment at the onset

of the event (“1”) suspended sediment originated almost entirely from the black marls. This source includes the badland that is very close to the outlet (Fig. C.1f). In the second phase of the event, the main source (i.e. molasse, Table 4.1) arrived and clearly dominated total solid discharge. Thereafter, the contribution of the molasses decreased while the one of the limestones and the Quaternary deposits increased (phase 3 and 4). This pattern was also coherent with the distribution of the sources in the catchment and their structural connectivity. The molasses are relatively far from the outlet (Fig. C.1f, Table 4.1), so they did not arrive at the outlet immediately at the onset of the event. The Quaternary deposits have the highest mean distance to the outlet and the limestones have the highest mean distance to the stream (Table 4.1) which is coherent with the late contribution of these sources.

To confirm the role of the distance to the outlet and the distance to the stream on the pattern of source contributions, the sources were subdivided based on these measures in the scenarios 4a and 4b. The results for the Galabre catchment are presented in Fig. 4.9 and Fig. 4.10. The limestone sources that are close to the river and the ones that are close to the outlet had a clockwise hysteresis pattern while the distant ones had an anticlockwise pattern. Here, the model confirmed typical interpretations of discharge-sediment flux hysteresis (Bača, 2008; Misset et al., 2019a). It should be stressed that the triangular rain applied here lasts a rather long period, much longer than the times of concentration of both catchments. Thus, the sedigraphs of all subsources were stretched over a time span that is comparable to the time span of the rain event. The distant sources arrived at the outlet long before the flux of the close sources ceased so the sedigraphs of the different subsources were superposed and did not lead to separate peaks. This holds true for both catchments and for the classification based on distance to the outlet as well as distance to the stream (see Fig. C.2 and Fig. C.3 for the Claduègne catchment).

Nonetheless, some of the temporal variability in the suspended sediment source contributions could be explained with the distance of the sources to the outlet. The first peak of black marls that arrived at the outlet of the Galabre during the onset of the event originated entirely from the subsources that are close to the outlet and adjacent to the river network (marked “1” in Fig. 4.9e and Fig. 4.10e). For the molasses and Quaternary deposits, the distance to the river or the outlet hardly impacted the variability of the

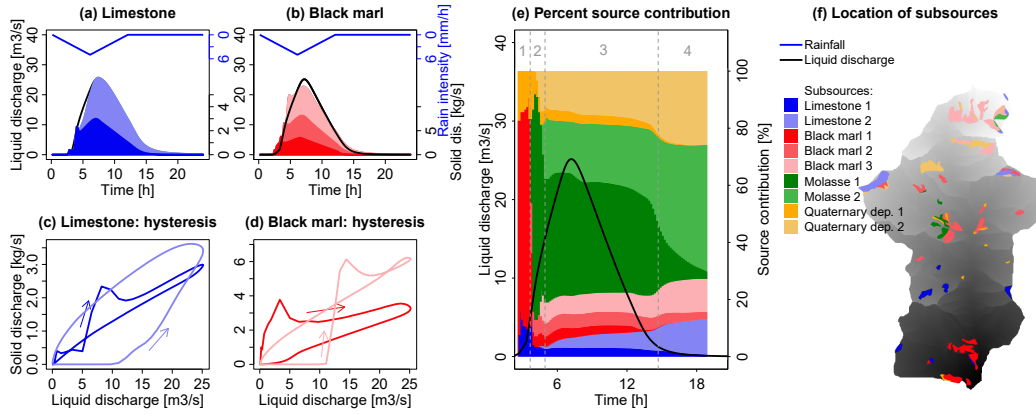


Figure 4.9: (a–b): Contribution of subsources of Limestone and Black marl that are classified according to their distance to the outlet. The colored areas show the contribution of sources close to the outlet (darker colors) and more distant sources (lighter colors) to the sedigraph. (c–d) and show the hysteresis loops of the subsources. Subfigure (e) shows the contribution of each subsurface to total solid discharge in percent. The dashed lines and the grey numbers above the figure distinguish different periods of the event as referred to in the text. (f) Location of the subsources in the Galabre catchment.

predicted source contributions. The first molassic sediments that arrived at the outlet during the rise of the hydrograph (“2”), originated almost entirely from the molassic patch that is directly adjacent to the river network. However, the decrease of the contribution of the adjacent sources during peak flow (“3”) occurred simultaneously with the arrival of the further sources.

A similar dynamic was observed in the Claduègne catchment. The first flush of sediments with a high contribution from the sedimentary source, originated entirely from sedimentary sources that are directly adjacent to the stream and from the badlands that are closest to the outlet (marked “1” in Fig. C.2). When the distance to the outlet was considered, it was remarkable that sediments which originated from the class badland 3 (corresponding to a distance to the outlet of 7.5 - 10 km; $T_{lag,Q_l} = 2.17 h$) arrived during the rising limb of the hydrograph (“2”) before the ones that originated from badland 2 (distance to the outlet of 5 - 7.5 km, $T_{lag,Q_l} = 2.67 h$) even though they are further away from the outlet. This is coherent with the distance to the river: While all patches belonging to the class badland 3 are directly adjacent to the river network, the ones belonging to the class badland 2 are further away from the river. However, this finding is related to the parameterization of the

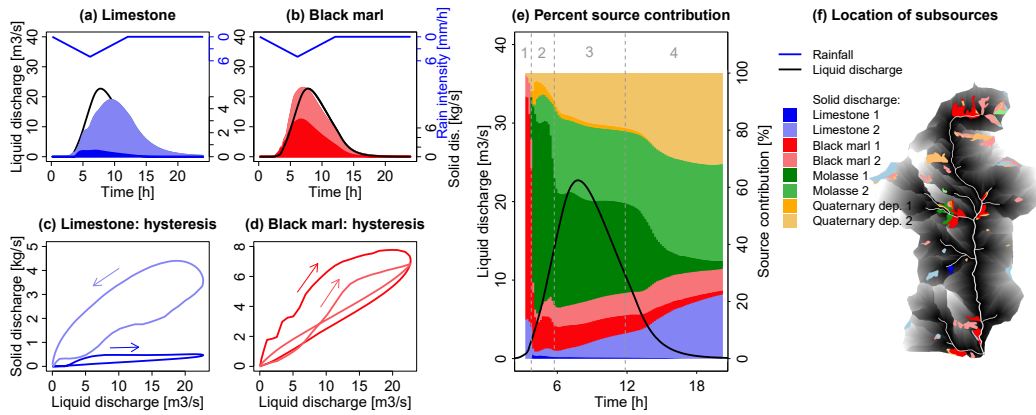


Figure 4.10: Contribution of subsources that are classified according to their distance to the stream in the Galabre catchment. For the description of the subfigures see the caption of Fig. 4.9.

model. In the results of scenario 4c where n_{river} was set to 0.1 and $n_{hillsl.}$ was set to 0.2 (i.e. less difference between n_{river} and $n_{hillsl.}$) this was not observed.

Our results showed that the location of the sources in the catchment highly influences the arrival time at the outlet and thus the modeled sediment flux dynamics. The main characteristics of the sediment flux dynamics were observed for all the modeling scenarios. As soon as appropriate CDA thresholds (typically 15 to 30 *ha*) and Manning’s n (in streams typically between 0.03 and 0.06, Barnes, 1967; Limerinos, 1970) were used, the temporal dynamics of the modeled contributions of the different sources were relatively independent of the modeling choices. Values could be varied in quite a high range without significantly changing these flux dynamics. However, this finding could be invalid for different types of rain events, notably shorter events. Nevertheless, one main result of this study was that for both mesoscale studied catchments, the actual location of sediment sources and their structural connectivity were more important than the discretization and parameterization of the model.

This first result allowed to provide a more detailed analysis on how catchment characteristics influence the hydro-sedimentary response. The results of our simulations showed that the Galabre catchment reacted faster than the Claduègne catchment. The hydrographs and the sedigraphs rose earlier

than in the Claduègne catchment and the rising limb of the hydrograph was steeper than the one of the Claduègne (shorter T_{lag} and T_c , Fig. 4.4, Table C.1). For the Galabre catchment the model was also less sensitive to the CDA threshold and to changes in Manning’s n . We assume that this is due to the smaller size of the Galabre catchment and the steeper slopes. Our results showed that the two catchments and also different sediment sources within the same catchment exhibited different sensitivities to model parameterization depending on their location in the catchment.

The results of the scenarios 4a-d further showed that the distance to the outlet and the distance to the stream influenced the sedigraph and the pattern of the source contributions. Different patches of closer and more distant subsources did not lead to multipeak sedigraphs when model was forced with a rather long unimodal hyetograph. Thus it did not explain the very high variability of source contributions observed during some events. Nevertheless, the classification into close and distant sources helped to understand the dynamics of source contributions. Other authors regarded hysteresis loops of discharge and suspended sediment concentrations to assess the role of close and distant sources where close sources are associated with clockwise hysteresis loops and distant ones with counterclockwise loops (e.g. Bača, 2008; Sun et al., 2016; Misset et al., 2019a). The finding that different hysteresis loops were observed for subsources of different connectivity shows that the subsources have a different hydro-sedimentary behavior and that even a simple classification as the one used here can help to understand the observed sediment flux dynamics. The lag times of the different sources were closely related to the distance to the stream and less so with the distance to the outlet suggesting that the distance to the stream is more important than the distance to the outlet in defining structural connectivity.

Many studies used the concept of structural connectivity to identify the main suspended sediment sources and transfer paths (e.g. Medeiros et al., 2010; Cavalli et al., 2013; D’Agostino and Bertoldi, 2014; López-Vicente et al., 2015). Others used the concept to interpret modeled sediment delivery ratios and erosion/deposition zones (Medeiros et al., 2010; Baartman et al., 2013a). Our results showed that the concept of structural connectivity can also be used to understand within-event dynamics of suspended sediment source contributions.

4.4 Conclusions and perspectives

This study aimed to improve our understanding of hydro-sedimentary processes leading to variability in the contribution of potential source soils to suspended sediments using a distributed, physical based numerical model. It allowed to assess how sensitive the model is to choices made during model discretization and parameterization. These methodological choices determine how structural connectivity is represented in the model and how the location of sources with respect to the river network and the outlet determined sediment fluxes.

We observed that the model was sensitive to the contributing drainage area threshold to define the river network and to Manning's roughness parameter n in the river network and on hillslopes. However, the model was less sensitive to all three values once the parameters varied only in a restricted, reasonable range. In our study sites, the pattern of modeled source contributions remained relatively stable when the CDA threshold was restricted to the range of 15 to 50 *ha* and n on the hillslopes to the range 0.4 - 0.8.

In the future, optimal choices of parameters should be based on a more precise search in these parameter ranges. More refined methodologies for calibration and uncertainty estimation such as Generalized Likelihood Uncertainty Estimation (GLUE, [Beven and Binley, 1992](#)) would be very helpful. They were not applied here because of the considerable calculation time of the complex model with a relatively large modeling domain but fine discretization (calculation times depended strongly on discretization but exceeded 20 *h* for individual model runs). A refined calibration of n based on available time series of water height at multiple sites in the Claduègne catchment ([Nord et al., 2017](#)) is in progress and will account for the distributed hydrological response.

The finding that the pattern of source contribution remained similar for quite broad ranges of CDA values and Manning's n is encouraging for the use of the modeling framework used here for the understanding of sediment fluxes. Comparing the two studied catchments showed that their hydro-sedimentary responses differed. The dynamics of source contributions varied due to different locations of the sources in the catchments, but the Galabre catchment also reacted much faster than the Claduègne catchment and was less sensitive to n and the CDA threshold. This could not only be attributed

to the smaller size of the catchment but was also due to the steeper slopes on the hillslopes and in the river network. This showed that the structural connectivity of the sources but also general catchment characteristics such as the slope determined hydro-sedimentary fluxes. In both studied catchment the actual location of sediment sources and their structural connectivity was found to be more important than choices made during discretization and parameterization of the model.

We further assessed how the structural connectivity of sources in the catchment influenced the sedigraphs at the outlet. The lag times and times of concentrations of the different sources were strongly related to their distance to the outlet and to the stream as well as to two indices of connectivity. Subsources that are closer to the outlet and the stream arrived earlier than more distant subsources. However, the sedigraphs of close and farther subsources were superposed and did not lead to separate peaks in the total sedigraph or the contribution of the different sources to total solid flux. This latter finding is certainly related to the rather long duration (12 *h*) of the rainfall time series that was used for all models analyzed in this chapter. We assume that different rainfall forcing would strongly impact the modeled hydro-sedimentary fluxes and the dynamics of sediment source contributions. Thus, in Chapter 5 the impact of spatio-temporal rainfall variability is addressed.

Chapter 5

Variability in source soil contributions to suspended sediments: the role of spatio-temporal rainfall variability

5.1 Introduction

This chapter is based on the draft of an article in preparation by Magdalena Uber, Guillaume Nord, Cédric Legout, Brice Boudevillain and Luis Cea. It is complemented by an interactive figure that can be found at https://modeloutputiber.shinyapps.io/Interactive_fig2/.

Rainfall contributes directly to soil erosion by water via splash erosion and indirectly by the generation of overland flow via rill, interrill and gully erosion. Overland flow is further needed to transport the eroded particles downhill to the river network. In this way, rainfall characteristics determine whether or not sediments get mobilized on erosion zones and whether these sources get connected to the outlet of the catchment. Rainfall is thus an

important aspect of functional connectivity that determines how landscape elements are linked via processes such as overland flow (Turnbull et al., 2008; Wainwright et al., 2011; Bracken et al., 2013).

In hydrological modeling the impact of the spatio-temporal rainfall variability on simulated discharge is an active research topic. Many studies tested the impact of different types of rainfall input (single rain gauge, semi-distributed rain gauge data, distributed radar data, combination of radar and rain gauge data) on modeled hydrographs (e.g. Sun et al., 2000; Sik Kim et al., 2008; Vieux et al., 2009; Anquetin et al., 2010; Looper and Vieux, 2012; He et al., 2013). Other studies found an effect of different spatial and temporal resolution of input data (Bronstert and Bárdossy, 2003; Ochoa-Rodriguez et al., 2015; Huang et al., 2019). For example Ochoa-Rodriguez et al. (2015) applied several aggregation factors to high spatio-temporal resolution data of 3 - 8 km^2 catchments and concluded that high temporal resolution is more important than high spatial resolution at this small scale.

However, there is no consensus on the impact of spatial rainfall variability on the hydrological model outputs (Emmanuel et al., 2015). Lobligeois et al. (2014) found that the sensitivity of a hydrological model on spatial rainfall variability depended on the catchment's size, rainfall intensity and on the degree of heterogeneity of the rain event. This latter finding was also confirmed by Emmanuel et al. (2017) and Anggraheni et al. (2018). They concluded that only if spatial rainfall variability was high and persistent, the hydrological response that was simulated with spatially uniform rainfall forcing differed significantly from the one obtained with distributed rainfall forcing data. For events with a relatively low spatial variability of cumulative event precipitation this was not the case. Smith et al. (2004) found that for a catchment with usually high spatial variability of precipitation, a distributed model yielded considerably better results than a lumped model, which was not the case for two other catchments with lower rainfall variability. Anquetin et al. (2010) concluded that the hydrological response of 32 catchments ranging from 2.5 - 99 km^2 was controlled by rainfall variability as soon as the soils were saturated.

Simulation approaches such as the one proposed by Emmanuel et al. (2015), can help to overcome the problem of measurement errors in radar data, rain gauge measurement and discharge measurements that are used

to evaluate model performance. They developed a simulation chain that includes (i) a rainfall simulator which generates artificial rain fields with varying spatio-temporal variability, (ii) a simulator which generated artificial stream networks and (iii) a distributed hydrological model. In this way, errors and uncertainty in the measurement of “real” catchment precipitation can be omitted and the effect of applying spatially uniform vs. distributed precipitation can be isolated. A similar approach was also adopted by [Seo et al. \(2012\)](#) who compared a stationary and a moving rainstorm and obtained different hydrological responses.

In soil erosion science, several studies also assessed the effect of spatio-temporal resolution of rainfall data on modeled erosion, but most of these studies were conducted at longer time scales using landscape evolution models ([Tucker and Bras, 2000](#); [Hancock and Coulthard, 2012](#); [Baartman et al., 2013b](#); [Coulthard and Skinner, 2016](#)). These studies showed that rain variability plays an important role in catchments ranging in size from 141 *ha* to > 400 *km*². For example, [Coulthard and Skinner \(2016\)](#) found that using spatially and temporally distributed rainfall time series instead of spatially lumped, daily rainfall time series increased mean annual sediment yield of the 415 *km*³ Swale catchment in northern England by > 100 %. Other studies regarded the effect of seasonal and spatial variations of rainfall forcing on the rainfall erosivity factor R of the USLE ([Renschler et al., 1999](#)) or addressed the impacts of climate change by estimating how expected changes of rainfall properties (mean annual precipitation, increased intensity, cumulative precipitation per storm) lead to increased soil erosion (review by [Wei et al., 2009](#)).

While the studies cited above underline the importance of rainfall data and its correct estimation as inputs for soil erosion and sediment transport models, they do not help to understand how spatio-temporal rain variability affects the hydro-sedimentary dynamics between and during flood events. A few studies addressed this topic at the event scale. [Baartman et al. \(2012\)](#) showed how rain intensity and duration determine differences of total sediment yield between events. In this way, the study confirmed observations that a few highly erosive events can contribute considerably to annual yields ([González-Hidalgo et al., 2007](#); [Navratil et al., 2011](#)). [Shen et al. \(2012\)](#) evaluated the impact of different spatial rainfall interpolation methods (Centroid method, Thiessen Polygon, Inverse Distance Weighting, two Kriging

techniques) on soil erosion modeled on a daily scale with SWAT. They found that sediment yield was more sensitive to rainfall spatialization than discharge. [Adams et al. \(2012\)](#) applied an approach similar to the one that [Emmanuel et al. \(2017\)](#) used for hydrological modeling by applying either spatially uniform or spatially distributed rainfall data in an erosion model that was based on the interrill erosion equation in WEPP. They observed that spatial variability led to increased erosion, due to locally higher rain intensity and higher runoff. Further, subcatchments were more sensitive to spatial rainfall variability than the entire catchment of about 150 km^2 . However, in the subcatchments, not only spatial variability differed but also spatially averaged precipitation, so the differences cannot be attributed to variability alone but also to different volumes. To our knowledge, no studies have analyzed the effect of spatio-temporal rain variability on within and between event dynamics of suspended sediment source contributions as is observed with fingerprinting studies (Chapter 3.3).

This chapter aims at improving our understanding of how rainfall characteristics affect hydro-sedimentary dynamics at the within and between event scale. We focus on the variability of sediment fluxes in terms of contributions of different sources to total suspended sediment flux in the Claduègne and Galabre catchments. The specific questions addressed in this chapter are:

- How do the temporal dynamics of rain events impact hydro-sedimentary fluxes at the outlet?
- Does spatial variability of rainfall forcing impact modeled hydro-sedimentary fluxes in the mesoscale catchments?
- How does the location of rain cells with respect to the sources determine contributions of different sources to sediment fluxes at the outlet?

To deal with these questions, we set up several scenarios to test the impact of temporal rainfall variability (intensity, duration, intermittency) and spatial variability (uniform vs. distributed precipitation, effect of approximating rainfall gradients). The characteristics of rain events is assumed to determine the functional or process-based connectivity of the sources to the outlet in the sense of [Wainwright et al. \(2011\)](#) and [Bracken et al. \(2013\)](#) (Chapter 1.2.2). Understanding the effect of these factors has two benefits. Firstly, it helps to assess the sensitivity of hydro-sedimentary models to the accuracy of rainfall forcing data. Secondly, it helps us to understand the

reasons for the observed variability of hydrosedimentary fluxes.

In this chapter, we used a simulation approach using synthetic uniformly distributed hyetographs and rain fields on the one hand and radar data of real rain events on the other hand. With the synthetic rain data we could test several scenarios of different representations of rainfall variability without having to consider uncertainties of actual rain data as well as hydro-sedimentary data. On the other hand, considering measured rain events is of interest to understand the observed hydro-sedimentary dynamics of real events and to compare the results obtained by modeling and sediment fingerprinting (Chapter 6.1).

In Chapter 4 the model was always forced with a uniformly distributed, synthetic, triangular hyetograph to separate the effect of choices made during model set up and the one of structural connectivity without considering the effect of the rainfall forcing. In this chapter on the other hand, we focus on rainfall characteristics that govern functional connectivity. Thus, rainfall forcing data was changed in different scenarios. The following sections are organized as follows: Firstly, a data quality control of the available radar precipitation data was performed in Chapter 5.2. As this data source is known to be prone to several sources of error, we evaluated this data by comparing it to ground based local measures of precipitation obtained from rain gauges. In Chapter 5.3.1 the rain events that are referred to later are described shortly. In Chapter 5.3.2 the modeling scenarios that were used to assess the impact of temporal and spatial variability of rainfall are described. Chapter 5.4 presents and discusses the results obtained with the different scenarios. Furthermore, we discuss the implications of these findings for hydro-sedimentary modeling and assess how rainfall variability can be an explanatory factor for observed variability of sediment fluxes.

5.2 Precipitation data quality control

For this chapter synthetic data as well as radar precipitation data was used. The latter was obtained for the entire country from 2007 to 2016 at a spatial resolution of 1 km^2 at a time step of 5 min (PANTHERE product of [Météo France, 2018](#); [Tabary, 2007](#)). Especially in mountainous areas, radar quantitative precipitation estimates are subject to several sources of errors

including ground clutter, beam shielding, signal attenuation in heavy rain or by a wet radome and variations in the rain drop size distribution (Borga, 2002; Pellarin et al., 2002; Germann et al., 2006; Ciach et al., 2007; Marra et al., 2014; Hachani et al., 2017). In addition, in the Galabre catchment the distance of the catchment to the closest S-band radar is $> 100 \text{ km}$ which increases the uncertainty considerably. In the Claduègne catchment, the closest radar is at 37 km distance to the catchment’s centroid, so we assume that the error is less important. To assess the uncertainty of the radar data, it was controlled and compared to local ground measurements of precipitation with rain gauges.

In a first step, we accumulated radar rain data over long periods to determine zones of systematic over- or underestimation of precipitation for example due to beam shielding. Neither the Galabre, nor the Claduègne catchment seemed to be highly affected by these types of error (Appendix D.1).

Secondly, for 57 events occurring between 2011 and 2016 in the Claduègne catchment and for 74 events in 2007 to 2016 in the Galabre catchment, radar data was compared to rain gauge data. In the Claduègne catchment the 22 rain gauges of the HPiconet data set (Nord et al., 2017) (available at the same 5 min resolution as the radar data) were used for this comparison. In the Galabre catchment the data from the three research rain gauges at Ainac (5 min resolution), Laval (5 min) and La-Robine-sur-Galabre (15 min) was used as well as the data from the operational rain gauges by Météo France at Digne-les-Bains (6 min), Thoard (1 d) and Beaujeu (1 d). Before undertaking this comparison, the data quality of the rain gauge data was controlled as well (Appendix D.1). In the Claduègne catchment radar and rain gauge data were compared at time steps 5 min , 15 min and 1 h while in the Galabre catchment the time step of the comparison depended on the resolution of the rain gauge data.

For all raster files the data of the cell that corresponded to the exact position of the rain gauge and the eight surrounding cells was extracted and averaged for the same time step as the rain gauge data. Only time steps where more than 0.1 mm of rain in 5 min or more than 1 mm of rain in 1 h were recorded by the rain gauge were considered. The residuals were calculated as $Res_i = G_i - R_i$, where G_i is the recording of the rain gauge and R_i

the precipitation estimate of the radar cell at the time step i . Further scores were calculated to compare the data, i.e. root mean square error $RMSE$, relative root mean square error $RRMSE$, Pearson’s correlation coefficient r , Spearman’s rank correlation coefficient ρ , Nash-Sutcliffe efficiency NSE and relative error E_{rel} (Eq. D.1 - D.6 in Appendix D.1). These scores were calculated (i) for all values, (ii) for low rain intensities (defined as the values lower than the 95th percentile Q_{95}) (iii) for medium rain intensities (Q_{95} - Q_{99}) and (iv) for high rain intensities ($> Q_{99}$). They were first calculated separately for each event and each rain gauge and then averaged over all events and / or rain gauges.

Table 5.1: Selected scores (Pearson’s correlation coefficient r , Nash-Sutcliffe efficiency NSE , relative error E_{rel}) calculated at different time steps and for low, medium and high rain intensities. The values are averaged over all events and over all rain gauges with the respective temporal resolution.

	Low intensities			Medium intensities			High intensities		
	$r[-]$	$NSE[-]$	$E_{rel}[%]$	$r[-]$	$NSE[-]$	$E_{rel}[%]$	$r[-]$	$NSE[-]$	$E_{rel}[%]$
Claduègne									
5 min	0.60	0.33	-0.98	0.42	0.08	0.98	0.45	-0.64	4.60
15 min	0.73	0.49	-0.96	0.50	0.13	3.40	0.52	-0.71	11.55
1 h	0.73	0.46	1.63	0.62	0.14	11.16	0.53	-1.99	32.94
Galabre									
5 min	0.34	-0.37	-0.44	0.17	-1.76	0.83	0.45	-6.49	3.36
15 min	0.48	-0.09	-0.34	0.12	-1.66	2.57	0.59	-2.78	7.67
1 h	0.70	0.02	1.00	0.43	-0.13	2.08	0.26	-2.38	8.57

The residuals of radar and rain gauge precipitation estimates at different time steps in the Claduègne catchment were usually lower than 0.5 mm for 5 min precipitation and lower than 2 mm for hourly precipitation and the systematic error was low (Fig. D.3). The errors were usually higher for smaller time steps and for higher rain intensity (Table. 5.1). For the high rain intensities E_{rel} was very high and the NSE was negative for all time steps. In the Galabre catchment the residuals were higher which resulted in scores that were worse than in the Claduègne catchment (Table. 5.1). It was especially evident by the negative NSE values for almost all intensities and time steps.

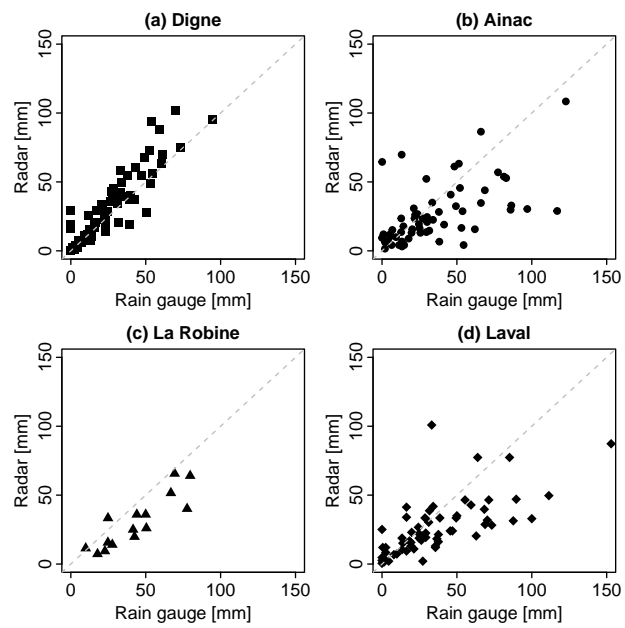


Figure 5.1: Comparison of cumulative event precipitation obtained with radar and rain gauge measurements at four locations in the Galabre catchment (Ainac and La Robine) or its vicinity. The dashed line is the line of identity.

We further assessed whether there was a seasonal or a spatial trend in the error between radar and rain gauge data. In the Claduègne there were no obvious trends even though events in autumn agreed less than those in the other seasons, especially at the rain gauge at St. Gineis en Coiron in the south of the basaltic plateau (Fig. D.4). However, at the rain gauge in Berzème in the north of the plateau, radar and rain gauges agreed well, so this did not represent a general spatial trend. In the Galabre catchment it was observed that there was a high dispersal from the line of identity of radar and rain gauge measurements, especially in summer and autumn (Fig. D.5). However, also in winter and spring there was a considerable underestimation of rain by the radar data. Concerning spatial trends, radar and rain gauge data of cumulative event precipitation agreed best at the rain gauge in Digne (Fig. 5.1a). At La-Robine-sur-Galabre there also was a good correlation, but precipitation was systematically underestimated by the radar data. At Ainac and Laval on the other hand there was a high scatter.

The analysis of seven rain events (four in the Claduègne catchment, three at the Galabre) that were regarded one by one (Chapter 5.3.1) showed that localized, convective events were often overestimated while stratiform, widespread events were often underestimated. The overestimation of convective events can be explained with the presence of very large rain drops or even hail, while the underestimation of stratiform events can be related to the numerous but small raindrops (Hachani et al., 2017; Diabi Skhakhfa et al., 2019). In mountainous regions a further aspect that contributes to this underestimation is the fact that the radar beam passes at a high altitude above the ground, thus it measures where drops are still smaller than when they reach the ground.

Given the considerable differences in rainfall amounts between radar and rain gauge data, we evaluated whether the spatial gradients in the radar data were similar to those observed by ground measurements. As can be seen in Fig. 5.2 this was not always the case. The data sets agreed mainly for small events with a low spatial precipitation gradient (encircled in Fig. 5.2). Only a few events were characterized by a difference of more than 10 mm in both data sets (green shaded area in Fig. 5.2) while there were several events where a gradient was present in one data set but not in the other (light gray shaded areas in Fig. 5.2). There were even events where there was an inverse gradient in the two data sets (darker gray shaded areas in Fig. 5.2). This

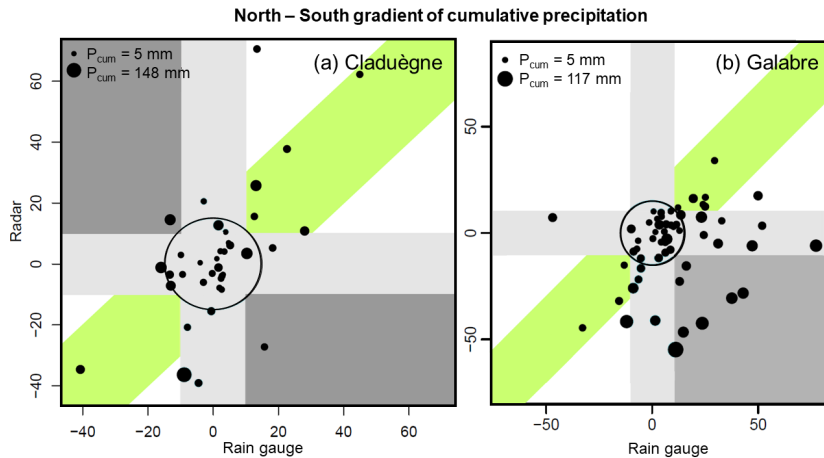


Figure 5.2: Difference of cumulative event Precipitation [mm] in the Claduègne (a) and Galabre (b) catchments recorded with rain gauges and radar. The values give the difference of event precipitation recorded at the northernmost and the southernmost rain gauge (Claduègne: distance of $15 km$ between Berzème and St. Germain; Galabre: distance of $16 km$ between Ainac and Digne). The size of the points is scaled to cumulative precipitation averaged over the two rain gauges.

concerned mainly the Galabre catchment.

Our results showed that especially in the Galabre catchment the radar data set is subject to large differences with ground measurements. At the scale of interest for our study, even the very basic structure of the rain field described as the rainfall gradient over a distance of about $15 km$ was oftentimes not represented correctly. Thus, there is a high interest in the advancement and application of methods for radar-rain gauge merging such as the one proposed by [Delrieu et al. \(2014\)](#) to obtain more accurate maps of quantitative precipitation estimates. This finding further confirmed the benefits of using simulated rain fields in modeling studies for process understanding and hypothesis testing ([Emmanuel et al., 2015](#)) as it is independent of errors of observed precipitation data.

For this study, the distributed rainfall maps obtained from radar data were used, but the considerable errors were kept in mind. They especially hindered the quantitative comparison of the modeled and observed hydro-sedimentary flux dynamics (Chapter 6.1). In the following chapter the events

considered in this chapter are regarded one by one.

5.3 Methods

5.3.1 Selected rain events

5.3.1.1 Claduègne

May 18th, 2013 The rain event was characterized by widespread, stratiform precipitation that coexisted with convective structures that were similar to the pattern classified as organized convective systems by [Hachani et al. \(2017\)](#). There was a low pressure system in western France, leading to strong south winds in southeastern France (Fig. [D.6c](#)). In the Claduègne catchment, this led to several very elongated rain cells with a north-south orientation that move northwards (Fig. [5.3a](#)). The cell that hit the catchment most intensively first reached the southwest of the catchment and then traversed it to the northeast. When precipitation was accumulated over the duration of the event (P_{cum}), there was a gradient from the northeast (highest P_{cum}) to the southwest (Fig. [5.3e](#)). The rain gauges recorded 86 mm of P_{cum} at Berzème in the north of the catchment and 67 mm at Mirabel further south, so P_{cum} was overestimated by the radar data (P_{cum} of 150 and 114 mm at the two rain gauges), but the gradient was represented correctly. The event led to an important hydrological response (peak discharge $Q_{l,max}$ of $> 80 m^3 s^{-1}$) and high sediment export of nearly 12000 t during that event alone.

October 23rd, 2013 The event was also caused by an organized meteorological structure with a large extent stretching from Northern Africa to Northern Europe (Fig. [5.3b](#)). In the Claduègne catchment this structure consisted again of elongated rain cells. They passed the catchment from the southwest to the northeast, parallel to their orientation, which led to high P_{cum} . The gradient of P_{cum} had a northwest-southeast orientation (Fig. [5.3f](#)) because the first cell passing the catchment only struck its northwestern border. This was consistent with the rainfall gradient observed with rain gauges (P_{cum} of 48 mm in Mirabel and 69 mm in Aubenas, about 7.5 km to the west of Mirabel). There also was a high $Q_{l,max}$ of about $60 m^3 s^{-1}$ and high sediment export of nearly 11000 t.

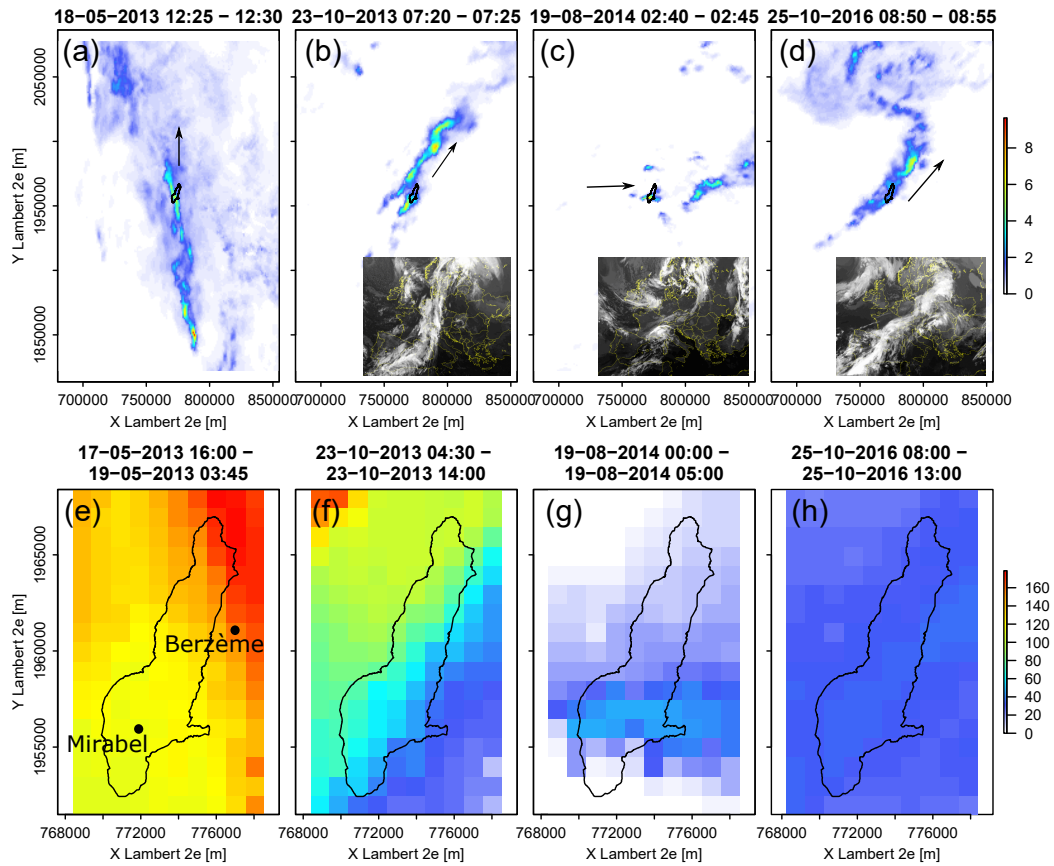


Figure 5.3: Precipitation characteristics of rain events in the Claduègne catchment. The top row shows maps of precipitation during single time steps [$mm/5\ min$] during four rain events (Météo France, 2018); the inset maps show infrared satellite images of cloud cover over Europe (Source: http://meteocentre.com/archive/archive.php?type=eur_ir&DAY=23&MONTH=10&YEAR=2013&HOUR=07&MIN=00&lang=en; not available in May 2013). The arrows show the displacement direction of the rain cells. Their orientation corresponds well to the one of the lines of geopotential height at 500 hPa (red dashed lines in Fig. D.6) which is an indicator for the movement of air masses at an altitude of about 5 km. The bottom row shows cumulative event precipitation [mm].

August 19th, 2014 This event was an example of a localized summer storm. It was not part of a larger, organized system. Even though clouds covered southeastern France and northern Italy (Fig. 5.3c), pressure gradients were very low across the entire country and wind speeds in southeastern France were low (Fig. D.6d). A particularity of the event was that it occurred - unlike the typical summer storm - during the night. One rather isolated, elliptical rain cell passed the southern part of the catchment shortly before 3 am UTC. The north of the catchment was barely affected while in the south it was very intense. At Mirabel a total of 35 mm was recorded between 2 am and 3 am, while at Berzème only 11 mm were measured. There was only a minor hydrological response with $Q_{l,max}$ of $1.1 m^3 s^{-1}$ due to the fact that the soils were far from saturation during this summer period. Sediment export (23 t) was much less than for the events in 2013.

October 25th, 2016 The event was part of an organized system over Europe, but at the Claduègne catchment rainfall is less intense than for the events in 2013 (Fig. 5.3d and h). A particularity of the event was that rainfall was distributed almost homogeneously over the entire catchment. Based on the radar data, P_{cum} was about 30 mm all over the catchment. On the other hand, the rain gauges at Berzème and Mirabel recorded 44 and 40 mm respectively, so radar data underestimated rainfall for this event. Nevertheless, the data sets agreed that precipitation is rather homogeneously distributed in the catchment. The rain event caused a flood with $Q_{l,max}$ of about $23 m^3 s^{-1}$ and an estimated sediment yield of 669 t.

5.3.1.2 Galabre

June 23rd, 2010 The event of June 2010 was a highly localized, intense summer thunderstorm. It was not part of an organized weather system (Fig. 5.4a) and lasted only about 1.5 h. In the Galabre catchment it was a distinct event because it only affected the southern part of the catchment while hardly any rain was recorded in the northern part. In the radar data a very strong precipitation gradient was observed (Fig. 5.4d). As the rain gauge at La-Robine-sur-Galabre was installed only in 2014, no data was available in the south of the catchment. This pattern was still consistent with observations because at Ainac in the north of the catchment only 4 mm of rain were recorded but a considerable hydrological response with $Q_{l,max}$ of about $8 m^3 s^{-1}$ was observed at the outlet. The quantitative precipitation estimates

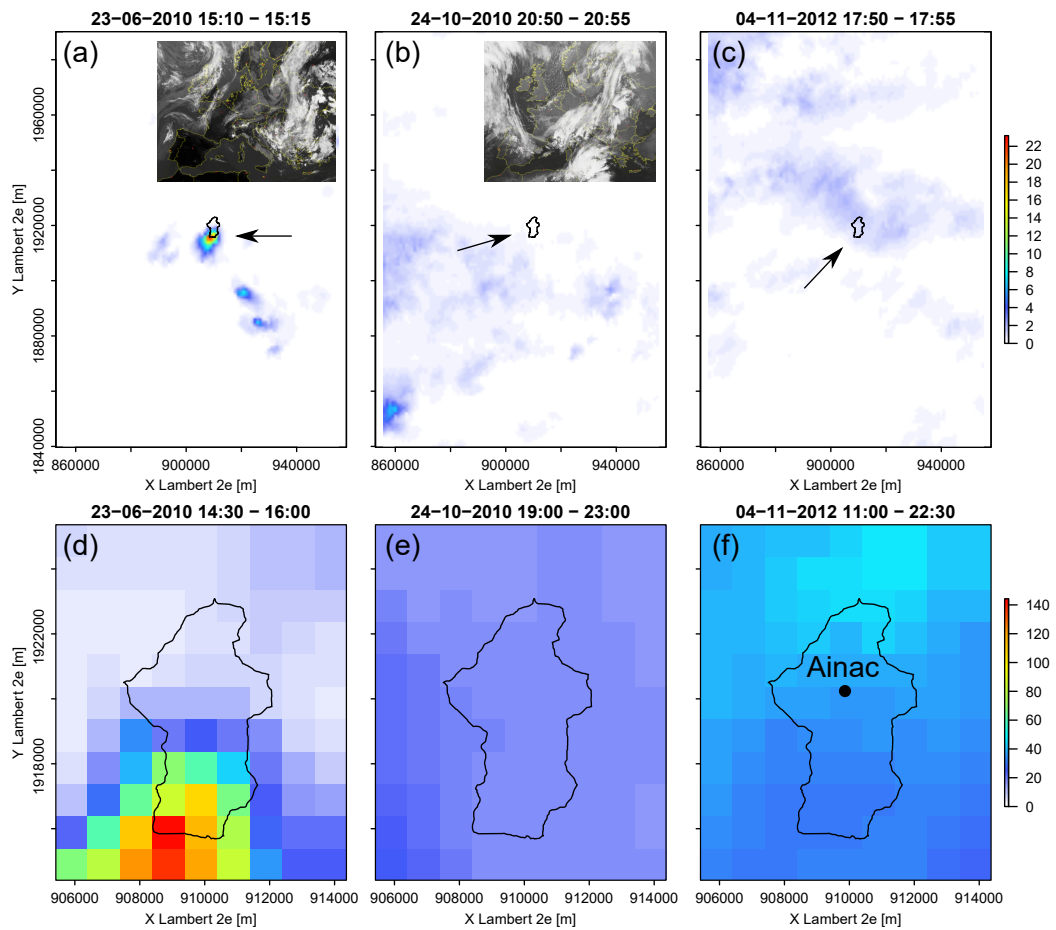


Figure 5.4: Precipitation characteristics of rain events in the Galabre catchment. The top row shows 5 min precipitation, the bottom row cumulative event precipitation. See caption of Fig. 5.3 for more details.

obtained from radar data are nonetheless highly likely to be overestimated as they locally reached extremely high, unrealistic intensities of 68 mm in 5 min in one pixel in the southwest of the catchment. In terms of sediment flux, the event led to the highest sediment yield of nearly 8500 t recorded in the study period 2007 - 2014 by [Esteves et al. \(2019\)](#) and the event stood out in the sediment fingerprinting study for the fact that the sediments originated almost entirely from black marls unlike all other events that were usually dominated by sediments originating from molasses (Chapter 3.3).

October 24th, 2010 This event was associated to a depression at the Mediterranean coast close to Marseille, thus, it was part of an organized system in southeastern France (Fig. 5.4b, Fig. D.6a). In the Galabre catchment this event was manifested as widespread, stratiform precipitation that lasted for about 4 h at moderate intensities (maximum 10 min rainfall intensity of 14 mm h^{-1}). It can be considered as a typical autumn event. Cumulative precipitation was distributed almost uniformly over the catchment (Fig. 5.4e), so the event presents a strong contrast to the one of June 2010. Cumulative event precipitation was considerably underestimated by the radar data as it ranged between 15 and 18 mm while 45 mm were recorded at Ainac. The observed hydrological response and sediment export were moderate with $Q_{l,max}$ of about $1.1 \text{ m}^3 \text{ s}^{-1}$ and about 150 t of exported sediment.

November 4th, 2012 The event was equally dominated by widespread, stratiform precipitation. It was related to a large depression between Ireland and Great Britain (Fig. D.6b). The event lasted about 12 h , maximum 10 min rainfall intensity was 17 mm h^{-1} and the shape of the hyetograph was similar to the synthetic triangular hyetograph applied in Chapter 4. The spatial distribution of precipitation in the catchment was also relatively uniform (Fig. 5.4f). Cumulative precipitation was again underestimated by the radar data (spatial average of 36 mm while 62 mm were recorded at Ainac). The observed hydrological response with $Q_{l,max}$ of about $9 \text{ m}^3 \text{ s}^{-1}$ was important and the sediment export of 3235 t ranks among the ten events with highest sediment yields from 2007 - 2014 ([Esteves et al., 2019](#)).

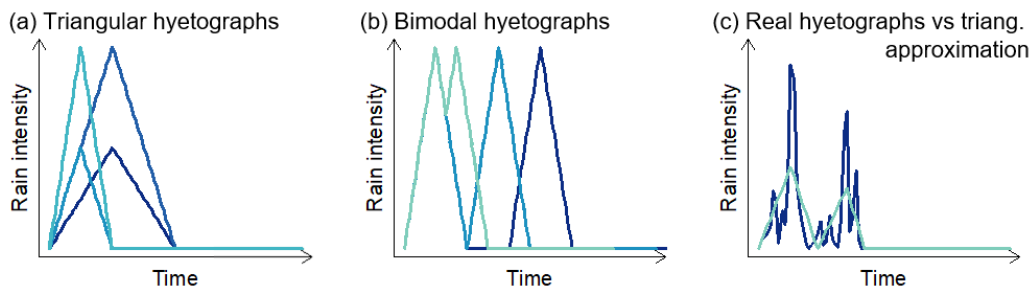


Figure 5.5: Schematic representation of hyetographs that were used as rainfall forcing in the scenarios that aimed at assessing the role of temporal rain variability.

5.3.2 Rainfall forcing used in the modeling scenarios

5.3.2.1 Temporal rain variability

In a first set of scenarios the impact of temporal rainfall variability on the modeled hydro-sedimentary fluxes and the dynamics of source contributions was tested. The model was set up as the basic scenario described in Chapter 4 and then the rainfall forcing was changed. To isolate the effect of temporal from spatial rain variability, rainfall was applied spatially uniform over the entire catchment. Details about the different scenarios are given in Table 5.2. In the basic scenario (Sc. 1), the model was forced with a synthetic triangular hyetograph where rain intensity increases linearly from 0 mm h^{-1} in the beginning of the event to a maximum of 5 mm h^{-1} after six hours and then decreases linearly to 0 mm h^{-1} twelve hours after the beginning of the rain event. In a first step the impact of rain intensity and duration was tested by still applying this synthetic triangular hyetograph but with higher intensity and/or shorter duration (Sc. 2a-2c; Fig. 5.5a). Further, the impact of two consecutive rain pulses was tested by applying bimodal hyetographs. They were each composed of two time-shifted synthetic triangular hyetographs with a duration of 6 h and a maximum intensity of 10 mm h^{-1} . Several bimodal hyetographs with different durations between the peaks were applied. The ones with 2 h and 4 h hours between the peaks had continuous precipitation because rain intensity between the peaks never decreased to 0 mm h^{-1} while the ones with 10 , 14 and 18 h between the peaks presented a time of 4 , 8 and 12 h without precipitation (Sc. 3a-3e; Fig. 5.5b). Thirdly, to test the effect of high frequency temporal variability of real hyetographs, the model was run (i) with real hyetographs of rain events that occurred in one of

Table 5.2: Duration and maximum 10 *min* precipitation intensity (I_{max}) of the hyetographs that were applied to test the impact of temporal variability. For bimodal hyetographs the time between the two peaks is given in addition. All hyetographs were applied to both catchments. A schematic representation of the hyetographs is shown in Fig. 5.5. Sc. 1 and 2 are shown in Fig. 5.5a, Sc. 3 in Fig. 5.5b and Sc. 4 in Fig. 5.5c.

Sc.	Description	Duration [h]	I_{max} [mm h ⁻¹]	Time betw. peaks [h]
1	Basic scenario	12	5	-
2a	Higher intensity	12	10	-
2b	Shorter	6	5	-
2c	Shorter & higher intensity	6	10	-
3a	Bimodal	8	10	2
3b	Bimodal 2	10	10	4
3c	Bimodal 3	12	10	6
3d	Bimodal 4	16	10	10
3e	Bimodal 5	20	10	14
3f	Bimodal 6	24	10	18
4a	Real event Gal 04-11-2012	11	17	-
4b	Real event Cld 23-10-2013	8.5	27	4.5
4c	Approximation of 4a	11	11	-
4d	Approximation of 4b	8.5	12	4.5

the catchments (time step 10 *min*) and (ii) with triangular approximations of these hyetographs. It was ensured that both real hyetographs and their triangular approximation had the same cumulative precipitation and the same time of peak rainfall. The first real hyetograph (event of November 4th, 2012 occurring at the Galabre) had a shape similar to the triangular hyetograph of the basic scenario. The second real hyetograph (event of October 23rd, 2013 occurring at the Claduègne, Fig 5.5c) had a clear bimodal shape. All hyetographs described above were applied to both catchments.

5.3.2.2 Spatial rain variability

A second set of scenarios was designed to test the impact of spatial and spatio-temporal variability. The highest detail of spatio-temporal information was contained in the time series of radar raster data at a resolution of 1 *km*² and 5 *min* (Sc. 8a-e ; Fig. 5.6d). We tested several ways to simplify this spatio-temporal pattern and assessed the impact of these simplifications on the modeled hydro-sedimentary response. Firstly, to test the impact of

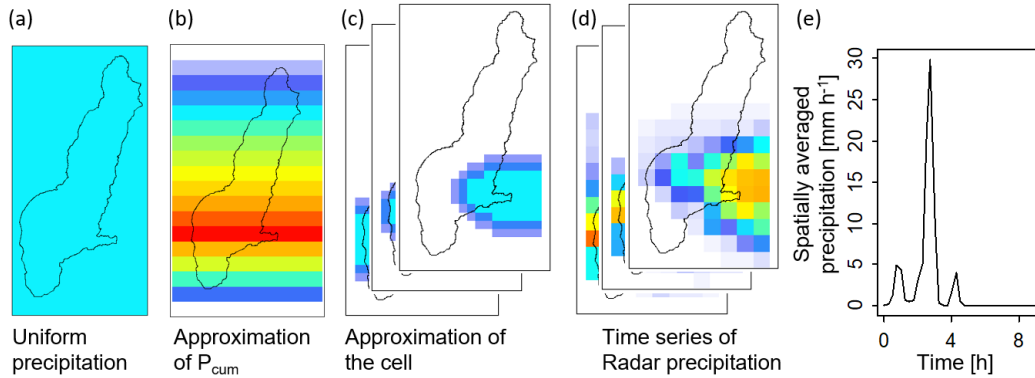


Figure 5.6: Schematic representation of distributed precipitation maps that were used as rainfall forcing to test the influence of spatial rainfall variability. The data represents the event of August 19th, 2014 in the Claduègne catchment. Subfigures a-c show different simplifications of the time series of distributed precipitation (d). Subfigure e shows the time series of spatially averaged averaged precipitation obtained from the radar precipitation (d).

small scale spatial variability, the shape of the rain cell that passed over the catchment was simplified by a geometric form that resembled the rain cell. Often, the shape of convective rain cells was found to resemble an ellipse (e.g. Barnolas et al., 2010; Peleg and Morin, 2012; Marra et al., 2016). Here, we applied an ellipse that passed the catchment from the west to the east (Sc. 7; Fig. 5.6c) as did the cell of the event on August 19th, 2014 in the Claduègne catchment. The rain intensity within the ellipse was fixed in a way that spatially averaged catchment rainfall was the same as for the time series of radar data. In the center of the ellipse rain intensity was spatially homogeneous and decreased linearly towards the edge of the ellipse (Fig. 5.6c). The dimensions (major axis: 8.5 km , minor axis: 5.0 km) and the displacement velocity (12 km h^{-1}) of the ellipse were chosen in a way that it resembled the “real” rain cell.

Secondly, we summed up in time all the radar rasters corresponding to a rain event to obtain a map of spatially distributed cumulative event precipitation (P_{cum} , as shown in Fig. 5.3e-h and 5.4d-f). This pattern of P_{cum} was simplified by creating a linear approximation of the spatial gradient in the catchment (Sc. 6a-b, Fig 5.6b). This map was normalized in a way that the spatial average in the catchment was 1. Then it was multiplied with the time series of spatially averaged catchment mean precipitation extracted from the

spatially distributed radar data (Fig. 5.6e). In this way, the information of the precipitation gradient of P_{cum} as well as the temporal dynamic remained but the small scale spatial variability was eliminated. This scenario was similar to rain fields that could be obtained in the absence of radar precipitation data when rain field have to be approximated by interpolation of rain gauge data with a low density in the catchment (e.g. Shen et al., 2012). The volumes of rain, the temporal dynamics and the spatial gradient of P_{cum} were the same in Sc. 6a and 8a as well as in Sc. 6b and 8b. By comparing the two pairs of scenarios, the effect of small scale rainfall variability was isolated. In the Claduègne catchment the quality of the spatially distributed radar data was assumed to be higher than in the Galabre catchment because it agreed better with rain gauge observations (Chapter 5.2). For this reason, the scenarios 6 and 7 were only applied in the Claduègne catchment and not in the Galabre catchment.

Lastly, spatial variability was completely eliminated by applying spatially uniform precipitation over the entire catchment (Sc. 5a-e, Fig 5.6a). To be able to compare these scenarios to the ones with spatially distributed precipitation input (Sc. 8a-e), spatially averaged catchment mean precipitation was calculated at each time step and applied uniformly over the entire catchment. Thus, the comparison of the results of Sc. 5a-e to the ones of Sc. 8a-e is similar to the approach that was taken by Emmanuel et al. (2017) for hydrological modeling and by Adams et al. (2012) for hydro-sedimentary modeling.

5.3.2.3 Location of the storm

A last set of scenarios (9a-c) was set up to assess how the hydro-sedimentary response and particularly the modeled source contributions changed depending on the location of the storm in the catchment. To this end, an artificial storm represented by a rain cell in the shape of an ellipse that passed over the catchment from the west to the east was simulated. The form of the ellipse and the displacement velocity were similar to the rain event in the Claduègne catchment on August 19th, 2014, but to simplify this artificial storm as much as possible, spatially homogeneous rain intensity was applied in this ellipse. It traveled over each catchment in the northern part, the central part and the southern part (Fig. 5.7). The size of the ellipse was kept the same for the two catchments, so it covers a larger fraction of the Galabre catchment

Table 5.3: Overview of the scenarios that were set up to assess the impact of spatial variability and location of the storm. The second column gives a short description of the spatial representation of the precipitation input. See the description in main text for more information. The third column gives the event that was used to derive the data (Cld: Claduègne, Gal: Galabre). For a short description of the rain events, see Chapter 5.3.1. The scenarios 5-8 were only applied to the catchment that rainfall data was obtained from. Scenario 9 was applied to both catchments because the rain data is highly abstracted from the recorded data.

Sc.	Spatial representation of precipitation	Event
5a	Uniform	Cld 18-05-2013
5b	Uniform	Cld 19-08-2014
5c	Uniform	Cld 25-10-2016
5d	Uniform	Gal 23-06-2010
5e	Uniform	Gal 24-10-2010
6a	Approximation of P_{cum}	Cld 18-05-2013
6b	Approximation of P_{cum}	Cld 19-08-2014
7	Approximation of the rain cell	Cld 19-08-2014
8a	Time series of raster precipitation	Cld 18-05-2013
8b	Time series of raster precipitation	Cld 19-08-2014
8c	Time series of raster precipitation	Cld 25-10-2016
8d	Time series of raster precipitation	Gal 23-06-2010
8e	Time series of raster precipitation	Gal 24-10-2010
9a	Ellipse, north of the catchment	-
9b	Ellipse, centre of the catchment	-
9c	Ellipse, south of the catchment	-

than of the Claduègne catchment as the latter is roughly two times larger than the former.

5.4 Results and discussion

5.4.1 How does temporal variability of rainfall forcing impact simulated hydro-sedimentary fluxes of different sediment sources?

Changing the intensity and the duration of the event strongly impacted maximum liquid and solid discharge ($Q_{l,max}$ and $Q_{s,max}$, Table 5.4). For example increasing maximum rain intensity with a factor two (Sc. 2a compared to

Table 5.4: Calculated characteristics of modeled hydrographs and sedigraphs for the scenarios assessing the role of temporal variability. Abbreviations: T_{lag,Q_l} : lag time of liquid discharge, T_{c,Q_l} : time of concentration of liquid discharge, T_{spr,Q_l} : spread of the hydrograph, $Q_{l,max}$: peak liquid discharge. Q_s refers to solid discharge and the characteristic times are calculated for each source separately (i.e. badlands, basaltic and sedimentary in the Claduègne catchment; limestone, black marl, molasses and Quaternary deposits in the Galabre catchment). The background color of the cells represents the percent change of each value with respect to the basic scenario for Sc. 2a - 3f and with respect to Sc. 4a and b for Sc. 4c and 4d (color legend in the bottom of the table).

	1 Basic Scenario	2a Higher intensity	2b Shorter	2c Shorter & higher int.	3a Bimodal $\Delta_t = 2h$	3b Bimodal $\Delta_t = 4h$	3c Bimodal $\Delta_t = 6h$	3d Bimodal $\Delta_t = 10h$	3e Bimodal $\Delta_t = 14h$	3f Bimodal $\Delta_t = 18h$	4a Real ev. Gal 04-11-2011	4b Real ev. Clid 23-10-2013	4c Approx. of 4a	4d Approx. of 4b
Claduègne														
T_{lag,Q_l} [h]	4.00	3.17	4.00	3.33	3.33	3.67	4.17	7.33	3.42	3.50	3.83	4.50	3.83	4.00
T_{c,Q_l} [h]	5.67	4.33	7.50	6.00	5.17	5.17	5.50	9.67	6.67	6.75	6.00	5.00	4.17	5.00
T_{spr,Q_l} [h]	12.33	11.67	9.33	8.50	9.67	11.67	14.17	18.33	19.50	19.33	13.33	10.75	11.00	11.00
$Q_{l,max}$ [$m^3 s^{-1}$]	42	93	25	62	87	85	77	69	66	65	62	131	79	130
$Q_{s,max}$ [$kg s^{-1}$]	191	300	200	345	346	345	345	293	345	345	239	638	312	532
T_{lag,Q_s} bad [h]	2.67	2.17	3.17	2.33	2.33	2.50	3.00	2.42	2.42	2.42	2.67	2.50	2.67	2.25
T_{c,Q_s} bad [h]	3.00	2.50	3.50	2.50	2.50	2.50	2.50	2.75	2.75	2.75	3.17	2.25	1.83	2.25
T_{spr,Q_s} bad [h]	9.17	9.67	4.67	4.50	6.67	8.67	10.67	10.83	10.67	10.50	10.17	7.75	8.33	8.00
T_{lag,Q_s} bas [h]	6.17	5.00	7.50	5.50	5.17	5.17	5.67	9.00	8.50	10.33	5.67	6.25	5.67	5.50
T_{c,Q_s} bas [h]	10.83	8.17	16.00	11.50	9.33	9.17	9.67	14.17	10.33	10.50	10.00	9.00	8.33	8.75
T_{spr,Q_s} bas [h]	16.00	14.17	16.83	13.00	12.83	14.50	17.17	21.67	25.83	30.00	15.33	14.00	14.00	14.00
T_{lag,Q_s} sed [h]	3.83	3.00	3.67	3.00	3.17	3.50	4.00	7.50	3.17	3.25	3.67	4.50	3.67	4.00
T_{c,Q_s} sed [h]	7.17	5.17	8.17	7.00	6.17	6.00	6.17	10.50	7.83	8.58	7.00	5.25	5.17	5.50
T_{spr,Q_s} sed [h]	14.00	12.83	10.00	9.50	10.83	12.67	14.83	19.17	23.17	23.83	14.83	11.25	12.17	11.75
Galabre														
T_{lag,Q_l} [h]	2.33	1.83	2.33	1.83	2.00	2.33	2.67	2.00	2.08	2.08	2.33	5.25	2.17	2.25
T_{c,Q_l} [h]	2.67	2.17	3.67	3.00	2.67	2.83	2.83	3.33	3.33	3.33	3.17	11.75	4.17	2.50
T_{spr,Q_l} [h]	10.83	10.83	6.67	6.50	8.33	10.50	12.50	14.83	14.33	14.17	12.50	15.75	13.17	9.50
$Q_{l,max}$ [$m^3 s^{-1}$]	23	48	16	39	46	43	41	40	39	39	31	93	43	82
$Q_{s,max}$ [$kg s^{-1}$]	96	171	90	176	176	176	176	181	192	194	126	425	168	329
T_{lag,Q_s} li [h]	3.67	3.00	3.33	2.83	3.00	3.33	3.83	5.17	6.67	3.17	3.67	4.50	3.33	3.75
T_{c,Q_s} li [h]	6.00	4.83	7.67	6.83	5.67	5.50	5.67	5.83	6.00	8.33	6.00	5.00	4.67	5.25
T_{spr,Q_s} li [h]	14.00	13.33	10.83	10.33	11.17	12.83	15.00	19.33	23.50	25.00	14.67	11.50	12.50	12.00
T_{lag,Q_s} ma [h]	1.83	1.33	2.00	1.50	1.67	1.83	2.33	1.58	1.58	1.58	1.83	1.75	1.67	1.50
T_{c,Q_s} ma [h]	2.67	1.83	3.00	2.17	2.17	2.17	2.17	2.50	2.33	2.33	2.67	1.25	1.33	1.75
T_{spr,Q_s} ma [h]	11.17	10.83	6.33	5.83	8.00	10.00	12.00	13.33	12.83	12.83	12.33	8.25	9.50	8.75
T_{lag,Q_s} mo [h]	1.83	1.33	2.00	1.50	1.50	1.83	2.17	1.58	1.58	1.58	1.83	1.25	1.67	1.50
T_{c,Q_s} mo [h]	2.33	1.67	2.50	1.83	1.83	1.83	1.83	2.08	2.00	1.92	2.50	1.13	1.17	1.50
T_{spr,Q_s} mo [h]	10.33	10.33	5.17	5.00	7.17	9.17	11.17	11.50	11.17	11.00	11.67	5.75	9.00	8.25
T_{lag,Q_s} qu [h]	2.67	2.00	2.83	2.17	2.33	2.50	3.00	2.17	2.17	2.17	2.67	2.75	2.33	2.50
T_{c,Q_s} qu [h]	4.00	3.17	4.67	3.67	3.67	3.67	3.67	3.75	3.67	3.75	4.17	2.75	2.67	3.00
T_{spr,Q_s} qu [h]	12.00	11.67	7.33	6.83	9.00	11.00	13.00	16.00	14.67	14.83	13.17	9.25	10.50	9.75
Change [%]	0 - 9	10 - 19	20 - 29	30 - 49	50 - 69	70 - 89	90 - 119	120 - 149	150 - 179	≥ 180				

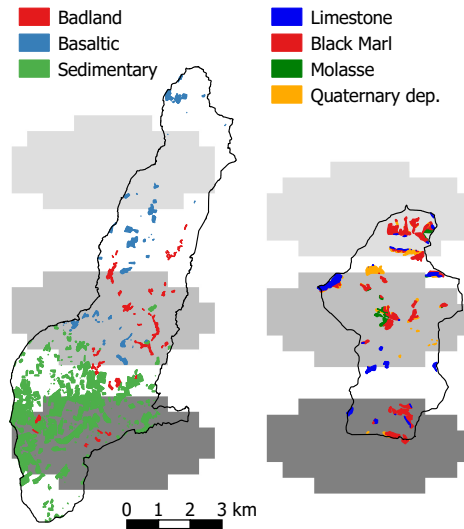


Figure 5.7: Location of the artificial, elliptic storms passing over the two catchments of the Claduègne (left) and the Galabre (right) from the west to the east with a constant displacement velocity and homogeneous rain intensity in Sc. 9a-c. The colored patches show the suspended sediment sources in the catchments.

the basic scenario) also increased $Q_{l,max}$ by slightly more than a factor two in both catchments. $Q_{s,max}$ was much less sensitive to changes in the duration of the hyetograph than to changes in the intensity which was not the case for $Q_{l,max}$. These results agreed with those of (Chaubey et al., 1999) and (Baartman et al., 2012). The correlation of sediment yield and maximum sediment fluxes with maximum rain intensity was also found in observed data (e.g. Mohamadi and Kavian, 2015; Tuset et al., 2016). However, the pattern of the predicted source contributions barely changed (Fig. 5.8). In the Claduègne catchment using the basic scenario (Sc. 1) as well as Sc. 2a-2c, the first sediments that reached the outlet originated from the sedimentary and the badland sources with each source contributing about 50% to total suspended sediment flux. Then the contribution of the badlands increased abruptly to about 90%. Subsequently, the contribution of the badlands decreased slowly while the contributions of the sedimentary and the basaltic sources increased. In the Galabre catchment this pattern was similar (Fig. 5.8). The first sediments originated almost entirely from the badlands on black marls which is the source that is closest to the outlet and well connected. However, the sediments originating from the main source, i.e. the badlands on molasses

arrived very soon at the outlet and thus the contribution of the black marls diminished rapidly to about 15%. Then, the contribution of the molasses decreased gradually while the contributions of the badlands on limestone and Quaternary deposits increased (Fig. 5.8). This general pattern was related to the location of the sources in the catchment and thus to their structural connectivity (Chapter 4).

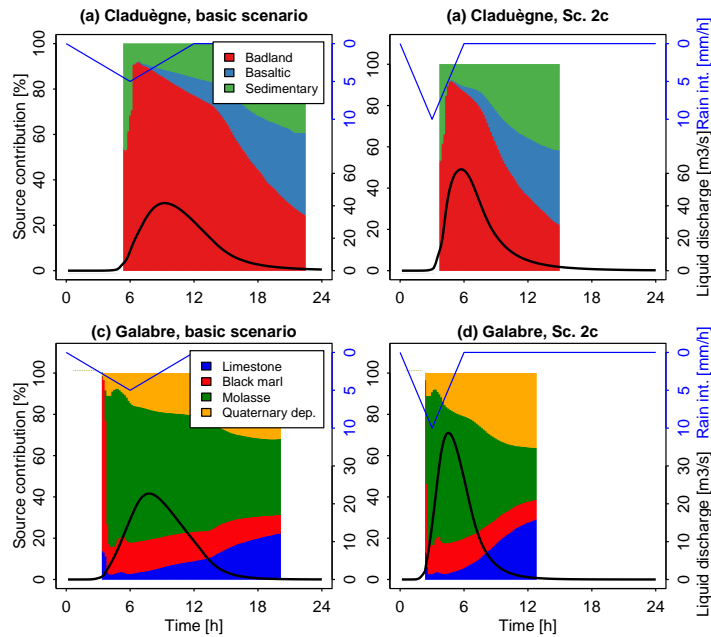


Figure 5.8: Modeled source contributions of the sediment sources in the Claduègne and Galabre catchment when rain intensity and duration were changed with respect to the basic scenario (left). Sc. 2c (right) used a hyetograph with a maximum rain intensity of 10 mm h^{-1} which was half the duration and twice the intensity of the basic scenario. The results of Sc. 2a and 2b can be seen in the [interactive figure](#).

These results showed that maximum rain intensity and duration alone were not sufficient to explain the significant changes in suspended sediment source contributions within events as observed with sediment fingerprinting (Chapter 3.3). Thus, we assumed that more temporarily variable hyetographs or spatially varying rain fields are needed to change the pattern of suspended sediment source contributions with respect to the one of the basic scenario.

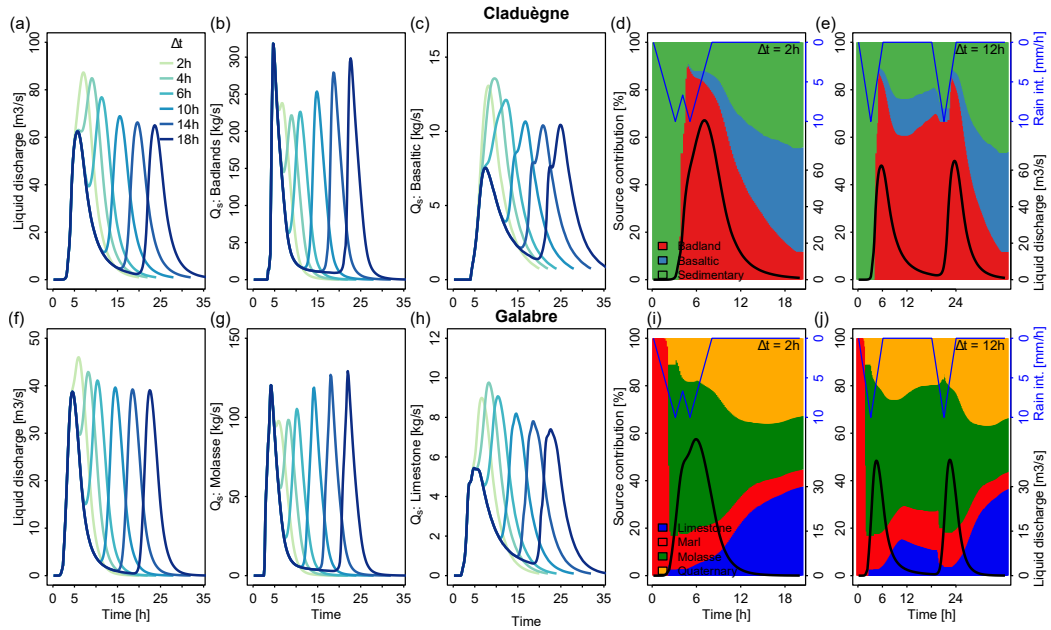


Figure 5.9: Results obtained with bimodal hyetographs with different times between the peaks (Δ_t , Sc. 3a-e). Figures (a) and (f) show the hydrographs in the Claduègne (top row) and Galabre (bottom row) catchments. Figures (b) and (g) show the sedigraph of the main source in each catchment, i.e. badlands in the Claduègne, molasses in the Galabre. (c) and (h) show the sedigraphs of the most distant sources, i.e. basaltic in the Claduègne, limestone in the Galabre. Figures (d) and (i) show the pattern of predicted source contributions to total suspended load for the hyetograph with $\Delta_t = 2 h$, (e) and (j) show the same for $\Delta_t = 12 h$

The results obtained with the bimodal hyetograph where the time between the peaks (Δ_t) was $2 h$ were very similar to the ones obtained with the unimodal hyetograph of Sc. 2a (Fig. 5.9 a and f, Table 5.4). For example, $Q_{l,max}$ in the Claduègne and Galabre catchments were 93 and $48 m^3 s^{-1}$ in Sc. 2a while they came to 87 and $46 m^3 s^{-1}$ respectively in Sc. 3a. The hydrographs as well as the sedigraphs of the sources remained unimodal or showed only a very small, secondary peak. Also the pattern of the contributions of the sediment sources (Fig. 5.9d and i) barely differed from Sc. 2a (similar to Fig. 5.8). This was due to the buffering effect of the catchments, the continuity of rainfall in this hyetograph and the time between peaks that was shorter than the time of concentration of the two catchments which is estimated to be $4.7 h$ in the Claduègne catchment (Hachgenei, 2018) and assumed to be in the order of $2 - 3 h$ in the Galabre catchment.

Table 5.5: Critical thresholds of Δ_t [h] where bimodal hyetographs lead to two distinct flood events. In order that events are considered independent from each other, flux has to decrease to $\leq 0.1 \cdot Q_{max}$. The thresholds are given for liquid discharge (Q_l) and solid discharge (Q_s) for the different source classes, ie. badlands, basaltic and sedimentary in the Claduègne; limestone, marl, molasse and Quaternary deposits in the Galabre catchment. The scheme on the right shows the example of liquid discharge in the Claduègne catchment. The hyetograph with $\Delta_t = 6 h$ leads to a bimodal hydrograph but a continuous flood event, whereas the hyetograph with $\Delta_t = 12 h$ leads to two independent events because Q decreased to $< 0.1 \cdot Q_{max}$ (dashed line).

Critical time between peaks, $\Delta_{t,crit}$ [h]					
Claduègne	Q_l	$Q_{s,bad}$	$Q_{s,bas}$	$Q_{s,sed}$	
	12	10	>18	12	
Galabre	Q_l	$Q_{s,li}$	$Q_{s,ma}$	$Q_{s,mo}$	$Q_{s,qu}$
	10	18	8	8	10

Different results were obtained for the scenarios with a longer Δ_t and especially the ones where rainfall stopped between the two peaks. With increasing Δ_t the pattern of the modeled source contributions became more different from the one obtained with a unimodal hyetograph (Fig. 5.9e and j). In both catchments, the main source (i.e. badlands in the Claduègne catchment, molasses in the Galabre catchment) remained dominant throughout the whole event. The dominance of the sources close to the outlet, i.e. sedimentary in the Claduègne catchment and black marls in the Galabre catchment, at the first stage of the event was not reproduced for the second peak. This was due to sediments of the main source remaining mobilized in the catchment.

In the Claduègne catchment Δ_t had to be $\geq 6 h$ to obtain a clearly bimodal hydrograph (Fig. 5.9a). In the smaller Galabre catchment this was already the case for the hyetograph with Δ_t of 4 h (Fig 5.9f). This difference between the catchments was related to the different sizes and times of concentrations of the two catchments. The sedigraphs of the different sources varied considerably. In the Claduègne catchment, the sedigraph of the badland sources receded quickly and even the sedigraph obtained with Δ_t of 2 h had a small, secondary peak (Fig. 5.9b). For the basaltic sources on the other hand, the recession was much slower and even the sedigraph obtained with Δ_t of 6 h remained unimodal (Fig. 5.9c). Not only the minimum value of Δ_t needed to produce bimodal hydrographs or sedigraphs, also the critical

value of Δ_t that was needed for two events to be considered independent from each other (i.e. flux receding to $< 0.1 \cdot Q_{max}$) was very variable (Table 5.5). It differed in the two catchments, between liquid and solid discharge and between the sedigraphs of the different sources. The different behavior of the sediment sources was strongly related to their location in the catchment and thus to structural connectivity. The results of the simulations run with the bimodal hyetographs showed how structural and functional connectivity interact to determine the shape of hydro-sedimentary fluxes at the outlet.

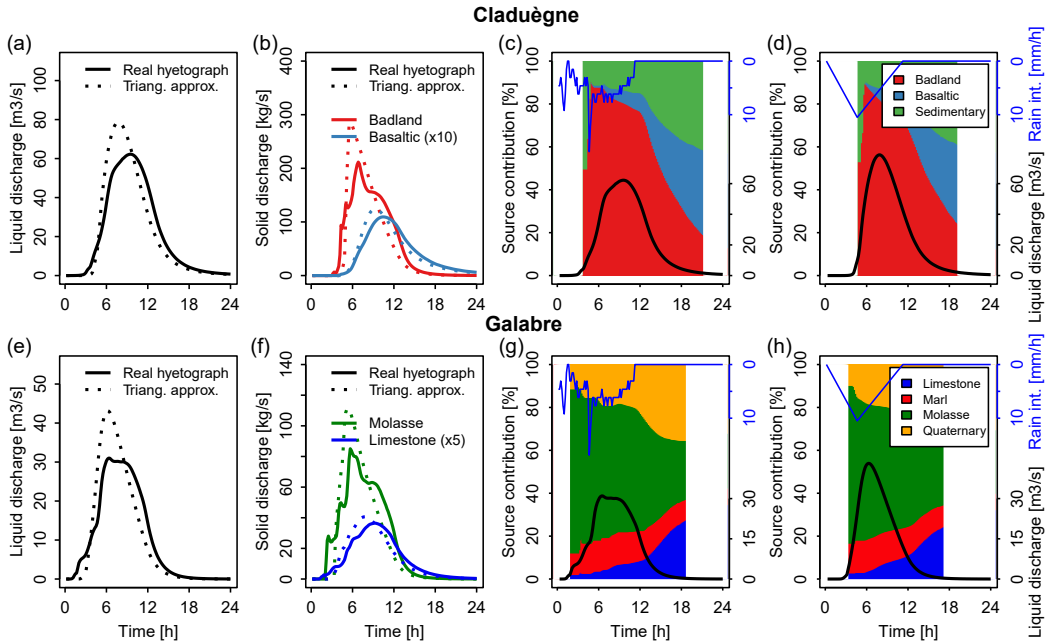


Figure 5.10: Modeling results obtained with Sc. 4a (real hyetograph of the event that occurred on November 4th, 2011 in the Galabre catchment) and 4c (artificial hyetograph, triangular approximation). Both hyetographs were applied spatially uniform over the entire catchment. The top row shows the results for the Claduègne catchment, the bottom row the ones of the Galabre catchment.

The results presented above showed that bimodal hyetographs led to considerable variability of modeled source contributions within an event that was not observed with unimodal hyetographs. However, the catchments act as buffers to dampen the effect of temporal rainfall variability. To further assess this dampening effect, we compared the results obtained with real hyetographs at 10 *min* resolution to the ones obtained with triangular approximations. In both catchments the hydrograph simulated with the rainfall

forcing of the event on November 4th, 2011 in the Galabre catchment was nearly as smooth as the one obtained with the triangular hyetograph (Fig. 5.10a and e). The hydrographs resembled each other. The spread T_{spr,Q_i} and lag times T_{lag,Q_i} of the event were similar but peak flow was overestimated by 27 % and 39 % in the Claduègne and Galabre catchments when the triangular hyetograph was used (Table 5.4). This was not the case for the other event on October 23rd, 2013 in the Claduègne, Sc. 4b and 4d. Here, the triangular approximation underestimated peak discharge by 11 % and 4 % (first and second peak of the event with two distinct rain peaks) in the Claduègne catchment and by 22 % and 9 % in the Galabre catchment. The sedigraphs of the badlands in the Claduègne catchment and the molasses in the Galabre catchment were less smooth when the real hyetograph was used than with the triangular approximation (Fig. 5.10b and f). Also peak solid discharge was overestimated by the triangular approximation in Sc. 4c and underestimated in Sc. 4d (Table 5.4). The pattern of the predicted source contributions, however, was nearly the same for the real hyetograph and the triangular approximation (Fig. 5.10c and d for the Claduègne catchment; Fig. 5.10g and h for the Galabre catchment. This holds true also for Sc. 4d.

These results are important for the determination of the maximum acceptable time step which is important for parsimonious hydrological modeling (Obled et al., 2009). Hachgenei (2018) found out, that a time step of 15 *min* was optimal for the small subcatchments of the Claduègne catchment ($< 5 km^2$) while a time step of 30 - 40 *min* was acceptable in the Claduègne catchment. This scale dependence might be the reason why the smaller Galabre catchment is affected stronger than the larger Claduègne catchment by the simplification of the rainfall time series.

5.4.2 Does spatial variability of rainfall forcing impact modeled hydro-sedimentary fluxes in mesoscale catchments?

5.4.2.1 Impact of simplifications of rainfall patterns

Before addressing the question whether spatially distributed precipitation is needed as model input or if knowledge of spatially averaged precipitation is sufficient, we tested to which extent simplifications of actual rain fields

Table 5.6: Calculated characteristics of modeled hydrographs and sedigraphs for the scenarios assessing the role of spatial variability. Abbreviations as in Table 5.4. The background color of the cells represents the percent change of each value with respect to Sc. 8a - e (distributed precipitation, color legend in the bottom of the table).

	5a Uniform	5b Uniform	5c Uniform	5d Uniform	5e Uniform	6a Approx. gradient	6b Approx. gradient	7 Approx. rain cell	8a Distributed	8b Distributed	8c Distributed	8d Distributed	8e Distributed	9a Ellipse, north	9b Ellipse, center	9c Ellipse, south
Claduègne																
T_{lag,Q_i} [h]	3.75	3.25	3.50	-	-	3.75	3.00	2.08	3.75	2.50	3.50	-	-	3.08	2.25	1.83
T_{c,Q_i} [h]	4.25	6.75	6.00	-	-	4.00	6.00	4.42	4.00	5.50	6.00	-	-	6.17	4.50	4.75
T_{spr,Q_i} [h]	9.25	7.75	8.25	-	-	9.25	7.00	5.67	9.25	6.50	8.25	-	-	4.92	4.00	4.83
$Q_{l,max}$ [$m^3 s^{-1}$]	105	40	52	-	-	107	43	58	102	53	53	-	-	47	86	81
$Q_{s,max}$ [$kg s^{-1}$]	387	336	365	-	-	382	318	211	368	356	375	-	-	1	815	283
T_{lag,Q_s} bad [h]	2.75	2.50	2.50	-	-	2.75	2.50	2.17	2.75	2.25	2.75	-	-	-	1.83	1.75
T_{c,Q_s} bad [h]	1.50	2.75	2.25	-	-	1.25	3.00	3.33	1.25	3.25	2.25	-	-	-	2.5	3.58
T_{spr,Q_s} bad [h]	6.50	3.00	4.00	-	-	6.50	4.00	4.58	6.50	4.25	4.00	-	-	-	1.75	3.75
T_{lag,Q_s} bas [h]	5.25	NA	6.25	-	-	5.25	NA	2.83	5.25	NA	6.25	-	-	5.67	3.17	2.17
T_{c,Q_s} bas [h]	8.75	NA	12.75	-	-	8.25	NA	5.50	8.25	NA	12.75	-	-	13.42	7.17	4.42
T_{spr,Q_s} bas [h]	12.50	NA	14.25	-	-	12.00	NA	5.92	12.00	NA	14.25	-	-	11.67	6.42	3.83
T_{lag,Q_s} sed [h]	3.25	3.00	3.25	-	-	3.50	2.75	2.08	3.25	2.50	3.25	-	-	-	1.83	1.83
T_{c,Q_s} sed [h]	4.75	6.75	6.50	-	-	5.00	6.75	5.00	4.75	5.50	6.50	-	-	-	3.33	5
T_{spr,Q_s} sed [h]	10.50	7.75	8.75	-	-	10.75	7.75	6.25	10.75	6.50	8.75	-	-	-	2.83	5.08
Galabre																
T_{lag,Q_i} [h]	-	-	-	1.50	3.50	-	-	-	-	-	-	0.50	3.75	1.08	0.92	0.58
T_{c,Q_i} [h]	-	-	-	3.75	4.75	-	-	-	-	-	-	2.00	4.75	2.17	2.17	1.25
T_{spr,Q_i} [h]	-	-	-	4.00	8.25	-	-	-	-	-	-	2.50	7.50	2	2.42	1.75
$Q_{l,max}$ [$m^3 s^{-1}$]	-	-	-	58	5	-	-	-	-	-	-	101	5	43	144	53
$Q_{s,max}$ [$kg s^{-1}$]	-	-	-	264	42	-	-	-	-	-	-	123	40	464	1233	91
T_{lag,Q_s} li [h]	-	-	-	2.25	4.00	-	-	-	-	-	-	0.75	4.00	2.08	2.42	0.33
T_{c,Q_s} li [h]	-	-	-	6.25	7.50	-	-	-	-	-	-	1.50	6.50	3.93	5.50	1.25
T_{spr,Q_s} li [h]	-	-	-	6.50	11.25	-	-	-	-	-	-	2.00	9.25	3.25	5.67	1.75
T_{lag,Q_s} ma [h]	-	-	-	1.25	3.50	-	-	-	-	-	-	0.25	3.50	1.08	0.67	0.33
T_{c,Q_s} ma [h]	-	-	-	2.50	5.00	-	-	-	-	-	-	0.50	4.75	1.42	0.83	0.75
T_{spr,Q_s} ma [h]	-	-	-	2.75	8.75	-	-	-	-	-	-	1.00	7.50	1.25	1.00	1.25
T_{lag,Q_s} mo [h]	-	-	-	1.25	3.50	-	-	-	-	-	-	2.00	3.75	1.33	0.58	-
T_{c,Q_s} mo [h]	-	-	-	2.00	4.75	-	-	-	-	-	-	3.25	4.75	1.67	0.58	-
T_{spr,Q_s} mo [h]	-	-	-	2.00	7.50	-	-	-	-	-	-	2.75	6.75	1.25	0.75	-
T_{lag,Q_s} qu [h]	-	-	-	2.00	4.75	-	-	-	-	-	-	0.50	4.50	1.33	0.67	0.58
T_{c,Q_s} qu [h]	-	-	-	3.75	7.75	-	-	-	-	-	-	1.25	7.25	2.17	1.50	0.75
T_{spr,Q_s} qu [h]	-	-	-	3.75	10.50	-	-	-	-	-	-	1.50	9.50	2.00	1.67	1.00
Change [%]	0 -	10 -	20 -	30 -	50 -	70 -	90 -	120 -	150 -	≥ 180						
	9	19	29	49	69	89	119	149	179							

influenced modeled results. The simplification of the patterns was done to reduce the complexity of actual precipitation and thus to simplify the interpretation of the processes that control the hydro-sedimentary response of the catchments. Further, given the ignorance of actual rain patterns due to uncertainty in radar data (Chapter 5.2) or lack of high resolution data, simplified patterns such as rainfall gradients in the catchment can be the only available information on spatial variability.

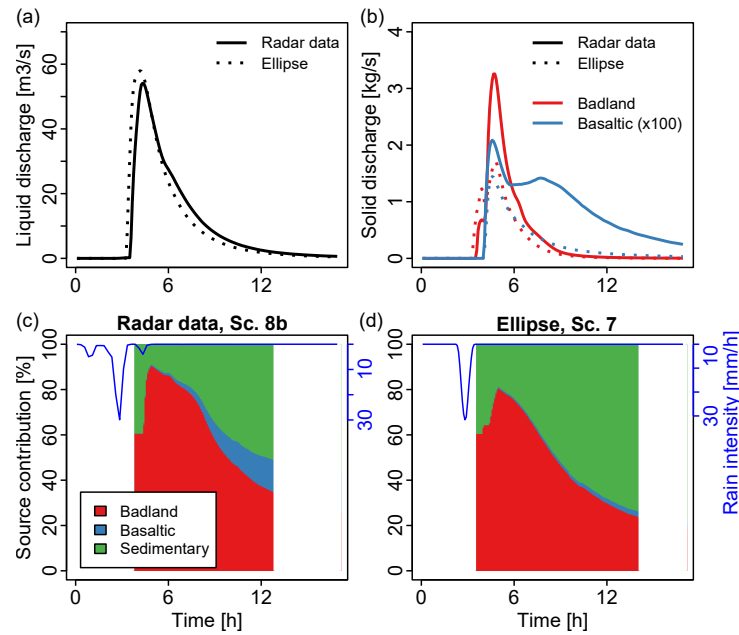


Figure 5.11: Modeling results obtained with distributed radar data of the flood event of the Claduègne on August 19th, 2014 (Sc. 8b) and with approximation of the shape of the rain cell with an ellipse (Sc. 7).

Firstly, the effect of eliminating small scale spatial variability was tested for the event on August 19th, 2014 in the Claduègne catchment (Fig. 5.3c and g, Fig. 5.6d). The shape of the convective storm that passed over the catchment from the west to the east was approximated with an ellipse (Sc. 7, Fig. 5.6c). The hydrograph was reproduced very well by the simplification (Fig. 5.11a). The sedigraphs, however, were strongly underestimated (Fig. 5.11b). For the badland source peak solid discharge was underestimated by about 50 %, total solid discharge by about 40 % (Table 5.6). For the basaltic source on the other hand, peak solid discharge was not as strongly underesti-

mated, but the flux receded much faster when the elliptic rain data was used than with the radar data. The general pattern of the source contributions was similar with both types of rain data. Nonetheless, the contribution of the basaltic source that was already very small with the radar data, was even smaller with the ellipse (Fig. 5.11d). The contribution of the sedimentary source on the other hand was larger with the ellipse.

These results suggested that an approximation of the rain cell can modify the hydro-sedimentary outputs and could thus lead to misinterpretation of the processes, particularly considering the sedigraphs. Indeed, the strong underestimation of the sedigraph of the badlands (which constitutes the large majority of total solid flux) showed that accurate rainfall data is needed for a correct representation of the sedigraph even though this was less the case for liquid discharge. Rainfall with lower intensity outside of the ellipse but on highly erodible sources such as the badlands played a role that cannot be neglected. Nevertheless, the hydrograph and the general pattern of source contributions were not affected significantly by an approximation of the rain cell shape.

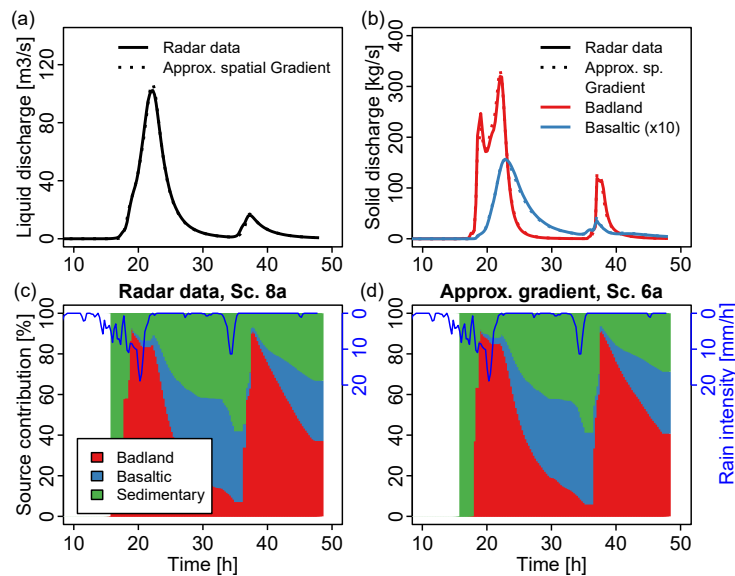


Figure 5.12: Modeling results obtained with distributed radar data of the flood event of the Claduègne on May 18th, 2013 (Sc. 8a) and with an approximated rainfall gradient (Sc. 6a).

Secondly, the effect of simplifying the radar data by approximating it with the spatial gradient of cumulative event precipitation was tested in Sc. 6a and b. These scenarios did not contain information on small scale spatial variability at the finest temporal resolution. They were rather characterized by a persistent spatial pattern throughout the event. The results for the event in the Claduègne catchment on May 18th, 2013 hardly differed between Sc. 6a and 8a corresponding to simplified and fully distributed precipitation data. The hydrographs, sedigraphs and the pattern of the source contributions were basically the same (Fig. 5.12, Table 5.6). It has to be noted that this event had a strong spatio-temporal dynamic with a very elongated rain cell moving over the catchment gaining intensity in the northern part of the catchment (Chapter 5.3.1).

However, for another event (i.e. August 18th, 2014), approximating the spatial rainfall gradient led to significant differences. The shape of the hydrograph was well reproduced but $Q_{l,max}$ was underestimated by 18 % (Table 5.6). This was similar for the sedigraph of the badland source where peak solid discharge was underestimated by 10 %. For the basaltic source, it was very well reproduced (underestimation of 0.9 %) but the shape of the sedigraph differed. We assumed that these differences were due to the fact that the approximation of the rain field was done with a linear gradient while the actual gradient was not linear. This gradient could decrease exponentially from the center as mentioned by von Hardenberg et al. (2003) or have a bivariate Gaussian distribution (Willems, 2001). Shen et al. (2012) compared different interpolation methods to obtain spatial precipitation from rain gauge networks for model input. They found that the sensitivity to rainfall variability increased from hydrological modeling to modeling of sediment and nutrient fluxes. Moreover, they suggested that the effect of spatial rainfall variability was scale dependent. Our results further suggested that sensitivity to small scale spatial variability and the dynamics of moving storms depend on the type of rain event. While both events showed a strong spatio-temporal dynamic, the one of May 18th, 2013 could be much better approximated with a linear rainfall gradient than the one of August 18th, 2014. This confirmed the conclusions of von Hardenberg et al. (2003) that it is important to consider a correct cell shape and radial intensity profile in distributed, process-based modeling.

5.4.2.2 Impact of neglecting spatial rainfall variability

The impact of spatial variability was further tested by applying either the time series of spatially distributed radar precipitation (Sc. 8a-e) or spatially averaged catchment precipitation that was applied homogeneously over the entire catchment (5a-e). For some events, considering spatial variability did not seem to be very important. This was the case for the events of October 25th, 2016 in the Claduègne catchment (Sc. 5c) and of October 24th, 2010 in the Galabre catchment (Sc. 5e; Fig. 5.13).

For other events this was not the case. For the highly localized event in the Claduègne catchment on August 19th, 2014 peak discharge was underestimated when uniform rainfall was applied (Sc. 5b, Fig. 5.13a, Table 5.6). Furthermore, the rising limb of the hydrograph was steeper when distributed precipitation with a rain cell that was located in the south of the catchment close to the outlet was used. Interestingly, the sedigraph of the badland source was nearly the same for the two scenarios (Fig. 5.13b). This was not the case for the other sources. When uniform precipitation was applied, the sedigraph of the basaltic source was delayed with respect to the sedigraph obtained with distributed precipitation. This was probably due to the fact that the sources further away from the outlet were not activated by the rain cell that was located in the south of the catchment. Furthermore, peak solid discharge and total exported sediment of the basaltic sources were much higher when uniform precipitation was used. This was also due to the location of the storm in the south of the catchment and the location of the sources in the north of the catchment. The opposite was the case for the sedimentary sources that are located in the south of the catchment and that were strongly affected by the distributed precipitation data. Here solid peak discharge was more than twice with the distributed precipitation compared to uniform precipitation (not shown here). These differences were also reflected in the pattern of the modeled source contributions. Especially the contribution of the basaltic sources varied between the two scenarios (Fig. 5.13c and d).

In the Galabre catchment the event on June 23rd, 2010 was very localized in the south of the catchment. This led to a steeper increase of discharge and to higher peak discharge when distributed precipitation is used (Sc. 8d, Fig. 5.13k). For this event, using distributed precipitation resulted in

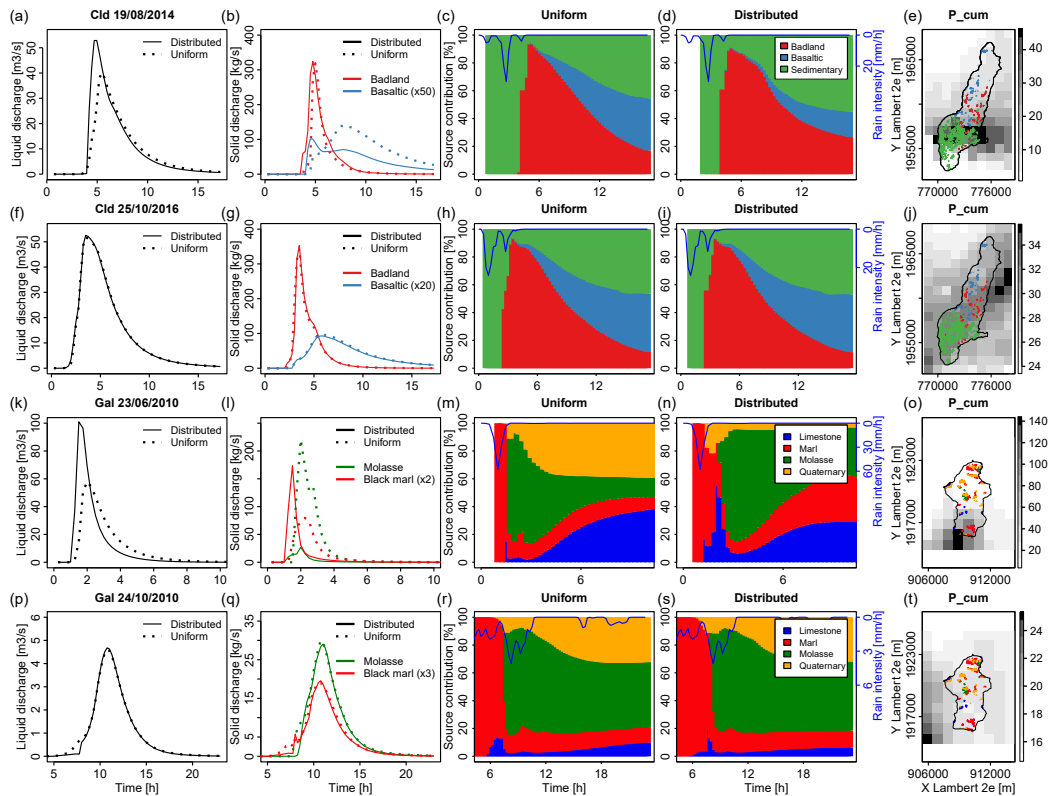


Figure 5.13: Comparison of the model run for several events with uniform (Sc. 5a-e) or spatially distributed precipitation (Sc. 8a-e). The four rows of figures correspond to different events. The first column of figures shows modeled hydrographs. The second column shows the sedigraph of the main source in each catchment (badland in the Claduègne and molasses in the Galabre catchment) and the sedigraph of one of the secondary sources. Note that the sedigraph of the secondary sources (basaltic in the Claduègne catchment, black marls in the Galabre catchment) was multiplied for better visualization. The third column shows the pattern of source contributions for uniform precipitation, the fourth column the same for distributed precipitation. The last column shows the map of cumulative event precipitation and the location of the erosion zones.

very different sedigraphs and a different pattern of source contributions (Fig. 5.13l-n). The black marls contributed much more to suspended sediments for this event than for other events. This was due to a large patch of black marls being located in the south of the catchment where the storm was concentrated. The molasses on the other hand were much less affected by the spatially distributed precipitation. As they are the main source, total solid discharge was overestimated by 130% when spatially uniform precipitation is used (Table 5.6). Also the lag times, times of concentrations and spread times differ strongly (> 180%) between Sc. 5d and Sc. 8d.

The question whether and at which spatio-temporal resolution distributed precipitation is needed for hydro-sedimentary modeling is addressed only in a few studies. Furthermore the results are inconclusive. While Shen et al. (2012) showed the sensitivity of the SWAT model to the spatial variability of rainfall input, Adams et al. (2012) concluded that if predictions at the outlet alone are required, the results obtained with spatially uniform or distributed precipitation were relatively similar. Thus, the latter authors concluded that a main source of uncertainty related to precipitation input is linked to errors of catchment mean (spatially averaged) precipitation and not to the ignorance of the spatial pattern. In our case, this conclusion was similar for events with relatively low spatial variability or when the rainfall volume and intensity on the main source were similar in both cases (uniform or distributed precipitation). For highly localized events where the main source received precipitation that was significantly different from the spatial average, knowledge on the spatial pattern of rainfall was very important. The different conclusions of the study by Adams et al. (2012) and our study seem to be mainly due to the kind of erosion sources. Indeed, Adams et al. (2012) assume erodibility of the soil to be either spatially uniform or linked to topography only. In our case, however, the erodibility of the sources is very different and the sources are localized on distinct patches. Thus, our findings about the importance of spatial variability of rainfall patterns are likely to be transferable to other environments with distinct and localized erosion zones, such as badlands, gullies, debris flow, landslides and other areas of extensive bare soils such as mining sites. For hydrological modeling Emmanuel et al. (2015, 2017) and Anggraheni et al. (2018) also stated the ambiguity of literature findings regarding the role of spatial variability. By comparing spatially distributed and uniform precipitation, they concluded that for events with considerable rainfall variability the hydrological response differed signif-

icantly while this was not the case for events with low variability. Our results suggested that this finding can be extended to hydro-sedimentary modeling but more studies on other scales and other study sites are needed to confirm or falsify this finding. As stated by [Emmanuel et al. \(2015\)](#), simulation approaches with artificially generated rainfall data are very helpful for this approach. Different from the comparison of radar and rain gauge data that is conducted by many authors, simulation approaches eliminate measurement errors and ensure that the total rain volume in scenarios that are compared are the same.

5.4.3 How does the location of rain cells with respect to the sources determine source contributions to sediment fluxes at the outlet?

As it was already observed for the highly localized events, the location of the storm in combination with the location of the sediment sources within the catchment strongly influenced the sedigraphs and the contribution of the sources to total sediment fluxes. In the Claduègne catchment the sources are strongly organized. The basaltic sources are located in the north, i.e. distant from the outlet, the sedimentary sources are located in the south and the badlands dispersed around a centroid in the central part of the catchment (Fig. 5.7, Fig. 4.1a). Thus, the results of Sc. 9a-c with an artificial storm traveling over the northern, central or southern part of the catchment were easy to interpret. When the storm hit the north, the sediments originated entirely from the basaltic sources because the other sources were not affected by the rain cell (Fig. 5.14a). Furthermore, peak solid discharge was reduced by about a factor 800 or 200 compared to the storm in the center or in the south respectively (Table 5.6). This was due to the small surface of sediment sources affected by this storm (Fig. 5.7) and the relatively low erodibility of the basaltic sources (Table 4.1). When the storm passed the southern part of the catchment, on the other hand, the basaltic sources were absent in sediment flux at the outlet (Fig. 5.14g). The sedimentary sources contributed more than when precipitation was applied over the entire catchment.

In the Galabre catchment these processes are more complicated because the sources are more dispersed in the catchment (Fig. 5.7, Fig. 4.1c, d). In the zone passed over by the storm in the north, all sources are present. The

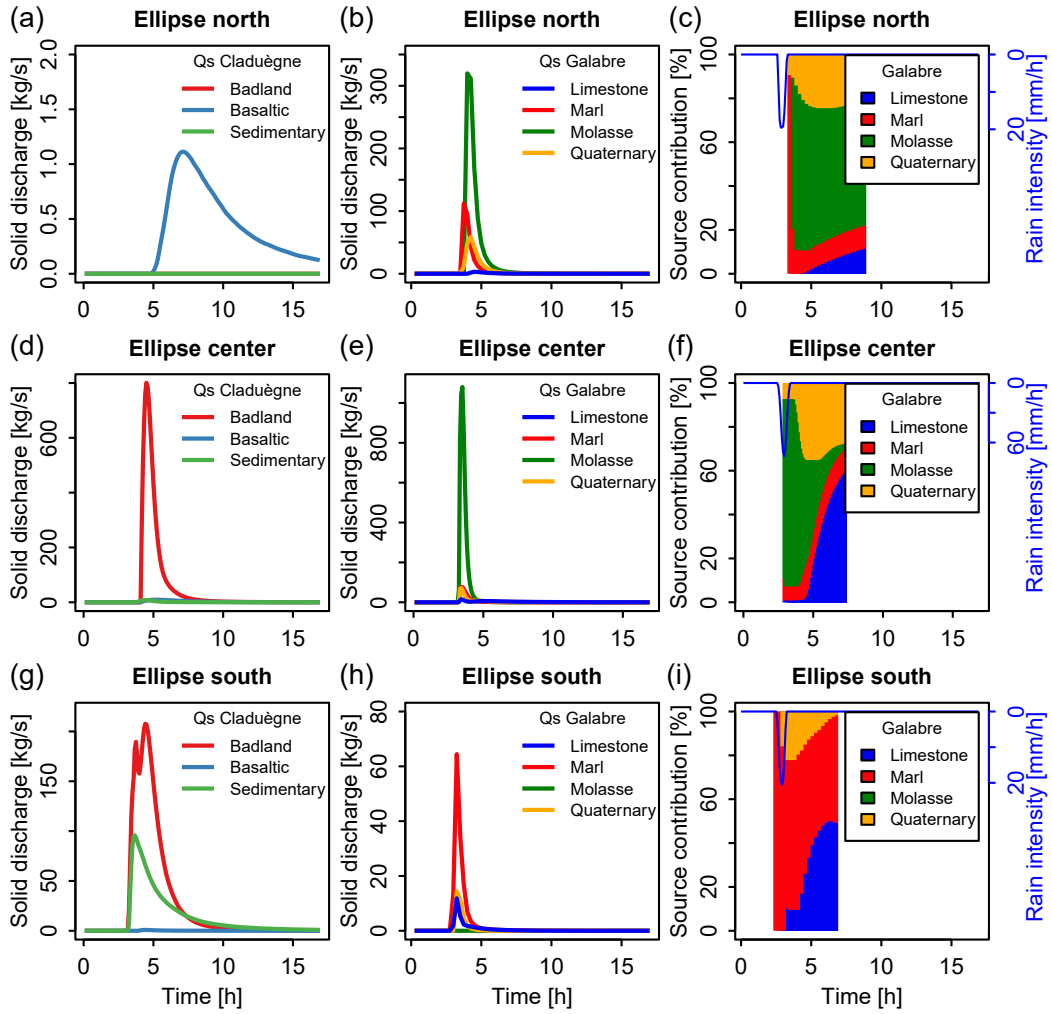


Figure 5.14: Sediment fluxes modeled with a synthetic, elliptic storm traveling over each catchment from the west to the east in the northern (top row), central (middle row) or southern part of the catchments (Sc. 9a-c).

marls are the source with the largest surface in this zone but there also is a patch of the molasses source which has the highest erodibility (Table 4.1). The patches of the limestone source and the Quaternary deposits are smaller and further away from the river network. These observations are quite similar to the distribution of these four sources in the entire catchment. Thus, the predicted pattern of source contributions was similar to a short and intense rain event applied over the entire catchment (Sc. 2c, Fig. 5.8d). In the central part of the catchment also all sources exist. As the main source, the molasses is very well connected to the river, sediments from this source arrived early at the outlet and dominated total suspended sediment flux from the beginning on (Fig. 5.14f). There are many limestone sources but they are less erodible and more distant from the river, thus they contributed only at the end of the event. In the southern part of the catchment there are no badlands on molasses. Thus, the sediments originated mainly from the secondary source black marls, but maximum solid discharge was much lower than for the scenarios where the molasses were affected (Fig. 5.14h and i, Table 5.6).

Forcing the model with artificial storms that were located in different parts of the catchment also showed how the location of the sources and thus structural connectivity in the catchment interacts with functional connectivity defined by the rainfall forcing. This finding was another example of the strong interplay between the two concepts found by other authors (Fryirs, 2013; Cossart et al., 2018; López-Vicente and Ben-Salem, 2019).

5.5 Conclusions and perspectives

Temporal rainfall variability It can be concluded that the temporal dynamics of rainfall strongly impacted the modeled hydro-sedimentary fluxes and that considerable within event variability of predicted source contribution could be obtained when the model was forced with highly variable hyetographs. However, there was a strong dampening effect of the catchment that smoothed high frequency signals of high-resolution rain data recorded during real events and bimodal hyetographs with short durations between the peaks that are smaller than the time of concentration of the catchments. This dampening effect was even more important for sediment fluxes than for liquid discharge. Thus, the high frequency signal of hyetographs recorded at

a high temporal resolution was less important than the general shape of the hyetograph (e.g. unimodal vs. multimodal), the duration and the maximum intensity of the event. This is reassuring, because high quality precipitation data obtained from dense rain gauge networks or radar-rain gauge reanalysis products might not always be available at sub-hourly temporal resolution.

Our results indicated that the temporal dynamics of highly variable hyetographs controlled the dynamics of hydro-sedimentary fluxes, thus they could explain within event variability of source contributions that was observed in sediment fingerprinting studies (Chapter 3).

Spatial variability and location of the storm The analysis of several rain events in two mesoscale study sites showed that the sensitivity to spatial rain variability could not be generalized. For some events it was sufficient to apply spatially averaged precipitation over the entire catchment. This applied to events with low variability of precipitation. For another event, knowledge of the general pattern of the rain fields, i.e. knowledge of the spatial gradient of cumulative event precipitation was sufficient to reproduce modeling results obtained with fully distributed data. For yet other events simplification of the rain fields led to misrepresentation of hydro-sedimentary fluxes, so correct knowledge of the fully distributed spatio-temporal dynamics of the rain event was needed.

These results have several implications for future research. Firstly, it is important to know in which environments, for which kind of events and on which scales event based hydro-sedimentary models are sensitive to spatial rainfall variability. To our knowledge, only [Adams et al. \(2012\)](#) and [Shen et al. \(2012\)](#) addressed this topic before, so further research is needed. In hydrological modeling, [Lobligeois et al. \(2014\)](#); [Emmanuel et al. \(2015, 2017\)](#) and [Anggraheni et al. \(2018\)](#) concluded that for highly spatially variable events, distributed precipitation yields better results than spatially uniform precipitation and our findings suggest that this can be extended to hydro-sedimentary modeling. To identify such spatially variable events, indices such as the ones proposed by [Zoccatelli et al. \(2011\)](#); [Emmanuel et al. \(2015\)](#) or [Wijbrans et al. \(2015\)](#) are valuable tools.

These results are also important to identify the data demand of hydro-

sedimentary models concerning rainfall forcing data. For events with low variability, knowledge of spatially averaged precipitation is sufficient. For highly variable events, on the other hand, much more detailed precipitation data is needed. Thus, in contexts where rainfall variability is usually low or where there are persistent gradients (e.g. due to topography) few rain gauges can be sufficient. In environments such as the Mediterranean where rainfall variability can be significant (Zanon et al., 2010; Borga et al., 2014; Lobligois et al., 2014) the precipitation data demand of hydro-sedimentary models is higher. In this context distributed data is needed and is usually obtained from precipitation radar. However, our analyses showed, that especially in the Galabre catchment this data was subject to considerable errors, so high quality data such as the reanalysis of radar and raingauge data that is available in the Claduègne catchment (Delrieu et al., 2014; Boudevillain et al., 2016) are very valuable for hydro-sedimentary modeling.

The location of the storm with respect to the sediment sources in the catchment was found to govern the mean source contributions during an event. This is especially true in the Claduègne catchment where the sources are highly organized (basaltic sources in the south and sedimentary sources in the north). In the Galabre catchment, the badland sources are more dispersed in the catchment. Thus, the location of the storm was less important as long as the main source (the badlands on molasses) was affected. Only the event in June 2010 that was very localized in the south of the catchment differed strongly from other events. Thus, the location of the storm also explained the variability of sediment source contributions between events that was observed by Poulenard et al. (2012) and Legout et al. (2013). These results showed how the interplay of structural connectivity (governed by the location of the sources in the catchment) and functional connectivity (governed by the spatio-temporal characteristics of the rain event) impacted hydro-sedimentary fluxes at the outlet.

Chapter 6

Conclusions and perspectives

6.1 Comparison of model results with source contributions estimated with sediment fingerprinting




The preceding chapters assessed the dynamics of hydro-sedimentary fluxes in two mesoscale Mediterranean catchments especially concerning the variability of the contributions of different sediment sources to total suspended load.

In this chapter it is discussed if the results obtained with sediment fingerprinting were consistent with those obtained with numerical modeling. We deliberately refrained from quantitatively comparing measured and modeled liquid and solid fluxes for two reasons:

Firstly, as other authors showed that hydro-sedimentary models perform weakly in exactly reproducing measured fluxes - especially at high spatio-temporal resolution - (Chapter 1.2.4), we abandoned the idea of accurately predicting exact values in favor of a more conceptual approach. Thus, as proposed by [Alewell et al. \(2019\)](#), we used the model as a tool to assess relative differences and trends of temporal variability.

Further, the modeling framework used here focused on the processes that are important to address the questions of this thesis on the origins of suspended sediments, their transfer in the catchment and the reasons for the observed variability of sediment fluxes. These processes include soil erosion by

Table 6.1: Classification of events into groups of different variability of suspended sediment fluxes. For results obtained with sediment fingerprinting the number of events that were assigned to the respective group are given; for modeling, examples of scenarios that created similar patterns are given. The first group comprises events with a low variability of source contributions, the second group events where only the beginning of the event varied from an otherwise constant pattern and the third group comprises events with a high variability of source contributions. See chapter 3.3 for a more detailed description of the groups.

	Claduègne		Galabre	
	Fingerprinting	Modeling	Fingerprinting	Modeling
Group 1	 6 events, e.g. May 18 th , 2013, Aug 19 th , 2014	-	15 events, e.g. June 23 rd , 2010	-
Group 2	 -	Basic scenario	18 events	Basic scenario, real ev. Oct. 24 th , 2010
Group 3	 5 events, e.g. Oct 25 th , 2016	Bimodal hyetographs, real ev. May 18 th , 2013, real ev. Aug 19 th , 2014, real ev. Oct 25 th , 2016	13 events, e.g. Oct 24 th , 2010	Bimodal hyetographs, real ev. June 23 rd , 2010

rainfall detachment, overland flow and sediment transport in the catchment. On the other hand, infiltration and subsurface fluxes were not represented in our modeling framework. Thus, modeled fluxes could not be compared quantitatively to measured ones that were surely governed also by these processes.

In Chapter 3 we qualitatively assessed the observed within event variability of sediment source contributions by classifying the events into three groups. Group 1 consisted of events with a low variability between samples taken during the same event ($\leq 25\%$ range of estimated source contributions), group 2 consisted of events where one sample in the beginning of the event differed from the others while the others had a low variability and group 3 consisted of events with a high variability ($> 25\%$ range of estimated source contributions for more than one sample; see Chapter 3.3).

In Chapter 4 general patterns of the temporal dynamics of the modeled source contributions were identified when a synthetic triangular hyetograph was applied (Fig. 6.1). In the Claduègne catchment the first sediments that arrived at the outlet originated about half and half from soils on sedimentary geology and from badlands (marked “1” in Fig. 6.1a). Shortly after, the badlands dominated total suspended yield and contributed more than 70 %

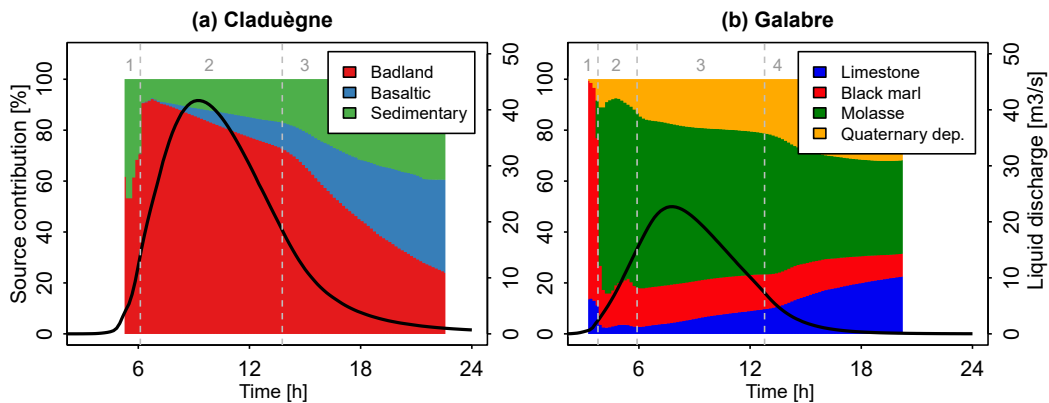


Figure 6.1: General pattern of source contributions to sediment fluxes in the Claduègne (a) and Galabre catchment (b) that were simulated with a synthetic triangular hyetograph in the basic scenario.

during the main part of the event (“2”). The contribution of the soils on basaltic and sedimentary geology increased gradually towards the end of the event.

In the Galabre catchment, in the very beginning of the event sediments originated almost entirely from badlands on black marl (marked “1” in Fig. 6.1b). Shortly after, the sediments originating from the main source (badlands on molasses) arrived and dominated solid fluxes during the rise of the hydrograph and the main part of the event (marked “2” and “3”). Then the contribution of the molasses decreased gradually while the ones of the more distant sources limestone and Quaternary deposits increased (“4”).

These patterns were ascribed to the structural connectivity of the sources (Chapter 4) and also persisted when the intensity or the duration of the hyetograph defining the rainfall forcing was changed (Chapter 5.4.1). In the Galabre catchment this pattern corresponds best to group 2 (one variable sample in the beginning of the event, low variability of the other samples). In the Claduègne it also corresponds best to group 2 or to group 3 (high variability) depending on how much of the tail of the hydrograph is considered.

Concerning the results obtained with sediment fingerprinting, the first peak of the contribution of the soils on sedimentary geology in the Claduègne catchment was only observed in the fingerprinting data for two events (October 23rd, 2013, Fig. 3.17d and November 4th, 2014, Fig. 3.17e), both events

were classified in group 3). However, not all events were sampled during the very beginning of the event, so it is likely that this first flush was missed in the observed data. This might be the reason why no events were classified in group 2 with the fingerprinting approach while it is observed with the modeling approach in the basic scenarios (Table 6.1). Another prominent feature of the modeled source contributions was the steady decrease of the contribution of the badlands. This was not observed systematically with the fingerprinting data. In the model output the arrival of the basaltic source was delayed compared to the other two sources due to their longer travel times. This was also not observed in the fingerprinting data. Given the uncertainty of the fingerprinting approach (estimated to be in the order of 20 %, Chapter 3.1), the pattern of the contribution of this minor source should be taken with care. However, the early arrival of sediments originating from the basaltic plateau during some events (e.g. November 4th, 2011, Fig. 3.17e, September 19th, 2014, October 25th, 2016, Fig. 3.17f) seemed to support the assumption that storage and remobilization of sediments from the river bed cannot be neglected. Several studies showed the importance of the river bed as a source of suspended sediment (e.g. Navratil et al., 2010; Misset, 2019).

In the Galabre catchment the comparison of results obtained with fingerprinting to the ones obtained with the model was complicated because the Quaternary deposits could not be differentiated by the fingerprinting methodology. The modeled first peak of the contribution of black marls was also observed for several events (those classified in group 2, e.g. May 29th, 2008, August 12th, 2008, November 12th, 2008, September 8th, 2010, July 13th, 2011, Fig. 3.17j-l, and some classified in group 3, e.g. October 24th, 2010, Fig. 3.17n). During the main part of the event, modeled source contributions remained relatively stable which was also observed with sediment fingerprinting for many events (group 2).

In order to identify whether general patterns of within event sediment flux variability exist in data obtained with fingerprinting, all samples were classified according to the stage of the hydrograph (rising limb, peak flow or falling limb; Chapter 3.3). In the Galabre catchment it was observed that the contribution of the badlands on black marl was highest during the rising limb and lowest during the falling limb (Fig. 3.18 and the inset figures in Fig. 6.2). This was consistent with the modeled results (Fig. 6.2). For the sources on molasses, however, the increase during the event observed with fingerprinting was not reproduced. On the contrary, the modeled contribu-

tions decreased during the event. This decrease could be partly ascribed to the increase of the Quaternary sources which hinder a direct comparison of results obtained with fingerprinting and modeling in this catchment. In the Claduègne catchment the modeled contributions were more variable than the observed ones. The contributions of the basaltic sources was highest during the falling limb, nearly zero during the rising limb and small during peak flow. This was not consistent with sediment fingerprinting where no significant differences between the contribution of this source were observed. Given the uncertainty of the fingerprinting approach and the small proportion of this source, this apparent difference between model and fingerprinting signatures might, however, be considered as non-significant.

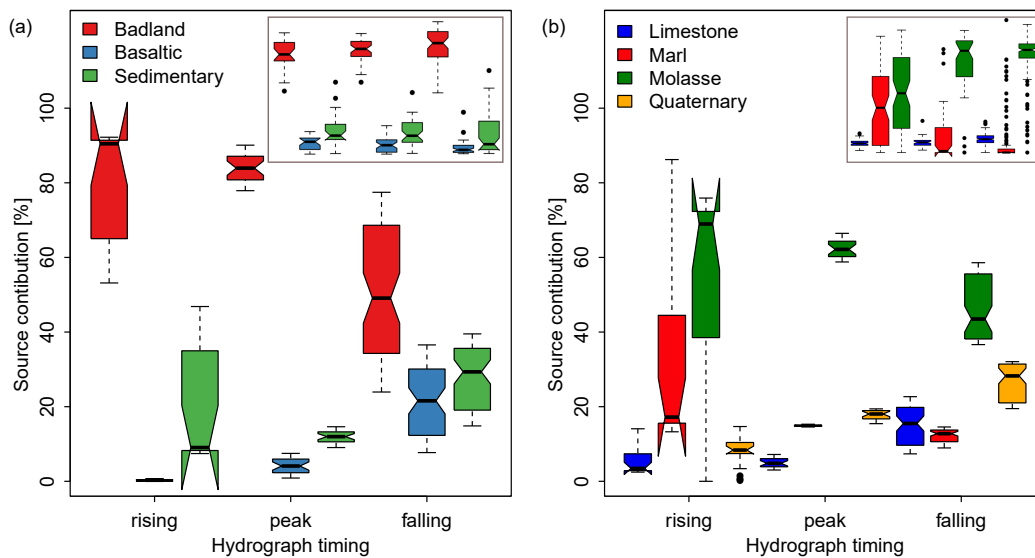


Figure 6.2: Modeled source contributions during different stages of the hydrograph (a) in the Claduègne and (b) in the Galabre catchment. The smaller inset plots show the pattern with observed data (Fig. 3.18).

For the five events that were modeled with distributed precipitation data, modeled and observed sediment fluxes could be compared for each event separately. Only one was classified in the same group of sediment flux variability with fingerprinting and modeling results (event in the Claduègne catchment on October 25th, 2016, Table 6.1). The simulated variability was usually higher than the observed one.

Indeed, in both catchments, several events were found to have a low variability of source contributions between samples taken during the same flood (events of group 1, Table 6.1, Fig. 3.17a-c, g-i). This concerned events, where the range of the most variable source ranged $< 25\%$ between samples. This low variability can be due to the fact that during the very beginning of the hydrograph when the source contributions were most variable, samples were not always taken. But a low within event variability can also indicate that storage and resuspension as well as mixing in the river bed can homogenize source contributions while these processes were not accounted for in the modeling framework.

On the other hand, there were also events where the source contributions obtained with sediment fingerprinting were much more variable than the general pattern described above (group 3). This high variability could be reproduced with the model when bimodal hyetographs were applied which led to higher temporal variability of the suspended sediment fluxes at the outlet (Chapter 5.4.1). However, in the model the contribution of black marls in the Galabre catchment remained relatively stable besides the first peak in the very beginning of the event while the variability was mainly due to variations in the contribution of the Quaternary deposits and the limestone sources. With fingerprinting this was different as the contribution of the limestones remained stable while the one of black marls could be highly variable throughout the event (e.g. events on January 11th, 2008, October 24th, 2011, November 4th, 2011).

Besides the variability of source contributions within events, the sediment fingerprinting studies presented in Chapter 3 also revealed a high variability between events. In the Claduègne catchment notably the summer event on August 19th, 2014 differed from the other events. During this event, which was the only storm occurring in summer for which fingerprinting was available, the contribution of the sedimentary sources was about twice the mean of all events. In the Galabre catchment, the event on June 23rd, 2010 stood out for the contribution of the black marls of about 100% while normally the molassic sources dominated suspended sediment fluxes. These anomalies could be explained by the distinct precipitation characteristics as both events were caused by highly localized rain cells that touched only parts of the catchments and thus caused a high spatial rainfall variability (Chapter 5) and for both events the higher than usual contribution of the sedimen-

tary sources in the Claduègne catchment and the black marls in the Galabre catchment were consistent between observed and modeled results. Nonetheless, differences remained. For instance, during the event in June 2010 the modeled contribution of limestone was up to 50 % which was not observed with fingerprinting, where the sources remained constantly dominated by black marls (group 1). Also the event of August 2014 was more variable in the model than observed with fingerprinting (group 1)

6.2 Synthesis and future research directions

With regard to the increasing on- and off-site problems caused by soil erosion and high sediment exports from headwater catchments, this thesis aimed at a better understanding of hydro-sedimentary fluxes in two mesoscale catchments. It was conducted in the Mediterranean region, which is especially prone to soil erosion due to its climate and land use; both of which are supposed to change significantly in the next decades. We addressed research questions on the origins of suspended sediments in the two studied catchments and on the variability of the contributions of different sediment sources to total suspended fluxes at the outlet. In this last part of the thesis the conclusions drawn in Chapters 3, 4 and 5 are synthesized and future research directions are proposed.

6.2.1 Where do suspended sediments passing the outlet of two mesoscale catchments originate and how do the contributions of different sources vary within and between flood events?

Based on tracer measurements, the sediment fingerprinting methodology provides a way to determine the origins of suspended sediments and to quantify the contributions of potential sources to individual sediment samples. In the Claduègne catchment the marly-calcareous badlands were the main source of sediment despite their small surface. In the Galabre catchment the studies by Poulénard et al. (2012) and Legout et al. (2013) identified badlands on molasses as the main sediment source. In both catchments the estimated source contributions could vary considerably both within flood events, i.e. from one sample to another and between flood events. Further, the studies

by Poulenard et al. (2012) and Legout et al. (2013) in the Galabre catchment as well as the one by Uber et al. (2019) in the Claduègne catchment stressed that the estimated source contributions are subject to important errors that can be in the order of 20 %. The main sources of error are the particle size selectivity during erosion and sediment transport and the heterogeneity of source samples. Furthermore, it was shown that different results were obtained when different tracer sets or mixing models were used. Here the choice of the tracer set seemed to be more important than the choice of the mixing model.

These findings have several implications for sediment fingerprinting studies in general and for the analysis of hydro-sedimentary processes in our study sites:

In the recent literature on sediment fingerprinting much effort is made on the development and the improvement of mixing models. Especially, Bayesian models have received increasing attention. Our results show, however, that a simple model which uses the least squares algorithm yields very similar results to the ones of a more sophisticated Bayesian model. Especially in the light of other sources of error, the choice of the mixing model seems to be of less importance. Thus, we suggest that future sediment fingerprinting research should focus on methods reducing the errors due to particle size effects, source heterogeneity and the choice of tracer sets.

Regarding the latter, we showed that while color tracers and X-ray fluorescence tracers agreed in the main sources, the predicted contributions to individual sources could differ strongly depending on the tracer set used. Comparing the results obtained with these alternative tracers to the ones of traditional tracer sets, i.e. magnetic susceptibility and radionuclids did not lead to unambiguous results either. Therefore, we suggest that using multi-tracer-multi-model means, i.e. ensemble predictions instead of predictions obtained with one tracer set and one mixing model, gives more robust results. Given the high analytic cost of traditional tracers, there is a high potential of using low-cost tracers.

The observed variability of predicted source contributions also has implications for research and practitioners. Identifying main sources of suspended sediment is important for planning effective erosion control or sediment retention measures. Our results showed that conclusions drawn from single,

instantaneous samples can be misleading as they might not be representative for long term mean values. Thus, it is important to either analyze cumulative samples or consider many samples taken at a high temporal resolution. For the latter, analytical costs may be important, so the possibility of using low-cost tracers is of interest.

High resolution sampling and analysis with low-cost fingerprinting techniques also has a high potential for process understanding. Which sources become activated during different events depends on the characteristics of the rain event and the location of the sources with respect to the outlet, so data obtained from fingerprinting can give indirect information on where erosion occurred and when sources arrive at the outlet. However, the methodology also has its limitation as only a limited number of source classes can be discriminated and the sampled events might not always represent the full range of variability of the meteorologic forcing.

To consider this issue, we believe that there is a high potential of combining sediment fingerprinting with distributed numerical modeling. Other studies have shown the benefit of combining fingerprinting with modeling to identify long-term mean sediment sources. Our results suggested, that there also is a strong interest to combine the two methodologies to understand the reasons for within and between event variability of suspended sediment fluxes. Future studies should elaborate procedures to determine how the two methodologies can complement each other optimally.

6.2.2 What are the reasons for the observed variability of source contributions between and within events?

In Chapters 4 and 5 we tested the hypothesis that the observed variability of source contributions was governed by the interplay of structural and functional connectivity in the catchment. To this end we used a physically-based, distributed numerical model of soil erosion and sediment transport. The use of the model allowed us to trace the sediments from the sources to the outlet numerically and to apply scenarios that assess the effect of the location of the sources in the catchment (i.e. their structural connectivity) and the effect of variable rainfall forcing on the contributions of source contributions at the

outlet to the catchment.

In Chapter 4, we first tested the sensitivity of the modeled hydro-sedimentary fluxes to model parameters (Manning’s roughness parameter n on the hillslopes and in the river network) and catchment discretization (by varying the threshold of contributing drainage area Th_{CDA} to define the river network). These parameters influence the way structural connectivity is represented in the model. Our results showed that while absolute values of modeled maximum liquid and solid discharge were sensitive to these parameters, the temporal dynamics of modeled source contributions remained relatively stable once parameters were varied only in a restricted range. Th_{CDA} could be varied from 15 to 50 *ha* and n on the hillslopes from 0.4 to 0.8. These values are reasonable and correspond to values that could be obtained from recommendations in the literature. These results were reassuring, because they justified the use of a modeling framework as presented here where the aim is not to reproduce exact values for liquid and solid fluxes but to contribute to a conceptual understanding of hydro-sedimentary processes that lead to the observed variability of suspended sediment fluxes.

We further tested how the distance of the sediment sources to the river network and to the outlet governed the temporal dynamics of source contributions to sediment fluxes at the outlet. These two measures served as proxies for structural connectivity that are easy to quantify. To isolate the effect of structural connectivity from the one of rainfall variability a synthetic, unimodal hyetograph was applied uniformly over the entire catchment. It was demonstrated, that the location of the sources in the catchment led to a general pattern of source contributions at the outlet that was determined by the distance of the sources to the outlet and to the river network. When this pattern was compared to the results obtained with sediment fingerprinting the results were only partly consistent; for instance the high variability of suspended sediment fluxes of the events classified in group 3 could not be reproduced but neither was the low variability of the events classified in group 1 (Chapter 6.1, Table 6.1).

We drew two main conclusions from this finding. Firstly, the results obtained with fingerprinting suggested that temporal storage in the river bed and later remobilization was important at least for some events. This hypothesis was supported by the events where the source contributions estimated

with fingerprinting were nearly constant throughout the event (group 1) and by the early arrival of basaltic sediments in the Claduègne catchment despite their high distance to the river network and the outlet. In the modeling framework, deposition, storage and remobilization of sediments in the river bed were not considered. This wash load hypothesis is supported by the relatively short time of concentration of the two catchments (in the order of $4.5 h$ in the Claduègne catchment and less in the Galabre catchment) that is shorter than the duration of the majority of rain events. Further, the river bed is mainly incised into the bedrock with a small active width of the river and thus the stock of fine material in the river bed is small. Nonetheless, the fact that deposition, storage and remobilization are neglected in the modeling framework used here shows a limitation of the study. In the future, it should be considered by simulating sequences of events and implementing in the model the deposition in the river bed and remobilization of fine deposits.

Secondly, structural connectivity alone could not explain the whole range of hydro-sedimentary dynamics at the event scale because observed sediment flux variability could be more important than the modeled one. For instance, the dynamics of events that were classified in group 3 could not be reproduced in Chapter 4. Future research should continue to develop methodologies to consider functional connectivity. Recent literature on sediment connectivity concluded that the methodology to assess structural connectivity is well advanced and several indicators are shown to be efficient to identify highly connected erosion zones that are main sources of sediment in a quantitative way. Functional connectivity on the other hand remains more vague; different definitions exist and it is less straightforward to quantify. Therefore, there is a need for further methodological development and for more case studies addressing this issue.

In Chapter 5, the effect of functional connectivity was tested by changing rainfall forcing. We found that temporal rain variability, notably multimodal hyetographs, led to considerable within event variability of hydro-sedimentary fluxes. Such strong variability was observed for some events with sediment fingerprinting but could not be reproduced in Chapter 4 where only structural connectivity was considered. We further observed that there was a considerable dampening effect of the catchment, that smoothed high-frequency signals of high resolution hyetographs. This effect was more important for solid fluxes than for liquid fluxes. This finding is important for the

precipitation data demands of hydro-sedimentary models and for the design of measurement networks. Our results suggested that high temporal resolution data was not necessarily needed but that accurate information of the general shape of the hyetograph, event duration and maximum rain intensity was important as the modeled hydro-sedimentary fluxes were very sensitive to this input data.

We further assessed how spatial variability affected the variability of hydro-sedimentary fluxes within and between events. To this end we forced the model (i) with spatially distributed precipitation data at a resolution of 1 km^2 and 5 min , (ii) simplified spatial patterns or (iii) spatially uniform precipitation. Our results showed that the sensitivity of the modeled hydro-sedimentary fluxes could not be generalized. For some events accurate knowledge of spatially averaged catchment precipitation seemed to be sufficient, for others knowledge of the general pattern such as a rainfall gradient was necessary while for yet others fully distributed precipitation data was needed. Identifying the kind of events (organized or local, convective or stratiform) that necessitate detailed spatial information remains an open issue. The question whether knowledge on the spatial pattern of rainfall forcing data is needed or whether it is more important to correctly estimate absolute rain volumes (i.e. spatially averaged) precipitation is an active research topic in hydrological modeling. Unfortunately, this question has hardly been addressed for hydro-sedimentary modeling even though our results and the ones of [Shen et al. \(2012\)](#) suggested that solid fluxes were more sensitive to spatial variability than liquid discharge. We assume that this is especially the case in catchments with highly localized active erosion zones while the results of [Adams et al. \(2012\)](#) suggest that this is less important when sediment sources are more diffuse.

The results of the modeling study further showed, that the location of the rain cell with respect to the location of the sources in the catchment determined which was the main source during the event. Thus, it determined the variability of source contribution between flood events. This was especially the case in the Claduègne catchment where the sources are highly organized along a north-south gradient. In the Galabre catchment this was only the case for highly localized storms that did not activate the main source.

Our study was limited to two catchments in a similar hydro-climatic con-

text and five rain events, so results cannot be generalized. An immediate next step would be to compare model output obtained with spatially uniform and distributed precipitation data for a high number of events in different catchments in various climatic regions. Such an approach was undertaken for hydrological modeling by [Lobligeois \(2014\)](#). This study gave valuable insights into the factors that determined the sensitivity to spatial rainfall variability notably catchment size, rain intensity and the heterogeneity of rain events. Concerning the latter point, the heterogeneity of spatial rainfall distribution can be quantified with indicators such as the ones proposed by [Zoccatelli et al. \(2011\)](#) and [Emmanuel et al. \(2015\)](#). We believe that extending these approaches from hydrological modeling to soil erosion and sediment transport modeling would have many benefits for the planning of measurement networks, model improvement and process understanding. In the Mediterranean context, rainfall can be highly variable, so accurate information on distributed precipitation is needed. In this context, reanalyses of radar and rain gauge data such as the one that was obtained using the methodology described by [Delrieu et al. \(2014\)](#) and provided at a high spatio-temporal resolution (1 km^2 , 15 min) by [Nord et al. \(2017\)](#) for the Claduègne catchment are very valuable to obtain accurate quantitative precipitation estimates.

Using indicators of rainfall variability further offers the perspective to assess functional connectivity in a more quantitative way. In this thesis, we applied a rather conceptual approach by classifying the events in three groups of sediment flux variability. The development of quantitative indicators of sediment flux variability in combination with indicators of rainfall variability could help to generalize findings on the impact of rainfall forcing on sediment flux dynamics. However, such indicators are not easy to calculate. Optimally a single index would be obtained for each event, but this is complicated to achieve from the multivariate, non-equidistant time series obtained with sediment fingerprinting. A preliminary attempt to do so ([Hachgenei, 2017](#)), showed that such indicators are highly sensitive to the sampling density within the event and thus the time step between samples.

6.2.3 Benefits of combining sediment fingerprinting and distributed numerical modeling

The question on the origins of suspended sediment passing the outlet of catchments has been addressed by researchers and practitioners for a long time. The two methodologies sediment fingerprinting and erosion modeling have both been used to identify main sediment sources and thus determine optimal areas for erosion control measures and they were shown to complement each other in a way that one methodology can confirm - or question - the results obtained with the other technique.

Here we applied sediment fingerprinting at a high temporal resolution (within event sampling) and distributed numerical modeling at the time scale of the event. In this way we aimed at going beyond the identification of mean source contribution towards a better understanding of the hydro-sedimentary processes that determine when and where erosion occurs and how long it takes the sediments to reach the outlet. These processes are supposed to govern the temporal dynamic of varying source contributions to solid fluxes at the outlet. Sediment fingerprinting and distributed, physically-based modeling both provide internal catchment information that can help to interpret fluxes at the outlet and identify the dominant processes. Understanding of such processes is important, e.g. for better comprehension and anticipation of contaminant transfer of pollutants or nutrients that are adsorbed to fine sediments.

In this thesis the results obtained with sediment fingerprinting and numerical modeling complemented each other. Oftentimes, soil erosion models are used to determine main sediment sources. In our study, the results obtained with sediment fingerprinting were used to calibrate the erodibility of the different sources. In this way, knowledge about the main sediment source was already given and we could use the model to address more detailed questions on the temporal dynamics of sediment fluxes and the reasons for the observed variability. Being able to simulate not only total solid fluxes but also separate sedigraphs for different sources can be important from an operational point of view, for example when contaminated sources such as mining sites are present in the catchment.

On the other hand, distributed modeling can also complement sediment fingerprinting studies. With high temporal resolution fingerprinting, a high

variability of sediment fluxes within and between events can be observed but it can only be guessed what are the reasons for this variability. Here, the numerical model can help to virtually trace sediment sources and to test hypotheses on how location of the sources in the catchment and characteristics of the rain event control travel times and the resulting sediment flux dynamics at the outlet. The results of sediment fingerprinting also revealed a limitation of our modeling approach, i.e the neglect of storage and remobilization of sediments during and between events, and thus pointed out to a future research direction to improve the modeling framework.

The combination of sediment fingerprinting and numerical modeling showed how the interplay of structural and functional connectivity determined sediment fluxes at the outlet. The former was defined by the location of the sources within the catchment as sources that are more distant from the river and the outlet needed longer to arrive than close sources. The latter was governed by the temporal and spatial variability of the rain event. In the future, studies should be conducted in a higher number of catchments in different hydro-climatic contexts and with a high number of rain events to generalize findings on how the characteristics of catchments and rain events determine variable hydro-sedimentary fluxes.

Appendices

Appendix A

Calculation of specific sediment yield

Specific sediment yield was calculated from the data set of discharge, turbidity and sediment concentration. Firstly, suspended sediment concentrations (*SSC*) were derived from measured turbidity (*T*) with a *T*–*SSC* rating curve as in Navratil et al. (2011). In the Claduègne catchment 238 suspended sediment samples were collected from 2011 to 2016, in the Galabre catchment 1155 samples were collected from 2007 to 2019. *SSC*, i.e. the mass of solids divided by the volume of liquid (expressed in $g\ l^{-1}$), is estimated by measuring the volume of the sample containing water and suspended sediment and by weighing the solid fraction after drying it at $105\ ^\circ C$ for 24 h (Nord et al., 2017).

A polynomial rating curve of the form $SSC = aT^2 + bT$ was fitted to the data (Fig. A.1) and the turbidity time series was converted to *SSC* with this curve. This time series was multiplied with the time series of discharge and summed up over a year to obtain yearly sediment yield. Between 2012 and 2016 yearly sediment yield varied strongly from 560 t to > 45000 t in the Claduègne catchment with a mean value of 15947 t. By dividing this value by the surface of the catchment we obtain a specific yield of $380\ t\ km^{-2}\ y^{-2}$. It has to be noted, that this value is subject to the error due to the *SSC* – *T* rating curve ($R^2 = 0.59$) as well as to the error due to the high temporal variability between years.

In the Galabre catchment the global rating curve was established as

$SSC = 0.03T^2 + 0.37T$ but there is a high variability in this relation that can partly be explained by the mineralogy of the sediments (Ronzani, 2019). Average sediment yields are also highly variable between the years (Esteves et al., 2019).

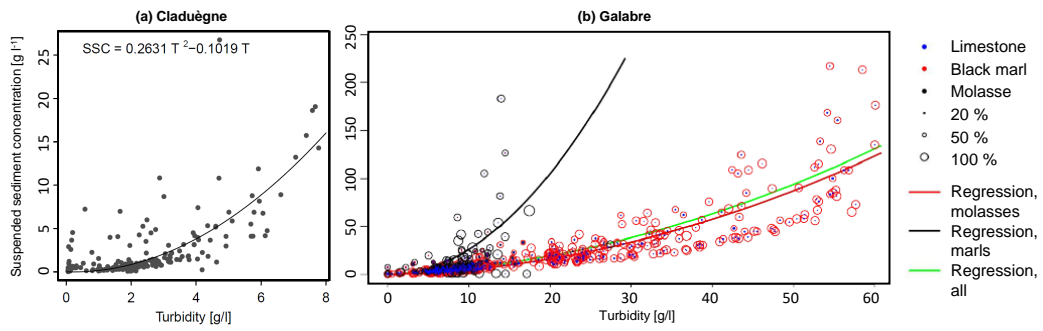


Figure A.1: Relation of suspended sediment concentration and turbidity and polynomial rating curve in the Claduègne (a) and in the Galabre catchment (b). (b) is adapted from Ronzani (2019). The red circles show the samples dominated by molasse, the black circles the ones dominated by black marls. It can be seen that the latter ones diverge from the global regression equation.

Appendix B

Supplementary information for Chapter [3.1](#)

B.1 Additional figures and tables

Table B.1: Tracer statistics of the L*, a* and b* parameters of the CIELAB color space (CIE, 2009) as examples of color tracers, exemplary element compositions measured with XRF and magnetic susceptibility X_{lf} that discriminate the source classes used for sediment fingerprinting.

	Color tracers			XRF tracers				Min. magnetism
	L*	a*	b*	Al ₂ O ₃	SiO ₂	CaO	Fe ₂ O ₃	X_{lf}
	[-]	[-]	[-]	[%]	[%]	[%]	[%]	[10 ⁻⁸ m ³ kg ⁻¹]
Basaltic bare topsoils								
min	33.38	4.09	12.39	8.66	22.27	1.16	5.99	371.22
max	46.68	14.04	21.32	14.39	32.26	3.93	16.26	2494.39
mean	39.18	7.45	17.10	11.30	25.48	2.50	12.09	1322.84
sd	3.24	1.95	2.19	1.47	2.20	0.79	3.07	551.38
Sedimentary bare topsoils								
min	42.34	3.38	13.45	2.71	26.23	2.54	1.63	4.14
max	64.64	7.23	25.09	7.53	54.36	27.85	6.56	357.87
mean	55.59	4.96	20.23	4.84	39.41	12.25	2.94	75.92
sd	3.96	0.86	2.67	1.14	7.00	7.15	1.32	79.40
Sedimentary badlands								
min	55.21	1.43	11.97	3.36	25.62	13.57	1.79	2.89
max	66.35	3.36	18.01	5.79	35.73	25.91	3.05	20.44
mean	61.20	2.08	13.61	3.89	31.17	21.12	2.20	5.39
sd	2.60	0.48	1.19	0.71	2.58	3.56	0.33	4.03

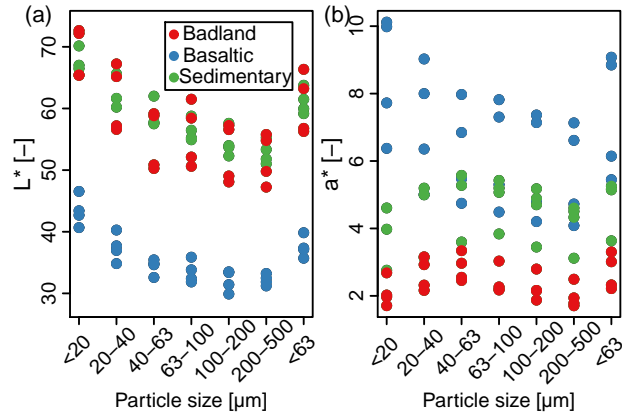


Figure B.1: The color tracers L^* and a^* of the CIELAB color space (CIE, 2009) as a function of particle size.

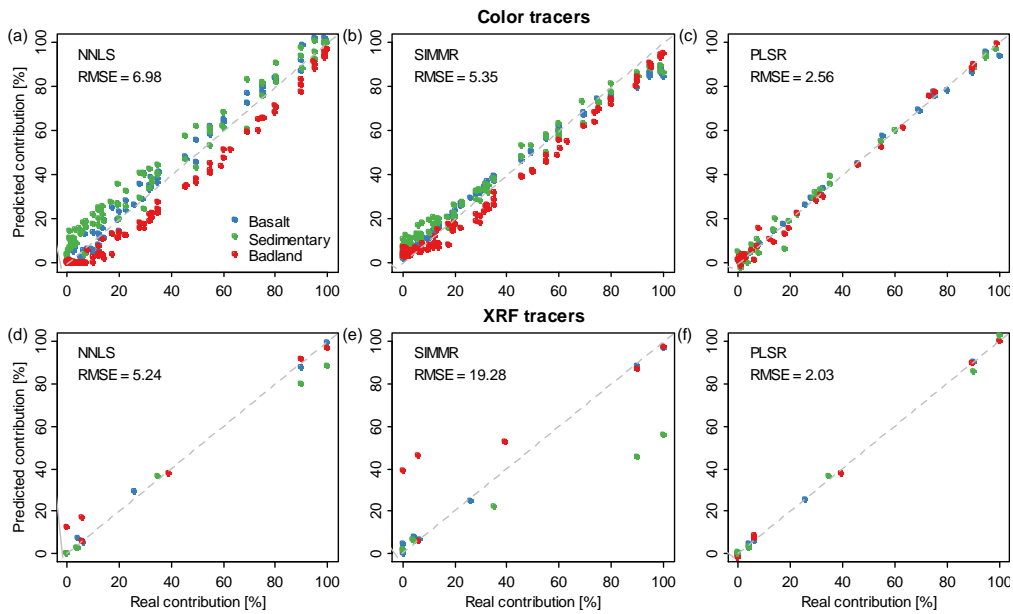


Figure B.2: Predicted versus real source contributions of the three sources to the artificial mixtures. For color tracers the number of artificial mixtures is 81, for XRF tracers there are 7 artificial mixtures. Please note that figure (c) shows the validation data set (i.e. one third of the artificial mixtures that was not used to train the PLSR model) while figure (f) shows the training data set as all 7 mixtures were used to train the model.

B.2 Comparison of the alternative tracer sets with conventional fingerprinting

The results obtained with the low cost tracers (presented in Chapter 3.1) indicated that the choice of tracers is very important for sediment fingerprinting as the results differed strongly between color tracers and XRF tracers. The magnetic tracers did not lead to unambiguous results either, so it could not be decided whether one tracer set led to better results than the other. In order to further investigate the role of the tracer set, we also compared our results to those obtained with a conventional tracer set commonly used in sediment fingerprinting studies, i.e. radionuclids (Motha et al., 2003; Evrard et al., 2011, 2013; Palazón et al., 2016; Palazón and Navas, 2017; Pulley et al., 2017b). This tracer set was not included in the article by Uber et al. (2019).

Measurements of radionuclid concentrations (Am-241, Be-7, Cs-137, Pb-210, excess Pb-210, K-40, Ra-226, Ra-228, Th-228 and Th-234) of nine source soil samples and 13 suspended sediment samples were determined by gamma-spectrometry at the Laboratoire des Sciences du Climat et de l'Environnement (Gif-sur-Yvette, France). The source samples comprise three samples of each source class, i.e. badlands, cultivated soils on basaltic geology and cultivated soils on sedimentary geology. The NNLS and the SIMMR mixing models (Chapter 3.1.2.4) were run with the radionuclid tracers. The PLSR mixing model could not be applied because it needs measurements on artificial mixtures which were not conducted due to the higher analytical costs of this tracer set.

The radionuclids discriminate well between the three source classes. The badlands can be easily distinguished based on their low concentration of Cs-137 while the basaltic and the sedimentary sources differ strongly in their concentration of Ra-228 and Th-234 (Table B.2). Several tracers did not

Table B.2: Values of selected radionuclid tracers. The mean and the range of three samples per source group and 13 sediment samples are given.

	Badland	Basaltic	Sedimentary	Suspended Sediment
Cs-137 [$Bq\ kg^{-1}$]	0.22 (0 - 0.66)	16.47 (10.21 - 19.62)	14.61 (12.10 - 16.86)	4.12 (2.05 - 7.08)
Ra-228 [$Bq\ kg^{-1}$]	21.44 (18.87 - 26.08)	37.20 (33.95 - 39.76)	25.18 (23.98 - 25.98)	19.43 (16.15 - 22.54)
Th-234 [$Bq\ kg^{-1}$]	17.56 (16.05-19.02)	31.11 (27.05 - 36.15)	19.24 (17.67 - 20.83)	17.59 (10.66 - 23.38)

pass the range test, but based on the low number of samples that were analyzed with this tracer set we could not assume that the full heterogeneity of source samples was covered with only three samples per class. Hence, this test could not be applied here.

Table B.3: Error due to source heterogeneity (Δ_{sh} , in % source contribution) estimated with the two mixing models run on source samples with radionuclid tracers (Chapter 3.1.2.5, Eq. 3.2).

	Badland	Basaltic	Sedimentary
NNLS	5.7	10.4	11.47
SIMMR	2.7	10.1	11.5

Model performance with the radionuclid tracer set was evaluated by calculating the error due to source heterogeneity (Δ_{sh} , see Chapter 3.1.2.5, Eq. 3.2). This measure tested whether the model was capable of correctly assigning the source samples to their respective class. In general, this type of error was in the order of the error estimated with color tracers and XRF tracers or slightly lower (Table B.3 for radionuclids and Table 3.2 for color and XRF tracers). With values exceeding 10 % estimated source contribution, the conventional tracer set confirmed the result obtained with alternative tracers that this source of error is important and has to be considered. Using the SIMMR model, Δ_{sh} was always smaller than when color and XRF tracers are used. Also for the sedimentary sources where Δ_{sh} was usually high, the radionuclids performed better than the alternative tracer sets.

Applied to suspended sediment samples, the models run with radionuclid tracers confirmed the result that the badlands are the main source of sediment (Fig. B.3). However the average contribution (65 and 51 % with NNLS and SIMMR) was lower than when color or XRF tracers were used (average contribution above 70 % regardless of the mixing model). The variability between samples was higher than with the other tracer sets, especially when the SIMMR model is used. The test whether the sum of the contributions of the three source classes predicted with the NNLS mixing model added up to about 100 % gave further insight in the model performance. The sums for seven out of 13 sediment samples exceed 110 % or were less than 90 % (Fig. B.3). With the color and XRF tracer this test gave better results which is probably due to the low number of samples used to build the model with

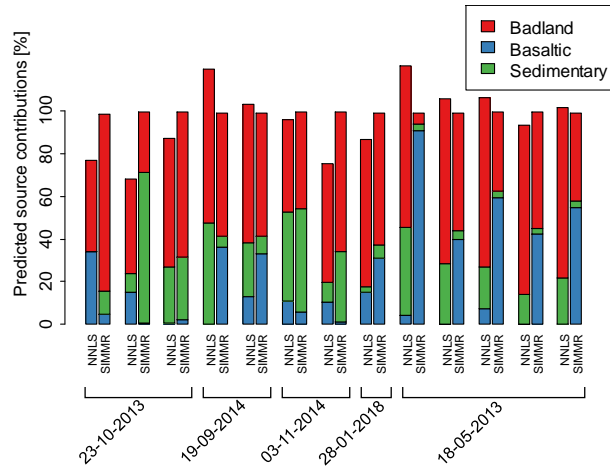


Figure B.3: Predicted contributions of the three source classes to suspended sediment samples. Each group of two bars represents a sediment sample and the two bars show the results obtained with the NNLS and the SIMMR mixing models.

radionuclids.

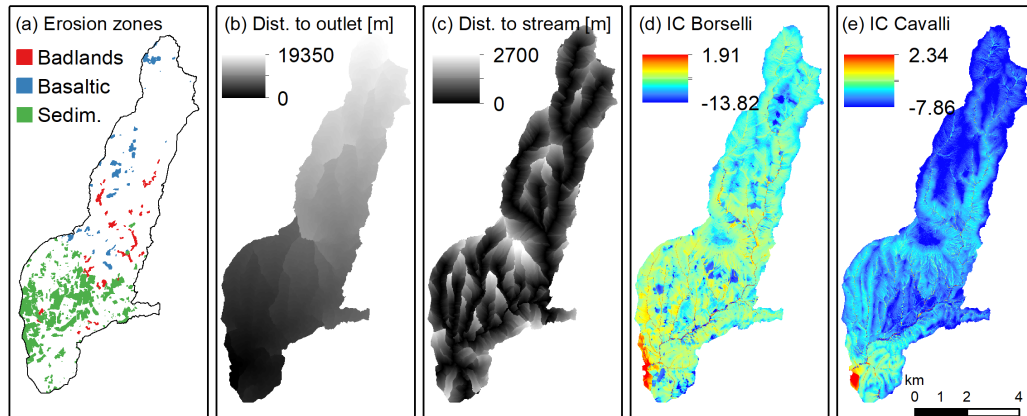
When the results obtained with radionuclids were compared to the ones obtained with spectral tracers significant differences in predicted source contributions were put forward (Chapter 3.1.3.3). This holds true for all tracer sets and all mixing models. This finding further supports the conclusion that multi-tracer/multi-model means provide a way to obtain more robust results. In this sense, complementing conventional fingerprinting studies with alternative tracers offers a high potential. It also underlines that many measurements on many source samples are needed to characterize the whole variability of sources. The possibility to do so is another advantage of low-cost tracers.

Appendix C

Supplementary information for Chapter [4](#)

C.1 Additional figures and tables

Claduègne



Galabre

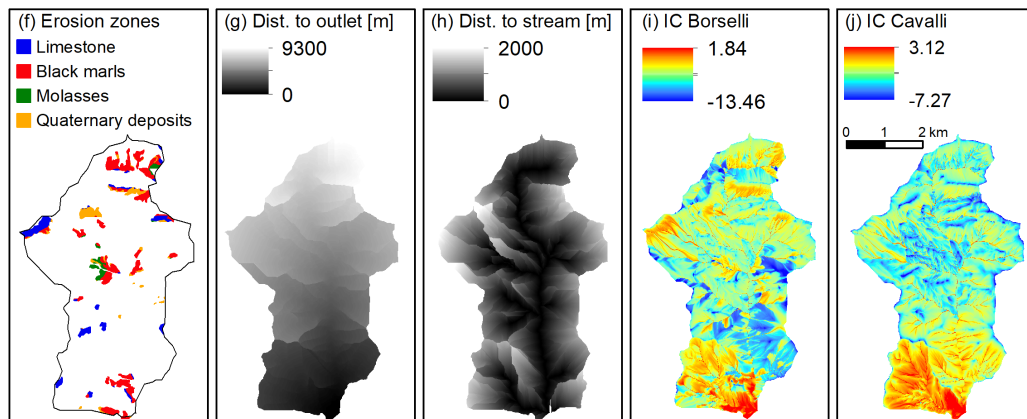


Figure C.1: Location of the erosion zones and maps of indicators of structural connectivity in the Claduègne (top row) and Galabre catchment (bottom row). The values for the indices of connectivity (*IC*) were calculated according to [Borselli et al. \(2008\)](#) and [Cavalli et al. \(2013\)](#).

Table C.1: Calculated characteristics of modeled hydrographs and sedigraphs for the different scenarios. Abbreviations: T_{lag,Q_l} : lag time of liquid discharge, T_{c,Q_l} : time of concentration of liquid discharge, T_{spr,Q_l} : spread of the hydrograph, $Q_{l,max}$: peak liquid discharge. Q_s refers to solid discharge and the characteristic times are calculated for each source separately (i.e. badlands, basaltic and sedimentary in the Claduègne catchment; limestone, black marl, molasses and Quaternary deposits in the Galabre catchment). The background color of the cells represents the percent change of each value with respect to the basic scenario (color legend in the bottom of the table). A visualization of this table is presented in Fig. 4.4.

	1 Basic Scenario	2a $Th_{CDA} = 35 ha$	2b $Th_{CDA} = 50 ha$	2c $Th_{CDA} = 150 ha$	2d $Th_{CDA} = 500 ha$	3a $n_{hillst.} = 0.2$	3b $n_{hillst.} = 0.4$	3c $n_{hillst.} = 0.6$	3d $n_{river} = 0.025$	3e $n_{river} = 0.075$	3f $n_{river} = 0.100$
Claduègne											
T_{lag,Q_l} [h]	4.00	4.33	4.50	5.33	NA	2.67	3.17	3.67	3.50	4.50	5.00
T_{c,Q_l} [h]	5.67	6.33	6.67	9.33	NA	3.17	4.00	4.83	4.67	6.50	7.33
T_{spr,Q_l} [h]	12.33	12.67	13.00	15.33	NA	10.67	11.17	11.67	11.83	12.67	13.17
$Q_{l,max}$ [$m^3 s^{-1}$]	41.65	40.16	39.14	32.91	22.14	51.44	48.00	44.57	42.51	40.67	39.64
$Q_{s,max}$ [$kg s^{-1}$]	191.04	198.67	183.24	169.41	108.65	197.45	201.52	196.98	163.88	217.06	230.97
T_{lag,Q_s} bad [h]	2.67	2.83	3.00	3.67	6.00	1.83	2.17	2.50	2.17	3.17	3.67
T_{c,Q_s} bad [h]	3.00	3.00	3.33	4.50	9.33	2.33	2.50	2.83	2.67	3.33	3.67
T_{spr,Q_s} bad [h]	9.17	9.00	9.17	10.00	14.67	9.50	9.17	9.17	9.67	8.83	8.50
T_{lag,Q_s} bas [h]	6.17	6.67	NA	NA	NA	3.67	4.83	5.50	5.50	NA	NA
T_{c,Q_s} bas [h]	10.83	11.17	NA	NA	NA	5.50	7.50	9.17	9.00	NA	NA
T_{spr,Q_s} bas [h]	16.00	15.83	NA	NA	NA	12.17	13.50	14.67	14.83	NA	NA
T_{lag,Q_s} sed [h]	3.83	4.17	4.33	4.83	NA	2.17	2.83	3.50	3.50	4.17	4.33
T_{c,Q_s} sed [h]	7.17	7.83	8.17	8.83	NA	3.00	4.67	6.00	6.67	7.50	7.67
T_{spr,Q_s} sed [h]	14.00	14.50	14.83	15.33	NA	10.67	12.00	13.00	14.17	13.83	13.67
Galabre											
T_{lag,Q_l} [h]	2.33	2.67	2.83	3.67	4.67	1.33	1.67	2.00	2.17	2.50	2.67
T_{c,Q_l} [h]	2.67	3.33	3.67	5.33	7.50	1.33	1.83	2.17	2.33	3.00	3.17
T_{spr,Q_l} [h]	10.83	11.33	11.50	12.83	14.50	10.33	10.50	10.50	10.83	10.83	10.83
$Q_{l,max}$ [$m^3 s^{-1}$]	22.71	21.83	21.50	19.47	17.89	25.38	24.43	23.58	22.79	22.61	22.54
$Q_{s,max}$ [$kg s^{-1}$]	95.70	94.73	94.29	103.65	69.15	96.64	95.15	94.54	94.08	97.66	99.52
T_{lag,Q_s} li [h]	3.67	4.33	4.50	5.50	NA	2.00	2.67	3.33	3.50	4.00	4.17
T_{c,Q_s} li [h]	6.00	7.83	8.17	10.83	NA	2.50	3.67	4.83	5.50	6.50	7.00
T_{spr,Q_s} li [h]	14.00	16.17	16.00	17.17	NA	11.33	12.00	13.00	13.67	14.17	14.33
T_{lag,Q_s} ma [h]	1.83	2.17	2.17	2.67	5.33	1.17	1.33	1.67	1.67	2.00	2.17
T_{c,Q_s} ma [h]	2.67	3.00	3.33	4.17	10.17	1.67	2.00	2.33	2.33	3.00	3.17
T_{spr,Q_s} ma [h]	11.17	11.33	11.67	12.33	18.17	11.17	11.00	11.00	11.33	11.33	11.50
T_{lag,Q_s} mo [h]	1.83	1.83	2.00	2.67	3.83	1.17	1.33	1.50	1.50	2.00	2.17
T_{c,Q_s} mo [h]	2.33	2.50	2.50	3.00	7.50	1.67	1.83	2.17	2.00	2.50	2.83
T_{spr,Q_s} mo [h]	10.33	10.33	10.17	10.17	13.33	10.33	10.17	10.33	10.50	10.00	10.00
T_{lag,Q_s} qu [h]	2.67	3.17	3.33	3.50	5.83	1.50	2.00	2.33	2.50	2.83	3.17
T_{c,Q_s} qu [h]	4.00	5.00	5.00	5.67	8.67	2.17	2.83	3.50	3.67	4.33	4.67
T_{spr,Q_s} qu [h]	12.00	12.67	12.67	12.67	14.83	10.83	11.17	11.67	11.83	11.83	11.83
Change [%]	0-9	10 - 19	20 - 29	30 - 49	50 - 69	70 - 89	90 - 119	120 - 149	150 - 179	≥ 180	

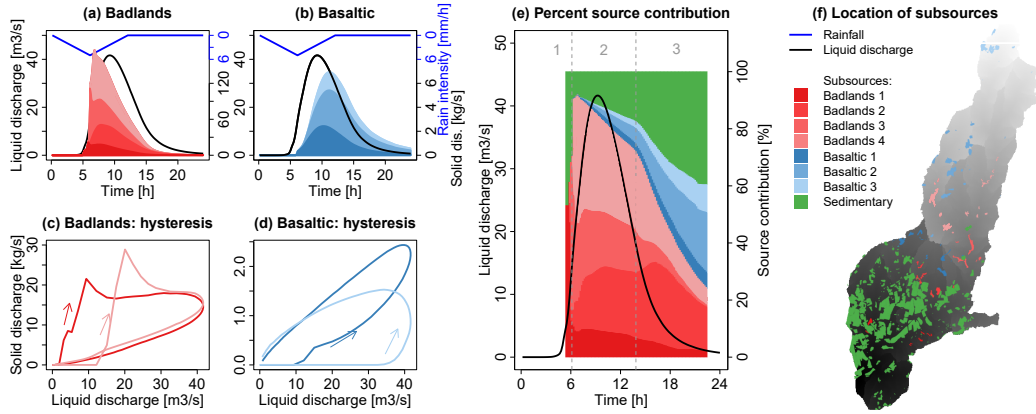


Figure C.2: (a–b): Contribution of subsources of badlands and basaltic sources that are classified according to their distance to the outlet. The colored areas show the contribution of sources close to the outlet (darker colors) and more distant sources (lighter colors) to the sedigraph. (c–d) and show the hysteresis loops of the subsources. Subfigure (e) shows the contribution of each subsurface to total solid discharge in percent. The dashed lines and the grey numbers above the figure distinguish different periods of the event as referred to in the text. (f) Location of the subsources in the Claduègne catchment.

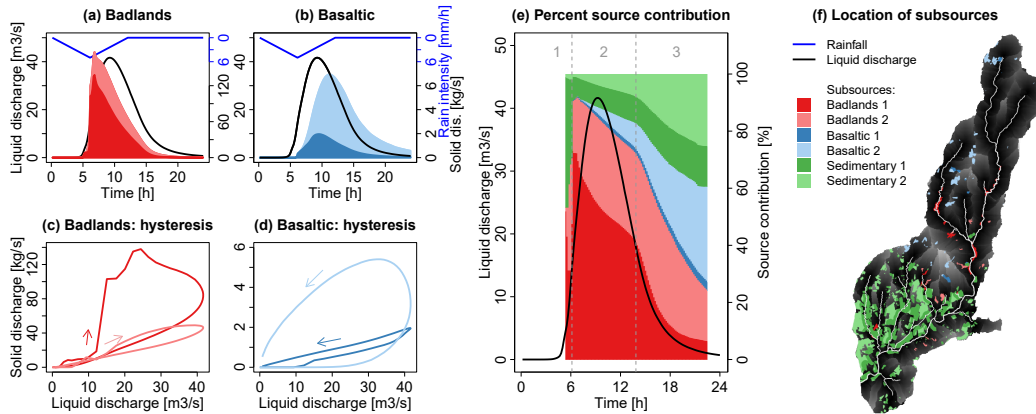


Figure C.3: Contribution of subsources that are classified according to their distance to the stream in the Claduègne catchment. For the description of the subfigures see the caption of Fig. C.2.

Appendix D

Supplementary information for Chapter 5

D.1 Precipitation data criticism (Chapter 5.2)

Criticism of the radar data In order to assess systematic errors, radar precipitation data was accumulated over long time periods. This procedure allows to identify radial features around the radar tower that are a sign of errors that are e.g. due to beam shielding in mountainous topography (Pellarin et al., 2002; Marra et al., 2014). This was observed around the radars at Colobrières south of the Galabre catchment and to a lesser degree at Nîmes south of the Claduègne catchment. Further there are some pixels where precipitation is systematically underestimated, e.g. east of the Bollène radar (Fig. D.1). However, neither the Galabre nor the Claduègne catchments seem to be highly affected by these errors.

Criticism of the rain gauge data The data quality control of the rain gauge precipitation data in the Claduègne catchment was undertaken by Nord et al. (2017). Firstly, the volume recorded by the tipping bucket rain gauge over the period between two visits was regularly compared to the volume collected during the same period of time in a 30 l water tank at the outlet of the bucket. The relative difference was $< 10\%$ for all rain gauges and $< 5\%$ for most of them. Where it exceeded 5% calibration was performed (Nord et al., 2017). Further, the temporal evolution of cumulative rainfall was plotted for rain gauges that are close to each other. In this way periods

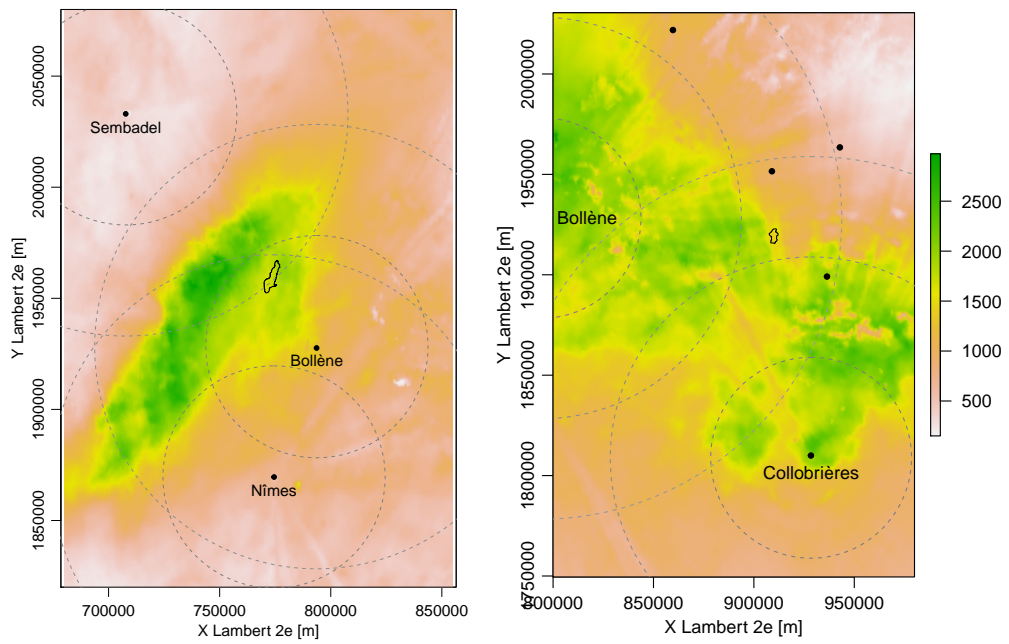


Figure D.1: Cumulated precipitation of 55 events in the Claduègne catchment (left) and 54 events in the Galabre catchment (right). The dashed circles represent the 50 , 100 and 150 km range markers around the S- and C band radars closest to the catchments.

where rain gauges did not record precipitation events could be identified and marked as missing data (Nord et al., 2017). Fig. D.2 shows the evolution of cumulative precipitation in the Galabre catchment. Problems were detected e.g. at Laval in March 2013 and at Ainac in August 2015, so these periods were marked as missing data.

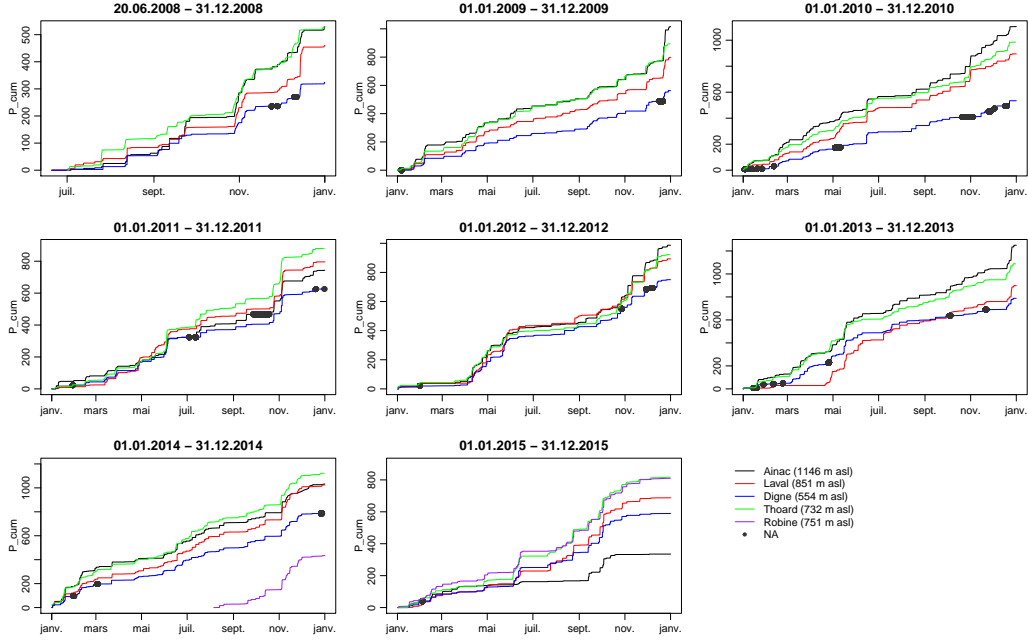


Figure D.2: Cumulative precipitation of the raingauges in the Galabre catchment. Problems of recordings become evident when one raingauge doesn't behave like the others.

Calculation of scores to compare rain gauge and raster data

Root mean square error

$$RMSE = \sqrt{\frac{1}{n} \sum_{i=1}^n (G_i - R_i)^2} \quad (D.1)$$

Relative root mean square error

$$RRMSE = \frac{RMSE}{\bar{G}} \quad (D.2)$$

Pearson's correlation coefficient:

$$r = \frac{\sum_{i=1}^n (R_i - \bar{R})(G_i - \bar{G})}{\sqrt{\sum_{i=1}^n (R_i - \bar{R})^2} \sqrt{\sum_{i=1}^n (G_i - \bar{G})^2}} \quad (\text{D.3})$$

Spearman's rank correlation coefficient

$$\rho = 1 - \frac{6 \sum_{i=1}^n D^2}{n^2 - n} \quad (\text{D.4})$$

Nash-Sutcliffe efficiency

$$NSE = 1 - \frac{\sum_{i=1}^n (R_i - G_i)^2}{\sum_{i=1}^n (G_i - \bar{G})^2} \quad (\text{D.5})$$

Relative error

$$E_{rel} = \frac{1}{n} \sum_{i=1}^n \frac{G_i - R_i}{G_i} \quad (\text{D.6})$$

where G are the recordings at the rain gauge, R are the precipitation estimates of the radar cell at the same time step, n is the number of observations, D is the difference between ranks of pairs of values.

D.2 Additional figures

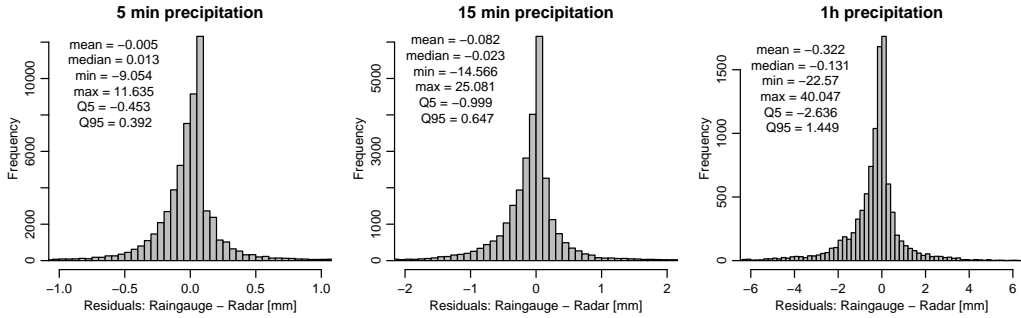


Figure D.3: Residuals of 5 min, 15 min and hourly precipitation obtained with radar and rain gauges during all events and for all gauges in the Claduègne catchment.

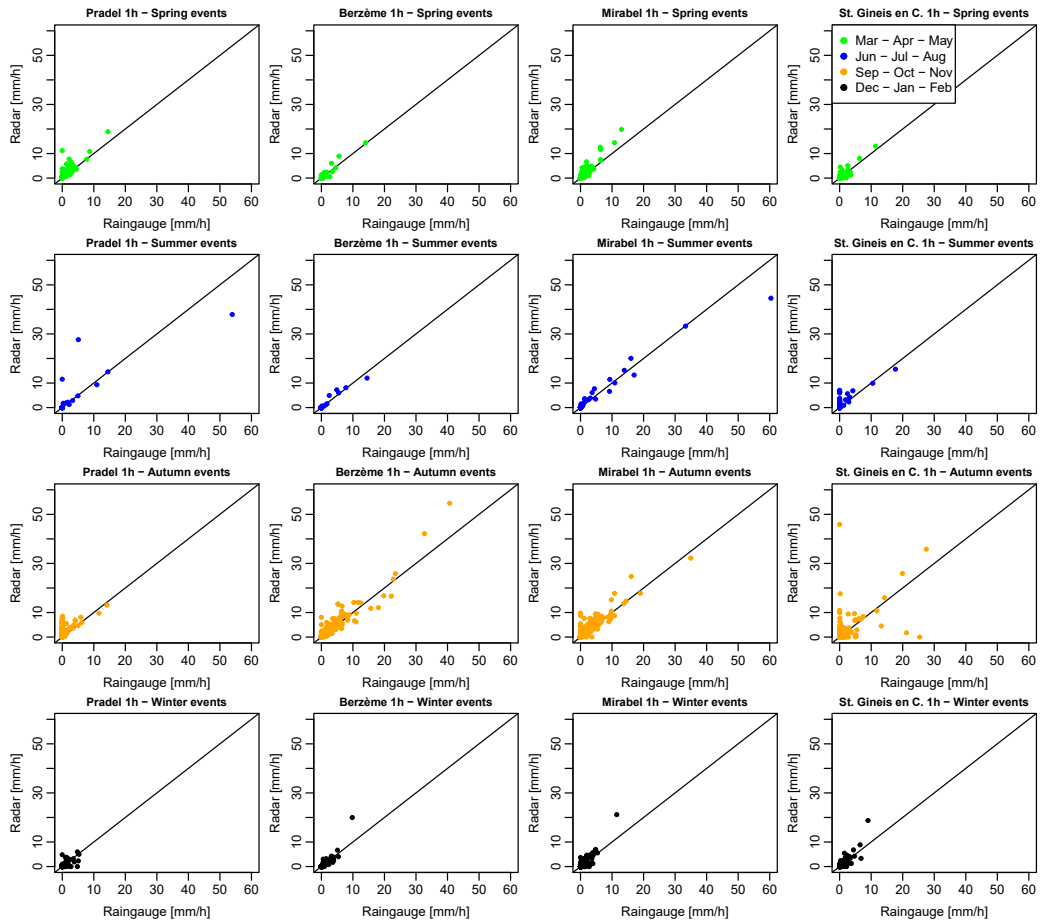


Figure D.4: Comparison of hourly precipitation data recorded by raingauges in the Claduègne catchment and estimated by radar in the different seasons. The rain gauges at Pradel and Mirabel are located on the sedimentary geology, the ones at St. Gineis en Coiron and Berzème are located on the basaltic plateau in the north of the catchment.

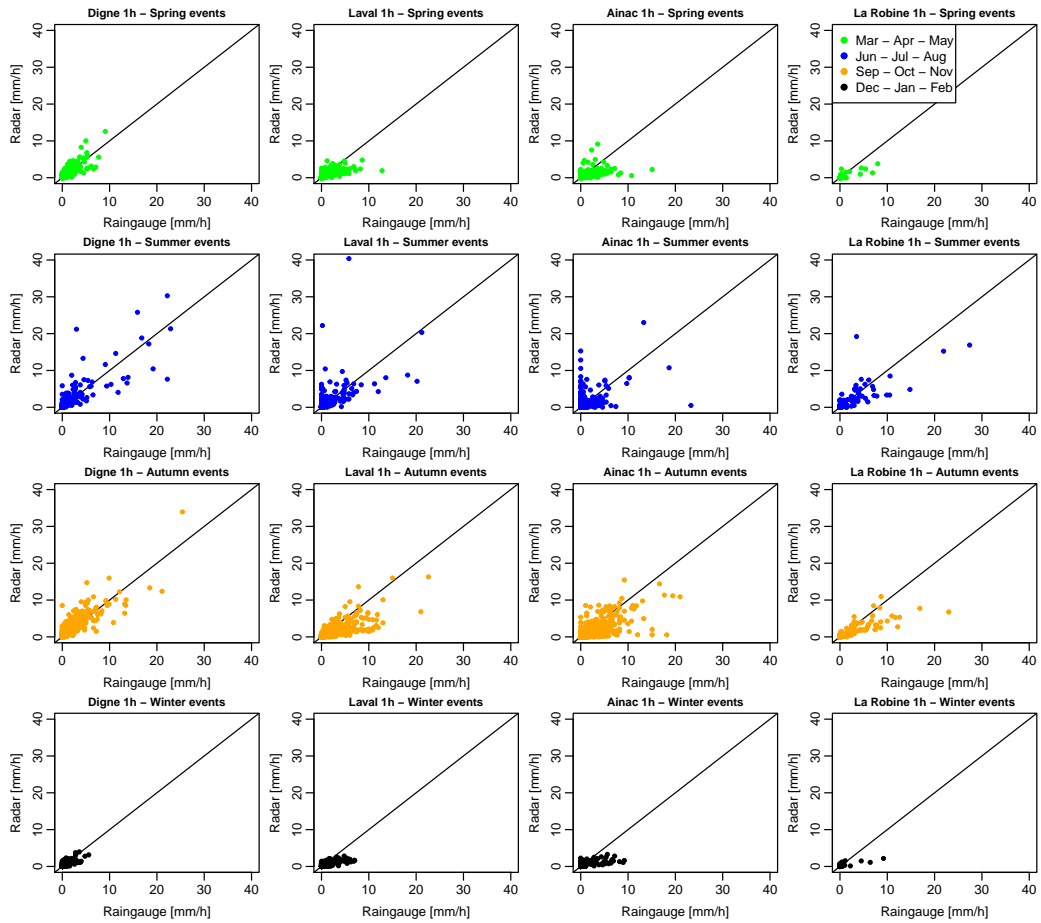


Figure D.5: Comparison of hourly precipitation data recorded by raingauges in the Galabre catchment and estimated by radar in the different seasons. All raingauges where hourly data is available are used (Ainac, Robine, Laval, Digne).

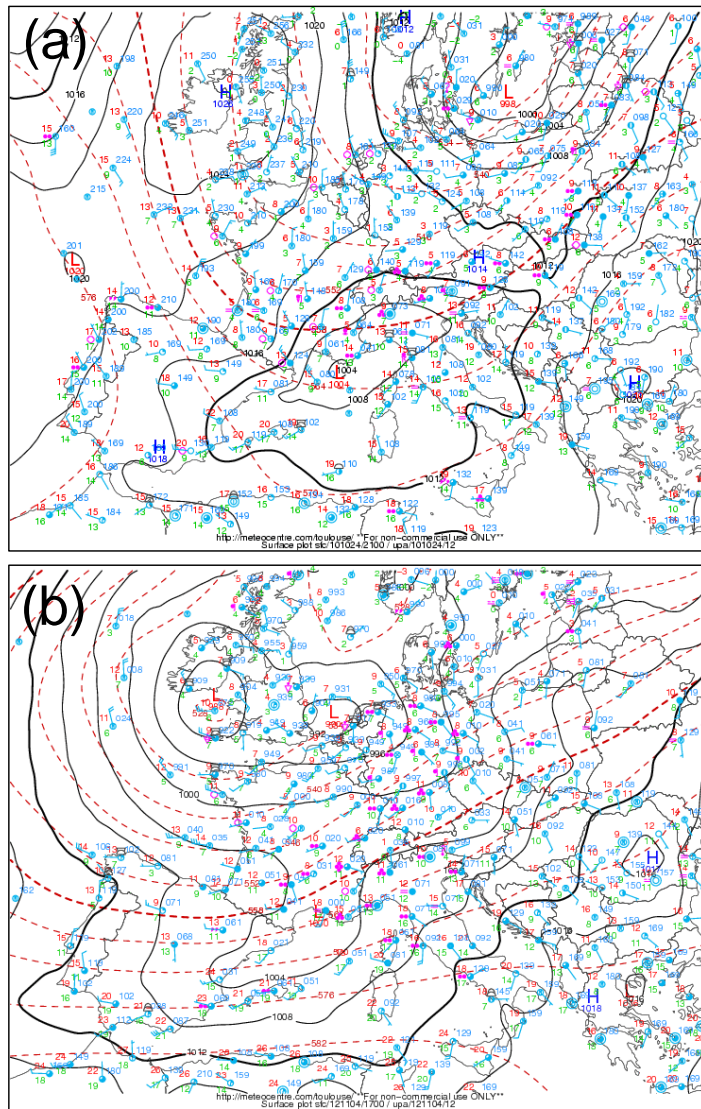


Figure D.6: Surface weather maps of Western Europe on October 24th, 2010 21:00 (a), November 4th, 2012 17:00 (b), May 18th, 2013 12:00 (c, next page) and August 19th, 2014 00:00 (d). Source: <http://meteocentre.com/archive/archive.php?lang=en>. The black lines are surface isobars. On November 4th, 2012, they were concentrated around a depression in Ireland and Great Britain (red “L”); the low density of isobars on August 19th indicates that the pressure gradient over France was low (d). The red dashed lines represent geopotential height at 500 hPa. The blue points or circles represent the locations of weather stations. The direction of the line extending from the point corresponds to the wind direction. Wind speed is represented by the barbs, i.e. the shorter lines that extend from the longer line. Multiple, longer barbs indicate high wind speeds, e.g. in the Rhone valley on May 18th, 2013 (c). The absence of barbs in most stations in southeastern France on August 19th, 2014 (d) indicates that wind speeds were low.

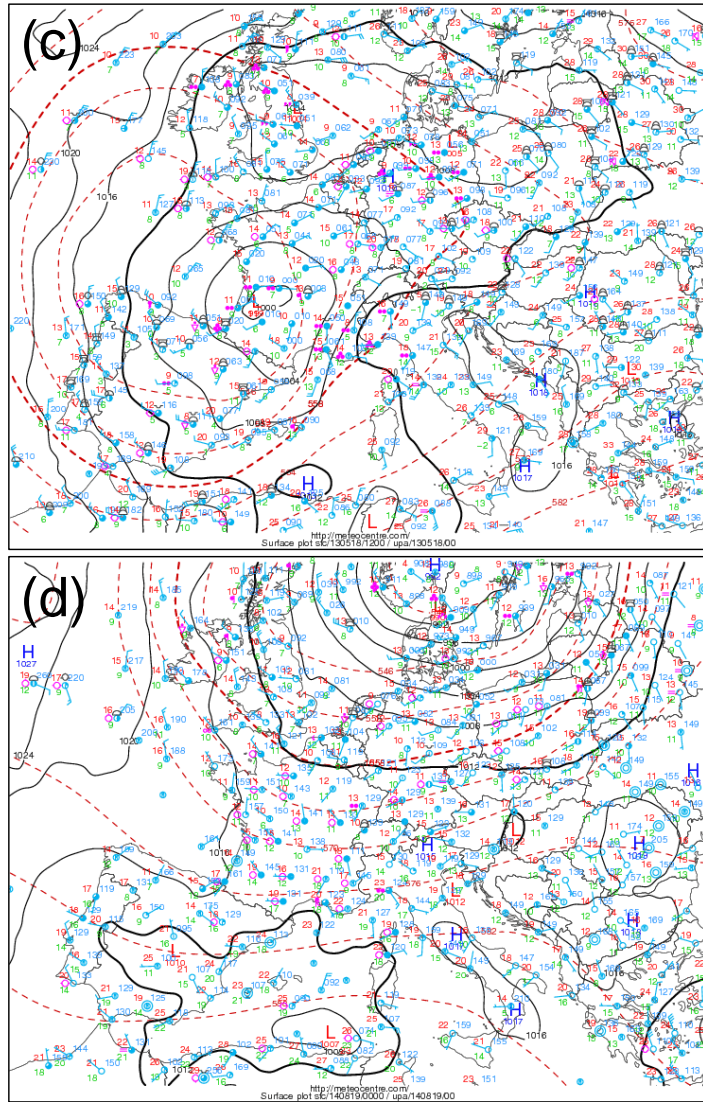


Figure D.6 (cont.): Surface weather maps of Western Europe on May 18th, 2013 12:00 (c) and August 19th, 2014 00:00 (d). See the explanations on the previous page.

Bibliography

- Abbott, M. B., Bathurst, J. C., Cunge, J. A., O'Connell, P. E., and Rasmussen, J. (1986a). An introduction to the european hydrological system—systeme hydrologique europeen, “SHE”, 1: History and philosophy of a physically-based, distributed modelling system. *Journal of Hydrology*, 87(1-2):45–59.
- Abbott, M. B., Bathurst, J. C., Cunge, J. A., O'Connell, P. E., and Rasmussen, J. (1986b). An introduction to the european hydrological system—systeme hydrologique europeen, “SHE”, 2: Structure of a physically-based, distributed modelling system. *Journal of Hydrology*, 87(1-2):61–77.
- Accornero, A., Gnerre, R., and Manfra, L. (2008). Sediment concentrations of trace metals in the Berre lagoon (France): an assessment of contamination. *Archives of environmental contamination and toxicology*, 54(3):372–385.
- Adams, R., Western, A. W., and Seed, A. W. (2012). An analysis of the impact of spatial variability in rainfall on runoff and sediment predictions from a distributed model. *Hydrological Processes*, 26(21):3263–3280.
- Alewell, C., Borelli, P., Meusburger, K., and Panagos, P. (2019). Using the USLE: Chances, challenges and limitations of soil erosion modelling. *International soil and water conservation research*.
- Alewell, C., Meusburger, K., Brodbeck, M., and Bänninger, D. (2008). Methods to describe and predict soil erosion in mountain regions. *Landscape and Urban Planning*, 88(2-4):46–53.
- Alpert, P., Ben-Gai, T., Baharad, A., Benjamini, Y., Yekutieli, D., Colacino, M., Diodato, L., Ramis, C., Homar, V., Romero, R., et al. (2002). The paradoxical increase of mediterranean extreme daily rainfall in spite of decrease in total values. *Geophysical research letters*, 29(11):31–1.
- Amundson, R., Berhe, A. A., Hopmans, J. W., Olson, C., Sztein, A. E., and Sparks, D. L. (2015). Soil and human security in the 21st century. *Science*, 348(6235):647.
- Anderton, S., Latron, J., White, S., Llorens, P., Gallart, F., Salvany, C., and O'Connell, P. (2002). Internal evaluation of a physically-based distributed model using data from a mediterranean mountain catchment. *Hydrology and Earth System Sciences*, 6(1):67–83.

- Andrieu, J. (2015). Landcover map claduègne catchment. https://mistrals.sedoo.fr/?editDatsId=1381&datsId=1381&project_name=HyMeX [access: 26-03-2020].
- Anggraheni, E., Sutjiningsih, D., Emmanuel, I., Payrastre, O., and Andrieu, H. (2018). Assessing the role of spatial rainfall variability on watershed response based on weather radar data (a case study of the Gard region, France). *International Journal of Technology*, 9(3):568–577.
- Anquetin, S., Braud, I., Vannier, O., Viallet, P., Boudevillain, B., Creutin, J.-D., and Manus, C. (2010). Sensitivity of the hydrological response to the variability of rainfall fields and soils for the Gard 2002 flash-flood event. *Journal of Hydrology*, 394(1–2):134–147.
- Antoine, P., Giraud, A., Meunier, M., and Van Asch, T. (1995). Geological and geotechnical properties of the “Terres Noires” in southeastern France: Weathering, erosion, solid transport and instability. *Engineering Geology*, 40(3):223–234.
- Arnaud, F., Révillon, S., Debret, M., Revel, M., Chapron, E., Jacob, J., Giguët-Covex, C., Poulenard, J., and Magny, M. (2012). Lake Bourget regional erosion patterns reconstruction reveals Holocene NW European Alps soil evolution and paleohydrology. *Quaternary Science Reviews*, 51:81–92.
- Arnold, J. G., Srinivasan, R., Muttiah, R. S., and Williams, J. R. (1998). Large area hydrologic modeling and assessment part i: model development 1. *JAWRA Journal of the American Water Resources Association*, 34(1):73–89.
- Asselman, N. (2000). Fitting and interpretation of sediment rating curves. *Journal of Hydrology*, 234(3-4):228–248.
- Baartman, J. E., Jetten, V. G., Ritsema, C. J., and de Vente, J. (2012). Exploring effects of rainfall intensity and duration on soil erosion at the catchment scale using openlsem: Prado catchment, se spain. *Hydrological Processes*, 26(7):1034–1049.
- Baartman, J. E., Masselink, R., Keesstra, S. D., and Temme, A. J. (2013a). Linking landscape morphological complexity and sediment connectivity. *Earth Surface Processes and Landforms*, 38(12):1457–1471.
- Baartman, J. E., Temme, A. J., Veldkamp, T., Jetten, V. G., and Schoorl, J. M. (2013b). Exploring the role of rainfall variability and extreme events in long-term landscape development. *Catena*, 109:25–38.
- Bača, P. (2008). Hysteresis effect in suspended sediment concentration in the Rybárik basin, Slovakia. *Hydrological Sciences Journal*, 53(1):224–235.
- Badoux, A., Turowski, J., Mao, L., Mathys, N., Rickenmann, D., Tzimopoulos, C., and Marchi, L. (2012). Rainfall intensity-duration thresholds for bedload transport initiation in small alpine watersheds. *Natural Hazards & Earth System Sciences*, 12(10).

- Baffaut, C., Nearing, M., Ascough II, J., and Liu, B. (1997). The WEPP watershed model: II. sensitivity analysis and discretization on small watersheds. *Transactions of the ASAE*, 40(4):935–943.
- Bajard, M., Sabatier, P., David, F., Develle, A.-L., Reyss, J.-L., Fanget, B., Malet, E., Arnaud, D., Augustin, L., Crouzet, C., et al. (2016). Erosion record in Lake La Thuile sediments (Prealps, France): Evidence of montane landscape dynamics throughout the Holocene. *The Holocene*, 26(3):350–364.
- Barnes, H. H. (1967). *Roughness characteristics of natural channels*. Number 1849. US Government Printing Office.
- Barnolas, M., Rigo, T., and Llasat, M. C. (2010). Characteristics of 2-D convective structures in Catalonia (NE Spain): an analysis using radar data and GIS. *Hydrology and Earth System Sciences*, 14(1):129–139.
- Barthod, L. R., Liu, K., Lobb, D. A., Owens, P. N., Martínez-Carreras, N., Koiter, A. J., Petticrew, E. L., McCullough, G. K., Liu, C., and Gaspar, L. (2015). Selecting color-based tracers and classifying sediment sources in the assessment of sediment dynamics using sediment source fingerprinting. *Journal of Environment Quality*, 44(5):1605.
- Bathurst, J., Ewen, J., Parkin, G., O’Connell, P., and Cooper, J. (2004). Validation of catchment models for predicting land-use and climate change impacts. 3. Blind validation for internal and outlet responses. *Journal of Hydrology*, 287(1-4):74–94.
- Bathurst, J. C., Lukey, B., Sheffield, J., Hiley, R. A., and Mathys, N. (1998). Modelling badlands erosion with SHETRAN at Draix, southeast France. In *Modelling Soil Erosion, Sediment Transport and Closely Related Hydrological Processes*, number 249 in IAHS Publications, pages 129–136.
- Belmont, P., Gran, K. B., Schottler, S. P., Wilcock, P. R., Day, S. S., Jennings, C., Lauer, J. W., Viparelli, E., Willenbring, J. K., Engstrom, D. R., and Parker, G. (2011). Large shift in source of fine sediment in the Upper Mississippi River. *Environmental science & technology*, 45(20):8804–8810.
- Ben Slimane, A., Raclot, D., Evrard, O., Sanaa, M., Lefèvre, I., Ahmadi, M., Tounsi, M., Rumpel, C., Ben Mammou, A., and Le Bissonnais, Y. (2013). Fingerprinting sediment sources in the outlet reservoir of a hilly cultivated catchment in Tunisia. *Journal of Soils and Sediments*, 13(4):801–815.
- Beven, K. (1996). Equifinality and uncertainty in geomorphological modelling. In *The Scientific Nature of Geomorphology: Proceedings of the 27th Binghamton Symposium in Geomorphology, Held 27-29 September, 1996*, volume 27, page 289. John Wiley & Sons.
- Beven, K. (2002). Towards an alternative blueprint for a physically based digitally simulated hydrologic response modelling system. *Hydrological Processes*, 16(2):189–206.

- Beven, K. and Binley, A. (1992). The future of distributed models: model calibration and uncertainty prediction. *Hydrological Processes*, 6(May 1991):279–298.
- Bhowmik, A. K., Metz, M., and Schäfer, R. B. (2015). An automated, objective and open source tool for stream threshold selection and upstream riparian corridor delineation. *Environmental Modelling & Software*, 63:240–250.
- Bilotta, G. and Brazier, R. (2008). Understanding the influence of suspended solids on water quality and aquatic biota. *Water Research*, 42(12):2849–2861.
- Bischetti, G., Gandolfi, C., and Whelan, M. (1998). The definition of stream channel head location using digital elevation data. *IAHS Publications-Series of Proceedings and Reports-Intern Assoc Hydrological Sciences*, 248:545–552.
- Bladé, E., Cea, L., Corestein, G., Escolano, E., Puertas, J., Vázquez-Cendón, E., Dolz, J., and Coll, A. (2014). Iber: herramienta de simulación numérica del flujo en ríos. *Revista Internacional de Métodos Numéricos para Cálculo y Diseño en Ingeniería*, 30(1):1–10.
- Blake, W., Walsh, R., Barnsley, M., Palmer, G., Dyrinda, P., and James, J. (2003). Heavy metal concentrations during storm events in a rehabilitated industrialized catchment. *Hydrological Processes*, 17(10):1923–1939.
- Blanchet, J., Molinié, G., and Touati, J. (2018). Spatial analysis of trend in extreme daily rainfall in southern France. *Climate Dynamics*, 51(3):799–812.
- Boardman, J., Vandaele, K., Evans, R., and Foster, I. D. (2019). Off-site impacts of soil erosion and runoff: why connectivity is more important than erosion rates. *Soil Use and Management*.
- Borga, M. (2002). Accuracy of radar rainfall estimates for streamflow simulation. *Journal of Hydrology*, 267(1-2):26–39.
- Borga, M., Stoffel, M., Marchi, L., Marra, F., and Jakob, M. (2014). Hydrogeomorphic response to extreme rainfall in headwater systems: flash floods and debris flows. *Journal of Hydrology*, 518:194–205.
- Borselli, L., Cassi, P., and Torri, D. (2008). Prolegomena to sediment and flow connectivity in the landscape: A GIS and field numerical assessment. *Catena*, 75(3):268–277.
- Borselli, L., Vigiak, O., Cavalli, M., and Ortiz Rodriguez, A. (2014). Using connectivity to assess soil erosion and mass movement processes in the landscape: applications and discussion of a new paradigm.
- Boudevillain, B., Delrieu, G., Galabertier, B., Bonnifait, L., Bouilloud, L., Kirstetter, P.-E., and Mosini, M.-L. (2011). The Cévennes-Vivarais Mediterranean Hydrometeorological Observatory database. *Water Resources Research*, 47(7):W07701.

- Boudevillain, B., Delrieu, G., Wijbrans, A., and Confoland, A. (2016). A high-resolution rainfall re-analysis based on radar-raingauge merging in the Cévennes-Vivarais region, France. *Journal of Hydrology*, 541:14–23.
- Boudreault, M., Koiter, A. J., Lobb, D. A., Liu, K., Benoy, G., Owens, P. N., and Li, S. (2019). Comparison of sampling designs for sediment source fingerprinting in an agricultural watershed in Atlantic Canada. *Journal of Soils and Sediments*, pages 1–17.
- Boukhrissa, Z., Khanchoul, K., Le Bissonnais, Y., and Tourki, M. (2013). Prediction of sediment load by sediment rating curve and neural network (ANN) in El Kebir catchment, Algeria. *Journal of Earth System Science*, 122(5):1303–1312.
- Bracken, L., Wainwright, J., Ali, G., Tetzlaff, D., Smith, M., Reaney, S., and Roy, A. (2013). Concepts of hydrological connectivity: Research approaches, pathways and future agendas. *Earth-Science Reviews*, 119:17–34.
- Bracken, L. J., Turnbull, L., Wainwright, J., and Bogaart, P. (2015). Sediment connectivity: a framework for understanding sediment transfer at multiple scales. *Earth Surface Processes and Landforms*, 40(2):177–188.
- Braud, I., Ayrat, P.-A., Bouvier, C., Branger, F., Delrieu, G., Dramais, G., Le Coz, J., Leblois, E., Nord, G., and Vandervaere, J.-P. (2016). Advances in flash floods understanding and modelling derived from the FloodScale project in south-east France. In *3rd European Conference on Flood Risk Management, Innovation, Implementation, Integration (FLOODrisk 2016), Oct 2016, Lyon, France*.
- Braud, I., Ayrat, P.-A., Bouvier, C., Branger, F., Delrieu, G., Le Coz, J., Nord, G., Vandervaere, J.-P., Anquetin, S., Adamovic, M., Andrieu, J., Batiot, C., Boudevillain, B., Brunet, P., Carreau, J., Confoland, A., Didon-Lescot, J.-F., Domergue, J.-M., Douvinet, J., Dramais, G., Freydier, R., Gérard, S., Huza, J., Leblois, E., Le Bourgeois, O., Le Boursicaud, R., Marchand, P., Martin, P., Nottale, L., Patris, N., Renard, B., Seidel, J.-L., Taupin, J.-D., Vannier, O., Vincendon, B., and Wijbrans, A. (2014). Multi-scale hydrometeorological observation and modelling for flash flood understanding. *Hydrology and Earth System Sciences*, 18(9):3733–3761.
- Braud, I. and Vandervaere, J. P. (2015). Analysis of infiltration tests and performed in the Claduègne catchment in May-June 2012. Technical report, Institut National de Recherche en Sciences et Technologies pour L’Environnement et L’Agriculture (IRSTEA), Laboratoire d’étude des Transferts en Hydrologie et Environnement (LTHE).
- Brazier, R. E., Beven, K. J., Freer, J., and Rowan, J. S. (2000). Equifinality and uncertainty in physically based soil erosion models: application of the GLUE methodology to WEPP—the water erosion prediction project—for sites in the UK and USA. *Earth Surface Processes and Landforms: The Journal of the British Geomorphological Research Group*, 25(8):825–845.

- Brils, J. (2008). Sediment monitoring and the European Water Framework Directive. *Annali dell'Istituto Superiore di Sanita*, 44(3):218.
- Brochot, S. and Meunier, M. (1995). Érosion de bad lands dans les Alpes du Sud. Synthèse. In Meunier, M., editor, *Compte-rendu de recherches n3 BVRE de Draix*, pages 141 – 174. Cemagref Editions.
- Bronstert, A. and Bárdossy, A. (2003). Uncertainty of runoff modelling at the hillslope scale due to temporal variations of rainfall intensity. *Physics and Chemistry of the Earth*, 28(6-7):283–288.
- Brosinsky, A., Foerster, S., Segl, K., and Kaufmann, H. (2014a). Spectral fingerprinting: sediment source discrimination and contribution modelling of artificial mixtures based on VNIR-SWIR spectral properties. *Journal of Soils and Sediments*, 14(12):1949–1964.
- Brosinsky, A., Foerster, S., Segl, K., López-Tarazón, J. A., Piqué, G., and Bronstert, A. (2014b). Spectral fingerprinting: characterizing suspended sediment sources by the use of VNIR-SWIR spectral information. *Journal of Soils and Sediments*, 14(12):1965–1981.
- Buendia, C., Bussi, G., Tuset, J., Vericat, D., Sabater, S., Palau, A., and Batalla, R. (2016a). Effects of afforestation on runoff and sediment load in an upland Mediterranean catchment. *Science of The Total Environment*, 540:144–157.
- Buendia, C., Vericat, D., Batalla, R. J., and Gibbins, C. N. (2016b). Temporal dynamics of sediment transport and transient in-channel storage in a highly erodible catchment. *Land Degradation & Development*, 27(4):1045–1063.
- Burylo, M., Dutoit, T., and Rey, F. (2014). Species traits as practical tools for ecological restoration of marly eroded lands. *Restoration Ecology*, 22(5):633–640.
- Burylo, M., Rey, F., Mathys, N., and Dutoit, T. (2012). Plant root traits affecting the resistance of soils to concentrated flow erosion: PLANT ROOT TRAITS AND SOIL STABILITY. *Earth Surface Processes and Landforms*, 37(14):1463–1470.
- Camenen, B., Jodeau, M., and Jaballah, M. (2013). Estimate of fine sediment deposit dynamics over a gravel bar using photography analysis. *International Journal of Sediment Research*, 28(2):220–233.
- Carrière, A. (2019). *Impact de la végétation sur l'érosion de bassins versants marneux*. Dissertation, Université Grenoble Alpes, Grenoble, France.
- Cavalli, M., Trevisani, S., Comiti, F., and Marchi, L. (2013). Geomorphometric assessment of spatial sediment connectivity in small alpine catchments. *Geomorphology*, 188:31–41.
- Cea, L., Bermudez, M., Puertas, J., Blade, E., Corestein, G., Escolano, E., Conde, A., Bockelmann-Evans, B., and Ahmadian, R. (2016). IberWQ: New simulation tool for 2D water quality modelling in rivers and shallow estuaries. *Journal of Hydroinformatics*, 18(5):816–830.

- Cea, L. and Bladé, E. (2015). A simple and efficient unstructured finite volume scheme for solving the shallow water equations in overland flow applications. *Water Resources Research*, 51(7):5464–5486.
- Cea, L., Legout, C., Grangeon, T., and Nord, G. (2015). Impact of model simplifications on soil erosion predictions: application of the GLUE methodology to a distributed event-based model at the hillslope scale. *Hydrological Processes*, 30(7):1096–1113.
- Cea, L., Puertas, J., and Vázquez-Cendón, M.-E. (2007). Depth averaged modelling of turbulent shallow water flow with wet-dry fronts. *Archives of Computational Methods in Engineering*, 14(3):303–341.
- Cea, L. and Vázquez-Cendón, M. E. (2012). Unstructured finite volume discretisation of bed friction and convective flux in solute transport models linked to the shallow water equations. *Journal of Computational Physics*, 231(8):3317–3339.
- Cerdan, O., Govers, G., Le Bissonnais, Y., Van Oost, K., Poesen, J., Saby, N., Gobin, A., Vacca, A., Quinton, J., Auerswald, K., Klik, A., Kwaad, F., Raclot, D., Ionita, I., Rejman, J., Rousseva, S., Muxart, T., Roxo, M., and Dostal, T. (2010). Rates and spatial variations of soil erosion in Europe: A study based on erosion plot data. *Geomorphology*, 122(1-2):167–177.
- Chaubey, I., Haan, C., Grunwald, S., and Salisbury, J. (1999). Uncertainty in the model parameters due to spatial variability of rainfall. *Journal of Hydrology*, 220(1-2):48–61.
- Chen, F., Zhang, F., Fang, N., and Shi, Z. (2016). Sediment source analysis using the fingerprinting method in a small catchment of the Loess Plateau, China. *Journal of Soils and Sediments*, 16(5):1655–1669.
- Ciach, G. J., Krajewski, W. F., and Villarini, G. (2007). Product-error-driven uncertainty model for probabilistic quantitative precipitation estimation with NEXRAD data. *Journal of Hydrometeorology*, 8(6):1325–1347.
- Ciszewski, D. and Grygar, T. M. (2016). A review of flood-related storage and remobilization of heavy metal pollutants in river systems. *Water, Air, & Soil Pollution*, 227(7):239.
- Collins, A., Pulley, S., Foster, I., Gellis, A., Porto, P., and Horowitz, A. (2017). Sediment source fingerprinting as an aid to catchment management: A review of the current state of knowledge and a methodological decision-tree for end-users. *Journal of Environmental Management*, 194:86–108.
- Collins, A. L., Walling, D. E., and Leeks, G. J. L. (1997). Source type ascription for fluvial suspended sediment based on a quantitative composite fingerprinting technique. *Catena*, 29(1):1–27.

- Collins, A. L., Walling, D. E., Webb, L., and King, P. (2010). Apportioning catchment scale sediment sources using a modified composite fingerprinting technique incorporating property weightings and prior information. *Geoderma*, 155(3–4):249–261.
- Colombo, R., Vogt, J. V., Soille, P., Paracchini, M. L., and de Jager, A. (2007). Deriving river networks and catchments at the European scale from medium resolution digital elevation data. *Catena*, 70(3):296–305.
- Comission Internationale de l’Eclairage (CIE) (1978). Recommendations on uniform color spaces, color-difference equations, psychometric color terms. *Colorimetry CIE, Paris, Suppl. No. 2 to publication no. 15*.
- Cooper, R. J., Krueger, T., Hiscock, K. M., and Rawlins, B. G. (2014). Sensitivity of fluvial sediment source apportionment to mixing model assumptions: A Bayesian model comparison. *Water Resources Research*, 50(11):9031–9047.
- Cooper, R. J., Krueger, T., Hiscock, K. M., and Rawlins, B. G. (2015). High-temporal resolution fluvial sediment source fingerprinting with uncertainty: a Bayesian approach. *Earth Surface Processes and Landforms*, 40(1):78–92.
- Cossart, E., Viel, V., Lissak, C., Reulier, R., Fressard, M., and Delahaye, D. (2018). How might sediment connectivity change in space and time? *Land Degradation & Development*, 29(8):2595–2613.
- Coulthard, T. J. and Skinner, C. J. (2016). The sensitivity of landscape evolution models to spatial and temporal rainfall resolution. *Earth Surface Dynamics*, 4(3):757–771.
- Cras, A., Marc, V., and Travi, Y. (2007). Hydrological behaviour of sub-Mediterranean alpine headwater streams in a badlands environment. *Journal of Hydrology*, 339(3–4):130–144.
- Crawford, C. G. (1991). Estimation of suspended-sediment rating curves and mean suspended-sediment loads. *Journal of Hydrology*, 129(1-4):331–348.
- Craz, A. (2005). *Etude et modélisation de la dynamique de fonctionnement hydrologique des bassins versants torrentiels marneux, apport du traçage naturel : application aux bassins versants de recherche et d’expérimentation (BVRE) de Draix, Alpes-de-Haute-Provence, France*. Dissertation, l’Université d’Avignon et des Pays de Vaucluse, Avignon, France.
- Crema, S. and Cavalli, M. (2017). SedInConnect: A stand-alone, free and open source tool for the assessment of sediment connectivity. *Computers & Geosciences*.
- Cronshey, R. G. and Theurer, F. D. (1998). AnnAGNPS-non point pollutant loading model. In *Proceedings of the First Federal Interagency Hydrologic Modeling Conference*, pages 19–23.

- Crutzen, P. J. (2006). The “anthropocene”. In Ehlers, E. and Krafft, T., editors, *Earth system science in the anthropocene*, pages 13–18. Springer.
- D’Agostino, V. and Bertoldi, G. (2014). On the assessment of the management priority of sediment source areas in a debris-flow catchment. *Earth Surface Processes and Landforms*, 39(5):656–668.
- Davis, C. M. and Fox, J. F. (2009). Sediment fingerprinting: Review of the method and future improvements for allocating nonpoint source pollution. *Journal of Environmental Engineering*, 135(7):490–504.
- de Deckere, E., De Cooman, W., Leloup, V., Meire, P., Schmitt, C., and Peter, C. (2011). Development of sediment quality guidelines for freshwater ecosystems. *Journal of Soils and Sediments*, 11(3):504–517.
- de Vente, J. and Poesen, J. (2005). Predicting soil erosion and sediment yield at the basin scale: Scale issues and semi-quantitative models. *Earth-Science Reviews*, 71(1-2):95–125.
- de Vente, J., Poesen, J., Verstraeten, G., Govers, G., Vanmaercke, M., Van Rompaey, A., Arabkhedri, M., and Boix-Fayos, C. (2013). Predicting soil erosion and sediment yield at regional scales: Where do we stand? *Earth-Science Reviews*, 127:16–29.
- Dearing, J., Hu, Y., Doody, P., James, P. A., and Brauer, A. (2001). Preliminary reconstruction of sediment-source linkages for the past 6000 yr at the Petit Lac d’Annecy, France, based on mineral magnetic data. *Journal of Paleolimnology*, 25(2):245–258.
- Dearing, J. A., Elner, J. K., and Happey-Wood, C. M. (1981). Recent sediment flux and erosional processes in a Welsh upland lake-catchment based on magnetic susceptibility measurements. *Quaternary Research*, 16(3):356–372.
- Dearing, J. A., Morton, R. I., Price, T. W., and Foster, I. D. L. (1986). Tracing movements of topsoil by magnetic measurements: two case studies. *Physics of the Earth and Planetary Interiors*, 42(1-2):93–104.
- Delrieu, G., Nicol, J., Yates, E., Kirstetter, P.-E., Creutin, J.-D., Anquetin, S., Obled, C., Saulnier, G.-M., Ducrocq, V., Gaume, E., et al. (2005). The catastrophic flash-flood event of 8–9 september 2002 in the Gard region, France: a first case study for the cévennes–vivaraïis mediterranean hydrometeorological observatory. *Journal of Hydrometeorology*, 6(1):34–52.
- Delrieu, G., Wijbrans, A., Boudevillain, B., Faure, D., Bonnifait, L., and Kirstetter, P.-E. (2014). Geostatistical radar–raingauge merging: A novel method for the quantification of rain estimation accuracy. *Advances in Water Resources*, 71:110–124.
- Descroix, L. and Gautier, E. (2002). Water erosion in the southern French alps: climatic and human mechanisms. *Catena*, 50(1):53–85.

- Descroix, L. and Mathys, N. (2003). Processes, spatio-temporal factors and measurements of current erosion in the French Southern Alps: a review. *Earth Surface Processes and Landforms*, 28(9):993–1011.
- Descroix, L. and Olivry, J.-C. (2002). Spatial and temporal factors of erosion by water of black marls in the badlands of the French southern Alps. *Hydrological Sciences Journal*, 47(2):227–242.
- Diabi Skhakhfa, I., Boudevillain, B., and Delrieu, G. (2019). Analysis of pseudo radar-based QPE errors due to the variability of the Z-R relationship from disdrometers dataset. In *Hymex Workshop*.
- Direction Régionale de l’Alimentation de l’Agriculture et de la Forêt d’Auvergne-Rhône-Alpes (DRAAF) (2017). Ilots déclarés à la PAC 2016 et le groupe de cultures dominant - Auvergne-Rhône-Alpes. https://www.data.gouv.fr/fr/datasets/ilots-declares-a-la-pac-2016-et-le-groupe-de-cultures-dominant-auvergne-rhone-alpes/#_ [access: 26-03-2020].
- Douglas, G., Caitcheon, G., and Palmer, M. (2009). Sediment source identification and residence times in the Maroochy River estuary, southeast Queensland, Australia. *Environmental Geology*, 57(3):629–639.
- Drobinski, P., Ducrocq, V., Alpert, P., Anagnostou, E., Béranger, K., Borga, M., Braud, I., Chanzy, A., Davolio, S., Delrieu, G., Estournel, C., Filali Boubrahmi, N., Font, J., Grubišić, V., Gualdi, S., Homar, V., Ivančan-Picek, B., Kottmeier, C., Kotroni, V., Lagouvardos, K., Lionello, P., Llasat, M., Ludwig, W., Lutoff, C., Mariotti, A., Richard, E., Romero, R., Rotunno, R., Roussot, O., Ruin, I., Somot, S., Taupier-Letage, I., Tintore, J., Uijlenhoet, R., and Wernli, H. (2014). HyMeX: a 10-year multidisciplinary program on the mediterranean water cycle. *Bulletin of the American Meteorological Society*, 95(7):1063–1082.
- Du, P. and Walling, D. E. (2017). Fingerprinting surficial sediment sources: Exploring some potential problems associated with the spatial variability of source material properties. *Journal of Environmental Management*, 194:4–15.
- Ducrocq, V., Braud, I., Davolio, S., Ferretti, R., Flamant, C., Jansa, A., Kalthoff, N., Richard, E., Taupier-Letage, I., Ayrat, P.-A., Belamari, S., Berne, A., Borga, M., Boudevillain, B., Bock, O., Boichard, J.-L., Bouin, M.-N., Bousquet, O., Bouvier, C., Chiggiato, J., Cimini, D., Corsmeier, U., Coppola, L., Cocquerez, P., Defer, E., Delanoë, J., Di Girolamo, P., Doerenbecher, A., Drobinski, P., Dufournet, Y., Fourrié, N., Gourley, J. J., Labatut, L., Lambert, D., Le Coz, J., Marzano, F. S., Molinié, G., Montani, A., Nord, G., Nuret, M., Ramage, K., Rison, W., Roussot, O., Said, F., Schwarzenboeck, A., Testor, P., Van Baelen, J., Vincendon, B., Aran, M., and Tamayo, J. (2014). HyMeX-SOP1: The field campaign dedicated to heavy precipitation and flash flooding in the northwestern Mediterranean. *Bulletin of the American Meteorological Society*, 95(7):1083–1100.

- Duvert, C., Nord, G., Gratiot, N., Navratil, O., Nadal-Romero, E., Mathys, N., Némery, J., Regüés, D., García-Ruiz, J., Gallart, F., and Esteves, M. (2012). Towards prediction of suspended sediment yield from peak discharge in small erodible mountainous catchments (0.45 – 22 km²) of France, Mexico and Spain. *Journal of Hydrology*, 454-455:42–55.
- Einstein, H., Anderson, A. G., and Johnson, J. W. (1940). A distinction between bed-load and suspended load in natural streams. *Eos, Transactions American Geophysical Union*, 21(2):628–633.
- Emmanuel, I., Andrieu, H., Leblois, E., Janey, N., and Payrastre, O. (2015). Influence of rainfall spatial variability on rainfall–runoff modelling: Benefit of a simulation approach? *Journal of Hydrology*, 531:337–348.
- Emmanuel, I., Payrastre, O., Andrieu, H., and Zuber, F. (2017). A method for assessing the influence of rainfall spatial variability on hydrograph modeling. First case study in the Cevennes Region, southern France. *Journal of Hydrology*, 555:314–322.
- Engelund, F. and Hansen, E. (1967). A monograph on sediment transport in alluvial streams. *Technical University of Denmark Østervoldgade 10, Copenhagen K*.
- Engman, E. T. (1986). Roughness coefficients for routing surface runoff. *Journal of Irrigation and Drainage Engineering*, 112(1):39–53.
- Erktan, A., Cécillon, L., Roose, E., Frascaria-Lacoste, N., and Rey, F. (2013). Morphological diversity of plant barriers does not increase sediment retention in eroded marly gullies under ecological restoration. *Plant and soil*, 370(1-2):653–669.
- Erktan, A. and Rey, F. (2013). Linking sediment trapping efficiency with morphological traits of *Salix* tiller barriers on marly gully floors under ecological rehabilitation. *Ecological Engineering*, 51:212–220.
- Esteves, M., Descroix, L., Mathys, N., and Lapetite, J. M. (2005). Soil hydraulic properties in a marly gully catchment (Draix, France). *Catena*, 63(2-3):282–298.
- Esteves, M., Legout, C., Navratil, O., and Evrard, O. (2019). Medium term high frequency observation of discharges and suspended sediment in a Mediterranean mountainous catchment. *Journal of Hydrology*, 568:562–574.
- Evrard, O., Laceby, J. P., Ficetola, G. F., Gielly, L., Huon, S., Lefèvre, I., Onda, Y., and Poulenard, J. (2019). Environmental DNA provides information on sediment sources: a study in catchments affected by Fukushima radioactive fallout. *Science of The Total Environment*, 665:873–881.
- Evrard, O., Navratil, O., Ayrault, S., Ahmadi, M., Némery, J., Legout, C., Lefèvre, I., Poirel, A., Bonté, P., and Esteves, M. (2011). Combining suspended sediment monitoring and fingerprinting to determine the spatial origin of fine sediment in a mountainous river catchment. *Earth Surface Processes and Landforms*, 36(8):1072–1089.

- Evrard, O., Poulenard, J., Némery, J., Ayrault, S., Gratiot, N., Duvert, C., Prat, C., Lefèvre, I., Bonté, P., and Esteves, M. (2013). Tracing sediment sources in a tropical highland catchment of central Mexico by using conventional and alternative fingerprinting methods. *Hydrological Processes*, 27(6):911–922.
- Fernández-Raga, M., Palencia, C., Keesstra, S., Jordán, A., Fraile, R., Angulo-Martínez, M., and Cerdà, A. (2017). Splash erosion: a review with unanswered questions. *Earth-Science Reviews*, 171:463–477.
- Ferreira, C. S., Walsh, R. P., Blake, W. H., Kikuchi, R., and Ferreira, A. J. (2017). Temporal dynamics of sediment sources in an urbanizing Mediterranean catchment. *Land Degradation & Development*.
- Fraga, I., Cea, L., and Puertas, J. (2013). Experimental study of the water depth and rainfall intensity effects on the bed roughness coefficient used in distributed urban drainage models. *Journal of Hydrology*, 505:266–275.
- Francke, T., Foerster, S., Brosinsky, A., Sommerer, E., Lopez-Tarazon, J. A., Güntner, A., Batalla, R. J., and Bronstert, A. (2018). Water and sediment fluxes in Mediterranean mountainous regions: comprehensive dataset for hydro-sedimentological analyses and modelling in a mesoscale catchment (River Isábena, NE Spain). *Earth System Science Data*, 10:1063–1075.
- Francke, T., López-Tarazón, J., and Schröder, B. (2008a). Estimation of suspended sediment concentration and yield using linear models, random forests and quantile regression forests. *Hydrological Processes*, 22(25):4892–4904.
- Francke, T., López-Tarazón, J. A., Vericat, D., Bronstert, A., and Batalla, R. J. (2008b). Flood-based analysis of high-magnitude sediment transport using a non-parametric method. *Earth Surface Processes and Landforms*, 33(13):2064–2077.
- Francke, T., Werb, S., Sommerer, E., and López-Tarazón, J. A. (2014). Analysis of runoff, sediment dynamics and sediment yield of subcatchments in the highly erodible Isábena catchment, Central Pyrenees. *Journal of Soils and Sediments*, 14(12):1909–1920.
- Franks, S. and Rowan, J. (2000). Multi-parameter fingerprinting of sediment sources: uncertainty estimation and tracer selection. *Computational Methods in Water Resources*, 13:1067–1074.
- Fryirs, K. (2013). (dis)connectivity in catchment sediment cascades: a fresh look at the sediment delivery problem. *Earth Surface Processes and Landforms*, 38(1):30–46.
- Gaillardet, J., Braud, I., Hankard, F., Anquetin, S., Bour, O., Dorfliger, N., De Dreuzy, J.-R., Galle, S., Galy, C., Gogo, S., Gourcy, L., Habets, F., Laggoun, F., Longuevergne, L., Le Borgne, T., Naaim-Bouvet, F., Nord, G., Simonneaux, V., Six, D., Tallec, T., Valentin, C., et al. (2018). OZCAR: the French network of critical zone observatories. *Vadose Zone Journal*, 17(1).

- Gallard, F., Balasch, J., Regüés, D., Soler, M., and Castelltort, X. (2005). Catchment dynamics in a Mediterranean mountain environment: the Vallcebre research basins (south eastern Pyrenees) II: temporal and spatial dynamics of erosion and stream sediment transport. In Garcia, C. and Batalla, R. J., editors, *Catchment Dynamics and River Processes: Mediterranean and Other Climate Regions*. Elsevier.
- Gallart, F., Latron, J., Llorens, P., and Beven, K. (2007). Using internal catchment information to reduce the uncertainty of discharge and baseflow predictions. *Advances in Water Resources*, 30(4):808–823.
- Gallart, F., Llorens, P., Latron, J., and Regüés, D. (2002). Hydrological processes and their seasonal controls in a small Mediterranean mountain catchment in the Pyrenees. *Hydrology and Earth System Sciences Discussions*, 6(3):527–537.
- Garcia, M. H. (2006). Sediment transport and morphodynamics. In Garcia, M. H., editor, *ASCE Manual of Practice 110 — Sedimentation engineering: Processes, measurements, modeling, and practice*, chapter 2, pages 22–164. American Society of Civil Engineers.
- Garel, E., Marc, V., Ruy, S., Cognard-Plancq, A.-L., Klotz, S., Emblanch, C., and Simler, R. (2012). Large scale rainfall simulation to investigate infiltration processes in a small landslide under dry initial conditions: the Draix hillslope experiment. *Hydrological Processes*, 26(14):2171–2186.
- Garzon-Garcia, A., Laceby, J. P., Olley, J. M., and Bunn, S. E. (2016). Differentiating the sources of fine sediment, organic matter and nitrogen in a subtropical Australian catchment. *Science of The Total Environment*.
- Gaume, E., Bain, V., Bernardara, P., Newinger, O., Barbuc, M., Bateman, A., Blaškovičová, L., Blöschl, G., Borga, M., Dumitrescu, A., Daliakopoulos, I., Garcia, J., Irimescu, A., Kohnova, S., Koutroulis, A., Marchi, L., Matreata, S., Medina, V., Preciso, E., Sempere-Torres, D., Stancalie, G., Szolgay, J., Tsanis, I., Velasco, D., and Viglione, A. (2009). A compilation of data on European flash floods. *Journal of Hydrology*, 367(1-2):70–78.
- Gellis, A. and Gorman Sanisaca, L. (2018). Sediment fingerprinting to delineate sources of sediment in the agricultural and forested Smith Creek watershed, Virginia, USA. *JAWRA Journal of the American Water Resources Association*.
- Germann, U., Galli, G., Boscacci, M., and Bolliger, M. (2006). Radar precipitation measurement in a mountainous region. *Quarterly Journal of the Royal Meteorological Society: A journal of the atmospheric sciences, applied meteorology and physical oceanography*, 132(618):1669–1692.
- González-Hidalgo, J. C., Peña-Monné, J. L., and de Luis, M. (2007). A review of daily soil erosion in western Mediterranean areas. *Catena*, 71(2):193–199.

- Gourdin, E., Evrard, O., Huon, S., Lefèvre, I., Ribolzi, O., Reyss, J.-L., Sengtaheuanghoung, O., and Ayrault, S. (2014). Suspended sediment dynamics in a Southeast Asian mountainous catchment: Combining river monitoring and fallout radionuclide tracers. *Journal of Hydrology*, 519:1811–1823.
- Grangeon, T. (2006). *Etude multi-échelle de la granulométrie des particules fines générées par érosion hydrique : apports pour la modélisation*. Dissertation, Université de Grenoble, Grenoble, France.
- Grangeon, T., Legout, C., Esteves, M., Gratiot, N., and Navratil, O. (2012). Variability of the particle size of suspended sediment during highly concentrated flood events in a small mountainous catchment. *Journal of Soils and Sediments*, 12(10):1549–1558.
- Grotzinger, J., Jordan, T. H., Press, F., and Siever, R. (2007). *Understanding earth*. W.H. Freeman and Company, 5th edition.
- Guo, L. and Lin, H. (2016). Critical zone research and observatories: Current status and future perspectives. *Vadose Zone Journal*, 15(9):0.
- Hachani, S., Boudevillain, B., Delrieu, G., and Bargaoui, Z. (2017). Drop size distribution climatology in Cévennes-Vivarais region, France. *Atmosphere*, 8(12):233.
- Hachgenei, N. (2017). *Tracing of suspended sediment sources in a meso-scale catchment using spectroradiometry*. Master 1 Report, Université Grenoble Alpes, Grenoble, France.
- Hachgenei, N. (2018). *Study of the distributed hydrologic response of the Claduègne catchment (Ardèche) using dense networks of rain and water level gauges*. Master thesis, Université Grenoble Alpes, Grenoble, France.
- Haddadchi, A., Olley, J., and Laceby, P. (2014). Accuracy of mixing models in predicting sediment source contributions. *Science of The Total Environment*, 497-498:139–152.
- Haddadchi, A., Ryder, D. S., Evrard, O., and Olley, J. (2013). Sediment fingerprinting in fluvial systems: review of tracers, sediment sources and mixing models. *International Journal of Sediment Research*, 28(4):560–578.
- Hallema, D. (2011). *Modélisation de l'impact des terrasses agricoles et du réseau d'écoulement artificiel sur la réponse hydrologique des versants*. Dissertation, Centre International d'Études Supérieures en Sciences Agronomiques, Montpellier, France.
- Hallema, D. W., Moussa, R., Andrieux, P., and Voltz, M. (2013). Parameterization and multi-criteria calibration of a distributed storm flow model applied to a Mediterranean agricultural catchment. *Hydrological Processes*, 27(10):1379–1398.
- Hancock, G. and Coulthard, T. (2012). Channel movement and erosion response to rainfall variability in southeast Australia. *Hydrological Processes*, 26(5):663–673.

- Hartmann, D., Klein Tank, A., Rusticucci, M., Alexander, L., Brönnimann, S., Charabi, Y., Dentener, F., Dlugokencky, E., Easterling, D., Kaplan, A., Soden, B., Thorne, P., Wild, M., and Zhai, P. (2013). Observations: atmosphere and surface. In Stocker, T., Qin, D., Plattner, G.-K., Tignor, M., Allen, S., Boschung, J., Nauels, A., Xia, Y., Bex, V., and Midgley, P., editors, *Climate Change 2013: The Physical Science Basis. Contribution of Working Group I to the Fifth Assessment Report of the Intergovernmental Panel on Climate Change*, chapter 2, page 159–254. Cambridge University Press, Cambridge, United Kingdom and New York, NY, USA.
- He, X., Sonnenborg, T. O., Refsgaard, J. C., Vejen, F., and Jensen, K. H. (2013). Evaluation of the value of radar QPE data and rain gauge data for hydrological modeling. *Water Resources Research*, 49(9):5989–6005.
- Heckmann, T., Cavalli, M., Cerdan, O., Foerster, S., Javaux, M., Lode, E., Smetanová, A., Vericat, D., and Brardinoni, F. (2018). Indices of sediment connectivity: opportunities, challenges and limitations. *Earth-Science Reviews*.
- Hessel, R., Jetten, V., and Guanhui, Z. (2003a). Estimating manning’s n for steep slopes. *Catena*, 54(1-2):77–91.
- Hessel, R., Jetten, V., Liu, B., Zhang, Y., and Stolte, J. (2003b). Calibration of the LISEM model for a small Loess Plateau catchment. *Catena*, 54(1-2):235–254.
- Hill, K. M., Gaffney, J., Baumgardner, S., Wilcock, P., and Paola, C. (2017). Experimental study of the effect of grain sizes in a bimodal mixture on bed slope, bed texture, and the transition to washload. *Water Resources Research*, 53(1):923–941.
- Huang, Y., Bárdossy, A., and Zhang, K. (2019). Sensitivity of hydrological models to temporal and spatial resolutions of rainfall data. *Hydrology and Earth System Sciences*, 23(6):2647–2663.
- Huon, S., Evrard, O., Gourdin, E., Lefèvre, I., Bariac, T., Reyss, J.-L., Henry des Tureaux, T., Sengtaheuanghoung, O., Ayrault, S., and Ribolzi, O. (2017). Suspended sediment source and propagation during monsoon events across nested sub-catchments with contrasted land uses in Laos. *Journal of Hydrology: Regional Studies*, 9:69–84.
- Huza, J., Teuling, A. J., Braud, I., Grazioli, J., Melsen, L. a., Nord, G., Raupach, T. H., and Uijlenhoet, R. (2014). Precipitation, soil moisture and runoff variability in a small river catchment (Ardèche, France) during HyMeX Special Observation Period 1. *Journal of Hydrology*, 516:330–342.
- Inglada, J., Vincent, A., and Thierion, V. (2017). Theia OSO land cover map 2106. <https://www.theia-land.fr/en/product/land-cover-map/> [access: 26-03-2020].
- Institut national de l’information géographique et forestière (IGN) (2018a). ORTHO HR. https://geoservices.ign.fr/ressources_documentaires/Espace_documentaire/ORTHO_IMAGES/BDORTHO_ORTHOHR/DC_BDORTHO_2-0_ORTHOHR_1-0.pdf [access: 26-03-2020].

- Institut national de l'information géographique et forestière (IGN) (2018b). RGE Alti. https://geoservices.ign.fr/ressources_documentaires/Espace_documentaire/MODELES_3D/RGE_ALTI/SE_RGEALTI.pdf [access: 26-03-2020].
- Jahn, R., Pfannschmidt, D., and Stahr, K. (1989). Soils from limestone, dolomite in the central Algarve (Portugal), their qualities in respect to groundwater recharge, runoff erodibility, present erosion. *Catena*, 14:25–42.
- Jetten, V., De Roo, A., and Favis-Mortlock, D. (1999). Evaluation of field-scale and catchment-scale soil erosion models. *Catena*, 37(3-4):521–541.
- Jetten, V. and Favis-Mortlock, D. (2006). Modelling soil erosion in europe. In Boardman, J. and Poesen, J., editors, *Soil Erosion in Europe*, chapter 50, pages 695 – 716. John Wiley and Sons, Ltd.
- Jetten, V., Govers, G., and Hessel, R. (2003). Erosion models: quality of spatial predictions. *Hydrological Processes*, 17(5):887–900.
- Keesstra, S., Nunes, J. P., Saco, P., Parsons, T., Poepl, R., Masselink, R., and Cerdà, A. (2018). The way forward: can connectivity be useful to design better measuring and modelling schemes for water and sediment dynamics? *Science of the Total Environment*, 644:1557–1572.
- Kirkby, M. and Cox, N. (1995). A climatic index for soil erosion potential (CSEP) including seasonal and vegetation factors. *Catena*, 25(1-4):333–352.
- Kirkby, M., Irvine, B., Jones, R. J., Govers, G., and team, P. (2008). The PESERA coarse scale erosion model for Europe. I.–model rationale and implementation. *European Journal of Soil Science*, 59(6):1293–1306.
- Kisi, O., Karahan, M. E., and Şen, Z. (2006). River suspended sediment modelling using a fuzzy logic approach. *Hydrological Processes*, 20(20):4351–4362.
- Koiter, A., Owens, P., Petticrew, E., and Lobb, D. (2013a). The behavioural characteristics of sediment properties and their implications for sediment fingerprinting as an approach for identifying sediment sources in river basins. *Earth-Science Reviews*, 125:24–42.
- Koiter, A. J., Lobb, D. A., Owens, P. N., Petticrew, E. L., Tiessen, K. H. D., and Li, S. (2013b). Investigating the role of connectivity and scale in assessing the sources of sediment in an agricultural watershed in the Canadian prairies using sediment source fingerprinting. *Journal of Soils and Sediments*, 13(10):1676–1691.
- Kondolf, G. M., Gao, Y., Annandale, G. W., Morris, G. L., Jiang, E., Zhang, J., Cao, Y., Carling, P., Fu, K., Guo, Q., Hotchkiss, R., Peteuil, C., Sumi, T., Wang, H. W., Wang, Z., Wei, Z., Wu, B., Wu, C., and Yang, C. T. (2014). Sustainable sediment management in reservoirs and regulated rivers: experiences from five continents. *Earth's Future*, 2(5):256–280.

- Krause, A., Franks, S., Kalma, J., Loughran, R., and Rowan, J. (2003). Multi-parameter fingerprinting of sediment deposition in a small gullied catchment in SE Australia. *Catena*, 53(4):327–348.
- Lacey, J. P., Evrard, O., Smith, H. G., Blake, W. H., Olley, J. M., Minella, J. P., and Owens, P. N. (2017). The challenges and opportunities of addressing particle size effects in sediment source fingerprinting: A review. *Earth-Science Reviews*.
- Lacey, J. P., Gellis, A. C., Koiter, A. J., Blake, W. H., and Evrard, O. (2019). Preface - evaluating the response of critical zone processes to human impacts with sediment source fingerprinting. *Journal of Soils and Sediments*, 19(9):3245–3254.
- Lacey, J. P. and Olley, J. (2015). An examination of geochemical modelling approaches to tracing sediment sources incorporating distribution mixing and elemental correlations. *Hydrological Processes*, 29(6):1669–1685.
- Lafren, J. M., Elliot, W., Flanagan, D., Meyer, C., and Nearing, M. (1997). WEPP - predicting water erosion using a process-based model. *Journal of Soil and Water Conservation*, 52(2):96–102.
- Lafren, J. M., Lane, L. J., and Foster, G. R. (1991). WEPP: a new generation of erosion prediction technology. *Journal of Soil and Water Conservation*, 46(1):34–38.
- Lawson, C. L. and Hanson, R. J. (1974). *Solving least squares problems*. Prentice-Hall, Englewood Cliffs.
- Le Bouteiller, C., Naaim-Bouvet, F., Mathys, N., and Lavé, J. (2011). A new framework for modeling sediment fining during transport with fragmentation and abrasion. *Journal of Geophysical Research*, 116(F3).
- Le Coz, J., Renard, B., Bonnifait, L., Branger, F., and Le Boursicaud, R. (2014). Combining hydraulic knowledge and uncertain gaugings in the estimation of hydrometric rating curves: a Bayesian approach. *Journal of Hydrology*, 509:573–587.
- Le Roux, J. J., Sumner, P. D., Lorentz, S. A., and Germishuys, T. (2013). Connectivity aspects in sediment migration modelling using the Soil and Water Assessment Tool. *Geosciences*, 3(1):1–12.
- Lecompte, M., Lhénaff, R., and Marre, A. (1998). Huit ans de mesures du ravinement des marnes dans les baronnies méridionales (Préalpes françaises du sud)/Gullying in the South Baronnies (southern French Alps). Results from eight years of monitoring. *Géomorphologie: relief, processus, environnement*, 4(4):351–373.
- Legout, C., Poulenard, J., Nemery, J., Navratil, O., Grangeon, T., Evrard, O., and Esteves, M. (2013). Quantifying suspended sediment sources during runoff events in headwater catchments using spectroradiometry. *Journal of Soils and Sediments*, 13(8):1478–1492.

- Lenzi, M., Mao, L., and Comiti, F. (2003). Interannual variation of suspended sediment load and sediment yield in an alpine catchment. *Hydrological Sciences Journal*, 48(6):899–915.
- Leonard, R., Knisel, W., and Still, D. (1987). GLEAMS: groundwater loading effects of agricultural management systems. *Transactions of the ASAE*, 30(5):1403–1418.
- Liébault, F., Bellot, H., Chapuis, M., Klotz, S., and Deschâtres, M. (2012). Bedload tracing in a high-sediment-load mountain stream. *Earth Surface Processes and Landforms*, 37(4):385–399.
- Liébault, F., Gomez, B., Page, M., Marden, M., Peacock, D., Richard, D., and Trotter, C. M. (2005). Land-use change, sediment production and channel response in upland regions. *River Research and Applications*, 21(7):739–756.
- Limerinos, J. T. (1970). Determination of the manning coefficient from measured bed roughness in natural channels. *US Geological Survey Water Supply Papers*, 1898(B):47.
- Lobligeois, F. (2014). *Mieux connaître la distribution spatiale des pluies améliore-t-il la modélisation des crues? Diagnostic sur 181 bassins versants français*. Dissertation, Institut des Sciences et Industries du Vivant et de l’Environnement - AgroParisTech, Antony, France.
- Lobligeois, F., Andréassian, V., Perrin, C., Tabary, P., and Loumagne, C. (2014). When does higher spatial resolution rainfall information improve streamflow simulation? An evaluation using 3620 flood events. *Hydrology and Earth System Sciences*, 18(2):575–594.
- Lofi, J., Pezard, P., Loggia, D., Garel, E., Gautier, S., Merry, C., and Bondabou, K. (2012). Geological discontinuities, main flow path and chemical alteration in a marly hill prone to slope instability: assessment from petrophysical measurements and borehole image analysis. *Hydrological Processes*, 26(14):2071–2084.
- Looper, J. P. and Vieux, B. E. (2012). An assessment of distributed flash flood forecasting accuracy using radar and rain gauge input for a physics-based distributed hydrologic model. *Journal of Hydrology*, 412:114–132.
- López Tarazón, J. A. (2011). *The sediment budget of a highly erodible catchment. The river Isábena (Ebro basin, central pyrennes)*. Dissertation, Universitat de Lleida, Lleida, Spain.
- López-Vicente, M. and Ben-Salem, N. (2019). Computing structural and functional flow and sediment connectivity with a new aggregated index: A case study in a large mediterranean catchment. *Science of The Total Environment*, 651:179–191.
- López-Vicente, M., Quijano, L., Palazón, L., Gaspar, L., and Izquierdo, A. N. (2015). Assessment of soil redistribution at catchment scale by coupling a soil erosion model and a sediment connectivity index (central Spanish Pre-Pyrenees). *Cuadernos de investigación geográfica*, 1(41):127–147.

- Lukey, B., Sheffield, J., Bathurst, J., Lavabre, J., Mathys, N., and Martin, C. (1995). Simulating the effect of vegetation cover on the sediment yield of Mediterranean catchments using SHETRAN. *Physics and Chemistry of the Earth*, 20(3-4):427–432.
- Lukey, B. T., Sheffield, J., Bathurst, J. C., Hiley, R. A., and Mathys, N. (2000). Test of the SHETRAN technology for modelling the impact of reforestation on badlands runoff and sediment yield at Draix, France. *Journal of Hydrology*, 235(1–2):44–62.
- Maher, B. A. (1986). Characterisation of soils by mineral magnetic measurements. *Physics of the Earth and planetary interiors*, 42(1-2):76–92.
- Mallet, F. (2018). *Spatialisation et modélisation de l'état hydrique des sols pour l'étude des processus de formation des écoulements en contexte torrentiel : application au bassin versant marneux du Laval (ORE Draix-Bléone, Alpes-de-Haute-Provence, France)*. Dissertation, l'Université d'Avignon et des Pays de Vaucluse, Avignon, France.
- Mano, V., Nemery, J., Belleudy, P., and Poirel, A. (2009). Assessment of suspended sediment transport in four alpine watersheds (France): influence of the climatic regime. *Hydrological Processes*, 23(5):777–792.
- Marra, F., Nikolopoulos, E., Creutin, J., and Borga, M. (2016). Space–time organization of debris flows-triggering rainfall and its effect on the identification of the rainfall threshold relationship. *Journal of Hydrology*, 541:246–255.
- Marra, F., Nikolopoulos, E. I., Creutin, J. D., and Borga, M. (2014). Radar rainfall estimation for the identification of debris-flow occurrence thresholds. *Journal of Hydrology*, 519:1607–1619.
- Martínez-Carreras, N., Krein, A., Gallart, F., Iffly, J. F., Pfister, L., Hoffmann, L., and Owens, P. N. (2010a). Assessment of different colour parameters for discriminating potential suspended sediment sources and provenance: A multi-scale study in Luxembourg. *Geomorphology*, 118(1–2):118–129.
- Martínez-Carreras, N., Krein, A., Udelhoven, T., Gallart, F., Iffly, J. F., Hoffmann, L., Pfister, L., and Walling, D. E. (2010b). A rapid spectral-reflectance-based fingerprinting approach for documenting suspended sediment sources during storm runoff events. *Journal of Soils and Sediments*, 10(3):400–413.
- Martínez-Carreras, N., Udelhoven, T., Krein, A., Gallart, F., Iffly, J. F., Ziebel, J., Hoffmann, L., Pfister, L., and Walling, D. E. (2010c). The use of sediment colour measured by diffuse reflectance spectrometry to determine sediment sources: Application to the Attert River catchment (Luxembourg). *Journal of Hydrology*, 382(1–4):49–63.
- Masselink, R. J., Keesstra, S. D., Temme, A. J., Seeger, M., Giménez, R., and Casali, J. (2016). Modelling discharge and sediment yield at catchment scale using connectivity components. *Land Degradation & Development*, 27(4):933–945.

- Mathys, N. (2006). *Analyse et modélisation à différentes échelles des mécanismes d'érosion et de transport de matériaux solides Cas des petits bassins versants de montagne sur marne (Draix, Alpes-de-Haute-Provence)*. Dissertation, Grenoble INP, Grenoble, France.
- Mathys, N., Brochot, S., Meunier, M., and Richard, D. (2003). Erosion quantification in the small marly experimental catchments of Draix (Alpes de Haute Provence, France). Calibration of the ETC rainfall-runoff-erosion model. *Catena*, 50(2-4):527-548.
- Mathys, N., Klotz, S., Esteves, M., Descroix, L., and Lapetite, J. M. (2005). Runoff and erosion in the Black Marls of the French Alps: Observations and measurements at the plot scale. *Catena*, 63(2-3):261-281.
- Medeiros, P. H., Güntner, A., Francke, T., Mamede, G. L., and Carlos de Araújo, J. (2010). Modelling spatio-temporal patterns of sediment yield and connectivity in a semi-arid catchment with the wasa-sed model. *Hydrological Sciences Journal*, 55(4):636-648.
- Melese, V. (2019). *Modélisation multi-échelle de l'aléa pluviométrique et incertitudes associées-Application à la région des Cévennes*. Dissertation, Université Grenoble Alpes, Grenoble, France.
- Merritt, W., Letcher, R., and Jakeman, A. (2003). A review of erosion and sediment transport models. *Environmental Modelling & Software*, 18(8-9):761-799.
- Mevik, B.-H., Wehrens, R., Liland, K., and Hiemstra, P. (2016). Package 'pls'. partial least squares and principal component regression. <https://cran.r-project.org/web/packages/pls/pls.pdf> [access: 20-01-2020].
- Micoud, B. (2018). *Étude du fonctionnement hydrologique d'un petit bassin versant montagneux méditerranéen*. Master 1 Report, Université Grenoble Alpes, Grenoble, France.
- Miller, J. R., Mackin, G., Lechler, P., Lord, M., and Lorentz, S. (2013). Influence of basin connectivity on sediment source, transport, and storage within the Mkabela Basin, South Africa. *Hydrology and Earth System Sciences*, 17(2):761-781.
- Misset, C. (2019). *The role of riverbed on suspended sediment transport dynamics in Alpine catchments*. Dissertation, Université Grenoble Alpes, Grenoble, France.
- Misset, C., Recking, A., Legout, C., Poirel, A., Cazilhac, M., Esteves, M., and Bertrand, M. (2019a). An attempt to link suspended load hysteresis patterns and sediment sources configuration in alpine catchments. *Journal of Hydrology*.
- Misset, C., Recking, A., Navratil, O., Legout, C., Poirel, A., Cazilhac, M., Briguet, V., and Esteves, M. (2019b). Quantifying bed-related suspended load in gravel bed rivers through an analysis of the bedload-suspended load relationship. *Earth Surface Processes and Landforms*, 44(9):1722-1733.

- Mohamadi, M. A. and Kavian, A. (2015). Effects of rainfall patterns on runoff and soil erosion in field plots. *International Soil and Water Conservation Research*, 3(4):273–281.
- Molinié, G., Ceresetti, D., Anquetin, S., Creutin, J. D., and Boudevillain, B. (2012). Rainfall regime of a mountainous Mediterranean region: Statistical analysis at short time steps. *Journal of Applied Meteorology and Climatology*, 51(3):429–448.
- Montety, V. d., Marc, V., Emblanch, C., Malet, J.-P., Bertrand, C., Maquaire, O., and Bogaard, T. (2007). Identifying the origin of groundwater and flow processes in complex landslides affecting black marls: insights from a hydrochemical survey. *Earth Surface Processes and Landforms*, 32(1):32–48.
- Montgomery, D. R. (2007). Soil erosion and agricultural sustainability. *Proceedings of the National Academy of Sciences*, 104(33):13268–13272.
- Montgomery, D. R. and Foufoula-Georgiou, E. (1993). Channel network source representation using digital elevation models. *Water Resources Research*, 29(12):3925–3934.
- Morgan, R., Quinton, J., Smith, R., Govers, G., Poesen, J., Auerswald, K., Chisci, G., Torri, D., and Styczen, M. (1998). The European Soil Erosion Model (EUROSEM): a dynamic approach for predicting sediment transport from fields and small catchments. *Earth Surface Processes and Landforms: The Journal of the British Geomorphological Group*, 23(6):527–544.
- Motha, J., Wallbrink, P., Hairsine, P., and Grayson, R. (2003). Determining the sources of suspended sediment in a forested catchment in southeastern Australia. *Water resources research*, 39(3).
- Météo France (2018). PANTHERE: Cumuls de lames d’eau radar métropole. https://donneespubliques.meteofrance.fr/?fond=produit&id_produit=103&id_rubrique=34 [access: 28-03-2020].
- Mueller, M., Bierschenk, A. M., Bierschenk, B. M., Pander, J., and Geist, J. (2020). Effects of multiple stressors on the distribution of fish communities in 203 headwater streams of Rhine, Elbe and Danube. *Science of The Total Environment*, 703:134523.
- Mukundan, R., Radcliffe, D., and Risse, L. (2010a). Spatial resolution of soil data and channel erosion effects on swat model predictions of flow and sediment. *Journal of Soil and Water Conservation*, 65(2):92–104.
- Mukundan, R., Radcliffe, D. E., Ritchie, J. C., Risse, L. M., and McKinley, R. A. (2010b). Sediment fingerprinting to determine the source of suspended sediment in a southern piedmont stream. *Journal of Environment Quality*, 39(4):1328.
- Mullen, K. M. and van Stokkum, I. H. (2015). Package ‘nnls’. The lawson-hanson algorithm for non-negative least squares (NNLS). <https://cran.r-project.org/web/packages/nnls/nnls.pdf> [access: 20-01-2020].

- Nadal-Romero, E., Martínez-Murillo, J. F., Vanmaercke, M., and Poesen, J. (2011). Scale-dependency of sediment yield from badland areas in Mediterranean environments. *Progress in Physical Geography*, 35(3):297–332.
- Nagy, H., Watanabe, K., and Hirano, M. (2002). Prediction of sediment load concentration in rivers using artificial neural network model. *Journal of Hydraulic Engineering*, 128(6):588–595.
- Navratil, O., Esteves, M., Legout, C., Gratiot, N., Nemery, J., Willmore, S., and Grangeon, T. (2011). Global uncertainty analysis of suspended sediment monitoring using turbidimeter in a small mountainous river catchment. *Journal of Hydrology*, 398(3-4):246–259.
- Navratil, O., Evrard, O., Esteves, M., Ayrault, S., Lefèvre, I., Legout, C., Reyss, J.-L., Gratiot, N., Nemery, J., Mathys, N., Poirel, A., and Bonté, P. (2012a). Core-derived historical records of suspended sediment origin in a mesoscale mountainous catchment: the River Bléone, French Alps. *Journal of Soils and Sediments*, 12(9):1463–1478.
- Navratil, O., Evrard, O., Esteves, M., Ayrault, S., Lefèvre, I., Legout, C., Reyss, J.-L., Gratiot, N., Nemery, J., Mathys, N., Poirel, A., and Bonté, P. (2012b). Core-derived historical records of suspended sediment origin in a mesoscale mountainous catchment: the River Bléone, French Alps. *Journal of Soils and Sediments*, 12(9):1463–1478.
- Navratil, O., Evrard, O., Esteves, M., Legout, C., Ayrault, S., Némery, J., Mate-Marin, A., Ahmadi, M., Lefèvre, I., Poirel, A., and Bonté, P. (2012c). Temporal variability of suspended sediment sources in an alpine catchment combining river/rainfall monitoring and sediment fingerprinting. *Earth Surface Processes and Landforms*, 37(8):828–846.
- Navratil, O., Legout, C., Gateuille, D., Esteves, M., and Liebault, F. (2010). Assessment of intermediate fine sediment storage in a braided river reach (southern French Prealps). *Hydrological Processes*, 24(10):1318–1332.
- Nearing, M., Jetten, V., Baffaut, C., Cerdan, O., Couturier, A., Hernandez, M., Le Bissonnais, Y., Nichols, M., Nunes, J., Renschler, C., Souchère, V., and van Oost, K. (2005). Modeling response of soil erosion and runoff to changes in precipitation and cover. *Catena*, 61(2-3):131–154.
- Nearing, M. A. (2004). Soil erosion and conservation. In Wainwright, J. and Mulligan, M., editors, *Environmental Modelling: Finding Simplicity in Complexity*, chapter 22, pages 277 – 290. John Wiley & Sons, Ltd.
- Nearing, M. A., Pruski, F. F., and O’Neal, M. R. (2004). Expected climate change impacts on soil erosion rates: A review. *Journal of Soil and Water Conservation*, 59(1):43 – 50.
- Neuville, A., Toussaint, R., and Schmittbuhl, J. (2012). Fracture aperture reconstruction and determination of hydrological properties: a case study at Draix (French Alps). *Hydrological processes*, 26(14):2095–2105.

- Nizou, J., Demory, F., and Dubrulle-Brunaud, C. (2016). Monitoring of dredged-dumped sediment dispersal off the Bay of the Seine (northern France) using environmental magnetism. *Comptes Rendus Geoscience*, 348(6):451–461.
- Nord, G., Berne, A., Boudevillain, B., Branger, F., Braud, I., Dramais, G., Gérard, S., Coz, J. L., Legout, C., Molinié, G., Baelen, J. V., Vandervaere, J., Andrieu, J., Aubert, C., Caliano, M., Delrieu, G., Grazioli, J., Horner, I., Huza, J., Boursicaud, R. L., Raupach, T., Teuling, A., Vincendon, B., and Wijbrans, A. (2015). A high space-time resolution dataset linking meteorological forcing and hydro-sedimentary response in a mesoscale Mediterranean catchment (auzon) of the ardèche region, France. In *AGU Fall Meeting*, San Francisco.
- Nord, G., Boudevillain, B., Berne, A., Branger, F., Braud, I., Dramais, G., Gérard, S., Le Coz, J., Legout, C., Molinié, G., Van Baelen, J., Vandervaere, J.-P., Andrieu, J., Aubert, C., Caliano, M., Delrieu, G., Grazioli, J., Hachani, S., Horner, I., Huza, J., Le Boursicaud, R., Raupach, T. H., Teuling, A. J., Uber, M., Vincendon, B., and Wijbrans, A. (2017). A high space–time resolution dataset linking meteorological forcing and hydro-sedimentary response in a mesoscale Mediterranean catchment (Auzon) of the Ardèche region, France. *Earth System Science Data*, 9(1):221–249.
- Nosrati, K., Collins, A. L., and Madankan, M. (2018). Fingerprinting sub-basin spatial sediment sources using different multivariate statistical techniques and the Modified MixSIR model. *Catena*, 164:32–43.
- Nosrati, K., Govers, G., Semmens, B. X., and Ward, E. J. (2014). A mixing model to incorporate uncertainty in sediment fingerprinting. *Geoderma*, 217–218:173–180.
- Oakes, E., Hughes, J., Jewitt, G., Lorentz, S., and Chaplot, V. (2012). Controls on a scale explicit analysis of sheet erosion. *Earth Surface Processes and Landforms*, 37(8):847–854.
- Obled, C., Zin, I., and Hingray, B. (2009). Choix des pas de temps et d’espace pour des modélisations parcimonieuses en hydrologie des crues. *La Houille Blanche*, (5):81–87.
- Observatoire Hydrométéorologique Méditerranéen Cévennes-Vivarais (OHM-CV) (2009). Runoff and erosion plots, pradel. <https://doi.osug.fr/public/OHMCV/OHMCV.ERO.PRA.10-13.1.html> [access: 26-03-2020].
- Ochoa-Rodriguez, S., Wang, L.-P., Gires, A., Pina, R. D., Reinoso-Rondinel, R., Bruni, G., Ichiba, A., Gaitan, S., Cristiano, E., van Assel, J., et al. (2015). Impact of spatial and temporal resolution of rainfall inputs on urban hydrodynamic modelling outputs: a multi-catchment investigation. *Journal of Hydrology*, 531:389–407.
- Oostwoud Wijdenes, D. J. and Ergenzinger, P. (1998). Erosion and sediment transport on steep marly hillslopes, Draix, Haute-Provence, France: an experimental field study. *Catena*, 33(3–4):179–200.

- Oreskes, N., Shrader-Frechette, K., and Belitz, K. (1994). Verification, validation, and confirmation of numerical models in the earth sciences. *Science*, 263(5147):641–646.
- Osman, K. T. (2014). *Soil Degradation, Conservation and Remediation*. Springer.
- Owens, P., Batalla, R., Collins, A., Gomez, B., Hicks, D., Horowitz, A., Kondolf, G., Marden, M., Page, M., Peacock, D., Peticrew, E., Salomons, W., and Trustrum, N. (2005). Fine-grained sediment in river systems: environmental significance and management issues. *River research and applications*, 21(7):693–717.
- Palazón, L., Latorre, B., Gaspar, L., Blake, W. H., Smith, H. G., and Navas, A. (2016). Combining catchment modelling and sediment fingerprinting to assess sediment dynamics in a Spanish Pyrenean river system. *Science of The Total Environment*, 569-570:1136–1148.
- Palazón, L. and Navas, A. (2017). Variability in source sediment contributions by applying different statistic test for a Pyrenean catchment. *Journal of Environmental Management*, 194:42–53.
- Palazón, L., Gaspar, L., Latorre, B., Blake, W., and Navas, A. (2014). Evaluating the importance of surface soil contributions to reservoir sediment in alpine environments: a combined modelling and fingerprinting approach in the posets-maladeta natural park. *Solid Earth*, 5(2):963–978.
- Panagos, P., Borrelli, P., Meusburger, K., Alewell, C., Lugato, E., and Montanarella, L. (2015a). Estimating the soil erosion cover-management factor at the European scale. *Land use policy*, 48:38–50.
- Panagos, P., Borrelli, P., Poesen, J., Ballabio, C., Lugato, E., Meusburger, K., Montanarella, L., and Alewell, C. (2015b). The new assessment of soil loss by water erosion in Europe. *Environmental science & policy*, 54:438–447.
- Panagos, P., Meusburger, K., Van Liedekerke, M., Alewell, C., Hiederer, R., and Montanarella, L. (2014). Assessing soil erosion in Europe based on data collected through a European network. *Soil science and plant nutrition*, 60(1):15–29.
- Pandey, A., Himanshu, S. K., Mishra, S., and Singh, V. P. (2016). Physically based soil erosion and sediment yield models revisited. *Catena*, 147:595–620.
- Parnell, A. (2016). Package ‘simmr’. A stable isotope mixing model. <https://cran.r-project.org/web/packages/simmr/simmr.pdf> [access: 20-01-2020].
- Parnell, A. C., Inger, R., Bearhop, S., and Jackson, A. L. (2010). Source partitioning using stable isotopes: Coping with too much variation. *PLoS ONE*, 5(3):e9672.
- Parnell, A. C., Phillips, D. L., Bearhop, S., Semmens, B. X., Ward, E. J., Moore, J. W., Jackson, A. L., Grey, J., Kelly, D. J., and Inger, R. (2013). Bayesian stable isotope mixing models. *Environmetrics*, 24(6):387–399.

- Parsons, A. J., Bracken, L., Poepl, R. E., Wainwright, J., and Keesstra, S. D. (2015). Introduction to special issue on connectivity in water and sediment dynamics. *Earth Surface Processes and Landforms*, 40(9):1275–1277.
- Parsons, A. J., Wainwright, J., Brazier, R. E., and Powell, D. M. (2006). Is sediment delivery a fallacy? *Earth Surface Processes and Landforms*, 31(10):1325–1328.
- Peleg, N. and Morin, E. (2012). Convective rain cells: Radar-derived spatiotemporal characteristics and synoptic patterns over the eastern Mediterranean. *Journal of Geophysical Research: Atmospheres*, 117(D15):D15116.
- Pellarin, T., Delrieu, G., Saulnier, G.-M., Andrieu, H., Vignal, B., and Creutin, J.-D. (2002). Hydrologic visibility of weather radar systems operating in mountainous regions: Case study for the Ardeche catchment (France). *Journal of Hydrometeorology*, 3(5):539–555.
- Perks, M., Warburton, J., Bracken, L., Reaney, S., Emery, S., and Hirst, S. (2017). Use of spatially distributed time-integrated sediment sampling networks and distributed fine sediment modelling to inform catchment management. *Journal of environmental management*, 202:469–478.
- Phillips, C. J., Rey, F., Marden, M., and Liébault, F. (2013). Revegetation of steeplands in france and new zealand: geomorphic and policy responses. *New Zealand Journal of Forestry Science*, 43(1):14.
- Phillips, D. L., Inger, R., Bearhop, S., Jackson, A. L., Moore, J. W., Parnell, A. C., Semmens, B. X., and Ward, E. J. (2014). Best practices for use of stable isotope mixing models in food-web studies. *Canadian Journal of Zoology*, 92(10):823–835.
- Pimentel, D. C., Harvey, C., Resosudarmo, P., Sinclair, K., Kurz, D., McNair, M., Crist, S., Shpritz, L., Fitton, L., Saffouri, R., and Blair, R. (1995). Environmental and economic costs of soil erosion and conservation benefits. *Science*, 267(5201):1117 – 1123.
- Poesen, J. (2018). Soil erosion in the anthropocene: Research needs. *Earth Surface Processes and Landforms*, 43(1):64–84.
- Poulenard, J., Legout, C., Némery, J., Bramorski, J., Navratil, O., Douchin, A., Fanget, B., Perrette, Y., Evrard, O., and Esteves, M. (2012). Tracing sediment sources during floods using Diffuse Reflectance Infrared Fourier Transform Spectrometry (DRIFTS): A case study in a highly erosive mountainous catchment (Southern French Alps). *Journal of Hydrology*, 414-415:452–462.
- Poulier, G., Launay, M., Le Bescond, C., Thollet, F., Coquery, M., and Le Coz, J. (2019). Combining flux monitoring and data reconstruction to establish annual budgets of suspended particulate matter, mercury and PCB in the Rhône River from Lake Geneva to the Mediterranean Sea. *Science of the Total Environment*, 658:457–473.

- Pradhanang, S. M. and Briggs, R. D. (2014). Effects of critical source area on sediment yield and streamflow. *Water and environment journal*, 28(2):222–232.
- Pulley, S., Foster, I., and Antunes, P. (2015). The uncertainties associated with sediment fingerprinting suspended and recently deposited fluvial sediment in the Nene river basin. *Geomorphology*, 228:303–319.
- Pulley, S., Foster, I., and Collins, A. L. (2017a). The impact of catchment source group classification on the accuracy of sediment fingerprinting outputs. *Journal of Environmental Management*, 194:16–26.
- Pulley, S. and Rowntree, K. (2016). The use of an ordinary colour scanner to fingerprint sediment sources in the South African Karoo. *Journal of Environmental Management*, 165:253–262.
- Pulley, S., Van Der Waal, B., Collins, A., Foster, I., and Rowntree, K. (2017b). Are source groups always appropriate when sediment fingerprinting? The direct comparison of source and sediment samples as a methodological step. *River Research and Applications*.
- Reiffarth, D., Petticrew, E., Owens, P., and Lobb, D. (2016). Sources of variability in fatty acid (FA) biomarkers in the application of compound-specific stable isotopes (CSSIs) to soil and sediment fingerprinting and tracing: a review. *Science of the Total Environment*, 565:8–27.
- Renschler, C., Mannaerts, C., and Diekkrüger, B. (1999). Evaluating spatial and temporal variability in soil erosion risk - rainfall erosivity and soil loss ratios in Andalusia, Spain. *Catena*, 34(3-4):209–225.
- Rey, F. (2004). Effectiveness of vegetation barriers for marly sediment trapping. *Earth Surface Processes and Landforms: The Journal of the British Geomorphological Research Group*, 29(9):1161–1169.
- Rey, F. (2009). A strategy for fine sediment retention with bioengineering works in eroded marly catchments in a mountainous Mediterranean climate (Southern Alps, France). *Land Degradation & Development*, 20(2):210–216.
- Rey, F. and Burylo, M. (2014). Can bioengineering structures made of willow cuttings trap sediment in eroded marly gullies in a Mediterranean mountainous climate? *Geomorphology*, 204:564–572.
- Ronzani, F. (2019). *Étude des relations entre turbidités et matières en suspension dans un bassin versant montagneux de mésoéchelle*. Master 1 Report, Université Grenoble Alpes, Grenoble, France.
- Ruin, I., Creutin, J.-D., Anquetin, S., and Lutoff, C. (2008). Human exposure to flash floods - relation between flood parameters and human vulnerability during a storm of September 2002 in southern France. *Journal of Hydrology*, 361(1-2):199–213.

- Salimi, E. T., Nohegar, A., Malekian, A., Hoseini, M., and Holisaz, A. (2017). Estimating time of concentration in large watersheds. *Paddy and Water Environment*, 15(1):123–132.
- Sánchez-Chardi, A., Ribeiro, C. A. O., and Nadal, J. (2009). Metals in liver and kidneys and the effects of chronic exposure to pyrite mine pollution in the shrew *Crocidura russula* inhabiting the protected wetland of Doñana. *Chemosphere*, 76(3):387–394.
- Schlunegger, F. and Schneider, H. (2005). Relief-rejuvenation and topographic length scales in a fluvial drainage basin, Napf area, Central Switzerland. *Geomorphology*, 69(1-4):102–117.
- Seo, Y., Schmidt, A. R., and Sivapalan, M. (2012). Effect of storm movement on flood peaks: Analysis framework based on characteristic timescales. *Water Resources Research*, 48(5).
- Shen, Z., Chen, L., Liao, Q., Liu, R., and Hong, Q. (2012). Impact of spatial rainfall variability on hydrology and nonpoint source pollution modeling. *Journal of Hydrology*, 472:205–215.
- Sik Kim, B., Kyung Kim, B., and Soo Kim, H. (2008). Flood simulation using the gauge-adjusted radar rainfall and physics-based distributed hydrologic model. *Hydrological Processes: An International Journal*, 22(22):4400–4414.
- Smith, H. G., Evrard, O., Blake, W. H., and Owens, P. N. (2015). Preface - addressing challenges to advance sediment fingerprinting research. *Journal of Soils and Sediments*, 15(10):2033–2037.
- Smith, M. B., Koren, V. I., Zhang, Z., Reed, S. M., Pan, J.-J., and Moreda, F. (2004). Runoff response to spatial variability in precipitation: an analysis of observed data. *Journal of Hydrology*, 298(1-4):267–286.
- Sun, L., Yan, M., Cai, Q., and Fang, H. (2016). Suspended sediment dynamics at different time scales in the Loushui River, south-central China. *Catena*, 136:152–161.
- Sun, X., Mein, R. G., Keenan, T. D., and Elliott, J. (2000). Flood estimation using radar and raingauge data. *Journal of Hydrology*, 239(1-4):4–18.
- Syvitski, J. P. and Kettner, A. (2011). Sediment flux and the Anthropocene. *Philosophical Transactions of the Royal Society A: Mathematical, Physical and Engineering Sciences*, 369(1938):957–975.
- Tabary, P. (2007). The new French operational radar rainfall product. Part I: Methodology. *Weather and forecasting*, 22(3):393–408.
- Takken, I., Beuselinck, L., Nachtergaele, J., Govers, G., Poesen, J., and Degraer, G. (1999). Spatial evaluation of a physically-based distributed erosion model (LISEM). *Catena*, 37(3-4):431–447.

- Tarboton, D. (2010). TauDEM (Terrain Analysis Using Digital Elevation Models). <http://hydrology.usu.edu/taudem/taudem5/> [access: 26-03-2020].
- Tarboton, D. G., Bras, R. L., and Rodriguez-Iturbe, I. (1991). On the extraction of channel networks from digital elevation data. *Hydrological Processes*, 5(1):81–100.
- Tarboton, D. G., Sazib, N., and Dash, P. (2015). Taudem 5.3 quick start guide to using the taudem, arcgis, toolbox.
- Te Chow, V. (1959). *Open-channel hydraulics*, volume 1. McGraw-Hill New York.
- Theuring, P., Rode, M., Behrens, S., Kirchner, G., and Jha, A. (2013). Identification of fluvial sediment sources in the Kharaa River catchment, northern Mongolia. *Hydrological Processes*, 27(6):845–856.
- Thommeret, N., Bailly, J.-S., and Puech, C. (2010). Extraction of thalweg networks from DTMs: application to badlands. *Hydrology and Earth System Science*, 14:1527–1536.
- Tiemeyer, B., Moussa, R., Lennartz, B., and Voltz, M. (2007). MHYDAS-DRAIN: A spatially distributed model for small, artificially drained lowland catchments. *Ecological modelling*, 209(1):2–20.
- Tramblay, Y., Neppel, L., Carreau, J., and Sanchez-Gomez, E. (2012). Extreme value modelling of daily areal rainfall over mediterranean catchments in a changing climate. *Hydrological Processes*, 26(25):3934–3944.
- Travelletti, J., Sailhac, P., Malet, J.-P., Grandjean, G., and Ponton, J. (2012). Hydrological response of weathered clay-shale slopes: Water infiltration monitoring with time-lapse electrical resistivity tomography. *Hydrological Processes*, 26(14):2106–2119.
- Tucker, G. E. and Bras, R. L. (2000). A stochastic approach to modeling the role of rainfall variability in drainage basin evolution. *Water Resources Research*, 36(7):1953–1964.
- Turcotte, R., Fortin, J.-P., Rousseau, A., Massicotte, S., and Villeneuve, J.-P. (2001). Determination of the drainage structure of a watershed using a digital elevation model and a digital river and lake network. *Journal of Hydrology*, 240(3-4):225–242.
- Turnbull, L., Wainwright, J., and Brazier, R. E. (2008). A conceptual framework for understanding semi-arid land degradation: Ecohydrological interactions across multiple-space and time scales. *Ecohydrology: Ecosystems, Land and Water Process Interactions, Ecohydrogeomorphology*, 1(1):23–34.
- Tuset, J., Vericat, D., and Batalla, R. (2016). Rainfall, runoff and sediment transport in a Mediterranean mountainous catchment. *Science of The Total Environment*, 540:114–132.

- Uber, M., Legout, C., Nord, G., Crouzet, C., Demory, F., and Poulenard, J. (2019). Comparing alternative tracing measurements and mixing models to fingerprint suspended sediment sources in a mesoscale Mediterranean catchment. *Journal of Soils and Sediments*, pages 1–19.
- Uber, M., Vandervaere, J.-P., Zin, I., Braud, I., Heisterman, M., Legoût, C., Molinié, G., and Nord, G. (2018). How does initial soil moisture influence the hydrological response? a case study from southern France. *Hydrology and Earth System Sciences*, 22:6127–6146.
- Upadhayay, H. R., Bodé, S., Griepentrog, M., Huygens, D., Bajracharya, R. M., Blake, W. H., Dercon, G., Mabit, L., Gibbs, M., Semmens, B. X., Stock, B. C., Cornelis, W., and Boeckx, P. (2017). Methodological perspectives on the application of compound-specific stable isotope fingerprinting for sediment source apportionment. *Journal of Soils and Sediments*, 17(6):1537–1553.
- Vale, S. (2016). *Application and evaluation of sediment fingerprinting techniques in the Manawatu River catchment, New Zealand*. Dissertation, Massey University, Palmerston North, New Zealand.
- Valentin, C., Poesen, J., and Li, Y. (2005). Gully erosion: impacts, factors and control. *Catena*, 63(2-3):132–153.
- Vallauri, D. R., Aronson, J., and Barbero, M. (2002). An analysis of forest restoration 120 years after reforestation on badlands in the southwestern alps. *Restoration ecology*, 10(1):16–26.
- van Rijn, L. C. (1984). Sediment transport, part II: suspended load transport. *Journal of hydraulic engineering*, 110(11):1613–1641.
- Van Rompaey, A. J., Verstraeten, G., Van Oost, K., Govers, G., and Poesen, J. (2001). Modelling mean annual sediment yield using a distributed approach. *Earth Surface Processes and Landforms*, 26(11):1221–1236.
- Vanmaercke, M., Maetens, W., Poesen, J., Jankauskas, B., Jankauskiene, G., Verstraeten, G., and de Vente, J. (2012). A comparison of measured catchment sediment yields with measured and predicted hillslope erosion rates in Europe. *Journal of Soils and Sediments*, 12(4):586–602.
- Vanmaercke, M., Poesen, J., Verstraeten, G., de Vente, J., and Ocakoglu, F. (2011). Sediment yield in Europe: spatial patterns and scale dependency. *Geomorphology*, 130(3-4):142–161.
- Vercruyssen, K. and Grabowski, R. C. (2019). Temporal variation in suspended sediment transport: linking sediment sources and hydro-meteorological drivers. *Earth Surface Processes and Landforms*.

- Vercruyssen, K., Grabowski, R. C., and Rickson, R. (2017). Suspended sediment transport dynamics in rivers: Multi-scale drivers of temporal variation. *Earth-Science Reviews*, 166:38–52.
- Vieux, B. E., Park, J.-H., and Kang, B. (2009). Distributed hydrologic prediction: sensitivity to accuracy of initial soil moisture conditions and radar rainfall input. *Journal of Hydrologic Engineering*, 14(7):671–689.
- Vogt, J., Soille, P., Colombo, R., Paracchini, M. L., and de Jager, A. (2007). Development of a pan-European river and catchment database. In *Digital terrain modelling*, pages 121–144. Springer.
- von Hardenberg, J., Ferraris, L., and Provenzale, A. (2003). The shape of convective rain cells. *Geophysical Research Letters*, 30(24):2280.
- Wainwright, J., Parsons, A. J., Müller, E. N., Brazier, R. E., Powell, D. M., and Fenti, B. (2008). A transport-distance approach to scaling erosion rates: 1. background and model development. *Earth Surface Processes and Landforms*, 33(5):813–826.
- Wainwright, J., Turnbull, L., Ibrahim, T. G., Lexartza-Artza, I., Thornton, S. F., and Brazier, R. E. (2011). Linking environmental régimes, space and time: Interpretations of structural and functional connectivity. *Geomorphology*, 126(3-4):387–404.
- Walden, J., Slattery, M. C., and Burt, T. P. (1997). Use of mineral magnetic measurements to fingerprint suspended sediment sources: approaches and techniques for data analysis. *Journal of Hydrology*, 202(1-4):353–372.
- Walling, D. (1977). Assessing the accuracy of suspended sediment rating curves for a small basin. *Water Resources Research*, 13(3):531–538.
- Walling, D. E. (1983). The sediment delivery problem. *Journal of Hydrology*, 65(1-3):209–237.
- Walling, D. E., Peart, M. R., Oldfield, F., and Thompson, R. (1979). Suspended sediment sources identified by magnetic measurements. *Nature*, 281:110 – 113.
- Wei, W., Chen, L., and Fu, B. (2009). Effects of rainfall change on water erosion processes in terrestrial ecosystems: a review. *Progress in Physical Geography*, 33(3):307–318.
- Whitaker, A., Alila, Y., Beckers, J., and Toews, D. (2003). Application of the distributed hydrology soil vegetation model to Redfish Creek, British Columbia: model evaluation using internal catchment data. *Hydrological Processes*, 17(2):199–224.
- Wijbrans, A., Delrieu, G., and Nord, G. (2015). Within catchment spatial rainfall variability over a range of spatio-temporal scales in the Cévennes-Vivarais Region, France. A study over the years 2007 – 2014 for ungauged basins(10-500 km²) and temporal resolution (1-6 hours). In *Hymex Workshop*.

- Wilkinson, S. N., Hancock, G. J., Bartley, R., Hawdon, A. A., and Keen, R. J. (2013). Using sediment tracing to assess processes and spatial patterns of erosion in grazed rangelands, Burdekin River basin, Australia. *Agriculture, Ecosystems & Environment*, 180:90–102.
- Willems, P. (2001). A spatial rainfall generator for small spatial scales. *Journal of Hydrology*, 252(1-4):126–144.
- Williams, J. (1985). The physical components of the EPIC model. *Soil Conservation Society of America*.
- Wischmeier, W. H. and Smith, D. D. (1978). Predicting rainfall erosion losses—a guide to conservation planning. *Predicting rainfall erosion losses—a guide to conservation planning*.
- Wisser, D., Frohling, S., Hagen, S., and Bierkens, M. F. (2013). Beyond peak reservoir storage? a global estimate of declining water storage capacity in large reservoirs. *Water Resources Research*, 49(9):5732–5739.
- Wold, S., Sjöström, M., and Eriksson, L. (2001). PLS-regression: a basic tool of chemometrics. *Chemometrics and intelligent laboratory systems*, 58(2):109–130.
- Yamakoshi, T., Mathys, N., and Klotz, S. (2009). Time-lapse video observation of erosion processes on the Black Marls badlands in the Southern Alps, France. *Earth Surface Processes and Landforms*, 34(2):314–318.
- Yang, D., Kanae, S., Oki, T., Koike, T., and Musiake, K. (2003). Global potential soil erosion with reference to land use and climate changes. *Hydrological Processes*, 17(14):2913–2928.
- Yu, L. and Oldfield, F. (1993). Quantitative sediment source ascription using magnetic measurements in a reservoir-catchment system near Nijar, SE Spain. *Earth Surface Processes and Landforms*, 18(5):441–454.
- Zalasiewicz, J., Williams, M., Smith, A., Barry, T. L., Coe, A. L., Bown, P. R., Brenchley, P., Cantrill, D., Gale, A., Gibbard, P., Gregory, F., Hounslow, M., Kerr, A., Pearson, P., Knox, R., Powell, J., Waters, C., Marshall, J., Oates, M., Rawson, P., and Stone, P. (2008). Are we now living in the Anthropocene? *GSA Today*, 18(2):4.
- Zanon, F., Borga, M., Zoccatelli, D., Marchi, L., Gaume, E., Bonnifait, L., and Delrieu, G. (2010). Hydrological analysis of a flash flood across a climatic and geologic gradient: The september 18, 2007 event in western slovenia. *Journal of Hydrology*, 394(1-2):182–197.
- Zhang, X. J. and Liu, B. (2016). Using multiple composite fingerprints to quantify fine sediment source contributions: a new direction. *Geoderma*, 268:108–118.

- Zimmermann, A., Francke, T., and Elsenbeer, H. (2012). Forests and erosion: insights from a study of suspended-sediment dynamics in an overland flow-prone rainforest catchment. *Journal of Hydrology*, 428:170–181.
- Zocatelli, D., Borga, M., Viglione, A., Chirico, G. B., and Blöschl, G. (2011). Spatial moments of catchment rainfall: rainfall spatial organisation, basin morphology, and flood response. *Hydrology and Earth System Sciences*, 15(12):3767–3783.